TriboBR

4th International Brazilian Conference on Tribology

26-29 November, 2023

Vitória -ES

Proceedings

Henara Lillian Costa
Cherlio Scandian

Proceedings of the Fourth International Brazilian Conference on Tribology

Vitoria, ES
2023

Revisão textual e gramatical: Resposanbilidade dos respectivos autores.

Dados Internacionais de Catalogação na Publicação (CIP)
(Câmara Brasileira do Livro, SP, Brasil)

Proceedings of the fourth international brazilian conference on tribology (4. : 2023 : Vitória, ES) 4th TRIBO BR [livro eletrônico] / organização Henara Lillian Costa , Cherlio Scandian. -- 1. ed. -- São Carlos, SP : Aptor Software, 2023.
PDF

Vários autores.
Bibliografia.
ISBN 978-85-63273-53-6

1. Tribologia I. Costa, Henara Lillian. II. Scandian, Cherlio. III. Título.

23-181085 CDD-621.89

Índices para catálogo sistemático:

1. Tribologia : Tecnologia 621.89

Aline Graziele Benitez - Bibliotecária - CRB-1/3129

Office of the President

International Tribology Council
C/o Empa, Überlandstrasse 129
8600 Dübendorf
Switzerland

Prof. em. Dr. Nicholas D. Spencer
President, ITC
www.itctribology.net

To the attendees of TriboBr

November 14, 2023

Welcome to TriboBr—4th International Conference on Tribology, Vitória -ES, Brazil

Dear Colleagues:

It is with great pleasure that, in the name of ITC, I welcome you to TriboBr in the beautiful city of Vitória.

The ITC exists to facilitate communication between tribologists worldwide, and this conference, with its many international participants, is an excellent demonstration of this principle. We also are responsible for ensuring that international congresses (the World Tribology Congress, WTC) take place at regular intervals, and are delighted that the next WTC will take place in Rio de Janeiro (20-25 September, 2026).

This conference happens in a period of crises: geopolitical and climatic. While we, as tribologists, can only hope that smarter politicians can solve the former, we hold some of the keys to the latter. Whether it be in the design of better lubricants to reduce CO_2 emissions and lower energy consumption or the design of better tribological systems to improve the reliability of wind turbines, tribologists can play a very significant role in meeting net-zero and sustainability goals.

Despite our importance in solving some of these vital issues, our role as tribologists is often invisible. We have a responsibility to educate not only the public as to the criticality of tribology, but also a significant number of engineers (especially non-mechanical engineers). Tribology should form a part of all engineering curricula, and high-school teachers should incorporate tribological projects into their school programs. Tribology societies, world-wide, have a responsibility to the field to implement such activities.

I look forward to meeting many of you and enjoying many presentations at the exciting conference that the organizers have planned. Please enjoy the next few days of intellectual stimulation in these beautiful surroundings.

Sincerely,

Nicholas D. Spencer
President, International Tribology Council

Dear participant,

The First International Brazilian Conference on Tribology (TriboBR 2010) was held in Rio de Janeiro, in November 2010. That meeting was certainly a milestone for the Brazilian Tribology, providing, along with other aspects, a forum for high-quality discussions on tribological issues.

Four years later, the Second International Brazilian Conference on Tribology (TriboBr 2014), in Foz do Iguaçu, celebrated the strengthening of the Brazilian tribological community. It involved not only the steady increase of the tribological activities in many already well-establish groups in Brazil but also the nucleation of new ones, with increasing number and depth of the interactions of Brazilian groups with institutions abroad, as well as industry-academy interactions. The Third International Brazilian Conference on Tribology (TriboBr 2018), in Florianópolis, showed further progress, with increased number of submissions, more international participation and consolidation of the Brazilian tribology.

The Fourth International Brazilian Conference on Tribology (TriboBr 2023), in Vitória, represents the continuity of this successful conference series. Most of the positive aspects of the previous events remain valid, including the increase in industry-academia and academia-academia interactions, the consolidation of emerging groups and further nucleation of new groups. The set of plenary and invited speakers is again remarkable, and the quality of the previous editions is attracting a growing number of tribologists from other countries. These signs indicate that the Brazilian tribological community has spread and matured, embracing new leading tribologists, to remain active independently of the oscillations in the economy.

The creation of the National Research Institute on Green Tribology for the Energy Transition (CT-Trib) in 2022 reflects the consolidation of the Brazilian tribology as a strong and collaborative network of leading groups on Tribology. CT-Trib has had a strong role and given substantial support to the organization of TriboBr 2023.

TriboBr 2023 will have 83 oral presentations and 62 poster presentations, with confirmed participants from 16 different countries.

The organizing committee would like to thank the endorsement from IFToMM. The power of social media was also explored to promote the conference by including it as a Project in the Research Gate platform. The committee also thanks the endorsement of Petronews, the financial support from all the sponsors, the International Advisory Board, the Scientific Committee and all others who have contributed to the success of TriboBr 2023. We welcome all participants, with the confidence of sharing with them another pleasant and fruitful conference in the beautiful island of Vitória.

COMMITTEE

Organizing committee

Prof. Henara Lillian Costa (FURG, Brazil) – Chair

Prof. Cherlio Scandian (UFES, Brazil) – Vice-chair

Prof. Cristiano Binder (UFSC, Brazil)

Dr. Gisele Hammes (UFSC, Brazil)

Prof. Giuseppe Pintaúde (UTFPR, Brazil)

Prof. José Daniel Biasoli de Mello (UFU, Brazil)

Prof. Lúcia Vieira (UNIVAP, Brazil)

Prof. Nathan Fantecelle Strey (UFES, Brazil)

Prof. Roberto Martins de Souza (Poli-USP, Brazil)

Prof. Salete Martins Alves (UFRN, Brazil)

INTERNATIONAL ADVISORY BOARD

SCIENTIFIC COMMITTEE

Adilson Rodrigues da Costa - UFOP- Brazil
Bernardo Tormos Martínez - Universitat Politècnica de València - Spain
Andreas Rosenkranz - Universidad Catolica de Chile - Chile
Carlos Figueroa – UCS - Brazil
Carlos Henrique da Silva – UTFPR – Brazil
Cristine Boher – Institut Clément Ader Albi - (ICAA) - France
Danielle Dini - Imperial College - UK
Eduardo Albertin – IPT - Brazil
Eduardo M. Tomanik - Gerdau Graphene - Brazil
Fabrice Dessanoy - Ecole Centrale de Lyon - France
Francisco José Profito – USP - Brazil
Geralda Cristina Durães de Godoy – UFMG - Brazil
Germán Prieto - Universidad del Sur - Argentina
Hélio Goldenstein – USP – Brazil
Izabel Fernanda Machado – USP - Brazil
João Henrique Corrêa de Souza - TechnNOVA -Brazil
John Jairo Coronado Marin – UniValle - Colombia
Julio Cesar Klein das Neves – UTFPR - Brazil
Kenneth G Budinski - Bud Labs - USA
Kent Salomonsson - Jönköping University - Sweden
Marcello Papini- Ryerson University - Canada
Marcia M. Maru – INMETRO – Brazil
Marcio Gustavo di Vernieri Cuppari – UFABC - Brazil
Maria Cristina Moré Farias – UCS - Brazil
Maria Isabel de Barros Bouchet- Ecole Centrale de Lyon - France
Massimo Pelizari - University of Trento - Italy
Paulo Cordeiro Machado – UFPA - Brazil
Ricardo C Dommarco - Universidad Nacional de Mar del Plata -Argentina
Richard R Chromik - McGill University - Canada
Steven Shaffer – Shaffer Tribology Consulting - USA
Sylvie Descartes - INSA/Lyon - France
Tanvir Hussain – University of Nottingham – UK
Tiago Cousseau – UTFPR - Brazil
Washington Martins da Silva Jr. – UFU - Brazil

PLENARY SPEAKERS

Prof. Ali Erdemir - Texas A&M - USA

Prof. Álvaro Prata - Federal University of Santa Catarina - Brazil

Prof. Hugh Spikes - Tribology Group, Imperial College London - UK

Prof. Mitjan Kalin - University of Ljubljana - Slovenia

Prof. Nick Spencer - ETH Zurich - Switzerland

Prof. Peter Gumbsch - Karlsruhe Institute of Technology - Germany

KEYNOTE SPEAKERS

Prof. Maria Isabel de Barros-Bouchet - Ecole Centrale de Lyon - France

Prof. Mehmet Baykara - University of California - Merced - USA

Prof. Mohamed El-Mansori - Arts et Metiers - France

Dr. Steve Shaffer - Schaffer Consulting - USA

SPONSORS AND EXIBITHORS

Gold sponsors

Sponsors

ENDORSEMENT

IFToMM Technical
Committee for Tribology

SUMMARY

PROGRAM

Sunday, 26/11/2023

16:00-18:00: Registration

18:45: Welcome address

18:30-22:30: Welcome drinks – Solarium Room

Special participation of "Chorinho and Samba" Brazilian band

Monday, November 27, 2023			
8h00	8h30	**Welcome and opening ceremony** ("**Ilha do Boi" Auditorium)**	
8h30	9h00	**Session 1:** (**"Ilha do Boi" Auditorium) Plenary lecture** – **Cartilage, contact lenses and car engines: lubrication with polymer brushes**, *N. Spencer, ETH Zurich, Switzerland* Moderator: *J.D.B de Mello*	
9h00	9h30		
9h30	10h30	**Poster Session A / Refreshments (Penedo Room)**	
		Session 2 ("Ilha das Caieiras" Room) Biotribology Moderator*: José Gomes*	**Session 3 ("Ilha do Boi" Auditorium) – Tribology in Manufacturing** Moderator: *G. Pintaude*
10h30	10h50	**4DRC** Study of the frictional behavior of soft contact lenses by an oscillatory free-vibration tribometer, *Amilcar Ramalho*, Universidade de Coimbra, Portugal	**4DME Invited:** Effect of Temperature on Fretting Wear of Additively Manufactured Inconel 718, *Muthuswamy Kamaraj*, Indian Institute of Technology Madras (IITM), India
10h50	11h10	**4DNQ** Surface topography evaluation of composite resin restored teeth by different finishing and polishing techniques, *Marcia Marie Maru de Moraes,* National Institute of Metrology, Quality and Technology (INMETRO), Brazil	**4DMW** High temperature tribological behavior of additively manufactured tool materials, *Gabriel Macêdo,* Luleå Tekniska Universitet, Sweden
11h10	11h30	**4DRZ** Biotribological behavior of ta-C coatings for load-bearing implants, *Max Marian* , Pontificia Universidad Católica de Chile (PUC), Chile	**4DQB** Influence of the turning process on the tribological performance of self-lubricating composites, *Caroline Francisco Dorneles* Universidade Federal de Santa Catarina, Brazil
11h30	11h50	**4DS2** Mechanical and tribological behavior of 2D material-reinforced metal matrix composites for biotribological applications, *Max Marian*, Pontificia Universidad Católica de Chile (PUC), Chile	**4DPS** Influence of sequential machining process on the surface of dies, *Sara Builes Diaz*, Universidade Federal de Santa Catarina (UFSC), Brazil
11h50	12h10	**4DR6** Effect of lamellar anisotropy produced by mechanical compression	**4DNM** Laser cladding and laser heat treatment process for tooling

		in UHMWPE on its tribological resistance**,** *Marcia Marie Maru de Moraes,* National Institute of Metrology, Quality and Technology (INMETRO), Brazil	applications, *Renan Oss Giacomelli* Instituto SENAI de Inovação em Processamento a Laser (ISI-LASER), Brazil
12h10	12h30	Sponsor Technical Talk 1, How to select the right tribological lab test for practical applications*, Lais Lopes,* Falex Group ("**Ilha do Boi" Auditorium)**	
12h30	14h	Lunch	
14h	14h30	**Session 4: Plenary lecture** – Lubrication in an inert atmosphere - a new route to sustainability - and much else…, *H. Spikes*, Tribology Group, Imperial College London, UK Moderator: *H.L. Costa* (**"Ilha do Boi" Auditorium)**	
14h30	15h		
		Session 5 Lubricants and Lubrication ("Ilha das Caieiras" Room) Moderator: *F. Profito*	**Session 6 Wear Testing ("Ilha do Boi" Auditorium)** Moderator: *N.F. Strey*
15h	15h20	**4DRJ** COF and wear variation of an anodized aluminum surface with different lubricant compositions, *Giuseppe Pintaude,* Universidade Tecnológica Federal do Paraná (UTFPR), Brazil	**Keynote** Wear testing and standards, *S. Schaffer,* Schaffer consulting, USA
15h20	15h40	**4DPY** Thermo-hydrodynamic analysis of journal bearings operating with non-Newtonian oils**,** *Mateus da Silva Cardoso*, Universidade Federal de Santa Catarina (UFSC), Brazil	
15h40	16h	**4DNW** Lubricating Performance of PAO Oils Additivated with Combinations of ZDDP, Metal Sulfides, and Carbon Nanotubes**,** *Germán Prieto,* Universidad Nacional del Sur (UNS), Argentina	**4DSP** Rotary barrel tumbling as a method of surface preparation for pin-on-disc wear testing samples, Leonardo Medeiros Xavier, Federal University of Espírito Santo (UFES), Brazil
16h	16h30	**Refreshments (Penedo Room)**	
		Session 7 Abrasion and erosion ("Ilha das Caieiras" Room) Moderator: *H. Goldenstein*	**Session 8 Lubricants and Lubrication ("Ilha do Boi" Auditorium)** Moderator: *H. L. Costa*
16h30	16h50	**4DPV** Erosion Simulation in Labyrinth Seals – CFD Analysis**,** *André Dantas Freire,* Polytechnic School of the University of São Paulo (USP), Brazil	**Keynote** Effects of lubricants and additives in DLC contacts, *M.I. de Barros-Bouchet* Ecole Centrale de Lyon, France
16h50	17h10	**4DMG** Micro abrasion in Fe-Cr-C-Nb alloys samples: the role of Niobium**,** *Adilson Rodrigues da Costa* Federal University of Ouro Preto (UFOP), Brazil	

17h10	17h30	**4DSV** Polishability of High-Chromium Cast Iron and Commercial Materials for Automotive Polymer Injection Molds, *Valdicleide Silva e Mello*, Universidade Federal do Espírito Santo (UFES), Brazil	**4DSN** Use of a test rig to evaluate effect of oil formulations on gearbox friction losses, *Eduardo Tomanik*, Gerdau Graphene, Brazil
17h30	17h50	**4DQM** The use of ASTM G-65 dry sand/rubber wheel test adapted to abrasiveness ranking of iron ores, *Daiane Münch*, Instituto Tecnológico Vale (ITV), Brazil	**4DP2** The Effect of Viscosity on Rail/Wheel Wear Resistance Using Calcium-Thickened Greases*, Ana Cecília de Carvalho,* Universidade Estadual de Campinas (UNICAMP) , Brazil
17h50	18h10	**4DSH** Scratch Tests onto Al-Fe-Cr Quasi-Crystal-Reinforced Aluminum Matrix Composite Fabricated by Selective Laser Melting, *Vinicius Alves de Lima,* Universidade de São Paulo (USP), Brazil	**4DPK** Designing MoS_2 based coatings for improved self-lubricating gears, *Newton Kiyoshi Fukumasu*, Universidade de São Paulo (USP), Brazil
18h10	18h30	**4DNJ** Effect of abrasive on the wear behaviour of synthetic and water based fluids in oil and gas drilling, Leonardo Rosa Ribeiro da Silva, Universidade Federal de Uberlândia (UFU), Brazil	**4DPW** A method to assess the tribological behaviour of solid lubricant nanoparticles in the macroscale applied to graphene and carbide-derived carbon, *Renan Oss Giacomelli,* Instituto SENAI de Inovação em Processamento a Laser, Brazil

Tuesday, November 28, 2023			
8h00	8h30	**Session 9: Plenary lecture** – Tribological Challenges and Opportunities for a Sustainable E-Mobility, *A. Erdemir*, Texas A&M, USA **("Ilha do Boi" Auditorium)** Moderator: *L. Vieira*	
8h30	9h00		
9h00	10h00	**Poster Session B / Refreshments (Penedo Room)**	
		Session 10 Wear ("Ilha das Caieiras" Room) Moderator: *A. R. Costa*	**Session 11 Surface Topography ("Ilha do Boi" Auditorium)** Moderator: *M. Marian*
10h00	10h20	**4DQJ** Analysis of rolling contact fatigue resistance in pearlitic and bainitic rail steel using twin-disc tests, *Roberto Martins de Souza*, Universidade de São Paulo (USP)	**4DM6 Keynote** True Atomic-Resolution Surface Imaging under Ambient Conditions via Conductive Atomic Force Microscopy, *M.Z. Baykara*, University of California – Merced, USA
10h20	10h40	*4DRS Modeling of Non-metalic Inclusions effects on Rails Performance, Eleir Mundim Bortoleto, Instituto Tecnológico Vale (ITV), Brazil*	

10h40	11h00	**4DMQ** Development of a High Temperature Friction and Wear Test in Liquid Lead Environment, *Daria Kolbas*, Luleå Tekniska Universitet (LTU), Sweden	**4DR4** Investigating Topography Effects on Tribological Performance of Graphite Nanoparticles Deposited by Drop-Casting, *Júlia Afonso Pires*, Universidade Federal de Santa Catarina (UFSC), Brazil
11h00	11h20	**4DRP** Investigating Wheel-Rail Contact: An Integrated Approach of Experimental Measurements and FEM-Based Rail Wear Profile Modeling, *Eleir Mundim Bortoleto*, Instituto Tecnológico Vale (ITV), Brazil	**4DQN** Deterministic Asperity-Based Elastic-Plastic Rough Contact Model, *João Carlos Fernandes de Queiróz*, Polytechnic School of the University of São Paulo (USP), Brazil
11h20	11h50	**4DNE** Investigation of the Evolution of Pores During Scuffing Resistance Tests Performed on Sintered Steel Vacuum Impregnated with Graphite, *Nicolás Ignacio Araya Rivera*, Universidad de Concepción (UDEC), Chile	**4DMM** Influence of Surface Texturing on Chrome-coated Cylinder Liners via Deterministic Mixed Lubrication Simulation, *Samuel Anisio Nunes Silva* Universidade Federal de Uberlândia (UFU), Brazil
11h50	12h10	**4DPB** Abrasion resistance of FeCrCV coatings for tillage tools, *Felipe Kevin Correia Luz*, Universidade Federal do Rio Grande (FURG), Brazil	**4DTS** AI-Driven tribological approach applied to on-machine surface roughness prediction, *Ricardo Knoblauch*, Arts et Metiers Institute of Technology, France
12h10	12h40	Sponsor Technical Talk 2, Friction and Wear Analysis: How to face new challenges, *Mohamadou Diew,* Bruker Group **("Ilha do Boi" Auditorium)**	
12h40	14h	Lunch	
14h	14h30	**Session 12: Plenary lecture** – What's going on below a tribologically loaded surface?, *P. Gumbsch*, Karlsruhe Institute of Technology, Germany **("Ilha do Boi" Auditorium)** Moderator: **C. Scandian**	
14h30	15h		
		Session 13 Coatings ("Ilha das Caieiras" Room) Moderator: *F. A. Xavier*	**Session 14 Tribology in Manufacturing ("Ilha do Boi" Auditorium)** Moderator: *R. M. Souza*
15h	15h20	**4DSF** Tribological characterization of laser cladding deposited stellite 6 coatings**,** *Viridiana Humarán Sarmiento,* Centro de Ingeniería y Desarrollo Industrial (CIDESI)	**Keynote**: Multiscale triboprocessing of complex functional surfaces in convergent manufacturing, *M. El-Mansori*, Arts et Metiers, France
15h20	15h40	**4DPH** Tribological behavior of duplex CrN/DLC and nanoscale multilayer DLC-W coatings at elevated temperatures**,** *André Paulo Tschiptschin*, Universidade de São Paulo (USP), Brazil	

15h40	16h00	**4DMZ** Effect of heat input on ultrahard Fe-Cr-B-C-W-Mo-Nb hardfacing**,** *Jonathan Gramajo* Universidade de Lomas de Zamora, Argentina	**4DSB** Tribological characterization of deterministic polyamide surfaces manufactured by additive and subtractive methods**,** *Luis Miguel Ballesteros*, Universidad Nacional de Colombia, Colombia
16h00	16h20	**4DPZ** Abrasive wear performance of tungsten carbide coatings**,** *Fábio Xavier*, Universidade Federal de Santa Catarina (UFSC), Brazil	**4DQH** Microstructure and Wear Behavior of Austenitic Stainless Steel AISI 316L Produced by rolled and Direct Metal Laser Sintering Methods**,** *Izabel Fernanda Machado*, Polytechnic School of the University of São Paulo (USP) , Brazil
16h20	16h40	**Refreshments (Penedo Room)**	
		Session 15 Friction reduction ("Ilha das Caieiras" Room) Moderator: *D. S. Berti*	**Session 16 Session Wear ("Ilha do Boi" Auditorium)** Moderator: *V. S. Mello*
16h40	17h00	**4DN6** Phototribology: active control of friction by light in solid and liquid states, *Carlos Alejandro Figueroa*, Universidade de Caxias do Sul (UCS), Brazil	**4DPQ** Relationship between mechanical properties and galling resistance of API grade steels, *Juan Pablo Abdelnabe*, Consejo Nacional de Investigaciones Científicas y Técnicas (CONICET), Argentina
17h00	17h20	**4DRB** Effect of electric current flow on the coefficient of friction of exfoliated and reassembled graphite films measured in reciprocating linear sliding tests, *Ronny Peterson da Nóbrega Gonçalves*, Universidade de São Paulo (USP), Brazil	**4DSS** Development of a graphic tool for rail corrugation assessment in a commercial Metro line, *Sebastian Gomez Durango*, Universidad Nacional de Colombia (UNAL), Colombia
17h20	17h40	**4DMJ** Tribological Performance of 410L Martensitic Stainless Steel Parts Manufactured by Laser Directed Energy Deposition, *Jurandir Marcos Sá de Sousa*, Universidade Federal de Santa Catarina (UFSC), Brazil	**4DSZ** Tribological response of ceramics by linear scratch test, *Renan Valter Magnol*, Instituto Federal do Espírito Santo (IFES)
17h40	18h00	**4DRY** Effects of coconut fruit fiber and Oyster seashell concentration and porosity on the impact energy and absorption of friction linings, *Eziwhuo Second Justice*, University of Port Harcourt, Nigeria	**4DSE** PEEK contact temperature sliding against brass, alumina and PEEK, *Rubson Mação Camporez* Federal University of Espírito Santo (UFES), Brazil
19h30	23h	**Conference dinner – Hotel Restaurant**	

Wednesday, November 29, 2023		
8h00	8h30	

8h30	9h00	**Session 17 Plenary lecture** - Green tribology for sustainable engineering and mobility, *M. Kalin*, University of Ljubljana, Slovenia **("Ilha do Boi" Auditorium)** Moderator: *R.M. Souza*	
		Session 18: New tribomaterials ("Ilha das Caieiras" Room) **Moderator:** *L. Vieira*	**Session 19: Wear testing ("Ilha do Boi" Auditorium)** **Moderator:** *G. Pintaúde*
9h00	9h20	**4DMT** Effect of NaCl Concentration on The Stainless Steels Tribocorrosion, *Arthur Santana de Mendonça*, Universidade Federal de Santa Catarina (UFSC), Brazil	**4DRN** Data automation for wheel-rail contact evaluation, *Modesto Valci Moreira Lopes*, Polytechnic School of the University of São Paulo (USP), Brazil
09h20	09h40	**4DT2** Improvement of wear resistance of a lean duplex stainless steel through low temperature plasma nitriding, *Josefina Andrea Dib*, Consejo Nacional de Investigaciones Científicas y Técnicas (CONICET), Argentina	**4DQE** Critical analysis between laboratory and industrial tests of niobium- and boron-modified high chromium white cast irons, *Maurício Waineraich Scal*, MScal Steelmaking Consulting, Brazil
9h40	10h10	Refreshments	
		Session 20 Surface engineering ("Ilha das Caieiras" Room) Moderator: *A. P. Tschiptchin*	**Session 21 Tribology and the energy transition ("Ilha do Boi" Auditorium)** Moderator: *E. Tomanik*
10h10	10h30	**4DMX** Thermally sprayed oxide-based coatings for tribological interfaces at high-temperature, *Andre Renan Mayer*, Concordia University Montreal, Canada	**4DMB Invited**: Electric Vehicle Traction Motor Bearing Tribology – Damage Assessment and Mitigations, *R. Gnanamoorthy*, Indian Institute of Technology Madras, India
10h30	10h50	**4DNS** Study of the effect of duplex treatments of nitrocarburizing and deposition of DLC films doped with nitrogen and silicon on the tribological properties of M2 steel, *Miguel Rubira Danelon*, Universidade de São Paulo (USP), Brazil	**4DMR** Compatibility assessment of PAO and POE with PA6 for potential EV application, *Bernardo Tormos*, Universidad Politécnica de Valencia, Spain
10h50	11h10	**4DTK** A wear map for the scratch behavior of Fe-Cr-C hardfacing, *Giuseppe Pintaude*, Universidade Tecnológica Federal do Paraná (UTFPR), Brazil	**4DTB** How can tribology help the energy transition? *Henara Lillian Costa,* Universidade Federal do Rio Grande (FURG), Brazil
11h10	11h30	**4DSQ** Influence of Polyethylene Glycol addition on the deposition and tribological performance of cobalt coatings prepared via cathodeplasma electrolytic deposition *Valdicleide da Silva Mello*, Universidade Federal do Espírito Santo (UFES), Brazil	**4DQQ** Exploring the Potential of Ti3C2TX MXene as a Lubricant Additive: Topography Evolution and Performance under Boundary Lubrication Conditions, *Davi Franzosi*, Polytechnic School of the University of São Paulo (USP), Brazil

11h30	11h50	**4DPP** Effect of Plasma Nitriding on Resistance to Microwear and Fatigue of AISI 321 Stainless Steel, *Marcos Dorigão Manfrinato*, Faculdade de Tecnologia de Sorocaba	**4DQX** Influence of Dimple Texturing on Coefficient of Friction of Piston Ring–Cylinder Liner Conjunction, *Felipe Kevin Correia Luz*, Universidade Federal do Rio Grande (FURG), Brazil
11h50	12h10	**4DPT** Abrasive wear of polymer coatings for sustainable energy Generation**,** *Fábio Xavier,* Universidade Federal de Santa Catarina, Brazil	**4DQP** Wear Coefficient Determination of Heterogeneous Microstructures using Numerical Simulation and Machine Learning, *Arnaldo Oliveira Lima*, Universidade de São Paulo (USP), Brazil
12h10	12h30	**Sponsor talk: RTec**	**4DPR** A Novel Nonlocal Wear Model for Assessing the Tribological Performance of Journal Bearings, *Javier Blanco Rodríguez,* Universidade de Vigo, Spain
12h30	14h	Lunch	
14h	14h30	**Session 22: Plenary lecture** – Brazilian challenges and opportunities in science and technology, *A.T. Prata*, Federal University of Santa Catarina, Brazil **(”Ilha do Boi” Auditorium)** Moderator: *J.D.B. de Mello*	
14h30	15h		
		Session 23 Tribology of mechanical components (“Ilha das Caieiras” Room) Moderator: *M.C.M. Farias*	**Session 24 Wear (”Ilha do Boi” Auditorium)** Moderator: *H. Goldenstein*
15h	15h20	**4DQC** Prediction of Friction Torque and Kinematics of Tapered Roller Bearings with detailed Multibody Simulation, *Oliver Koch*, Universität Kaiserslautern, Germany	**4DTA** Comparative Sliding Wear Behavior of Pearlite and Tempered Upper Bainite Microstructures, *Arnaldo Oliveira Lima*, Universidade de São Paulo (USP), Brazil
15h20	15h40	**4DQK** Effects of Highly Dynamic Rotational Cycles on Radial Shaft Seals with Dust Lip, *Lenine Marques de Castro Silva*, Universität Kaiserslautern (UNI-KL), Germany	*4DQF Evaluation of the micro-scratch resistance in different directions of a directionally solidified high chromium cast iron, Leandro Bastos Bergami, Universidade de São Paulo (USP), Brazil*
15h40	16h	Refreshments	
16h	16h20	Closure Ceremony **(“Ilha do Boi” Auditorium)**	

Poster Session A – 27/11/2023 – 09:30 to 10:30

4DMH Soft Tribology and Rheology of Functional Soy Yogurts Supplemented with Prebiotics, *José Ramos Gomes*, Universidade do Minho, Portugal

4DT4 Effect of potential on the friction coefficient and wear of the Co-Cr-Mo alloy in Ringer´s lactate solution, *Vagner Eduardo Caetano Marques,* Universidade do Vale do Paraíba (UNIVAP), Brazil

4DNF Influence of Particle Size and Porosity on The Tribological Behaviour of Vacuum-Impregnated Sintered Steel, *Nicolás Ignacio Araya Rivera*, Universidad de Concepción (UDEC), Chile

4DNG Production of Biolubricant by the Enzymatic Esterification of Ricinoleic Acid with TMP**,** *Rodolpho Ramilton de Castro Monteiro*, Universidade Federal do Ceará (UFC), Brazil

4DNN Investigation on the improvement of tribological resistance of UHMWPE GUR 1020 by application of a DLC film on argon and oxygen etched surfaces, *Vanessa Kapps*, National Institute of Metrology, Quality and Technology (INMETRO), Brazil

4DNP Importance of data acquisition rate selection for reliable evaluation of resistance to friction of tribomaterials, *Vanessa Kapps*, National Institute of Metrology, Quality and Technology (INMETRO), Brazil

4DNT Effect of plasma nitriding temperature on wear resistance of Hadfield steel, *Miguel Rubira Danelon*, Universidade de São Paulo (USP), Brazil

4DNV Increased energy efficiency in iron ore milling, changing lubricant from mineral oil to synthetic oil, *Danilo Mota Campos*, Universidade Federal de Ouro Preto (UFOP), Brazil

4DP4 Effect of Glass Fiber Concentration in PA Based Composites Tribology, *Arthur Santana de Mendonça*, Universidade Federal de Santa Catarina (UFSC), Brazil

4DPD Evaluation of point contact areas and contact pressure distribution between railway sleeper and ballast: field measurements and FEM modelling, *Erivaldo Santos Jales*, Instituto Tecnológico Vale (ITV), Brazil

4DPE Rough Contact Models for Multibody Tribodynamics Simulation of Crank–Connecting Rod–Piston Mechanisms: A Critical Assessment, Isaac Vinícius do Nascimento, Universidade de São Paulo (USP), Brazil

4DPG Effect of Reinforcement with Nanosheets of MXenes (Ti3C2Tx) on the Compressive and Wear Resistance of Structural Concrete, *Cristiane Arpino*, Universidade Federal de Pelotas (UFPEL), Brazil

4DQ2 Image processing for automatic wear track measurements, *Caio Augusto Garcia Sampaio Valente*, Universidade Tecnológica Federal do Paraná (UTFPR), Brazil

4DQ6 Effects of Surface Texturing of Sheet Metal Forming Tools in Strip Drawing Tests, *Diego Tolotti de Almeida*, Bruning Tecnometal, Brazil

4DQV Study of Adherence evaluation the feasibility of using stainless steel coated with a film of TiO2 in the treatment of sanitary effluents, *Vagner Eduardo Caetano Marques*, Universidade do Vale do Paraíba (UNIVAP), Brazil

4DQZ Reduction of mechanical energy dissipation in hierarchical titanium coatings, *Jean Valdir Uchôa Teixeira*, Universidade Estadual Paulista (UNESP), Brazil

4DR2 Study on the tribological behavior of new titanium alloys for biomedical applications, *Jean Valdir Uchôa Teixeira*, Universidade Estadual Paulista (UNESP), Brazil

4DRK Tribological Characterization of Nanoporous Anodized Anodic Alumina Coatings for Biomedical Applications, *Eurico Felix Pieretti,* Instituto de Pesquisas Energeticas e Nucleares (IPEN), Brazil

4DRR Laboratory evaluation of tribological performance of biodegradable grease with magnetite nanoparticles coated with stearic acid for wheel/rail interface, *Bruno Pereira Ferrer,* Universidade Tecnológica Federal do Paraná (UTFPR), Brazil

4DRT Friction and wear of graphene-based polymer nanocomposites for dental applications, *María Cristina Moré Farias*, Universidade de Caxias do Sul (UCS), Brazil

4DRX Biotribological Characterization of Laser Textured Ti6Al4V Produced by Addictive Manufacturing, *Eurico Felix Pieretti*, Universidade de São Paulo (USP), Brazil

4DSJ Quantification of powder evaporation for optimization of coating deposition by plasma spray, *Franciele Dias de Castro*, Universidade Federal de Pelotas (UFPEL), Brazil

4DSM Determination of lubricant film thickness using ultrasonic reflection**,** *Alvaro Santos Piovesan* Universidade Federal de Pelotas (UFPEL), Brazil

4DSW Effect of Plasma Nitriding Pressure on Micro-abrasive Wear of AISI 316 l Austenitic Stainless Steel, *Antonio Ferreira*, Instituto Federal do Espírito Santo (IFES), Brazil

4DSY Effect of the Nitrogen Content Used in the Plasma Nitriding Atmosphere on the Abrasive Wear Resistance of AISI H13 Hot Work Tool Steel**,** *Adonias Ribeiro Franco Júnior*, Instituto Federal do Espírito Santo (IFES), Brazil

4DMV Simulation-based Optimization of Fluid Distribution for Enhanced Grinding Performance, *Sharlane Maria Costa*, Universidade do Minho, Portugal

4DSA Evaluation of parameters of an analytical solution for the surface temperatures of the pin-on-disk tribological test, *Mateus Lube Uliana*, Federal University of Espírito Santo (UFES), Brazil

4DTP Influence of vapor on the next generation gas turbine engines, *Bruno César Noronha Marques de Castilho*, Concordia University Montreal, Canada

4DPF Numerical Simulation of the Tribological Behavior of Hybrid Textured Surfaces (Stochastic Texturing + Honing) of Textured Cylinder Liners of Two-Stroke Engines, *Elton Yvens Godoy de Oliveira* Universidade Federal do Rio Grande (FURG), Brazil

4DTT Opportunities to produce and operate waste-based lubricants, *Isaac dos Santos Nunes*, Universidade Federal do Rio Grande (FURG), Brazil

4DNH The role of manufacturing-induced texture on the tribological performance of cold work tool steels, *Henara Lillian Costa*, Universidade Federal do Rio Grande (FURG), Brazil

4DRH Influence of carbon content on the hardness and microstructure of different stainless steels hardenable by surface laser remelting, *Lucas Kalebe Araujo de Almeida*, Univerdade Federal de São Carlos (UFSCAR), Brazil

4DRM The behavior of annealed and quenched AISI 410 steel in sliding wear tests, *Guilherme Yuuki Koga*, Univerdade Federal de São Carlos (UFSCAR)

Poster Session B – 28/11/2023 – 09:30 to 10:30

4DSG Particle Abrasivity of Perlite Determined under Microscale Abrasion Testing, *Marjorie Benegra*, Universidade Tecnológica Federal do Paraná (UTFPR)**, Brazil**

4DPN Evaluation of Abrasive Wear Resitance of FeMnCr Coating on ASTM A128 grade C Steel, *Marcos Dorigão Manfrinato*, Faculdade de Tecnologia de Sorocaba, Brazil

4DMN Identification of the Wear Mechanisms in the Homogenizer Plunger in Tomato Processing Industry, *Thales Rodrigues*, Universidade Federal de Goiás (UFG)

4DSK Analysis of homogeneity of the white etching layer in a deformed pearlitic steel, *Alejandro Pulgarin Cuero*, School of the University of São Paulo (USP)

4DNK Effect of abrasive granulometry on the wear of electrical submersible pumps, *Leonardo Rosa Ribeiro da Silva*, Universidade Federal de Uberlândia (UFU)

4DNX Galling Resistance of a Cryogenically Treated L80 13Cr Stainless Steel for OCTG Premium Connections, *Germán Prieto* Universidad Nacional del Sur (UNS), Argentina

4DRV The role of microstructure in the mechanical properties and wear resistance of a post-heat-treated white cast iron alloy, *Mário José Bueno de Souza Freitas*, Instituto Tecnológico Vale (ITV)

4DST Thermal and Thermochemical Treatments in Co-30Cr Superalloy: Influence on Hardness and Surface Resistance, *Matheus da Costa Mattos Azeredo*, Instituto Federal de Educação, Ciência e Tecnologia do Espírito Santo (IFES), Brazil

4DSX Comparative analysis of the wear resistance by pure slip and rolling/sliding of two super premium heavy haul steel rails, Hélio Goldenstein Polytechnic School of the University of São Paulo (USP), Brazil

4DMS Dry Sand/Rubber Wheel tests for Abrasiveness analysis, *Adilson Rodrigues da Costa*, Federal University of Ouro Preto (UFOP), Brazil

4DN2 Study of the rotating arc on the tri bological behavior of hardbanding for oildrilling tubes, *Jonathan Gramajo*, Universidade de Lomas de Zamora, Argentina

4DNA The effect of test parameters on CERCHAR abrasiveness index of iron ores, *Daiane Münch*, Instituto Tecnológico Vale (ITV), Brazil

4DNR The effects of heat treatment on the mechanical properties of 450 HB wear resistant steel, *Fábio Dian Murari*, Usiminas, Brazil

4DQD Abrasive wear resistance of commercial ceramic materials used as chute linings, *Isabella Maria Mota de Souza*, Instituto Tecnológico Vale (ITV), Brazil

4DQR Influence of The Ball (Counter-Body) Material on Micro-Abrasion-Corrosion, *Miguel Angel Narvaez Ardila*, Universidade Federal de Uberlândia (UFU), Brazil

4DRA Abrasive wear resistance of wear plate materials for chute linings, with different test configurations using astm-g65 test tribometer, *Luis Alfredo Acevedo Suarez*, Instituto Tecnológico Vale (ITV), Brazil

4DTD The removal coefficient (fab)of high chromium white cast irons and tool steels, *Kaio Lucas Sousa Vieira*, Universidade Federal do Espírito Santo (UFES), Brazil

4DRE Microstructural and Wear Resistance Analysis of CoCr Alloy after Plasma Carbonitriding Using Cathodic Cage, *Rodolfo Miranda Binda*, Instituto Federal do Espírito Santo (IFES), Brazil

4DRF Correlation of field and laboratory wear results of commercial materials for transfer chute linings, *Jose Jimmy Penagos*, Instituto Tecnológico Vale (ITV), Brazil

4DRQ Abrasion Resistance of Work Hardening Layer of Hadfield Steel, *Paulo Cordeiro Machado*, Universidade Federal do Pará (UFPA), Brazil

4DN4 Influence of austenitising temperature on micro-scale abrasive wear of Ni-modified ferritic stainless steel, *Vinicius Carvalho Teles,* Federal University of Ouro Preto (UFOP), Brazil

4DPM Tribological Behavior of Composite Epoxy Coatings for Premium OCTG Threaded Connections, *Juan Pablo Abdelnabe* Consejo Nacional de Investigaciones Científicas y Técnicas (CONICET), Argentina

4DPX Production and tribological characterization of bronze composites reinforced with silica from rice husk deposited by thermal plasma spray, *Marcelo Gautério Fonseca*, Universidade Federal de Pelotas (UFPEL)

4DTQ Chromium- and cobalt-based oxide materials for elevated temperature applications, *Bruno César Noronha Marques de Castilho*, Concordia University Montreal, Canada

4DSR Effect of the shielding gas and heat treatment on microstructure and sliding wear behavior of Inconel 625 coatings onto carbon steel, *Eliane Alves Kihara*, Universidade Federal de Goiás (UFG), Brazil

4DSC Microabrasion Resistance of Laser-cladded 316L/NbC Composite Coating, *Nathan F. Strey*, Federal University of Espírito Santo, Brazil

4DSD On the relationship between contact temperature and tribological behavior of wagon brake shoes, *Rubson Mação Camporez*, Federal University of Espírito Santo (UFES), Brazil

4DS6 Characterization of tribolayers formed during sliding wear of railway wheels, *Daniela Nunes Oliveira,* Federal University of Espírito Santo (UFES), Brazil

4DTR Design, manufacturing, assembly and operation of high-stress abrasion tester according to ASTM B611-21, *Natália de Oliveira Sousa*, Federal University of Espírito Santo (UFES) , Brasil

4DP6 Computational method for evaluating the sliding wear rate in a pin-on-disc tribometer*, João Vitor Raimundo Silva e Silva*, Universidade Federal do Espírito Santos (UFES), Brazil

4DTC Adhesion of protective patinas formed in high-performance weathering steels, *Henara Lillian Costa*, Universidade Federal do Rio Grande (FURG)

4DQG The impact of high chromium cast iron modified with niobium and boron on abrasive wear assessed by industrial tests under different severity conditions, *Geralda Cristina Duraes de Godoy*, Universidade Federal de Minas Gerais (UFMG), Brazil

4DMP Improving the tribotechnical properties of friction surfaces by using mineral coatings, *Roman Polyakov*, Orel State University, Russia

STUDY OF THE FRICTIONAL BEHAVIOR OF SOFT CONTACT LENSES BY AN OSCILLATORY FREE-VIBRATION TRIBOMETER

L.M. Vilhena, A. Ramalho*

CEMMPRE, Centre for Mechanical Engineering, Materials and Processes, Department of Mechanical Engineering, University of Coimbra, Rua Luís Reis Santos, 3030-788 Coimbra, Portugal

* amilcar.ramalho@dem.uc.pt

Abstract

Understanding the Biotribology involved between contact lenses and the eye, namely the friction between the eyelid and the surface of the contact lens during the blink movement, is a crucial factor in avoiding irritation, discomfort and other eye infections. The aim of the present research work is to investigate the tribological behaviour of different soft contact lenses under different contact conditions. During blinking, the eyelid motion occurs with very specific conditions, with sliding speed up to 200 mm/s and contact pressure of around 5 to 10 kPa, making it difficult to replicate these conditions using commercial equipment. A tribometer has been developed for this purpose, which operates with vibration horizontal movement. The friction assessment method is based on the evaluation of the free damping vibration movement, of the mass - spring system. This technique proved to have adequate sensitivity for the biologically relevant conditions, light normal load, high speed and hydrodynamic lubrication. This equipment was been used to evaluate the friction behaviour of different soft contact lenses and to discriminate the influence of several factor, namely the ageing action cycling the effect of UV light and adsorbed proteins.

Keywords: Biotribology; vibration tribometer; Soft Contact Lenses

Surface topography evaluation of composite resin restored teeth by different finishing and polishing techniques

Calmon K[1)], Souza WLR[1)], Vieira LCGC[1)], Maru MM[2)], Perez CR[1)]

[1)] Department of Prosthodontics, School of Dentistry, University of Rio de Janeiro, Rio de Janeiro, RJ, Brazil
[2)] Materials Metrology Division, National Institute of Metrology, Quality and Technology - Inmetro, Duque de Caxias, 25250 020, Brazil
*Corresponding author: mmmaru@inmetro.gov.br

Introduction

Through roughness analysis, this in vitro study evaluated the polishing capacity of three finishing and polishing techniques applied to composite resin cervical restorations. It is claimed that biofilm accumulation may occur depending on the surface's roughness level, leading to carious lesions and gingivitis [1]. An acceptable in vivo threshold Ra roughness for avoiding plaque accumulation varies in the literature with values of 0.2 µm [2], 0.7 µm [3], and 0.25-0.50 µm [4]. Evaluations of surface finishing and polishing techniques of restorative materials are commonly done in flat specimens, and results can significantly differ from clinical scenarios. The present work discloses how heterogeneous the surface quality may result when dealing with the complex topography of natural teeth.

Methodology

Class V cavities were produced in natural premolar teeth at the amelodentinal junction on the buccal surface and restored with a nanoparticulate composite resin (Z350 Filtek Supreme XT). Three different clinical finishing and polishing techniques were tested (n=3 teeth per group): **G1** - diamond burs and rubber points; **G2** - diamond burs and surface sealant; **G3** – finishing and polishing discs associated with spiral discs. The teeth were positioned in an artificial dental arch inside a dummy head to simulate a clinical restoration condition. Ra roughness (n>20 measurements, 0.25 mm cut-off) was obtained from 3D profilometry (PGI830 Taylor Hobson), Figure 1. T-test statistics (a=0.05; p=0.05) was applied to compare Ra between groups.

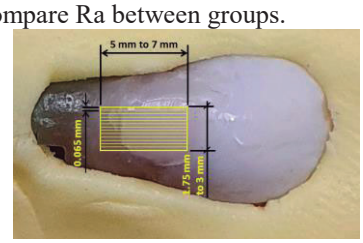

Figure 1 Dimensions of the area of the tooth measured in the profilometer.

Results and Discussion

Figure 2 shows 3D topography maps of a tooth before and after restoration. Figure 3 shows one as-measured profile and the respective roughness profile. Table 1 presents the Ra roughness values for each group. The best results were obtained from G3, considering the lowest mean value as well as the lowest dispersion of Ra roughness, in opposite to group G1, which was significantly distinct from G3 (p=0.047).

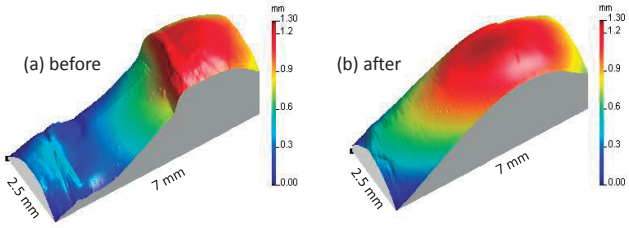

Figure 2 3D topography maps of a tooth before and after restoration.

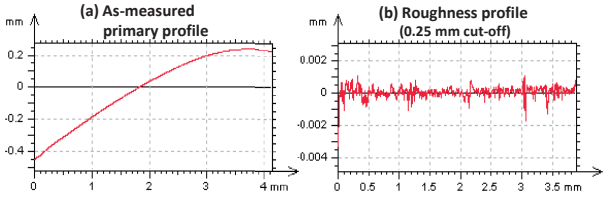

Figure 3 Profiles extracted from 3D map of a restored tooth. (a) As-measured; (b) 0.25 mm cut-off roughness.

Table 1 Ra roughness obtained for the three groups.

Parameter	Mean Ra [µm] (n>20)		
Group	**G1**	**G2**	**G3**
Tooth #1, #4, #8	1.38	0.42	0.41
Tooth #2, #6, #9	0.77	0.52	0.47
Tooth #3, #7, #10	0.75	0.90	0.26
Mean	0.97	0.61	0.38
Standard deviation	0.36	0.25	0.11
Coefficient of variation	37%	41%	29%
T test (α= 0.05)	**G1 x G3**	**G1 x G2**	**G2 x G3**
p-value	0.047	0.120	0.120

References

[1] Rosin, M., et al., *One-year evaluation of an Ormocer restorative-a multi-practice clinical trial*. Clin. Oral Investig., 2003. **7**: 20–6.

[2] Bollen, C.M.L., et al., *Comparison of surface roughnessof oral hard materialsto the threshold surface roughness for bacterial plaque retention: A review of the literature*. Dent. Mater., 1997. **13**:258-269.

[3] Kaplan, B.A., et al., *The effect of three polishing systems on the surface roughness of four hybrid composites: a profilometric and scanning electron microscopy study*. J. Prost. Dent., 1996. **76**:34-38.

[4] Jones, C.S., Billington, R.W., Pearson, G.J., *Laboratory study of the loads, speeds and times to finish and polish direct restorative materials*. J. Oral Rehab., 2005. **32:**686–692.

Biotribological behavior of ta-C coatings for load-bearing implants

Rothammer, B.[1)*], Bartz, M. [1)], Wartzack, S. [1)], Weihnacht, V. [2)], and Marian, M.[3)*]

1) Engineering Design, Friedrich-Alexander-University (FAU) Erlangen-Nuremberg, Erlangen, Germany
2) Fraunhofer Institute for Material and Beam Technology IWS, Dresden, Germany
3) Department of Mechanical and Metallurgical Engineering, School of Engineering, Pontificia Universidad Católica de Chile, Santiago, Chile
*Corresponding authors: rothammer@mfk.fau.de, max.marian@uc.cl

1. Introduction

Amorphous/diamond-like carbon (DLC) coatings deposited on the articulating surfaces of total hip (THR) or total knee replacements (TKR) have the potential to enhance the overall biotribological behavior and longevity [1-2]. This requires excellent adhesion to soft and hard implant materials, biocompatibility as well as superior mechanical properties and wear resistance [3].

2. Materials and methods

Medical grade Co28Cr6Mo (CoCr), Ti6Al4V (Ti64) and ultrahigh molecular weight polyethylene (UHMWPE) were studied as substrate materials. Tetrahedral amorphous carbon (ta-C) coatings were deposited by plasma-filtered pulsed laser-arc technique using a commercial PVD coating system. The surface topography, cytocompatibility as well as mechanical properties and adhesion of ta-C coatings were analyzed. The biotribological behavior was studied in pin-on-disk sliding experiments under substitute synovial fluid lubrication. The wear behavior was investigated through laser scanning microscopy (LSM), Raman spectroscopy as well as focused ion beam scanning electron microscopy (FIB-SEM). [4]

3. Results and discussion

The ta-C coatings exhibited typical morphology and composition and featured higher roughness compared to the substrates. Contact angle measurement as well as indirect and direct cell testing suggested sufficient biocompatibility and suitability for biomedical applications. The ta-C coatings demonstrated excellent mechanical properties with improved hardness-to-elasticity ratio. The adhesion between the coatings and CoCr, Ti64, and UHMWPE substrates was excellent. Despite higher friction, the ta-C coatings significantly reduced wear on both contacting bodies (Figure 1). The intact coating effectively protected the UHMWPE disk from adhesive or abrasive wear. However, crack networks and near-surface fatigue were observed after prolonged testing. Particle analysis revealed minimal release of nanometer-sized particles compared to the reference groups. The biotribological behavior remained consistent over time. [4]

Cracking and folding in the ta-C coating on UHMWPE substrates were attributed to the mismatch in thermal expansion coefficients between the coating and substrate materials, which led to varied expansion and shrinkage during temperature changes, along with the high intrinsic compressive stress typical of ta-C coatings. The compressive stress in the coating, combined with time-dependent plastic deformation of the PE substrate, resulted in fold formation, coating shearing, crack formation, and subduction (Figure 1, left). Furthermore, cyclic tribological stress exceeded the compressive stress resistance of the ta-C coating, leading to the formation and propagation of microcracks near the surface (near-surface fatigue; Figure 1, right). Anyways, the durability of the ta-C coating is expected to extend the service life of metallic and polymeric implant materials. [4]

4. References

[1] B. Rothammer et al.: Amorphous Carbon Coatings for Total Knee Replacements—Part II: Tribological Behavior, Polymers, 13, 2021, 1880, DOI: 10.3390/polym13111880
[2] B. Rothammer, K. Neusser, M. Bartz, S. Wartzack, A. Schubert, M. Marian: Evaluation of the Wear-Resistance of DLC-Coated Hard-on-Soft Pairings for Biomedical Applications, Wear, 523, 2023, 204728, DOI: 10.1016/j.wear.2023.204728
[3] R. Shah et al.: Enhancing mechanical and biomedical properties of protheses - Surface and material design, Surfaces and Interfaces, 27, 2021, 101498, DOI: 10.1016/j.surfin.2021.101498
[4] B. Rothammer et al.: Wear mechanism of superhard tetrahedral amorphous carbon (ta-C) coatings for biomedical applications, Advanced Materials Interfaces, 2023, 2202370, DOI: 10.1002/admi.202202370

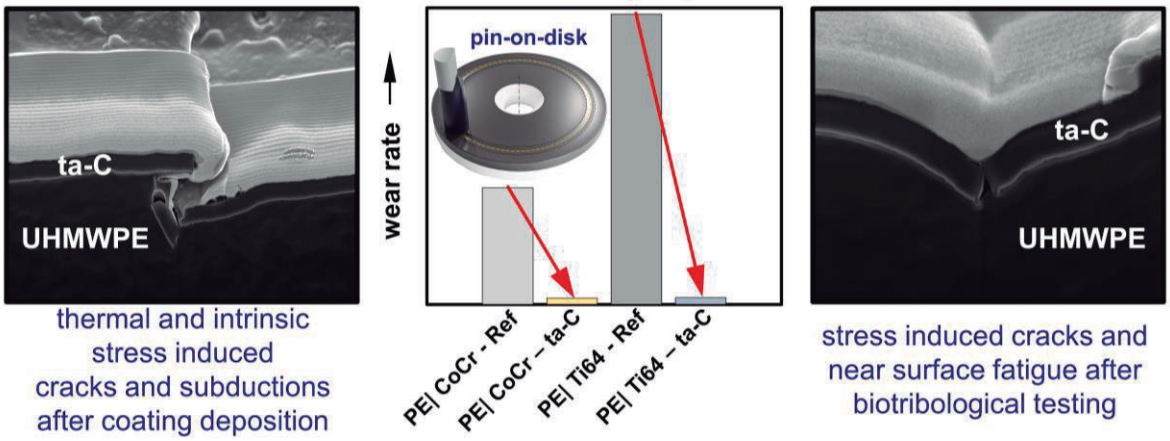

Figure 1 Wear rate and mechanisms of ta-C coated UHMWPE

Mechanical and tribological behavior of 2D material-reinforced metal matrix composites for biotribological applications

Ramteke, S. [1] and Marian, M.[1] *

[1] Department of Mechanical and Metallurgical Engineering, School of Engineering, Pontificia Universidad Católica de Chile, Santiago, Chile,
*Corresponding author: max.marian@ing.puc.cl

1. Introduction

Several medical devices are utilized to treat and alleviate various diseases, injuries, and provide support for anatomical and physiological processes. However, these devices often encounter issues or malfunctions at rubbing interfaces, leading to problems such as tissue damage from high friction, excessive wear, fretting, corrosion, or loosening. Therefore, it is crucial to improve the biotribological behavior of these systems to ensure their safe and reliable operation over an extended period. To address this need, it is essential to enhance the mechanical properties and biotribological behavior of materials, particularly cobalt-chromium (CoCr) or titanium (Ti) alloys [1]. One approach to achieve this enhancement is by incorporating fillers into the materials, see Figure 1. Promising options for biological and biomedical applications are 2D materials like graphene, graphene oxide (GO), and transition metal carbides, nitrides, and carbonitrides (MXenes) [2]. These materials exhibit significant potential in reducing friction and wear of various substrate or matrix materials under both dry and lubricated conditions. However, the utilization of 2D materials in biotribological applications for metallic materials has been relatively unexplored [2]. Additionally, there is a lack of research on the fabrication of multifunctional composite structures using additive manufacturing (AM) techniques such as selective laser melting (SLM) for biomedical and biotribological applications. The combination of additive manufacturing with 2D material-based metal matrix composites (MMCs) holds great promise for creating patient-specific (tailor-made) implants and prostheses that are highly resistant to wear.

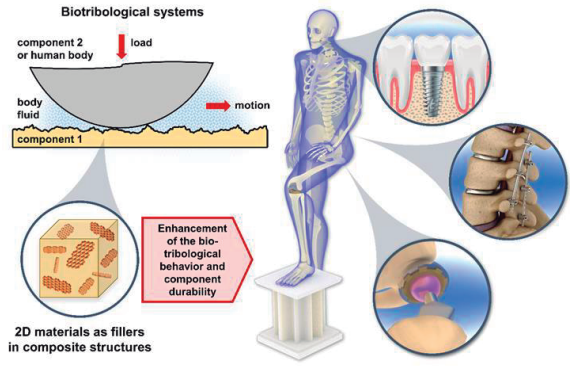

Figure 1 Enhancement of the biotribological behavior and durability of dental implants, bone fracture fixations, or load-bearing prostheses through 2D materials as reinforcement phase in composite structures. Reprinted from [2].

2. Materials, methods and results

In this study, we focused on investigating the effects of incorporating 2D material nanosheets, including graphite, graphene, graphene oxide, reduced graphene oxide, and Ti_3C_2 MXenes, as reinforcement phases in CoCr matrix composite materials. These composite materials were fabricated using selective laser melting (SLM) additive manufacturing. Thereby, the structural and chemical changes during the SLM process were analyzed and the presence of the 2D materials in the fabricated samples could be verified. Furthermore, the mechanical properties, such as hardness (see Figure 2) and the tribological behavior (steel and ceramic ball-on-disk under dry and lubricated conditions) of the reinforced composites were studied and compared with pure CoCr references.

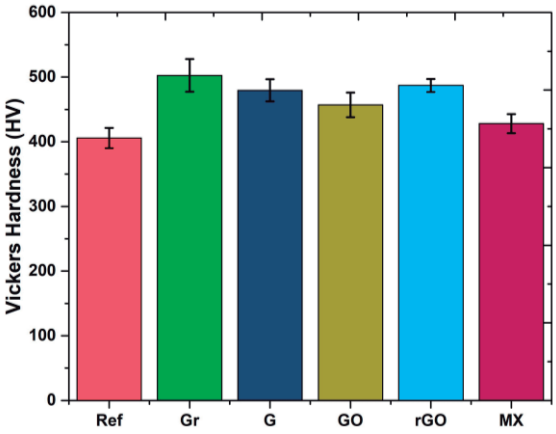

Figure 2 Vickers hardness of the CoCr matrix composites fabricated by SLM without (Ref) or with the addition of 0.3 wt.% of graphite (Gr), graphene (G), graphene oxide (GO), reduced graphene oxide (rGO), and MXenes (MX).

3. References

[1] R. Shah, B. Gashi, S. Hoque, M. Marian, A. Rosenkranz, Enhancing mechanical and biomedical properties of protheses - Surface and material design, Surfaces and Interfaces 27, 2021, 101498, DOI: 10.1016/j.surfin.2021.101498.

[2] M. Marian, D. Berman, D. Nečas, N. Emami, A. Ruggiero, A. Rosenkranz: Roadmap for 2D Materials in Biotribological/Biomedical Applications – A Review, Advances in Colloid and Interface Science, 307, 2022, 102747, DOI: 10.1016/j.cis.2022.102747

Effect of lamellar anisotropy produced by mechanical compression in UHMWPE on its tribological resistance

Moura, LG[1,2], Maru, MM[1], Almeida, CM[1], Fancello, EA[2], Roesler, CRM[2]

[1] Materials Metrology Division, National Institute of Metrology, Quality and Technology - Inmetro, Duque de Caxias, 25250-020, Brazil
[2] Biomechanics Engineering Laboratory, Federal University of Santa Catarina, Santa Catarina, 88040-900, Brazil
[3] Department of Mechanical Engineering, Federal University of Santa Catarina, 88040-900, Brazil
*Corresponding author: mmmaru@inmetro.gov.br

1. Introduction

An alternative preprocessing route for improving mechanical strength, as well as wear resistance of ultra-high molecular weight polyethylene (UHMWPE) used in orthopedic artificial joints is by submitting it to mechanical compression [1]. Therefore, this work aimed at evaluating the tribological response of commercial UHMWPE through linear scratching tests after submitting the polymer to mechanical compression.

2. Methodology

Plate specimens of (6×36×36) mm^3 size made of commercial GUR1050 UHMWPE resin were mechanically compressed in a homemade channel-die device at a true deformation ratio of 2.5, in plain strain mode, resulting in a deformed shape as seen in Figure 1.

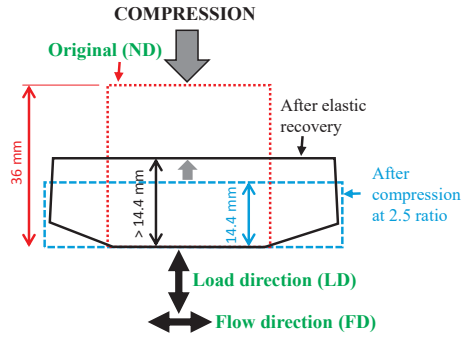

Figure 1 Geometric representation of the UHMWPE plate specimen before and after mechanical compression, and after elastic recovery.

The polymer lamella morphology was observed by atomic force microscopy (JPK Nanowizard AFM) in tapping mode. Linear scratching tests under linearly increasing load were performed in the specimens before and after compression, parallel and orthogonal to the compression direction, as in the scheme in Figure 2.

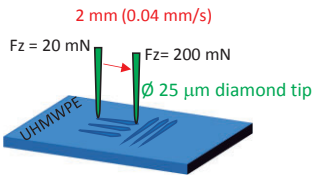

Figure 2 Schematics of the performed scratching tests.

3. Results and Discussion

The results revealed directional modification of the tribological behavior, in which the resistance to scratch visibly reduced (t-test, $p<<0.05$) in the flow direction, seen by both the resistance force and the permanent depth of the scratch, while in the compression direction the force increased but the depth was unchanging (ANOVA, $p=0.27$) compared to the original material. This has led one to conclude that applying mechanical compression at a deformation ratio of 2.5 has not provided tribological enhancement to the UHMWPE in spite of the structural anisotropy induced in the material.

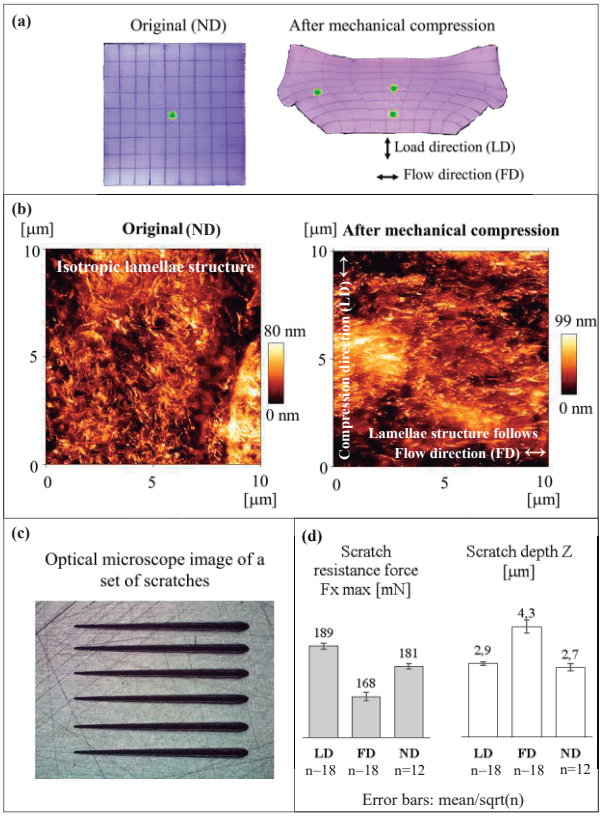

Figure 3 (a) Tested surfaces; green dots indicate the scratched regions; (b) AFM images before and after compression showing lamellae orientation; (c) optical images of a scratched region; (d) scratch resistance force and final depth left by the scratches.

4. References

[1] Barylski, A., Maszybrocka, J. and Cybo, J., *The Influence of Plastic Deformation Performed Before and After Electron Beam Irradiation on Mechanical Properties and Wear of UHMWPE*. Solid State Phenomena. 2015. 220-221: 565–70.

Effect of temperature on fretting wear of additively manufactured Inconel 718

A. Sahu[1], D. Kesavan[2], and M. Kamaraj[1*]

[1]Department of Metallurgical and Materials Engineering,
Indian Institute of Technology Madras, Chennai, Tamil Nadu, India-600036
[2]Department of Mechanical Engineering,
Indian Institute of Technology Palakkad, Kerala, India-678623

[*]Email: kamaraj@iitm.ac.in

Abstract

The current study compares the high-temperature fretting wear resistance of AM Inconel 718 processed by Laser Powder Bed Fusion (L-PBF) to conventional wrought samples. The AM coupons were homogenized at 1080°C followed by double aging heat treatment to increase hardness from 350 HV to 500 HV approximately. Prior to testing, X-ray diffraction, nanoindentation, scanning and transmission electron microscopy were used to characterize the material, indicating the difference in the microstructure. In a series of point contact tests with alumina balls as rider materials, three levels of variable fretting wear test temperature were tested (RT, 250°, and 500°), as well as constant fretting wear test parameters for normal load, stroke length, and frequency. Fretting loops for the tests were predominantly in gross slip regimes. Wear volume decreased at 500°C compared to the sample test at room and 250°C test temperatures. The subsurface analysis of the wear region showed variation in the depth of spinel oxide layer formed by the variation in operating temperature. Wear track characterization showed an increased presence of Cr oxide with increasing temperature. Wear mechanisms was found to change from abrasive and tribo-oxidation to adhesive and oxidation wear with variation in the content of spinel oxides on the top surface.

High temperature tribological behavior of additively manufactured tool materials

Macêdo, G.[1)*], Pelcastre, L.[1)], Prakash, B.[1)] and Hardell, J.[1)]

[1)] Division of Machine Elements, Luleå University of Technology, Luleå, 971 87, Sweden
[*]Corresponding author: gabriel.macedo@ltu.se

1. Introduction

Additive manufacturing (AM) of metallic materials has been constantly evolving since the past decade. Many defects that were believed to be intrinsic of AM have been tackled in different ways such as optimization of process parameters, post heat treatments and post machining. AM has now achieved a technological maturity level that opens up the possibility of its use in advanced applications, such as hot forming tool materials. Tools in hot forming processes are subjected to harsh contact conditions at elevated temperatures, where adhesive and abrasive wear are a challenge [1, 2]. There are few studies on the tribological behavior of AM tool materials, and even fewer involving elevated temperatures. In this context, the aim of this study is to investigate the high temperature tribological behavior of additively manufactured tool materials with emphasis on their wear resistance, drawing a direct comparison to a conventionally produced tool steel.

2. Methodology

A reciprocating sliding tribometer (SRV Optimol) was used in this study. Three different tool materials were used as disk specimen: additively manufactured tool steel (AM-TS); conventionally produced tool steel (Ref-TS); and additively manufactured maraging steel (AM-MR). AM-TS and Ref-TS have the same composition and can be described as a tempered martensitic carbon-based tool steel (X35CrMoV5-2). The counter-body (ball specimen) was tungsten carbide (Cobalt binder). The test temperatures (tool material temperature) were 40°C, 200°C and 400°C. The test parameters were frequency of 25 Hz; stroke length of 2 mm; load of 50 N; and test duration of 15 min.

3. Results

Figure 1 shows the tool material wear volume for all test conditions. AM-TS and Ref-TS show similar behavior: a large decrease in material removal with increasing temperature. At 400°C, however, Ref-TS had 40% lower wear volume than AM-TS. The wear volume for AM-MR was not significantly affected by the change in temperature, and it also showed a much larger wear volume at all temperatures when compared to both AM-TS and Ref-TS. At 400°C, the wear volume for AM-MR was 266 times larger than for Ref-TS.

The reduction in wear volume with higher temperatures for the AM-TS and Ref-TS specimens was attributed to the formation of a protective tribolayer. EDS analysis showed that at 200°C, the tribolayers contained mostly of oxidized tool material wear debris (Fe and O), but also a significant amount of W. At 400°C, the tribolayer formed contained mostly W, with some amount of Fe and O. This shows that material transfer from the WC/Co specimens was significant at elevated temperatures, mainly at 400°C. For AM-MR, tribolayer formation from oxidized tool material wear debris (Fe and O) was also observed, but a negligible amount of W was found during analysis.

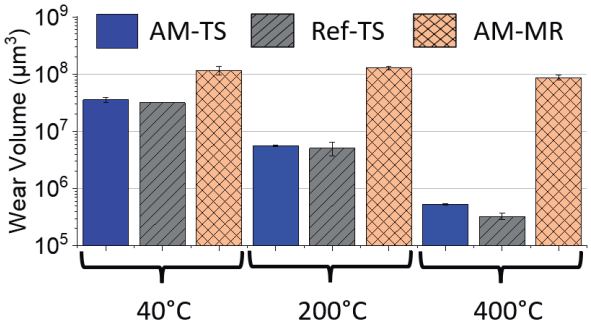

***Figure 1**. Wear volume from tool material.*

4. Conclusions

This study investigated the friction and wear behavior of two additively manufactured tool materials (AM-TS and AM-MR) and a conventionally produced tool steel (Ref-TS) when sliding against a WC/Co counter-body at elevated temperatures. AM-TS showed very similar friction and wear behavior to Ref-TS, regardless of test temperature. AM-MR showed a much higher degree of material removal at all test temperatures. Difference in wear behavior between the different materials and temperatures was attributed to the formation of tribolayers of different compositions.

5. References

[1] Pelcastre, L.; Hardell, J.; Prakash, B.: *Investigations into the occurrence of galling during hot forming of Al-Si-coated high-strength steel*. In: Journal of Engineering Tribology. **225** (2011). pp. 487–498.
[2] Venema, J. et al.: *Friction and wear mechanisms during hot stamping of AlSi coated press hardening steel*. In: Wear. **380–38**1 (2017). pp. 137–145.

Influence of the turning process on the tribological performance of self-lubricating composites

Dorneles, C. F. [1)], Builes, S. D. [1)], Ebersbach, F. G. [1)]; Schroeter, R. B. [1)], Binder, C. [1)] and Klein, A. N. [1)]

[1)] Department of Mechanical Engineering, Federal University of Santa Catarina, Florianópolis, 88040 900, Brazil
*Corresponding author: carol.fdorneles@gmail.com

1. Introduction

Lubrication deficiency is one of the main causes that directly affect the performance of mechanical systems, thus generating a large amount of mechanical energy [1]. In this context, self-lubricating composites are a viable alternative to other lubricants, combining satisfactory mechanical properties and a low coefficient of friction that contribute to reducing energy consumption [2]. This work evaluates the tribological performance of self-lubricating composites (Fe–4Ni–0.5Si + 6.5%vol graphite and 1%vol h-BN) obtained by the powder metallurgy process after the turning process.

2. Material and methods

For the production of composites studied, that was used a mix of iron powder as raw material and add Si powder (Fe45Si), Ni powder, and solid lubricants (6.5%vol of graphite and 1%vol of h-BN). The powders were pressed in a double action hydraulic press (600 MPa). The sintering was carried out in a tubular furnace (95% Ar, 5% H) with 2 stages. In the first stage, a heating rate of 5 ºC/min and a 30-minute stay at a temperature of 550 ºC were used; in the second stage, the final sintering was isothermal, at a temperature of 1125 °C for 1 hour, using a heating time of 10 °C/min. After this process, the specimens were carried out dry turning, varying the cutting speed (v_c) in 6 levels: 350, 450, 550, 650, 750, and 850 m/min. The tribological tests were carried out in a UMT-3 CETR tribometer for reciprocating sliding tests in a sphere/cylinder configuration with a frequency of 2 Hz and 10 mm stroke. To determine the coefficient of friction and the wear rates tests were carried out at constant load with 2 N for 1 hour (Hertz stress 0.82 GPa). The wear marks were analyzed in a SEM.

3. Results and Discussions

Figure 1 shows the values of the wear rate and friction coefficient after the tribological wear test. It was observed that all surfaces show the friction coefficient within the value established for the lubricant film (μ=0.2). Thus, it is concluded that during the tests there was the presence of lubricating solids in the formation of the film [3]. However, for the turned surfaces with cutting speeds of 450, 550, 650 and 750 m/min, there was an increase in wear of approximately 62 times when compared to the material only sintered. When wear of less than $4x10^{-6}$ $mm^3.N^{-1}.m^{-1}$ was achieved on the turned surfaces, the morphology of the wear marks was characterized by showing wear only at roughness peaks and the presence of a tribolayer composed of matrix elements, solid lubricant, and oxides. In Figure 2, it is possible to observe that for the test with the lowest friction coefficient (Fig. 2a), the wear mark is characterized by plastic deformation only at the peak of the roughness and for the test with the highest friction coefficient (Fig. 2b), and the plastic deformation is increased until reaching the valley of the roughness profile.

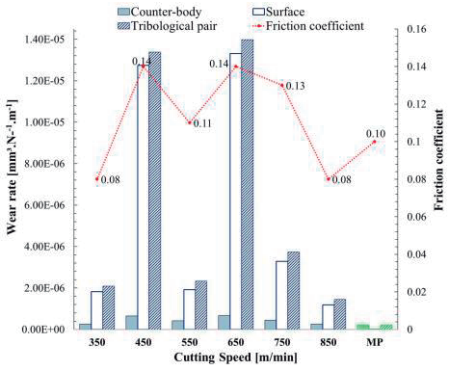

Figure 1 Wear rate and friction coefficient for machined and sintered surfaces.

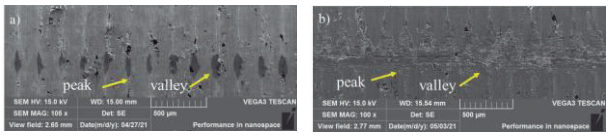

Figure 2 Morphology of wear marks for (a) surface with wear less than $4x10^{-6}$ $mm^3.N^{-1}.m^{-1}$ and (b) surface with wear more than $4x10^{-6}$ $mm^3.N^{-1}.m^{-1}$.

4. Conclusions

All surfaces show a friction coefficient below 0.2, as expected. However, the wear results showed higher variation, being more intense on surfaces made with cutting speeds of 450, 550, 650, and 750 m/min.

5. References

[1] Holmberg K, Andersson P, Erdemir A. *Global energy consumption due to friction in passenger cars*. Tribol Int., 2012. **47**: p. 221–234.

[2] Holmberg K, Erdemir, A. *The impact of tribology on energy use and CO^2 emission globally and in combustion engine and electric cars*. Tribol Int, 2019. **135**: p. 389–396.

[3] Erdemir, A. *Solid lubricants and self-lubricating films.* Modern Tribology Handbook, 2000. p. 787–825.

Influence of sequential machining process on the surface of dies

Xavier, F.A.[1)], Builes, S.D.[1)], Bordin, F.M.[1)*], Costa, E.C.[1)], Filho, C.H.[2)]

[1)] Department of Mechanical Engineering, Universidade Federal de Santa Catarina, Florianópolis, 88040 900, Brazil.
[2)]Zen S.A., Brusque, 88355 110, Brazil.
[*]Corresponding author: f.m.bordin@posgrad.ufsc.br

1. Introduction

The wear of cold forging dies in the metalworking industry is highly dependent on the tribological contact between the cold-forged material and die surface integrity (surface texture and subsurface modifications) [1]. However, frequently, only the last steps of manufacturing are characterized, giving no regard to the whole process chain.

Therefore, this study evaluates the characteristics of the surface and subsurface of geometrically complex dies after the machining.

2. Materials and methods

The complex geometry of the dies is generated after a pre-machining step. The inner geometry is composed of sharp angles and splines, requiring subsequent electro-discharge machining (EDM) in roughing and finishing regimes, followed by stress relief heat treatment and further polishing, PVD coating and subsequent finishing step by polishing of the coated surface.

The machined material is a sintered high-speed steel, S790 grade, quench and tempered to a hardness of 60 HR_C. Each sequential surface was analyzed by surface texture/roughness and subsurface damage.

3. Results

The surface roughness profile of the process sequence can be observed in figure 1.

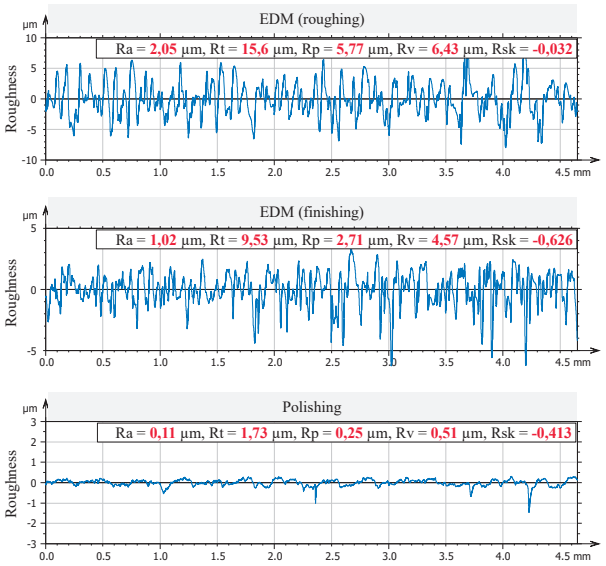

Figure 1 Surface roughness profiles.

The resulting surface and subsurface in machining process is highly dependent on the type of material removal mechanism. Due to the thermal nature of the EDM process, the resulting surface is constituted of stochastic craters (Figure 2).

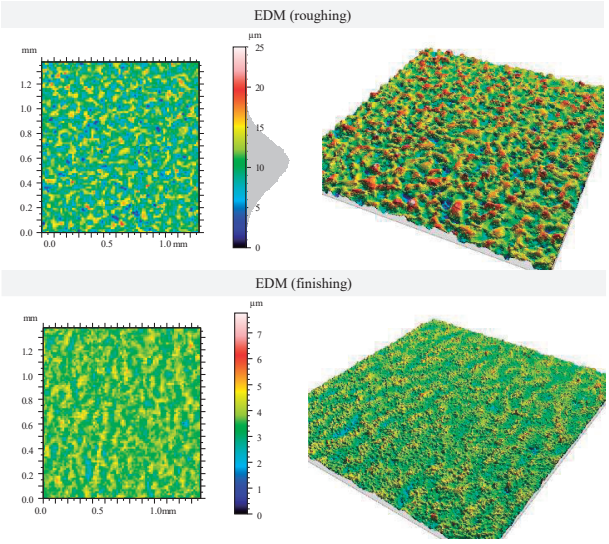

Figure 2 3D reconstruction of the EDM surfaces.

However, not only the surface is subject to the process mechanisms of material removal, but also the subsurface. Figure 3 introduces a sequence of alterations beneath the surface, caused by the heat generated, heat affected zones (HAZ), which reduces the die lifetime in operation.

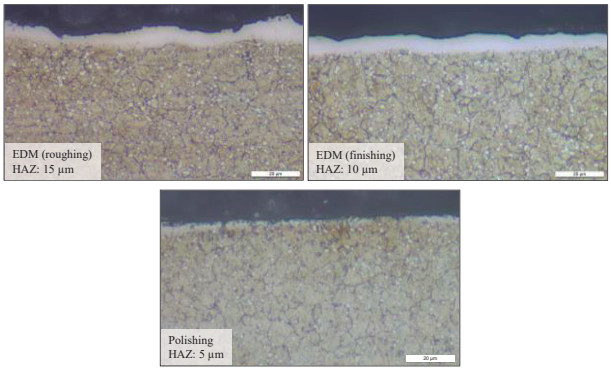

Figure 3 Subsurface alterations.

4. References

[1] Andreas, K., M. Merklein, *Influence of surface integrity on the tribological performance of cold forging tools*. Procedia CIRP, 2014. **13**: pp. 61-66.

Laser cladding and laser heat treatment process for tooling applications

O.C. de Moura Filho*[1),2)], R.O. Giacomelli [2)], F. Correa[2)], J.T. Pacheco [2)], N.W. Dreveck[2)], C.E. Niño Bohórquez [1)]

[1)] Universidade Federal de Santa Catarina, Brazil. [2)] SENAI Innovation Institute for Laser Processing, Brazil,

*Corresponding author: osmar.custodio@sc.senai.br

1. Introduction

One of the most used materials for manufacturing stamping tools is the AISI D2 steel, due to its high mechanical strength and wear resistance [1]. This material, however, has a high carbon and alloying elements content that greatly reduces its weldability. In order to reduce the lead time and increase the quality of tooling repair processes, L-DED (Laser Directed Energy Deposition), is being extensively used mainly due to its low heat input and dilution of the cladded layers and high precision [2]. The current work is focused on the development of the Laser Cladding process for the AISI D2 tool steel adding AISI 420 martensitic stainless steel in metallic powder form as clad material with post-repair laser heat treatment. The strategy used consisted of an experimental approach, using a diode laser with a maximum power of 6 kW. The results indicate the possibility of depositing multilayers with desirable geometrical parameters, free from defects, without the requirement of preheating. The laser heat treatment applied as a post-process step was found to be highly effective in enhancing the hardness of the deposited layer. Additionally, it successfully reduced the coefficient of friction, resulting in improved tribological properties.

2. Methods

The equipment used for both processes was the PRECO SL8600. The laser source used is a Laserline LDF 6000-60 VG-Power. The processing head for Laser Cladding was a Fraunhofer-Coax 8 and for the Laser Heat Treatment was the Laserline OTS 2 – F200 with an integrated pyrometer. Table 1 shows the parameters used during the processes. Regarding tribological characterizations by reciprocating test, CETR-UMT-2 equipment model was used. The normal load, frequency, stroke, test time, counter-body diameter and material are respectively 5 N, 20 Hz, 5 mm, 30 min, ø 4 mm and Si_3N_4.

Table 1: Parameters used for the laser processes.

Parameters	Laser Cladding	Laser Heat Treatment
Laser Power [W]	570	-
Speed [mm/min]	700	300
Hatch Distance [mm]	1.1	-
Powder feed rate [g/min]	8	-
Laser Spot size	ϕ2 mm	20 mm x 3 mm
Temperature [°C]	-	1350
Work distance [mm]	13	168

3. Results

The cross-sectional analysis of the repair deposition (Figure 1) revealed an adequate geometry, free of cracks and with a minimal occurrence of pores. Subsequently, the samples underwent laser heat treatment, and the outcomes are depicted in Figure 2. In terms of the average coefficient of friction, the as built repair condition exhibited a value of 0.56 ± 0.02, whereas the laser heat-treated condition showed a lower value of 0.50 ± 0.01.

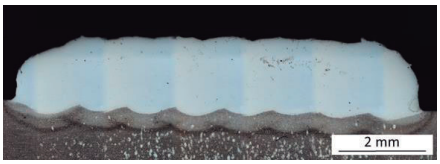

Figure 1: Cross-section of the three layers of AISI 420 steel deposited on AISI D2 by laser cladding as built.

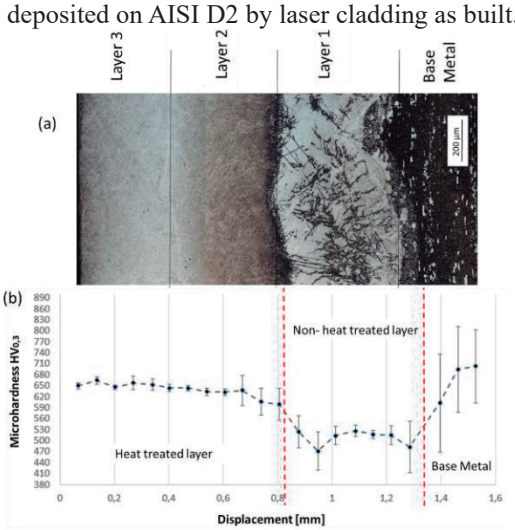

Figure 2: Laser cladded layers after laser heat treatment. (a) Cross section and (b) Microhardness profile.

4. Discussion

The microstructure of the laser heat-treated samples showed a refined martensitic structure and exhibited higher hardness in comparison to the samples without laser heat treatment. In the wear tests, the laser heat-treated samples presented lower average values of the coefficient of friction when compared to the non-heat-treated conditions.

5. References

[1] Lim et al; Process Control for Sheet-Metal Stamping Process, 2014.

[2] Gedda, H. Laser cladding: an experimental and theoretical investigation 2004.

How to select the right tribological lab test for practical applications

Lais M. Lopes[1)*], Dr. Dirk Drees[1)], Dr. Emmanouil Georgiou[2)]

[1)] Falex Tribology, Rotselaar, B3110, Belgium
[2)] Hellenic Air-Force Academy, Faculty of Aerospace Studies
Dekelia Air Force Base, GR 19005, Greece
[*]Corresponding author: lais.lopes@falex.eu

1. Introduction

The selection of a relevant laboratory test, to simulate an industrial application, is very challenging. Although some standard test methods exist, they are usually not suitable to provide the answers that are needed by a product developer, maintenance engineer or failure analyst. This is because tribological problems result from a vast combination of factors. Tribology is a system property, and there are many limitations when translating a field problem to a lab program. In this presentation, we will illustrate some of the more practical challenges, and show how we can address them at a practical level.

2. Tribology testing challenges

The major problem is to simplify the field problem to a controlled laboratory test.

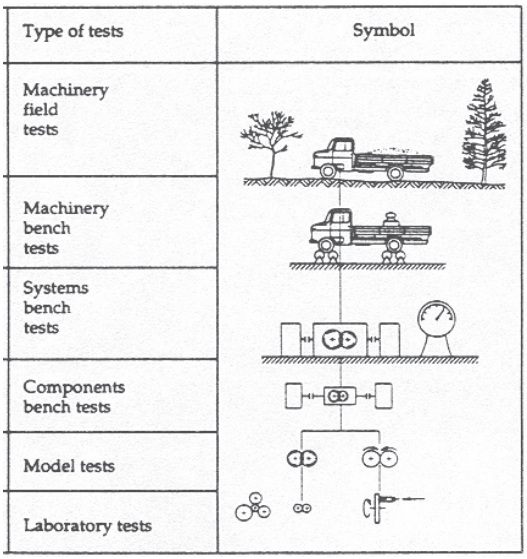

Figure 1 : From field problem to lab test

Obviously, the best simulation of a field problem is to conduct field tests. However, these have two primary issues: 1) field tests are time-consuming and expensive 2) field tests are a black box: there is lack of control over the test conditions, and there is limited information on component level. The general strategy is to simplify field tests, to reduce their duration and to increase control and repeatability.
A major challenge is that when simplifying models and conducting lab tests, the correlation to the real application is often lost. This can occur because tests are performed on smaller components, under more severe conditions, or fail to replicate the actual wear mechanisms observed in industrial practice.
The three main challenges in lab-scale testing are simplification without loss of correlation, wear mechanism convergence, and testing efficiency.

2.1. Simplify the field conditions

For this stage of the project setup, a lot of information must be collected from field experience, and thus an intensive dialogue between the project manager on lab testing, and the industrial client is needed. There is no simple scenario to reach this stage, but in general one can investigate the mechanical conditions, try to classify them and then incorporate the environmental conditions into the program. Every application will be unique, which means that each approach to lab testing will also be different, but some generalities can be used.

2.2. Match the wear mechanism

Once a suitable lab simulation has been identified, the testing conditions on lab scale must be optimized, aiming to match the wear mechanism observed in the lab with that in the practical application. Figure 2 illustrates the wear mechanisms observed in the application and in the vane pump testing.

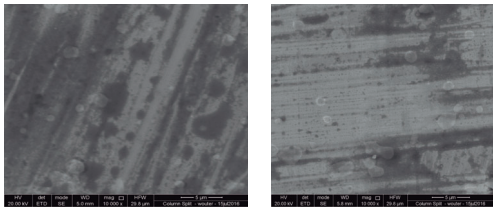

(a) (b)

Figure 2 : Matching the wear mechanisms: (a) Original component (b) Lab test result.

2.3. Multiple sectors, multiple approaches

The presentation will show examples from a variety of industrial sectors, and how we have made specific adjustments for each problem to simulate it as efficiently as possible on the lab scale.

2.4. Make testing more efficient

In the end, laboratory testing proves valuable only when it can generate sufficient data, along with repeatability, within an economically realistic timeframe. Because a lot of tests are focused on durability of materials (or wear rate), they are long tests by definition. Our approach sometimes is to use multi-station test machines that multiply the number of data points by 10 or 50 times, generating significantly more statistical data than a single station machine could ever achieve. But this will be the topic of a next presentation.

COF and wear variation of an anodized aluminum surface with different lubricant compositions

Vasco, M.C.[1)] and Pintaude, G.[1)*]

[1)] Department of Mechanical Engineering, Universidade Tecnológica Federal do Paraná, Curitiba, 81280-340, Brazil
[*]Corresponding author: pintaude@utfpr.edu.br

1. Introduction

Aluminum alloys are widely used in various industries due to their mechanical behavior and high strength / weight ratio, however, their low hardness generally limit their application in situations where high wear resistance is required [1]. Anodizing is a surface modification process that produces a high hardness alumina film that can contribute to wear reduction. Anti-wear additives (AW) act by forming a protective tribofilm in the contact area. Furthermore, the addition of nanoparticles, such as nanoalumina, can further improve wear resistance in various applications [2].

Based on this possibility, this work presented an investigation on the coefficient of friction (COF) and wear of an anodized aluminum oxide layer, employing different lubricant compositions in reciprocating tribological tests.

2. Experimental procedures

The aluminum alloy employed in this work was Alumold 500™. Anodizing was performed at room temperature utilizing a 5%wt H_2SO_4 solution for 60 minutes, with constant current density of 45 mA/cm². Polyalphaolefin-6 (PAO 6) oils, with and without the addition of 0.8%wt ZDDP, served as base lubricants. The amount of 0.01% wt% of alumina nano particles was dispersed in the lubricant oils.

For the ball-on-flat reciprocating tribological tests, high alumina spheres (E=400 GPa, Ø 3 mm) were chosen as the counterpart material. Applied load was of 2N, stroke magnitude of 10mm, frequency of 2.5Hz and varying times of 5 to 30 minutes.

The coefficient of friction was measured using the load sensors of the CETR-UMT equipment. Wear volume was determined using a non-contact interferometer.

3. Results and Discussion

Average COF values, *Figure 1*, show no statistically significant variation for lubricants with added nano particles, indicating that self-lamination, micro polishing, and self-mending may be the main anti-wear mechanisms for these lubricant compositions. There is a progressive increase on the wear track volume with time, *Figure 2*, regardless of the lubricant composition employed. Such behavior could be expected since the maximum contact pressure occurs below the maximum AAO layer thickness and is higher that the substrate's yield stress value, allowing for plastic deformation of the substrate.

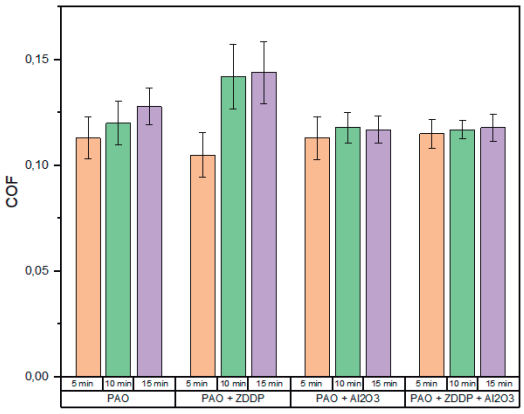

Figure 1 Average COF variation with lubricant composition in time.

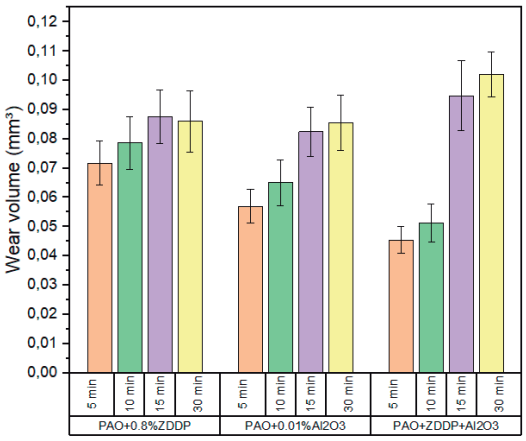

Figure 2 Variation of the wear tracks' volume with reciprocating time and lubricant composition.

4. Conclusion

We studied COF and wear variation of an anodized aluminum surface with varying lubricants. Lubricant composition plays a major role regarding COF variation but a minor role regarding wear resistance.

5. References

[1] C. Soffritti *et al.*, "Dry Sliding Behavior of an Aluminum Alloy after Innovative Hard Anodizing Treatments," *Materials (Basel).*, vol. 14, no. 12, p. 3281, 2021, doi: 10.3390/ma14123281.

[2] F. Ma *et al.*, "Evaluation of tribological performance of oxide nanoparticles in fully formulated engine oil and possible interacting mechanism at sliding contacts," *Surfaces and Interfaces*, vol. 24, Jun. 2021, doi: 10.1016/j.surfin.2021.101127.

Thermo-hydrodynamic analysis of journal bearings operating with non-Newtonian oils

Cardoso, M.[1*], Salvaro, D.[1], Klein, A.N.[1], Prata, A.T.[1] and Binder, C.[1]

[1] Universidade Federal de Santa Catarina, Brazil
*Corresponding author: mateus.c@labmat.ufsc.br

1. Introduction

The refrigeration industry, responsible for 20% of global electricity usage, demands improved efficiency [1]. In high-efficiency hermetic compressors, journal bearings with tight clearances and low-viscosity oils operate under high pressures and shear rates, potentially causing non-Newtonian behavior. Assessing non-Newtonian effects aids in selecting and developing more efficient lubricants, contributing to significant energy savings in the refrigeration industry. This study investigates the effects of different oils on the journal bearing of a high-efficient household refrigerator hermetic compressor. A thermo-hydrodynamic model, solving the modified Reynolds equation and energy equation iteratively using the finite volume method, is proposed, and used.

2. Methods

The modified Reynolds equation proposed by [2] coupled with the energy equation (adiabatic condition) were solved using the finite volume method in an iterative process. The cavitation boundary was calculated using the equation of conservation of mass [3]. The parameters of the power law curve fitting were obtained from experimental data fitting. The viscosity curves rheological properties were measured using a rotational rheometer ($\dot{\gamma} = 0 - 20000\ s^{-1}\ e\ T = 25,50\ e\ 75°C$). The oils analyzed and their properties are displayed in Table 1.

Table 1: Oil lubricants properties.

Oil	ID	Viscosity Parameters			$(\rho \times c_p)$
		$m_o(T_o = 25°C)$ $[mPa.s]$	n	β	$[J/Kcm^3]$
Alkylbenzene	ALQ 1	1.595	1.050	0.025	1.710
Alkylbenzene	ALQ 2	2.989	1.037	0.020	1.710
Alkylbenzene	ALQ 3	27.871	1.018	0.043	1.710
Mineral	Mineral	12.675	1.024	0.035	1.790
Polyolester	POE 1	12.696	1.000	0.041	1.900
Polyolester	POE 2	29.202	0.997	0.043	1.910

3. Results

When comparing two oils of similar value of m_o, mineral oil and POE 1 ($m_{o_{mineral}} = 12.68\ Pa.s \cong m_{o_{\mathrm{POE\,1}}} = 12.70\ Pa.s$) the hydrodynamic force (Figure 1) generated in the bearing when mineral oil is used is greater than that when POE is used (for $\varepsilon = 0.8$, $W_{mineral} = 383.66\ \mathrm{N} > W_{\mathrm{POE\,1}} = 266.86\ \mathrm{N}$) the difference in the resulting hydrodynamic force can be explained by two factors, the first and most significant, being the difference in shear rate behavior that these two lubricants exhibit. Mineral oil has a shear thickening behavior ($n_{\mathrm{mineral}} = 1.024$), while POE 1 exhibits Newtonian behavior ($n_{\mathrm{POE\,1}} = 1$). In addition, polyolester has a higher temperature-viscosity index (β) than mineral oil ($\beta_{POE\,1} = 0.041 > \beta_{mineral} = 0.035$).

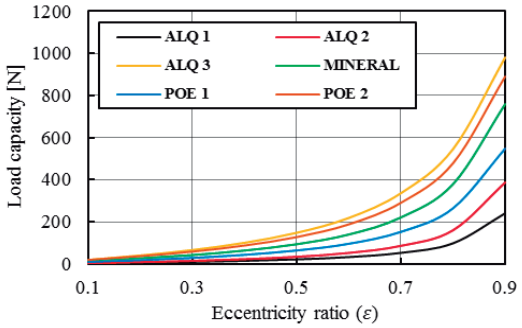

Figure 1: Load capacity.

The bearing operating with mineral oil ($C_f = 2.59 \cdot 10^{-3}$) has lower friction coefficients than operating with POE 1 ($C_f = 2.69 \cdot 10^{-3}$), despite its higher load capacity. This is due to the viscosity of shear thickening oil increasing in the region of high pressure (responsible for hydrodynamic force), while viscosity decreases in regions of low pressure (mostly contributing to friction). This phenomenon is illustrated in Figure 2.

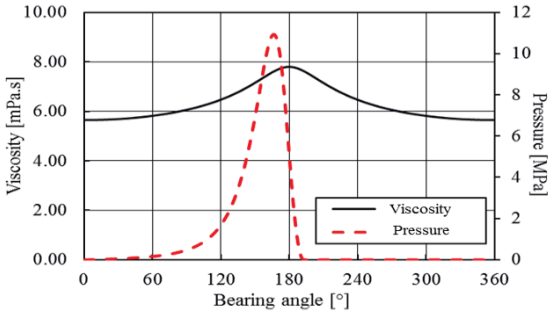

Figure 2: Pressure and viscosity distribution in journal bearing and dilatant fluid.

4. Conclusions

Even small deviations from Newtonian behavior, such as those presented by the investigated oils, resulted in significant changes in the bearing performance. When thermal and non-Newtonian behaviour are ignored, the journal bearing load capacity and friction force are directly proportional to the viscosity of the fluid. However, in the present work, where these effects were explored, a different behavior was observed. Under the same operating conditions, the load capacity and friction force are 67% and 64%, respectively, lower for the bearing operating with ALQ 2 than with POE 2, even though the consistency parameter at $T_o(m_o)$ is an order of magnitude lower.

5. References

[1] Dupont J. L., IIF-IIR, doi:10.18462/IIF.NITE C38.06.2019.
[2] I. K. Dien and H. G. Elrod, J Tribol, doi:10.111 5/1.3254619.
[3] A. T. Prata and R. T. S. Ferreira, J Tribol, doi:10.1115/1.2920311.

Lubricating Performance of PAO Oils Additivated with Combinations of ZDDP, Metal Sulfides, and Carbon Nanotubes

Prieto, G.[1)2)*], Ovando, E.[2)], Abdelnabe, J.P.[1)2)], Silva Cárdenas, I.[2)], Antonelli, M. M.[2)], and Tuckart, W.R.[1)2)]
[1)] IFISUR, CONICET-UNS, Bahía Blanca, CP8000, Argentina
[2)] Engineering Department, Universidad Nacional del Sur, Bahía Blanca, CP8000, Argentina
[*]Corresponding author: german.prieto@uns.edu.ar

1. Introduction

Wind turbines rely on efficient lubrication of their gearboxes to operate effectively. The complexity of the gearbox's lubrication requirements, due to the size and nature of its components, operating conditions, and need for long service life, is addressed by using advanced base oils, such as Polyalphaolephins, and additives.

Zinc dialkyldithiophosphate (ZDDP) is a traditional anti-wear additive, thanks to its capacity to form tribolayers that reduce friction and protect surfaces against wear. Solid lubricants, such as metal sulfides and carbon nanotubes (CNTs), can also improve lubricating properties.

In this work, different oil formulations containing a PAO 6 base oil additivated with ZDDP and solid lubricants were evaluated in block-on-ring tests.

It found that oils with ZDDP and CNTs exhibited the best tribological behavior, reducing friction by 24% and wear by 70%.

2. Materials and Methods

Oils were formulated using a Durasyn 6 PAO base oil (INEOS), additivated with different amounts of ZDDP (HiTEC), MoS_2 (Climax Molybdenum), Bi_2S_3 (Tribotecc), WS_2 (Tribotecc) and CNTs (Cheap Tubes). The resulting formulations were identified as follows:

Table 1 Lubricating oil formulations (wt%)

ID	ZDDP	Bi2S3	MoS2	WS2	CNT
A	1	0	0	0	0
B	1	4	0	0	0
C	1	0	4	0	0
D	1	2	2	0	0
E	1	0	0	4	0
F	1	0	0	0	0.1
G	1	0	4	0	0.1
H	1	0	0	4	0.1
I	1	0	2	2	0.1
J	1	2	2	0	0.1

Block-on-ring tests were carried out, using a ring (ϕ: 0.04 m) and a block both made with SAE 52100 steel. The sliding speed was 1.0 m/s, the contact pressure was 1.0 GPa and the total sliding distance was 3,600 m. The lower third of the rotating disc was submerged in oil.

Friction was continuously recorded and after the tests, the wear volume was determined using laser confocal microscopy (Fig. 1), while the formation of tribofilms was evaluated using SEM-EDS and Raman microspectroscopy.

3. Results

It was found that in all cases, the addition of a solid lubricant to the formulation contributed to lowering the friction. The lowest average COF was obtained using a combination of ZDDP and CNTs (Fig. 1). However, for some formulations the wear rate exhibited a significant increase, as in the case in the B formulation which contained ZDDP and Bi_2S_3. The lowest wear rates were observed for the combination between ZDDP and MoS_2, closely followed by the ZDDP+CNTs formulation (Fig. 1).

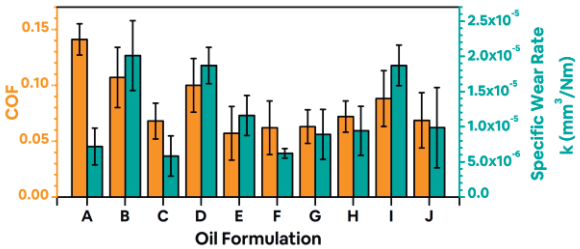

Figure 1 Average COF and Specific Wear Rate (k) for the different oil formulations.

The presence of ZDDP resulted in the formation of typical phosphate pads, while the addition of metal sulfides in some cases hindered the pad-formation process due to a competition between sulfide tribolayers and phosphate pads [1]. On the other hand, the addition of CNTs facilitated the formation of phosphate pads and their regeneration when worn out, likely due to their high thermal conductivity that promotes the tribochemical reactions between the ZDDP and the steel surfaces [2].

4. References

[1] Prieto, G., Dennehy, J., Tuckart, W. R. (2021). *Synergetic effect of metal sulfides and ZDDP on the lubricating performance of a PAO oil.* 10th Global Conference on Materials Science and Engineering.

[2] Dzięgielewski, W., Kowalczyk, J., Kulczycki, A., Madej, M., & Ozimina, D. (2020). *Tribochemical interactions between carbon nanotubes and ZDDP antiwear additive during tribofilm formation on uncoated and DLC-Coated steel*. Materials, 13(10), 2409.

Rotary barrel tumbling as a method of surface preparation for pin-on-disc wear testing samples

Xavier, L.M.[1)*], Rosa Neto, C.A.[1)], Strey, N.F.[1)], Boher, C.[2)] and Scandian, C.[1)]

[1)] Tribology, Corrosion and Materials Laboratory – TRICORRMAT, Department of Mechanical Engineering, Federal University of Espírito Santo - UFES, Vitória, 29075-910, Brazil

[2)] Institut Clément Ader - ICA, Université de Toulouse, IMT Mines Albi, SUMO, Campus Jarlard, 81013 Albi, France

[*]Corresponding author: leonardo.xavier@edu.ufes.br

1. Introduction

Sample homogeneity regarding surface roughness and mechanical properties is an important factor to consider, prior to wear testing. A rough surface and abnormal surface hardness values can significantly affect wear behavior [1]. Ideally, for pin-on-disc wear testing, samples' surface roughness average (Ra) should be under 0.8 µm, and their mechanical properties and microstructure shouldn`t be considerably altered [2]. Conventional machining processes (e.g., turning) can harden the samples' uppermost layers and produce undesired, non-uniform values of surface roughness parameters, hence, a careful and thorough sample surface preparation is necessary prior to testing.

This work proposes rotary barrel tumbling as a reliable and inexpensive method to prepare the surface of samples intended for later pin-on-disc wear testing.

2. Materials and method

The surfaces of 15 discs (75 mm in diameter, 8 mm thick) and 23 pins (cylindrical with semispherical head, 7.95 mm in diameter and 68 mm long) were prepared.

Six discs were machined from forged AAR Class D wheels (CDf), 6 from cast AAR Class D wheels (CDc), and 3 from cast AAR Class C wheels (CCc). Nominal rim hardness values for Class D and Class C wheels are in the range of 341-415 BHN and 321-363 BHN, respectively. Pins were machined from the head of a high-strength steel (352-397 HBW) AREMA TR68 rail.

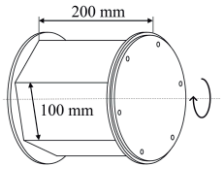

Figure 1 Barrel's hexagonal prism geometry

A 4-stage tumbling process was utilized. Operational parameters and media composition varied for each stage, as shown in Table 1. The tumblers' (OTOCARVA 2x5L) barrel geometry is shown in Figure 1.

Table 1 Tumbling parameters

Stage	Media	rpm	Time
1	abrasive chips, water and abrasive powder	60	4–12h
2	abrasive chips, water and cleaning compound	60	4h
3	abrasive chips, water and cleaning compound	60	2h
4	corn cob granules and polishing paste	80	8h

Mass loss, surface roughness parameters and surfaces` microhardness Vickers (10 gf) were measured before tumbling, after each stage, and after the complete tumbling process. Optical microscopy and optical 3D profilometry were carried out to aid in the visualization of the surfaces` roughness evolution.

3. Results

Considerable reduction was attained on the samples' surface roughness parameters. As displayed in Figure 2, final values of Ra for CDf, CDc, CCc discs and for pins were, respectively, 14%, 33%, 33 % and 33% of their original values. Final surface HV values were closer to the nominal for each steel, being, for CDf, CDc and CCc discs respectively, 55%, 64% and 78% of their original values.

Little deviation was found across sample categories after tumbling, and the standard deviation among samples of the same category was either reduced or not significantly altered, except for HV of CDc discs.

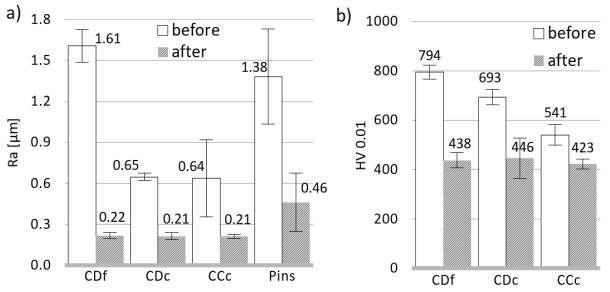

Figure 2 (a) Ra and (b) HV, before and after tumbling

4. Conclusions

The proposed method was efficient in reducing samples surfaces' roughness and hardness to desired levels. Deviation across sample categories and standard deviations among samples of same category indicate that greater homogeneity was attained after tumbling.

5. References

[1] Dzierwa, A. *Influence of surface preparation on surface topography and tribological behaviours.* Archives of Civil and Mechanical Engineering, v. 17, n. 3, p. 502–510, 2017.

[2] ASTM Standard G99-17, *"Standard Test Method for Wear Testing with a Pin-on-Disk Apparatus"* ASTM International, West Conshohocken, PA, 2017, DOI: 10.1520/G0099-17, www.astm.org

Erosion Simulation in Labyrinth Seals – CFD Analysis

Freire, A.D.[1)*], Silva, E. C. N.[1)], and Machado, I. F.[1)]

[1)] Department of Mechatronics and Mechanical Systems Engineering, Escola Politécnica, University of São Paulo, São Paulo, 05508-030, Brazil
[*]Corresponding author: andredf@usp.br

1. Introduction

Labyrinth seals (LS) are commonly used to minimize leakage but are susceptible to erosive wear caused by small particles in turbomachinery systems. This study aims to simulate erosion rates in labyrinth seals on the rotor using Finnie's model to quantify the impact of erosion on leakage [1].

2. Methodology

The erosion wear in the labyrinth seal (ten teeth) made of Ti-6Al-4V alloy is predicted using the Finnie erosion model, which considers particle velocity, diameter, and impact angle [2]. The alloy, obtained by additive manufacturing, density (ρ) (4252, 4297 and 4341 kg/m³) and surface hardness (H) (3.0, 3.5 and 4.0 GPa – corresponding to 313.4, 365.8 and 418HV/10) were varied considering [3]. The fluid flow within the LS on a rotor is modeled using the incompressible Navier-Stokes equations using the software COMSOL. The turbulent flow of CO_2 is simulated using the Reynolds-averaged Navier-Stokes (RANS) equations. The dynamic viscosity of 1.47e-5 [Pa s] and density of 1.84 [kg/m³] of CO_2 were used. Reynolds numbers (Re) of 200 and 2000 were evaluated to represent low and high inlet velocities. The rotational speed was 1018 rpm (rotor rotation). SiC spheric particles (Dp) were added to cause erosion during simulation (100µm, 150µm, and 200µm), which can be found in oil and gas transportation [4].

3. Results

Figure 1 shows that the most important effect can be related to the particle velocity. At low inlet velocities, the erosion results follow Finnie's equation since as Dp increases, the erosion also increases.

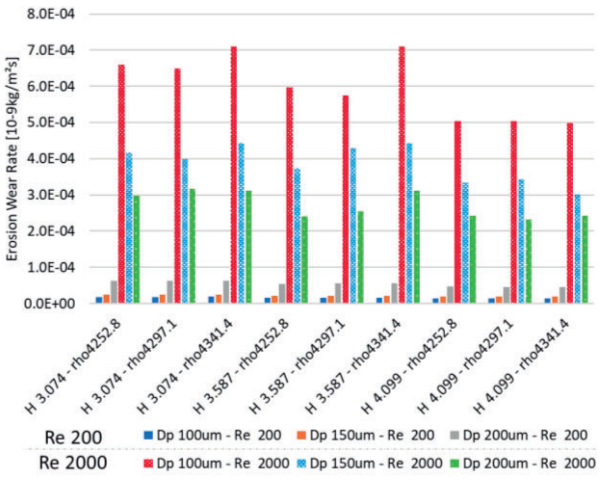

Figure 1 Erosion mass loss with density, hardness, the diameter of the particle, and Re velocity

However, the opposite result was found for high Re. More investigation must be conducted since Finnie's model erosion equation was based on a different geometry (elbow pipeline) [5].

Figure 2 shows the main factors that represent the significant levels: Re and Dp. The other factors (the H and Density) do not significantly affect erosion ($p > 0.05$).

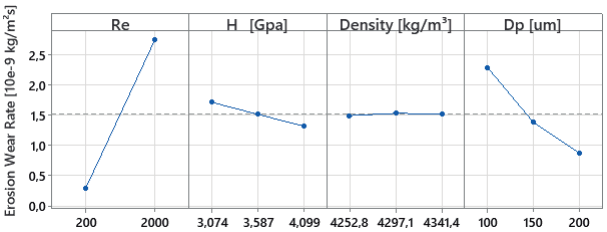

Figure 2 ANOVA Statics for Erosion wear

Table 1 summarizes the significant factors levels of the study of erosion wear in the rotor labyrinth seals. The factor Re contributes 22.66% to the variability at level 200 and 22.66% at level 2000. The factor Dp contributes 3.42% to the variability at level 100, 3.42% at level 150, and 3.42% at level 200. The interaction Re*Dp contributes 2.60% to the variability at all levels. All percentage representation considered the error.

Table 1 Factors Significant Levels

Factor	Levels	Effect Size	% Representation
Re	200; 2000	108.319	45.32%
Dp	100; 150; 200	24.543	10.27%
Re*Dp	200 2000	100 150 200	37.306	15.61%

4. Conclusion

Hardness and density have not had a significant effect. Finnie's model can better predict erosion when the particle is dragged and collide against the wall at small impact angles (low Re). In high Re, the particle is pushed and hit on the wall with bigger angles (close to the 90º - Coriolis effect). Therefore, Finnie's model shows the best results for small Dp and low Re.

5. References

[1] S. Chitrakar, H. P. Neopane, and O. G. Dahlhaug, in Sedimentation Engineering, 2018.
[2] I. Finnie, Wear, 19, 1, 81–90, Jan. 1972.
[3] H. Chen, J. I. Frankel, and M. Keyhani, Numer. Heat Transf. Part B Fundam., 72, 109–129, Aug. 2017.
[4] L. Zhao, Y. Yan, and X. Yan, J. Pet. Sci. Eng., 196, 107992, Jan. 2021.
[5] B. ; Li et al., Energies 2022, 15, 1901, 15, 5, 1901, Mar. 2022.

Micro abrasion in Fe-Cr-C-Nb alloys samples: the role of Niobium

Costa, A. R*.[1]; Wieslaw Grabon[2]; Oliveira, T. G.[1]; Silva, R. C. P.[1]
[1]REDEMAT – Rede Temática em Engenharia de Materiais – UFOP - Ouro Preto - MG – Brazil
[2] Rzeszow University of Technology - Poland
*Corresponding author: arcosta55@gmail.com

1 ABSTRACT

This paper addresses to analyze the role played by Niobium (Nb) in the microstructure of Fe-Cr-C alloys being tested in micro abrasion conditions (ball abrasion test). Three alloys with differences in Cr content and one of them with 5% Nb have been prepared as weld tracks under Fe-C substrate. The resulting microstructures contain carbides embedding in a metallic matrix. Significant changes in mechanical properties are reported depending on the morphology, size and distribution of carbides [1, 3]. Results pointed out to an improvement in wear resistance of Fe-Cr-C-Nb alloy although it showed lower values of hardness and volume fraction of carbides in comparison to the other alloys. The coefficient of friction was also affected by Nb addition. Such results evidence the possibility of using such alloy in applications that require high performance in wear resistance as mining and agricultural equipment.

Key words: Niobium, Chromium, Wear, Ball Abrasion Test.

2 INTRODUCTION

Fe-Cr-C alloys are useful as coatings, sometimes with others elements, providing a great variety of microstructures showing better response to wear, especially under abrasion. Often, these alloys have carbides of MC, M_6C, M_7C_3, $M_{23}C_6$ and Cr_2C_3 type depending on the composition, solidification and cooling rates. Berns [2] reports how size, distribution, adherence to matrix, volume fraction and morphology can affect the wear rate of microstructures. Accordingly to [2, 3], Nb in Fe-Cr-C systems provides NbC carbides resulting in better wear resistance. However, hard micro constituents bring some limitations as coarse morphologies and poor adherence.

Our contribution to this area had been done measuring specific wear rate and wear coefficients of thick coatings deposited upon ASTM A36 steel plate - (150 x 50 x 11,7) mm. The deposition was performed by means of welding methods providing thick tracks of Fe-Cr-C and Fe-Cr-C-Nb. The wear tests have been done in a ball abrasion tester. This test provides craters which diameters allow to follow the loss of mass evolution during tests among other features.

3 MATERIALS AND METHODS

Fifteen samples of the ASTM A36 carbon steel of dimensions (150x50x11.7mm) were produced for the coating's application of the alloys A, B and C by the welding process. In each sample, four weld beads of 5mm high and 150mm length were deposited in a single layer.

Micro abrasion tests have been performed in order to verify the influence of the introduction of Nb into the microstructure on wear resistance. The micro wear behavior of these microstructures has been verified by means of ball abrasion test coupled with SEM/EDS observations.

3 RESULTS AND DISCUSSION

It was possible to measure and interpret the wear behavior of each alloy following the evolution of the diameters of the craters and observing the microstructures. Our discussion takes into account the correlation between micro hardness, the microstructures, the volume loss of the samples/specific wear rates and the evolution of friction coefficients.

4 CONCLUSION

The best performance in terms of abrasion resistance was observed to Fe-Cr-C (5%Nb) (Alloy C), instead of lower carbides volume fraction present in the microstructure and lower matrix hardness values. This result points to suggest it as hard facing material candidate.

5 REFERENCES

[1] Kirchgaßner, M.; Badisch, E.; Franek, F. "Behaviour of iron-based hard facing alloys under abrasion and impact". Wear, v. 265, n. 5, pp. 772-779, 2008.

[2] Berns, H.; "Microstructural properties of wear-resistant alloys". Wear, v. 181, pp. 271-279, 1995.

[3] T. G. de Oliveira, A. R. da Costa. Influence of microstructure on micro-abrasive wear resistance of alloys Fe-Cr-C and Fe-Cr-C-Nb. ISSN 1517-7076 Revista Matéria, e-12281, 2019.

Acknowledgemnts: UFOP and CAPES.

Polishability of High-Chromium Cast Iron and Commercial Materials for Automotive Polymer Injection Molds

Mello, V,S,[1)*], Strey, N.F[1)], Vieira, S.L, K [1)], Scandian, C[1)] and Alves, S, M.[2)]

[1)]Tribology, Corrosion and Materials Laboratory - TRICORRMAT, Department of Mechanical Engineering, Federal University of Espírito Santo - UFES, Vitória, 29075-910, Brazil
[2)] Science and Technology School, Universidade Federal do Rio Grande do Norte, Natal, 59075-000, Brazil
[*]Corresponding author: valdicleide.mello@ufes.br

1. Introduction

The manufacturing of automotive parts requires precision, strength to wear, mechanical, variations in temperature and pressure. Besides this, the material of the mold needs to exhibit a high polishing capability to promote high-quality finishing. In this context, the polishing capability of polymer injection molds plays a crucial role in achieving finished surfaces free from imperfections. The combination of resistance to mechanic and thermal fatigue makes high-chromium cast iron a possible choice for applications that require high durability under challenging conditions. In this research, we focused on investigating the polishing capacity of high-chromium cast iron alloys, using the P20 and H13 steels as references. These steels are widely recognized in the literature for their good and excellent polishing capabilities [1].

2. Methods

2.1. Materials

Four high-chromium cast iron were investigated, coded according to the chromium percentage and arrangement of chromium carbides in the matrix. These alloys are 19E - 19 %wt Cr, eutectic, (56 ± 1,0) HRC, 19H - 19 % wt Cr, hypoeutectic, (60 ±0,9) HRC, 26E - 26 %wt Cr, eutectic, (55 ± 0,7) HRC and 26H - 26 % wt hypoeutectic,(55 ± 0,5) HRC. As reference standards, P20 (29± 1.3) HRC and H13 steels were investigated (85 ± 1,5 HRB).

2.2. Polishing procedures

The preparation of surfaces samples were performed in two step using a Struers TegraPol-25 automatic polishing machine under 10 and 70 N of load. Polishing disc and polishing head were set to rotation speeds of 200 rpm and 50 rpm, respectively, both rotating in the same direction. Step one: the samples were grounded for 10 minutes, using the P80, P120, P320, P500 and P800 FEPA sandpapers (Struers); Step two: the polishing were performed for 3 minutes using a water-based suspensions of monocrystalline diamond particles (Struers DiaDuo-2 3 µm and 1 µm) and the polishing cloth (Struers MD-Mol and MD-Nap, respectively).

Before and after each one of the steps of finishing, roughness parameters measurements were performed with a Taylor Hobson Surtronic 25 portable profilometer. Surface topography parameters were obtained using a confocal profilometer (S neox- Sensofar). The metalographic analysis of samples was performed by the Murakami etchant.

3. Results and discussions

The results suggest that the 19E alloy demonstrated performance comparable to that of H13 and superior to that of P20 in terms of surface roughness after the polishing process, resulting in a smoother surface. These findings can be attributed to the distributions and volume fraction of chromium carbides in this alloy leading to improved surface quality. This characteristic provides an advantage in applications where a high-quality finish is desired.

Figure 1: Microstructres: a) 19E and b)H13

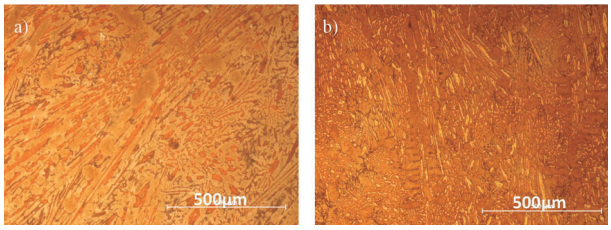

Table 1: Roughness parameters of sample surfaces after final polishing step (1 µm) under 70 N of load.

Roughness Parameter	19E	19H	26E	26H	P20	H13
Ra	0.02	0.02	0.06	0.09	0.07	0.02
Rz	0.19	0.18	0.53	0.70	0.55	0.12
Rsm	46.70	30.4	29.50	49.56	232	31.16
Rsk	-110	-0.28	-1.93	-1.86	-1.62	0.04

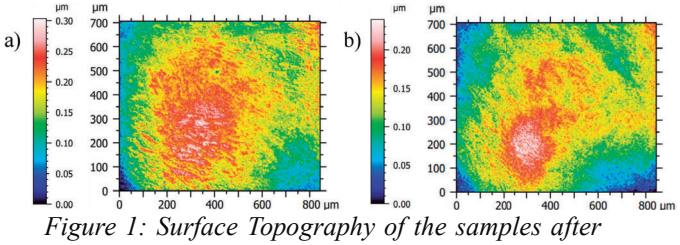

Figure 1: Surface Topography of the samples after the final polishing step: a) 19E and b)H13

4. References

[1] S.N. Lekakh, M. Buchely, R. O'Malley, L. Godlewski, Mei Li,*Thermo-cycling fatigue of SiMo ductile iron using a modified thermo-mechanical test.*International Journal of Fatigue,2021.**148.**

The use of ASTM G-65 dry sand/rubber wheel test adapted to abrasiveness ranking of iron ores

Münch, D.[1)*], Moreira, L.[1)], Nins, B.[1)], Penagos, J. J.[1)] and Bortoleto, E.M.[1)]

[1)] Instituto Tecnológico Vale, Ouro Preto, MG, Brazil.
[*]Corresponding author: daianemunch90@gmail.com

1. Introduction

The established methods for evaluating rock abrasiveness are unsuitable for friable rocks associated with dry applications. ASTM G65 [1] is a laboratory test that determines the resistance of metallic materials to scratching abrasion using a dry sand/rubber wheel. This method was already used to establish an abrasiveness ranking related to conveyor belt materials [2]. This study aimed to investigate the abrasiveness ranking of iron ores compared with the standard sand abrasive in the wear of metallic material (AISI H13).

2. Materials and methods

The experiments were adapted from ASTM G65 [1], using H-13 steel samples, normal Brazilian sand, and four types of iron ores as abrasives. The particle size class ranges of -0,6+0,3 and -0,3+0,15 mm were used, similar to AFS 50/70. The test parameters were 56N of applied force, 10 minutes, 200 rpm wheel rotation, and the abrasive flow rate varied between 320 and 530 g/min due to density difference. The abrasives were characterized according to their mineralogy, density, microhardness, and shape parameters.

3. Results

Friable hematite and compact hematite represent high-grade iron ore with a predominance of compact hematite (90 wt%). Jaspilite has a contribution of quartz of about 12 wt%, while sand is composed primarily of quartz (95 wt%). In hydrated ore predominates goethite (67 wt%). The microhardness values obtained are presented in Table 1. Higher values (> 1000 HK) were related to Friable, Compact hematite, and sand. The average sphericity for all abrasives was approximately 0.79 mm, and the aspect ratio was 0.69 mm.

Table 1 Knoop microhardness values for abrasives.

	Knoop microhardness (HK)	
Abrasive	**-0.6+0.3mm**	**-0.3+0.15mm**
Friable hematite	1240 ± 98	1265 ± 58
Jaspilite	970 ± 121	1138 ± 79
Compact hematite	1101 ± 140	1105 ± 78
Sand	1213 ± 51	1280 ± 108
Hydrated ore	910 ± 174	892 ± 80

The abrasiveness ranking followed the increasing order of hydrated ore, sand, compact hematite, jaspilite, and friable hematite (Figure 1), as already observed for rubber samples [2]. Coarse size (-0.6+0.3 mm) caused greater wear rate than fine size class (-0.3+0.15 mm).

4. Discussion

Although friable hematite and sand have similar hardness and shape parameters, the wear rate of friable hematite was four times higher. As hardness solely does not explain this phenomenon, an evaluation of methods for determining particle shape parameters should be sought. While standard sand tends to have more rounded quartz grains, compact hematite mineral comprises more sinuous, microcrystalline, and lamellar morphologies. However, optical-electronic analysis of the morphology did not distinguish the shape parameters among the abrasives.

The ASTM G65 as an abrasiveness test has proven helpful for rock materials that cannot be tested with the CERCHAR abrasiveness test and Miller Slurry Abrasion Response (SAR) method. Although using the same particle size class, one must pay attention to the influence of different abrasive properties on the abrasiveness.

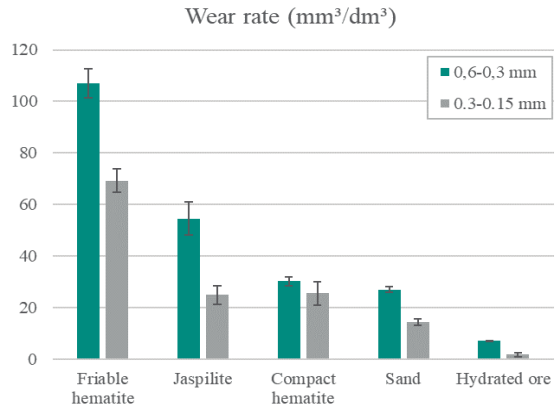

Figure 1 Wear rate produced by the abrasives.

5. Conclusions

The abrasiveness classification showed a higher wear rate for friable hematite and a lower for hydrated ore. Also, standard sand was shown to underestimate the wear in the condition of loose abrasive compared to iron ores.

References

[1] ASTM G65. *Standard Test Method for Measuring Abrasion Using the Dry Sand/Rubber Wheel Apparatus.* ASTM Standards, 2010. 1–6.
[2] NINS, B. et al. *Abrasiveness of iron ores: Analysis of service-worn conveyor belts and laboratory Dry Sand/Rubber Wheel tests.* Wear, 2022, **506:** p. 204439.

SCRATCH TESTS ONTO Al-Fe-Cr QUASI-CRYSTAL-REINFORCED ALUMINUM MATRIX COMPOSITE FABRICATED BY SELECTIVE LASER MELTING

Souza, R.M[1)], Kang, N.[2)], Lima, A.O.[1)] , Lima, V.A.*[1)], Seriacopi, V.[1)], Machado, I.F[1)], El Mansori, M.[2)]

[1)] Laboratório de Fenômenos de Superfície, Escola Politécnica da Universidade de São Paulo, São Paulo, 05508-030, Brazil
[2)] Arts et Metiers Institute of Technology, MSMP, France
*Corresponding author: vinicius.alves.lima@usp.br

1. Introduction

Additive manufacturing (AM) processes, and the corresponding process parameters, provide a wide range of structures and mechanical properties. In some cases, AM processing results in materials with improved tribological behavior. For example, the development of a composite structure with harder particles embedded in a softer metallic matrix may lead to the formation of a mechanical mixing layer (MML) that significantly decreases the coefficient of friction (COF) and improves the wear resistance [1]. In this work, scratch tests were carried out to analyze the action of a single abrasive particle in an Al-Fe-Cr quasi-crystal reinforced aluminum matrix composite, fabricated by selective laser melting (SLM).

2. Experimental Procedure

Aluminum-matrix composite samples were prepared by SLM using a prealloyed Al-Fe-Cr powder. After AM processing, the sample microstructure was composed of a region with coarse quasi-crystals (QCs) particles and a region with fine QC particles, as indicated in Figure 1. Samples were later characterized by nanoindentation, with loads from 0.5 to 10 mN, for evaluation of hardness and elastic modulus of both regions.

Three Scratch test procedures [2] were conducted on the sample surface, to characterize the effect of a single abrasive particle on both regions. One procedure was conducted with increasing load, from 0 to 100 mN. The other two procedures were conducted with constant load, one with 5 mN and the other with 80 mN (Figure 1).

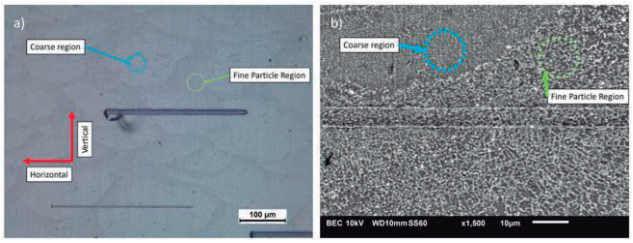

Figure 1 - Al-Fe-Cr microstructure highlighting two distinct regions: a coarse region and fine particle region by (a) OM and (b) SEM.

3. Results

Nanoindentation measurements indicated a dispersion in hardness values, especially for the lowest values of normal load, as indicated in Figure 2.

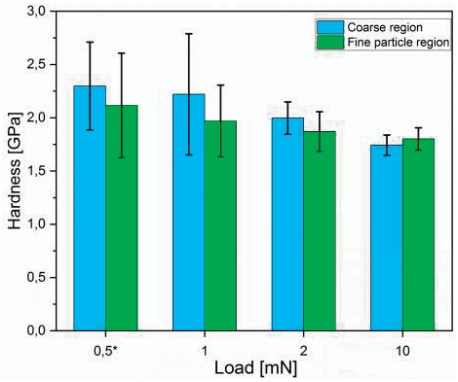

Figure 2 - Hardness of the coarse and fine particle region as function of the load.

Scratch tests were with progressive load were able to reveal a change in abrasion micromechanism as a function of the normal load (Figure 3). Scratch tests have also indicated how the friction and wear behavior was affected by microstructural features, such as quasi-crystal particle distribution.

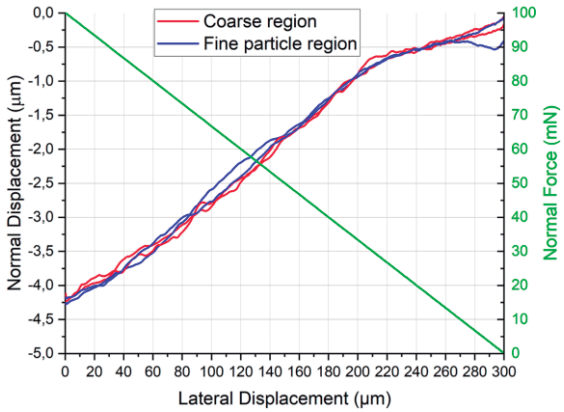

Figure 3 – Evolution of vertical displacement and load as a function of lateral displacement of scratch tests with progressive load

4. References

[1] Kang, N.; Zhang, Y.; El Mansori, M.; Lin, X. *Laser powder bed fusion of a novel high strength quasicrystalline Al–Fe–Cr reinforced Al matrix composite*. Advanced Powder Materials, 2023. 2: 100108.

[2] Seriacopi, V.; Prados, E.F.; Fukumasu, N.K.; Souza, R.M.; Machado, I.F. *Mechanical behavior and abrasive mechanism mapping applied to micro-scratch tests on homogeneous and heterogeneous materials: fem and experimental analyses*. Wear, 2020. 450-451: 203240.

Effect of abrasive on the wear behavior of synthetic and water based fluids in oil and gas drilling

Moura, E.I.F.[1)*], Silva, L.R. R.[1)], Riente, A.F.[2)], Percy, J.G.[2)] and Franco, S.F.[1)]
[1)] Department of Mechanical Engineering, Universidade Federal de Uberlandia, Uberlandia, 38400 901, Brazil
[2)] PETROBRAS, Rio de Janeiro, 21941-915, Brazil
[*]Corresponding author: edja.moura@ltad.com.br

1. Introduction

Concerns about environmental hazards caused by synthetic-based drilling fluids have led to an increased demand for water-based drilling fluids that meet many environmental requirements. It is known [1] that synthetic fluids have better tribological behavior because they are more lubricating than aqueous, however, some studies show the opposite [2, 3]. To better understand this issue, this study evaluates the effect of abrasives on the performance of water-based and synthetic drilling fluids.

2. Methodology

A reduced scale test based on the API 7CW standard, that simulates cylinder-cylinder contact, was used to evaluate the proposed tribological conditions. The tests used samples of the material from the casing and the drill string. The parameters used in the test are compatible with those proposed by the API7CW standard and are shown in Table 1.

3. Results

According to the results of mass loss of the casing sample for the aqueous and synthetic fluids shown in Figure 1 and the wear marks shown in Figure 2, the effect of the abrasive in increasing the wear is clear, especially when using synthetic fluid. In the condition where there is no presence of abrasive, the ANOVA analysis shows that, statistically, the averages are equal. To justify this behavior, it is observed, in addition to a change in the wear mechanisms, the formation of a film on the worn surface of the casing of the well under both conditions. In the literature, authors [4] identified the existence of a film composed of carbon on the weathered surface of hydrocarbon fluids under atmospheric conditions at zero or low levels of oxygen. The formation of the tribofilm found in greater quantity in the condition of water base fluid with abrasive may be related to the difference in viscosity between the fluids and the presence of abrasives. In view of this, the higher viscosity measured for the synthetic fluid (733 cP, against 129 cP for aqueous fluid) can carry more particles to the contact region, causing the breakdown or non-formation of the tribofilm.

Table 1 Test parameters

Force	Speed	Abrasive	% abrasive
44 N/mm	155 rpm	NBR 100 mesh	7 % of the volume

4. Conclusion

It is concluded that viscosity and abrasive can influence the performance of aqueous and synthetic fluids.

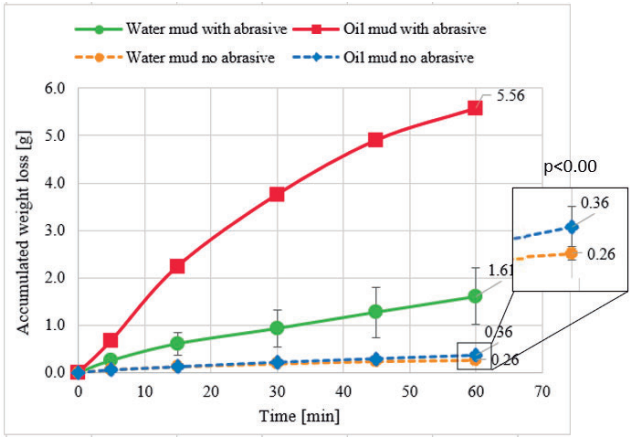

Figure 1 Mass loss in the casing over time.

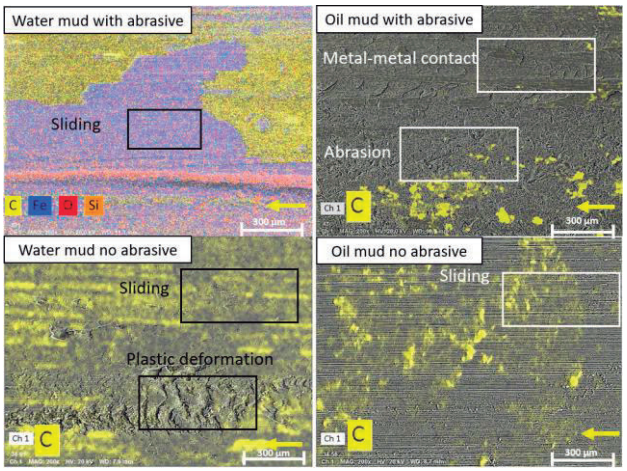

Figure 2 Worn surface observed via SEM

5. References

[1] R. Gheisari, A.A. Polycarpou, Synergistic physical and chemical interactions of selected additives and base oil used in extended reach drilling applications, Wear. 478–479(2021)203889. https://doi.org/10.1016/j.wear.2021.203889.
[2] E.I.F. Moura, J.O. De Moraes, J.G. Percy, S.D. Franco, L.J. Da Silva, A.F. Riente, Effect of drilling fluid type on oil well casing wear, Rio Oil Gas Expo Conf. 22 (2022) 19–20. https://doi.org/10.48072/2525-7579.rog.2022.019.
[3] S. Sayindla, B. Lund, J.D. Ytrehus, A. Saasen, Hole-cleaning performance comparison of oil-based and water-based drilling fluids, J. Pet. Sci. Eng. 159 (2017) 49–57. https://doi.org/10.1016/j.petrol.2017.08.069.
[4] J. Zhang, S. Campen, J. Wong, H. Spikes, Oxidational wear in lubricated contacts – Or is it?, Tribol. Int. 165 (2022)107287. https://doi.org/10.1016/j.triboint.2021.107287.

Use of a test rig to evaluate effect of oil formulations on gearbox friction losses.

Tomanik, E.[1)], Miagava, J.[2)], Papoulias, G.[3)], Getschko, N[1)], Profito, F.[1)]

[1)] University of São Paulo, São Paulo, 05508 030, Brazil
[2)] Insper Institute of Education and Research, São Paulo, 04546-042, Brazil
[3)] Instituto de Pesquisas Tecnologicas, São Paulo, 3767-4000, Brazil
*Corresponding author: eduardo.tomanik@usp.br

1. Introduction

Gearboxes are used in a myriad of mechanical systems, from high-speed electric cars to very large and relatively slow wind turbines. There is a crescent search for downsizing, higher mechanical efficiency, longer time before maintenance and more recently, development of lubricants with improved thermal and dielectric properties conductivity [1]. Improved oil formulation, including use of novel additives, is one of the main paths to improve gearbox performance. Use of improved lubricants have the additional advantage that they have the potential to be applied to existent machinery, reducing cost and time when compared with new designs and materials. However, most of the current development tests are either expensive or not representative of the gearbox complex mechanisms. A simpler, small, test rig to test oil formulations for gearboxes would allow a more extensive and time saving research on novel solutions.

2. Simplified tests rig for gearbox friction losses

To conduct investigation on novel oil formulations for gearboxes, a small gearbox was built. The rig has a 1:9 gear ratio to achieve higher speeds but it can also be converted to an usual reductor just inverting the sides for the input / output. In the current configuration, friction losses are measured by the time taken to go from 1000rpm to full stop. Longer times mean lower friction losses.

The rig is being upgraded to have a continuous recording of temperature, vibrations, and speed, which would allow more comprehensive investigations of the impact of oil formulation. By the paper final version, improved test conditions and novel additives will be carried-out.

3. Preliminary Results

Figure 1 shows the gearbox before installation of the sensors for temperature, vibration time to stop with different oil volumes. Oil volume affects the churning losses (work done by the gears to drag the oil). Using an ISO 68 mineral oil, 27% lower oil volume led to 40% higher time to stop. Figures 2 shows tests with different oils with same nominal viscosity. 10.9% lower friction/churning losses was observed with an ICE oil. Figure 3 shows the effect of adding 3.5% FM additive to the gear oil.

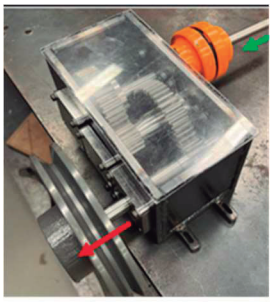

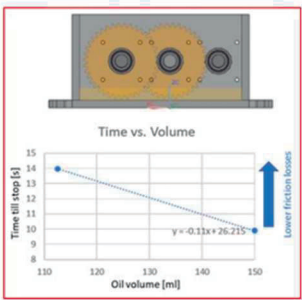

Figure 1- Photo of rig prototype (currently being upgraded with sensors) RIGHT: effect of oil on churning losses.

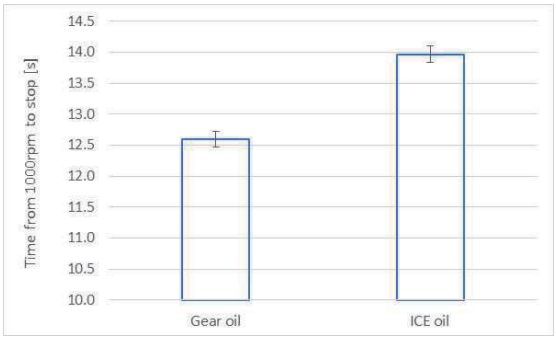

Figure 2-Test with different oil formulations with same nominal viscosity.

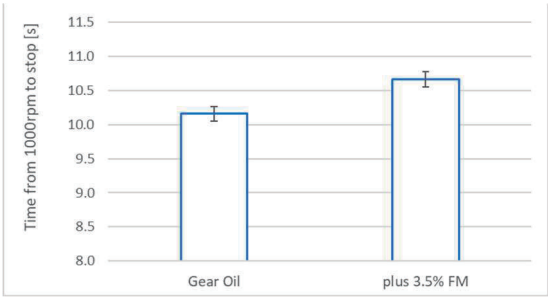

Figure 2- Test with addition of Friction Modifier. test done with lower oil volume to maximize effect of the FM.

References

[1] Canter, N. *Tribology and Lubrication for E-Mobility: Findings from the Inaugural STLE Conference on Electric Vehicles*, 2022

[2] Siebert, H.; Holm, A., Protecting Gears in Wind Power Applications.2009. Lu, 2020 CFD-Based Investigation of Lubrication and Temperature

The Effect of Viscosity on Rail/Wheel Wear Resistance Using Calcium-Thickened Greases

Carvalho, A.C.[1)*.1)], Miranda, R.S.[1)] , Fernandes, F.M.[1)], Carvalho, J.G.A[1)], Cousseau, T.[2)] and Mei, P.R[1)]

[1)] School of Mechanical Engineering, Universidade Estadual de Campinas, Campinas, 13080 970, Brazil
[3)]Federal University of Technology - Paraná, Mechanical Engineering Department, Curitiba, 80230 901, Brazil

[*]Corresponding author: decarvalho.anacecilia@gmail.com

1. Introduction

Over the past 30 years, extensive research has been conducted to develop a solution plan aimed at increasing the lifespan of rails and improving the safety standards of rail transport. This plan focuses on friction management, which involves controlling the friction coefficient between the wheel and the rail to ensure optimal values for safe traction and braking. By implementing this management strategy, wear rates can be reduced, leading to improved fuel efficiency. In the context of curves, friction control is achieved through the application of lubricating greases specifically on the gauge corner of the rail[1-2]. However, there is a lack of understanding regarding the relationship between the grease formulation and its performance. This study aims to investigate the impact of grease viscosity on its ability to reduce wear.

2. Materials and methods

The wear tests were performed in a twin disc tribometer shown in **Figure 1**. The greases were formulated and provided by the Federal University of Technology – Paraná.

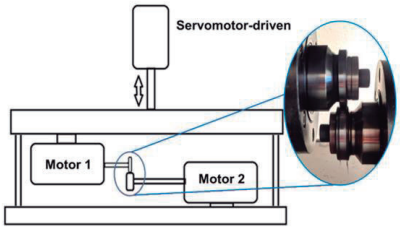

Figure 1 – Schematic drawing of twin disc machine.

3. Results and discussion

The findings are depicted in Figure 2. In the dry condition, the wheel wear is significantly greater than the rail wear, primarily due to the disparity in hardness between the two discs. The rail disc's higher hardness leads to abrasive wear on the wheel, resulting in a more substantial loss of mass. In the lubricated test, the viscosity greases function through distinct mechanisms on the rail discs. This can be attributed to the dual effect of grease hydro-pressurization within cracks. Although the lower viscosity grease easily enters the cracks, it does not generate as significant of a hydraulic effect in promoting crack growth as the higher viscosity greases do. This phenomenon was previously observed by WANG et al. (2017)[3]. Nonetheless, even with the accelerated crack growth effect, the use of greases reduced the wear of the wheel-rail system under all tested conditions compared to the dry test.

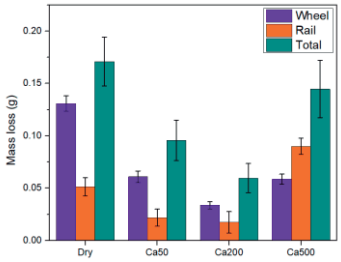

Figure 2 - Mass loss dry and lubricated test conditions.

Figure 3 illustrates the variation in the coefficient of friction (COF) during the lubricated tests. The COF values for the lubricated conditions were determined by averaging the results of the final 8,000 cycles for each test. It can be concluded that all the tested greases effectively reduced the COF, resulting in an approximate 70% decrease in this parameter upon application. However, there were no significant differences observed in the COF values among the different greases employed.

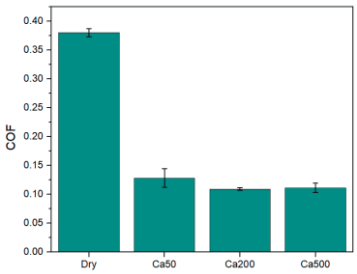

Figure 3 - COF values for the dry and lubricated tests.

4. References

[1] Seo J-W, Jun H-K, Kwon S-J, Lee D-H. *Rolling contact fatigue and wear of two different rail steels under rolling–sliding contact.* Int J Fatigue.2016.**83**:p.184-194.

[2] Hardwick C, Lewis R, Stock R. *The effects of friction management materials on rail with pre existing rcf surface damage*. Wear. 2017. **384-385**: p50-60.

[3] Wang WJ, Lewis R, Evans MD, Liu QY. *Influence of different application of lubricants on wear and pre-existing rolling contact fatigue cracks of rail materials*. Tribol Lett. 2017;**65(2)**:p.1-15.

Designing MoS_2 based coatings for improved self-lubricating gears

Fukumasu, N.K.[1*], Carvalho, A.A.[2], Rego, R.[2], Tschiptschin, A.P.[1], Souza, R.M.[1] and Machado, I.F.[1]

[1)] Universidade de São Paulo, São Paulo, 05508-030, Brazil
[2)] Instituto Tecnológico de Aeronáutica, São José dos Campos, 12228-900, Brazil

[*]Corresponding author: newton.fukumasu@usp.br

1. Introduction

Optimal lubrication plays a vital role in preventing gear failure. Insufficient lubrication deprives gear surfaces of a protective film, resulting in metal-to-metal contact which may lead to increased friction and wear. To mitigate a premature failure, self-lubricating coatings offer a promising solution. Materials, such as graphite or molybdenum disulfide, provide long-lasting lubrication even in harsh conditions, reducing friction and wear between gear surfaces, ensuring reliable performance and enhanced durability [1].

In this work, MoS_2 based coating was produced to support the stresses developed at the contact between surfaces that present a combined rolling and sliding movement under boundary lubrication conditions.

2. Methodology

Ball on disc configuration was used to analyze the tribological behavior under mixed to boundary lubrication transition of the coated surface. AISI 52100 steel was used on both ball and disc. Only discs were coated.

The deposition process was carried out at an in-house developed hybrid reactor, using Nb and MoS_2 targets to produce a doped Nb:MoS_2 coating.

Tribological tests were performed with a Mini-Traction Machine from PCS Instruments, which allows the individual control of ball and disc velocities, leading to variable lubrication conditions and sliding to rolling ratio (SRR) at the contact. A constant normal load of 33 N was applied at a fixed SRR of 100%. PAO ISO VG 8 base oil at 90°C was used as lubricant.

The as-deposited coating and the worn surface were characterized using optical microscopy, Raman spectroscopy and instrumented indentation. A Xplora One Raman Spectroscopy system, from Horiba Inc., equipped with a laser wavelength of 532 nm was used to measure Raman spectra in mapping mode. The Ti950 triboindenter system from Brucker Inc. was used to measured load-displacement curves, allowing the evaluation of hardness and reduced elastic modulus using the Oliver & Pharr method.

3. Results

Tribological tests are presented in Figure 1. In this figure, coated condition (blue circles) presented lower traction coefficient compared to the reference uncoated condition (black squares) along all the tested velocities. In Figure 2a, hardness (H) and reduced Elastic Module (Er) were measured in three surface conditions: as-deposited coating (dark gray), inside the wear track (light gray) and spalled region (white). Raman spectra of those selected regions are presented in Figure 2c. Figure 2b shows the superposition of a colored image representing the intensity of Raman shift of 400 cm^{-1}. This figure suggests the existence of crystalline MoS_2 on regions inside the wear track, induced by tribological conditions of an amorphous MoS_2 based coating [2].

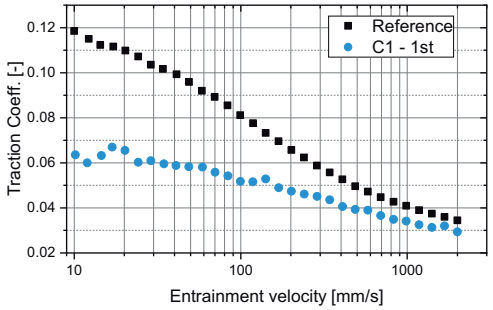

Figure 1 – Stribeck curve for the analyzed system: black squares represent the reference condition, while blue circles indicate the coated disc condition.

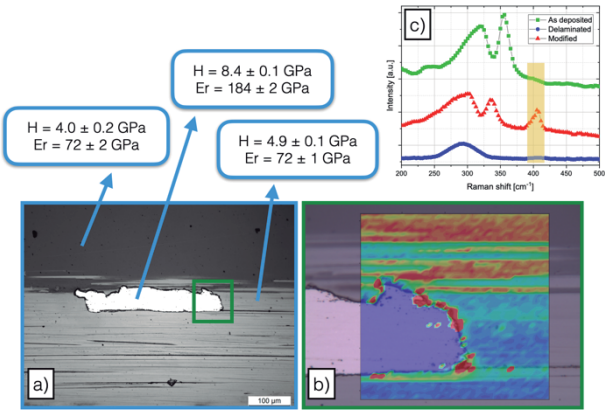

Figure 2 – Analyses of the wear track: a) hardness of selected regions, in which dark gray represent the original coating, light gray is the coating inside the wear track and the white region represent an exposed substrate; b) Raman spectra mapping near the spalled region and c) Raman spectra of different regions.

4. Conclusions

In this work, cyclic elevated pressure under sliding/rolling contact condition induced the crystallization of MoS_2 from the as-deposited amorphous coating, sustaining a lower friction compared to uncoated reference condition.

5. References

[1] Polcar, T. and Cavaleiro, A., Surf. Coat. Technol., 20122, 206, 686-695
[2] Beilstein, J., Nanotechnol., 2017, 8, 1115–1126.

A method to assess the tribological behaviour of solid lubricant nanoparticles in the macroscale applied to graphene and carbide-derived carbon

Renan Oss Giacomelli[1, 2)*]; Guilherme Oliveira Neves[1)]; Nicolás Araya[1)]; Diego Salvaro[1)]; Cristiano Binder[1)]; Aloisio Nelmo Klein[1)]; José Daniel Biasoli de Mello[2)]

[1)] Laboratório de Materiais, Universidade Federal de Santa Catarina, Brazil.
[2)] SENAI Innovation Institute for Laser Processing, Brazil
[3)]Faculdade de Engenharia Mecânica, Universidade Federal de Uberlândia, Brazil.
[*]Corresponding author: renan.og@posgrad.ufsc.br

1. Introduction

Solid lubrication is a fundamental protection and performance tool. Its use, however, is hindered in many cases due to the high costs of self-lubricant coatings and composites associated with complex manufacturing processes [1]. Furthermore, the main aspects that govern the tribological performance of solid lubricant nanoparticles in the macroscale remain largely uncharted due to the absence of quantitative comparison criteria and evaluation tools. Therefore, this work aimed to develop a simple, low-cost, robust and efficient method to deposit and evaluate solid lubricants nanoparticles in the macroscale. The effectiveness of the proposed methods was proven in a complete tribological investigation of steel tribopairs lubricated using graphene and novel carbide-derived-carbon (CDC) nanoparticles, showing an optimal topography and particle coverage to enable excellent tribological performance regarding both friction and wear.

2. Materials and method

The nanoparticles used were Ammonia functionalized multi-layer graphene (MLG) (HDPlas® - Graphene Supermarket) and CDC nanoparticles obtained via dissociation of Cr_3C_2 and B_4C (patented process). Specimens with different particle coverage were obtained by varying the total volume of nanoparticle solution (0.05wt.%) dispensed via drop-casting, with three levels of coverage: 4, 20 and 40 µl/cm².

The coverage obtained in each specimen was evaluated via BSE image analysis using a custom Python v3.0 script and via WLI with a protocol using the software MountainsMap® 7.4. Constant load reciprocating cylinder (SAE 52100 steel) on flat specimens (AISI 1020 steel) tests were performed with the following parameters: initial contact pressure of 154.3 MPa, 10 N normal load, 2 Hz frequency with 10 mm stroke (40 mm/s) and 1 h duration (144 m of sliding distance). Wear marks of tribosystems were investigated using SEM, OM, WLI, micro-Raman spectroscopy and EDS mapping. In addition, a novel Raman quantitative analysis was performed to determine the carbon-based materials crystallite size and point defects density.

3. Results and discussion

Figure 1 shows examples of techniques used to quantify nanoparticle coverage (WLI and BSE) as well as the quantitative Raman analysis (c) with the corresponding typical tribolayers (d).

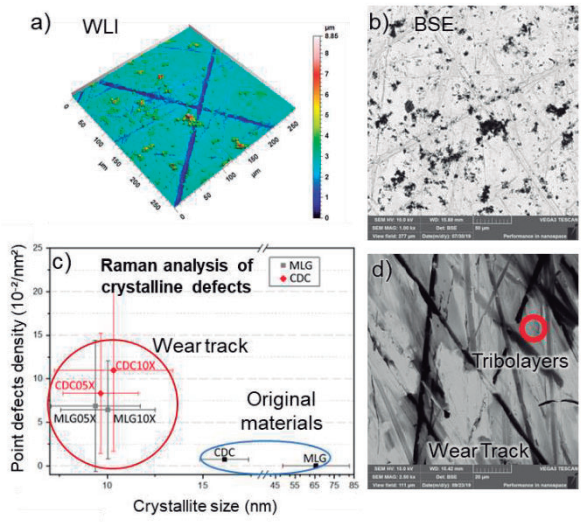

Figure 1. White light interferometry (WLI) (a) and Back-scattered electrons (BSE) (b) analysis. Quantitative Raman analysis in (c) and SEM analysis of wear track from constant load tests in (d).

4. Discussion

By using the drop-casting technique to precisely deposit nanoparticles together with the quantification methods, it was possible to determine a minimum amount of coverage to obtain the benefits of solid lubricant nanoparticles. Average friction coefficients of 0.09 for MLG and of 0.11 for CDC and immeasurable wear were found, with only mild topography modifications. Furthermore, quantitative Raman analysis showed that the tribolayers generated were similar regarding the disorder level (Figure 1(c)), despite the significant differences in original nanoparticles crystallite sizes.

5. References

[1] M. Marian, D. Berman, A. Rota, R.L. and Jackson, A. Rosenkranz, *Layered 2D Nanomaterials to Tailor Friction and Wear in Machine Elements—A Review*, Adv. Mater. Interfaces. 9 (2022) 1–19.

Analysis of rolling contact fatigue resistance in pearlitic and bainitic rail steel using twin-disc tests.

Moreno, S.[1)*], Tressia, G[1,2)], Souza, R.M.[1)] and Sinatora, A.[1,2)]

[1)] Laboratório de Fenômenos de Superfície, Escola Politécnica da Universidade de São Paulo, Departamento de Engenharia Mecânica, Av. Prof. Mello Moraes 2231, 05508-970, SP, Brazil
[2)] Instituto Tecnológico Vale, R. Prof. Paulo Magalhães Gomes s/n. Conjunto de laboratórios da Escola de Minas – UFOP, Morro do Cruzeiro, Ouro Preto MG, Brazil
[*]Corresponding author: samorenosa@usp.br

1. Introduction

In response to the increase of heavy haul railway operations, developers must improve not only the vehicle-track interaction but also rail-wheel interface [1]. In the rail-wheel interface due to the high contact pressure, and usual unlubricated excessive wear, many defects are developed in the rail and wheel. For this reason, studies have been carried out to improve the rail-wheel steel compositions and microstructures features [2]. To increase hardness and wear resistance, the chemical composition of the rails has been changed over the years, in particular the amounts of C have been increased. The increase in C promotes brittleness of the rail and difficulties in welding. An alternative is to work on heat treatments for rails with C between 0.7 wt.% and 0.8 wt.%, to promote microstructural changes, in particular obtaining lower bainite, to improve the hardness and other mechanical properties [3]. In this work, twin disc tests were performed, to compare the rolling contact fatigue and wear resistance of pearlitic and bainitic rail steel, with same chemical composition, under the following hypothesis: dry tangent track, pearlitic wheel and low creepage conditions.

2. Materials and methods

The specimens (discs) were manufactured from a pearlitic rail steel with composition presented in Table 1.

Table 1 Chemical composition.

(wt %)					
C	Si	Mn	Cr	P	S
0,79	0,24	1,06	0,32	0,017	0,01

Top of rail hardness measurements show values close to 387 ± 10 HV. Five discs were heat treated to obtain bainitic microstructure. This treatment was performed by heating up to 910 ºC for 1200 s and with 13 ºC/s cooling rate up to 450 ºC for 900 s, where the bainitic microstructure starts. This procedure was performed by TTT curves obtained earlier. The hardness of bainitic microstructure was on the order of 390 ± 11 HV. The twin disc test was carried out in a tribometer with the following settings (Table 2).

Table 2 Twin disc test settings

Parameter	Value	Unit
Contact Pressure	1420	Mpa
Angular velocity	382	RPM
Creepage	0,4	%
Load	2395	N
Cycles	300000	-

After tests, the analysis is going to divide in three sections, surface analysis, microstructure changes, RCF and wear behavior. In the surface analysis, more common defects will be identified, and roughness measurements will be done. To evaluate the RCF and wear behavior, the internal and external cracks will be measured. The angle and length of cracks turn to importance, since the mass loss due to spalling behavior, is governed by the direction of crack propagation [4]. At last, in the microstructure analysis the deformed and hardened zone will be measure for the purpose to understand which microstructure transform the contact energy better.

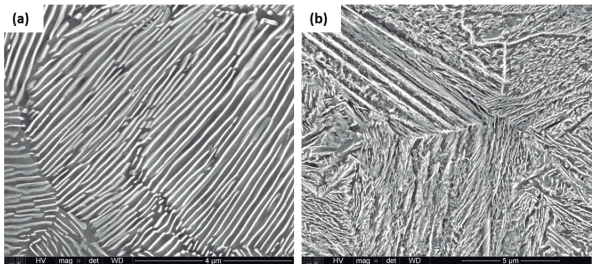

Figure 1. Microstructure observed in SEM of the (a) pearlitic steel and (b) bainitic steel.

3.References

[1] S. M. Zakharov, “F OR H EAVY H AUL R AILWAY O PERATIONS : Click Here to View Table of Contents,” no. May 2001, 2018.

[2] R. S. Miranda, A. B. Rezende, S. T. Fonseca, F. M. Fernandes, A. Sinatora, and P. R. Mei, “Fatigue and wear behavior of pearlitic and bainitic microstructures with the same chemical composition and hardness using twin-disc tests,” *Wear*, vol. 494–495, no. July 2021, p. 204253, 2022, doi: 10.1016/j.wear.2022.204253.

[3] G. Tressia and L. H. D. Alves, “Effect of bainitic transformation on the microstructure and wear resistance of pearlitic rail steel,” vol. 9, no. September, pp. 1095–1102, 2020, doi: 10.1108/ILT-07-2019-0282.

[4] R. C. Rocha, H. Ewald, A. B. Rezende, S. T. Fonseca, and P. R. Mei, “Using twin disc for applications in the railway: a systematic review,” *J. Brazilian Soc. Mech. Sci. Eng.*, vol. 45, no. 4, 2023, doi: 10.1007/s40430-023-04104-1.

Modeling of Non-metalic Inclusions effects on Rails Performance

Bortoleto, E.M.[1)*], Penagos, J.J.[1)] and Tressia, G.[1)]

[1)] Instituto Tecnológico Vale, Ouro Preto, Brazil
[*]Corresponding author: eleir.bortoleto@itv.org

1. Introduction

The material of rails has generally a pearlitic (or sometimes bainitic) structure, with a small content of cementite along the grain boundaries and trace amounts of non-metallic inclusions in the form of oxides and sulphides produced in the smelting process [1].

One of the factors influencing the strength parameters of rail steel is Sulphur, which can combine with Iron generating iron sulfide, a phase with low melting point, which can cause hot forming difficulties and ruptures. The addition of sufficient manganese prevents the formation of FeS and preferentially converts the sulfur to higher melting point manganese sulfides [2]. The presence of these non-metallic inclusions in the microstructure of rail steel is an important cause of fatigue-crack initiation in the material.

This work presents a finite element method (FEM) study of the contact between wheel and rail by evaluating the effects of the presence of non-metallic inclusions in the microstructure of rail steel. Different types of rail microstructures were evaluated in order to analyze the effects of type (oxide or MnS), size, density and distribution characteristics (depth from rail surface) of inclusions on the critical damage in rails. Microstructures with oxide and sulfide inclusions were modeled. The results reveal that crack initiation is more likely to occur at elongated MnS inclusions. Besides, this analysis may be the basis for the creation of some inspection criteria for rails.

2. Material and Methods

A finite element analysis was conducted to investigate the contact phenomenon of a rigid wheel over an elastic-plastic deformable rail, simulating the microscale deformation process near to the surface of a rail under rolling sliding contact loads and evaluating the material behavior of the rail by the presence of non-metallic inclusions. Rail surface is subjected to cyclic loading and strain is evaluated as a function of number of load cycles and elastic-plastic response of the rail material.

FEM meshes were generated based on material micrographs and the finite element solver Abaqus was used to model the wheel and rail contact interaction and the mechanical material behavior of the rail. Rolling contact fatigue was modeled by means of cracks nucleation and propagation at rail microstructure using eXtended Finite Element Method (XFEM) [3]. Figure 1 illustrates a micrograph that was transformed into a finite element method (FEM) mesh. Additionally, it is accompanied by an energy-dispersive X-ray spectroscopy (EDS) analysis of the manganese (Mn) inclusion.

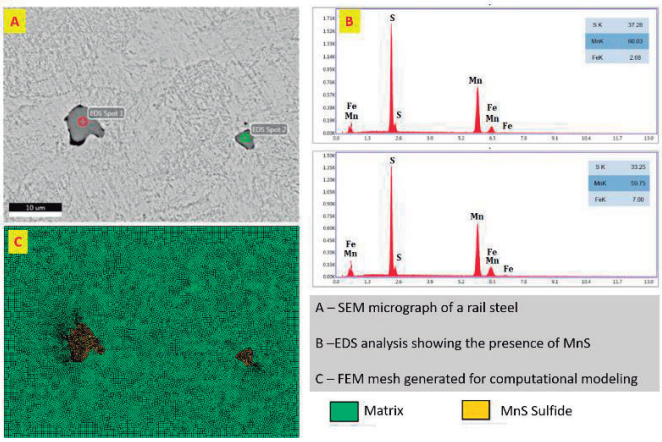

Figure 1 One of the typical micrographs (A) of MnS inclusions (B) and the FEM mesh generated for computational modeling (C).

Nanoindentation technique was applied to obtain mechanical properties values of non-metallic inclusions, which allowed the determination of hardness, elastic modulus, and other mechanical properties at the microscale, aiding in the understanding and characterization of their impact on material performance.

3. Results and Discussions

Nonmetallic inclusions act as stress concentrators since tensile strength is incompletely maintained within the inclusion. Inclusions affect mechanical properties by chemical composition, density, size, shape and distribution and contribute to the formation of microcracks after a large number of load cycles. The results reveal that crack initiation occurs at elongated inclusions. Inclusion shape control can reduce the aspect ratio of the manganese sulfides modifying its mechanical behavior [2].

4. References

[1] Mikłaszewicz Ireneusz, Czarnecki Marcin, 'A Cause for Cracking of Head-Check Rails', Materials Research Proceedings, Vol. 5, pp 11-16, 2018.
[2] J. Maciejewski, The Effects of Sulfide Inclusions on Mechanical Properties and Failures of Steel Components, J. Fail. Anal.Prev. 15 (2015) 169–178.
[3] Trolle B, Baietto MC, Gravouil A et al (2014) 2D fatigue crack propagation in rails taking into account actual plastic stresses. Eng Fract Mech 123(1):163–181.

Development of a High Temperature Friction and Wear Test in Liquid Lead Environment

Kolbas D.[1)*], Pelcastre L.[1)], Prakash B. [1)], Antti M-L. [2)], and Hardell J[1)].

[1)] Division of Machine Elements, Department of Engineering Sciences and Mathematics, Luleå University of Technology, Luleå, 971 87, Sweden
[2)] Division of Materials Science, Department of Engineering Sciences and Mathematics, Luleå University of Technology, Luleå, 971 87, Sweden
[*]Corresponding author: daria.kolbas@ltu.se

1. Introduction

The development of small lead-cooled nuclear reactors provides technical and scientific challenges such as the understanding, prevention, and prediction of the degradation of components in liquid lead. Critical components include the fuel rods, heat exchanger, and pump impeller. These functional elements are exposed to mechanical loading (up to 40 MPa), high temperatures (450–550 C°), and flow-induced vibrations (up to 25 Hz, amplitude about 100 µm) [1]. Under such conditions, fretting wear can occur between the spacer wire or supports and the outer surface of the fuel- or heat exchanger tubes. Due to the harsh operating environment, only few test rigs are available that enable tribological characterisation under liquid metal conditions. The aim of this work is to adapt an existing high temperature oscillating friction and wear tester, to enable the use of liquid metals as the test environment and assess the applicability of the developed methodology to study different materials and contact configurations.

2. Experimental techniques and materials

Modification of a high temperature reciprocating tribometer includes a liquid lead bath, oxygen concentration and temperature control sensors, and an atmosphere control system for providing a reducing atmosphere (95% Ar 5% H_2). Different surface roughness values were used for investigating the wettability of the steel surface by molten lead. Line and area contact configurations were evaluated to assess how lead enters the contact zone. Samples for experiments were made of stainless steel 316L and AISI 52100 bearing steel (100Cr6).

3. Salient results

The self-mated 316L tribo pair showed a friction level of 1.2±0.2 (Fig. 1) in line contact configuration. The significant standard deviation is explained by the influence of an initial sample waviness on the tribolayer formation and subsequent varying severity of adhesive wear. Using a self-mated 100Cr6 steel in line contact configuration resulted in COF level of 0.79±0.03 and changing the contact geometry from line to area contact increased the coefficient of friction by 46% (Fig. 1).

The dominant wear mechanism for both tested materials is adhesive wear. For the self-mated 316L tribo pair, the protruding load bearing areas show adhesive marks and the valleys in-between accumulated wear particles (Fig. 2 (a)).

The preliminary EDS analysis shows a considerable amount of lead on the worn surfaces for all tested contact configurations (Fig. 2 (b)) after dissolution. The study has shown that the test set-up enables tribological tests in liquid lead and the methodology provides repeatable friction and wear results.

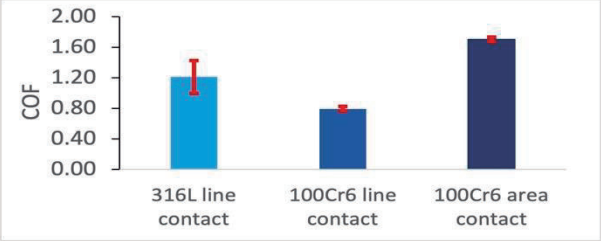

Figure 1 Steady-state average COF.

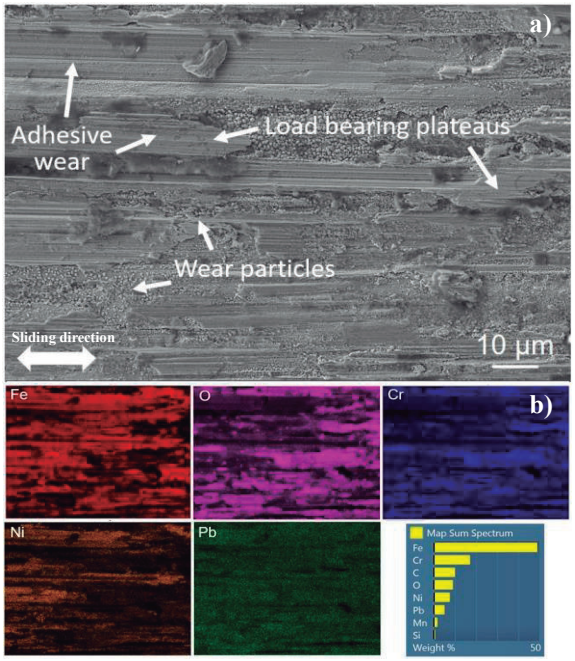

Figure 2 (a) SEM micrographs, (b) EDS map analysis and elemental spectrum of 316L disk.

4. References

[1] Lai, J., Sun, L., Li, P. et al. *Study on vortex-induced vibration of the tubes in a nuclear engineering test reactor*. Nucl. Eng. Des, 2014. 330: p. 391– 399.

Investigating Wheel-Rail Contact: An Integrated Approach of Experimental Measurements and FEM-Based Rail Wear Profile Modeling

Bortoleto, E.M.[1)*] and Tressia, G.[1)]

[1)] Instituto Tecnológico Vale, Ouro Preto, Brazil
*Corresponding author: eleir.bortoleto@itv.org

1. Introduction

Rail wear is a critical issue in railway operations, affecting safety, efficiency, and maintenance costs. Accurate prediction of rail wear can provide valuable insights for optimizing maintenance practices, prolonging the lifespan of rails, and reducing operational disruptions. In this context, this work presents a numerical model that aims to predict rail wear in railway operation, based on the linear Archard's wear law and finite element modeling (FEM). This computational study was carried out using finite element software Abaqus®, 3-D deformable geometries and elastic–plastic material properties, while Archard's wear model was implemented into a FORTRAN ad-hoc user subroutine (UMESHMOTION) in order to incorporate the rail wear profile computation in the numerical model [1]. The code incorporates adaptive mesh tools that reorganize local nodal positions to enable an incremental computation of surface wear based on nodal displacements.

The motivation behind developing this numerical model stems from the limitations of traditional empirical approaches, which often lack the ability to capture the complex dynamics and interactions involved in rail wear. The proposed numerical model utilizes finite element method (FEM) and considers various factors, including wheel-rail contact conditions [2], material properties, operating conditions (such as slip ratio and axel load), and maintenance strategies (e.g. rail grinding frequency and rail profile grinding). By accurately simulating the contact between the wheel and rail, the model can predict wear patterns, identify high-wear areas, and quantify wear rates under different operational scenarios. This information can assist railway operators in making informed decisions regarding maintenance scheduling, rail replacement, and optimizing maintenance interventions.

2. Materials and Methods

The geometry for FEM modeling considered a class C wheel with a diameter of 914 mm and a freight profile, along with a TR-68 rail type. The mesh employed for both components was carefully refined to accurately capture the contact and sliding regions, utilizing smaller elements in the contact area.

Material properties for the wheel and rail determined through experimental measurements, encompassing Elastic modulus, Poisson's ratio, hardness, and the friction coefficient.

To obtain precise and reliable measurements of the stresses experienced by the rail during train passage and the rail profile after usage, advanced instrumentation techniques such as strain gauges and 3D laser scanning were utilized. Rail wear was also obtained by hand-held measuring equipment called MiniProf. These experimental data serve as a benchmark for model calibration and facilitate the comparison of results obtained from FEM-based rail wear profile modeling.

The wear profile is predicted based on the accumulated contact stresses and sliding distances. In each time increment, the contact forces, contact area, and wear depth are recalculated and updated by considering the new surface profile resulting from the changes in nodal positions and element connectivity due to wear progression.

A sensitivity analysis was performed by varying the input parameters such as friction coefficient, material properties, and wear model parameters. The sensitivity of the wear profile to these parameters indicated that axel load and slip ratio are the critical factors influencing wear behavior.

3. Results

The comparison between the simulated wear profiles with experimental data from wear tests and field measurements profiles could validate the numerical model. The results showed that higher contact pressures, generated by higher axel loads, and higher slip ratios led to increased wear rates. The difference in load conditions due to track geometry are also important in rail wear [Figure 1]. Besides, the FEM model enabled the prediction of wear depth distribution along the rail.

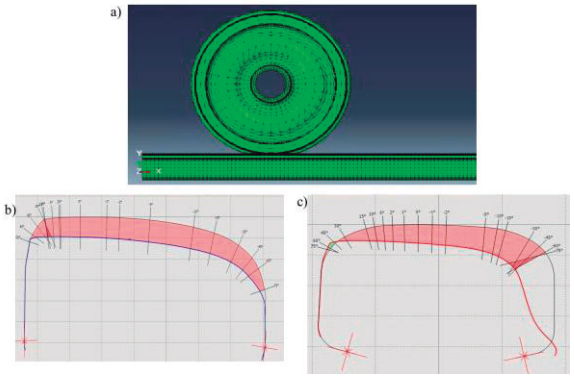

Figure 1 a) FEM mesh for wheel-rail contact modeling, b) wear in rail head generated in a straight rail track and c) gauge corner wear in a curve radius rail track.

4. References

[1] Bortoleto, E.; Rovani, A.; Seriacopi, V.; Profito, F.; Zachariadis, D.; Machado, I.; Sinatora, A.; Souza, R. Experimental and numerical analysis of dry contact in the pin on disc test. Wear 2013, 301, 19–26.
[2] Lewis, R., & Olofsson, U. (2004). Mapping rail wear regimes and transitions. Wear, 257(7–8), 721–729.

Investigation of the Evolution of Pores During Scuffing Resistance Tests Performed on Sintered Steel Vacuum Impregnated with Graphite

Araya, N.[1-2)*], Neves, G.O.[2-3)], Arenhart, R. [3)], Binder, C.[3)], Klein, A.N. [3)], de Mello, J.D.B.[3-4)].

[1)] Department of Materials Engineering, Concepcion University
Concepción, 4070 386, Chile
[2)] Department of Mechanical Engineering, Bio Bio University,
Concepción, 4081 112, Chile
[3)] Department of Mechanical Engineering, Santa Catarina Federal University,
Florianópolis, 88040 900, Brazil
[4)] College of Mechanical Engineering, Uberlândia Federal University,
Uberlandia, 38400 901, Brazil
*Corresponding author: nicolasiaraya@udec.cl

1. Introduction

Self-replenishable ways of applying solid lubrication in tribological systems are mainly limited to the use of self-lubricating composites produced by powder metallurgy by either mixing solid lubricant and metallic powders or producing the lubricating phase via in-situ reactions during sintering [1]. Impregnating the pores of sintered materials with solid lubricants is the only technique that allows studying the dynamic behaviour of the lubricant reservoirs without having to consider the thermodynamical interactions between the metallic phase and the lubricant during the sintering process, which drastically modifies the mechanical properties of the metallic phase as a function of the amount and nature of the solid lubricant used.

2. Experimental Procedure

In this work, mixtures of ASTALOY CRL and 0.6 wt.% C were pressed at 200, 400 and 600 MPa and then sintered for 1 hour at 1100 °C in an Ar/5 vol.% H_2 flowing atmosphere. The samples were then subjected to eight impregnation cycles using a dispersion of graphite powders (d50 = 1.10 µm) in acetone.

The impregnated specimens were subjected to scuffing resistance tests [2] using a reciprocating ball on flat configuration with a 10 mm diameter AISI 52100, a 10 mm stroke and a frequency of 2 Hz. The scuffing resistance tests started at a 7 N load with 7 N increments every 10 minutes and ended when the COF consistently surpassed the 0.2 threshold. The evolution of the size and morphology of the pores inside the wear scar was studied by performing several scuffing resistance tests that were paused at the end of each step before failure. Then the wear scars were observed using a Scanning Electron Microscope coupled with an EDS chemical analysis. A custom-made Python Image Analysis script was used to quantify the number, size and form factors as a function of the load during the scuffing resistance tests. Also, the dynamic wear rates during the tests were calculated by analysing the wear scars using White Light Interferometry.

3. Results and Discussion

A summary of the results of this work is shown in Figure 1. The image analysis showed that, the porosity inside the wear scars is reduced during the dry sliding process. In contrast, the number of pores remains stable due to the sealing process, which divides larger pores into smaller ones, reducing the size of pores but increasing their number. This process results in a stable wear rate as a function of porosity, except for highly porous specimens, which started with higher wear rates.

.

4. Conclusions

The main conclusion of this work is that during the sliding process, pores are sealed resulting in the reduction of the size of pores which in turns may prevent lubricant from being rapidly released from them which is favourable to maintain lubricity.

.

5. References

[1] Binder, C. et al., *'Fine tuned' steels point the way to a focused future.* Met. Powder Rep., 2010. **65**: 4.
[2] de Mello, J.D.B. and Binder, R., *A methodology to determine surface durability in multifunctional coatings applied to soft substrates.* Tribol. Int., 2006. **39**: 8.

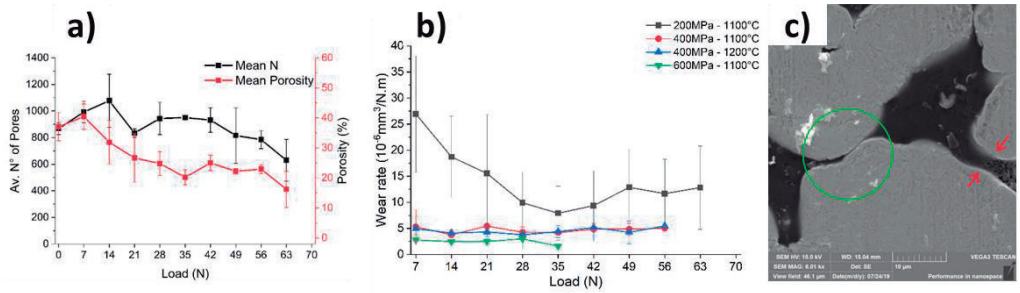

Figure 1- a) Evolution of number of pores and porosity inside the wear scars; b) Evolution of the wear rate as a function of load; c) Pore sealing phenomenon.

Abrasion resistance of FeCrCV coatings for tillage tools

Passos, T. A.[1,2)*], Costa, H.L[2)] and Pintaude, G.[1)]

[1)] Surface and Contact Laboratory, Universidade Tecnológica Federal do Paraná, Curitiba, 81280-340, Brazil
[2)] Surface Engineering Group, Universidade Federal do Rio Grande, Rio Grande, 96203-900, UK
[*]Corresponding author: tpassos@furg.br

1. Introduction

Fe-Cr-C-V coatings are commonly used to increase the abrasion resistance of tillage tools, commonly applied by arc transferred plasma (PTA) welding. Optimization of process parameters (current, voltage, powder feed rate and cooling rate) can help control the microstructure to achieve desired properties. PTA-welded Fe-Cr-C-V coatings exhibit better abrasion resistance due to the presence of hard carbides and hardened martensitic phase in the microstructure. Carbides, such as chromium carbides and vanadium carbides, are known for their high hardness, which helps reduce wear and increase coated tool life. The presence of martensite further increases the hardness and wear resistance of the coating. The precise abrasion resistance of PTA-welded Fe-Cr-C-V coatings can be influenced by factors such as coating thickness, carbide particle size, and overall microstructure. Fine carbide particles evenly distributed in the matrix and a well-controlled microstructure contribute to increased abrasion resistance. The specific composition and deposition parameters can be tailored to meet the specific requirements of preparation tools and optimize their performance in abrasive environments. This investigation characterized the microstructure of hardfacings made of Fe Cr C and vanadium concentration greater than 5%, deposited by PTA, in addition to evaluating the abrasive wear behavior of these coatings.

2. Methods

A welding equipment model IMC Digitec A7ACPO 450 was used at a flat position to produce Fe-Cr-C-V coatings onto A36 carbon steel plates (100mm x 200mm). Single-layer deposits were obtained using a 50% superimposition between individual beads, with a maximum temperature of the previous bead of 40°C. Two thickness values for the plates (12.5 and 25.4 mm) were used to vary the deposit cooling rate, monitored using thermocouples. Microhardness profiles, optical microscopy, and SEM/EDX investigated the microstructure of the deposits. Rubber-wheel abrasion tests evaluated the overlay wear rates using two severity conditions (A and D) defined in ASTM G65.

3. Results and discussion

Upon solidification, primary carbides rich in vanadium (yellow circles) are formed in a martensitic matrix (dark gray in Figure 1a). Solidification is likely to start with the formation of vanadium-rich primary carbides (yellow circles) followed by the formation of primary austenitic dendrites and transformed martensite laths after cooling. Figure 1b shows primary vanadium carbides (VC) more agglomerated when compared to Figure 1a. VC formation as spherical, petal-like particles and thin scale-like segments can be seen in Figure 1b, as reported in the literature [1]. Primary carbides were found in the 25.4 mm substrate coatings along with the coarse structure of vanadium carbides (marked as 1 and 3 in Figure 1b). The main difference in the microstructures is the appearance of coarser carbides in the coating deposited on the thicker plate. Particle dynamics during the abrasion test may have influenced the wear rate (Figure 2). Generally, when the normal load is higher, the load per particle is higher. It becomes more severe when the abrasive size is larger, since larger abrasives result in fewer particles in the contact and, thus, higher load per particle. For lower loads and/or finer abrasives, the load per abrasive is lower so that instead of the abrasives becoming fixed on the rubber and grooving the specimen surface, they remain as free particles rolling between the rubber and the surface, leading to multiple indentations. This micromechanism is less severe, often leading to lower wear rates [2].

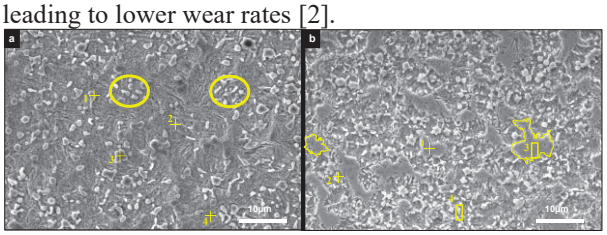

Figure 1 SEI SEM of Fe-CrC-V coating cross section (a) 12.5 mm thick substrate and (b) 25.4 mm thick substrate

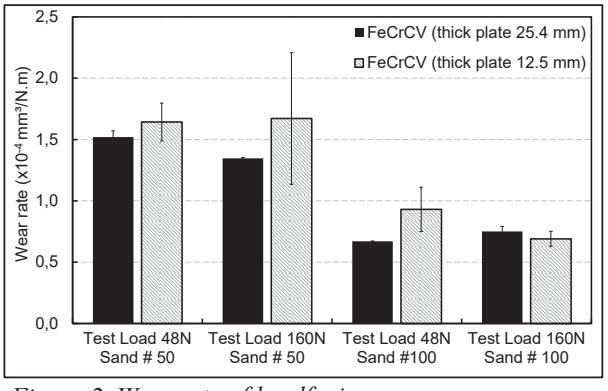

Figure 2 Wear rate of hardfacing

4. References

1. Takeda M, Mitome M, Hayakawa H, Nishiuchi S, Tanabe T, Yamamoto S. Morphology and crystallographic phase of V–C particles formed in Fe–Cr–Ni–V–C alloys. Materials Science and Technology. 2013;29(6):672-8.
2. Gates J. Two-body and three-body abrasion: a critical discussion. Wear. 1998;214(1):139-46.

True Atomic-Resolution Surface Imaging under Ambient Conditions via Conductive Atomic Force Microscopy

Baykara, M.Z.[1)*]

[1)] Department of Mechanical Engineering, University of California Merced, Merced, CA 95343, USA
[*]Corresponding author: mehmet.baykara@ucmerced.edu

1. Introduction

A great number of mechanical phenomena, including friction, are dictated by the atomic-scale structure and properties of material surfaces. Yet, the principal tools utilized to characterize surfaces at the atomic level rely on strict environmental conditions such as ultrahigh vacuum (UHV) and low temperature. Results obtained under such well-controlled, pristine conditions bear little relevance for the great majority of mechanical processes that often occur under ambient conditions. In this talk, we present conductive atomic force microscopy (C-AFM) as a powerful tool for the true atomic-resolution imaging of material surfaces, predominantly from the two-dimensional (2D) materials family, *under ambient conditions* [1]. We expect our C-AFM method to provide atomic-scale, fundamental information about surfaces that will be relevant for not only tribology, but all areas of science where surfaces play an important role.

2. Results

C-AFM, when applied under ambient conditions at high scanning speeds, provides true atomic-resolution images of material surfaces. As a representative example, Figure 1 shows two images where a cluster of sulfur vacancies and a single sulfur vacancy are detected on a flake of MoS_2 that has been exfoliated from the bulk onto a SiO_2 substrate. The capability of imaging a single atomic vacancy proves that the method achieves ultimate, i.e. true atomic resolution. Going one step further, Figure 2 shows a C-AFM image that has been acquired on a thin crystal of Mo_2C, a member of the emerging transition metal carbide (TMC) material family. The image not only shows an atomic-scale background with a periodicity of 2.2 Å but also an additional modulation with larger periodicity (11.4 Å) on top of the atomic lattice. The latter feature is indicative of *charge ordering*, the first instance where such an exotic electronic phenomenon has been observed at room temperature on a TMC.

In order to explore the physical mechanisms behind the atomic-resolution imaging capabilities of C-AFM, a number of experiments with varying operational parameters were performed. By way of such a systematic procedure, it was determined that scanning speed played a key factor in atomic-resolution imaging, as only images recorded at tens of nm/s featured robust atomic-scale data. Additional experiments are underway to pinpoint exactly why high scanning speeds are a pre-requisite for atomic-scale imaging.

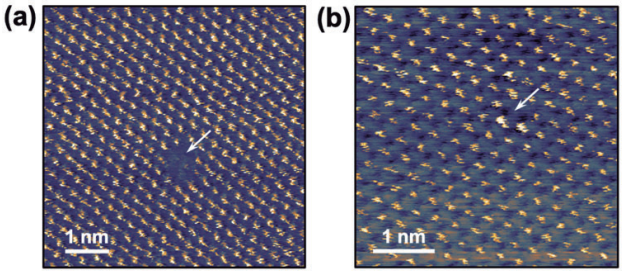

Figure 1 Atomic-resolution images recorded on MoS_2 via C-AFM under ambient conditions. While (a) shows a cluster of sulfur vacancies on the surface, (b) demonstrates the capability of our method to resolve a single atomic vacancy.

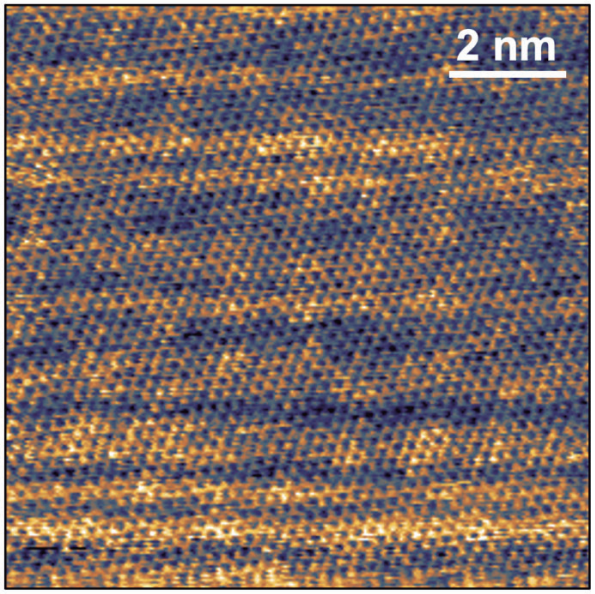

Figure 2 An atomic-resolution image recorded on a thin crystal of Mo_2C via C-AFM under ambient conditions. While the atomic-scale background is clearly visible, the image is modulated by a super-structure that is indicative of room-temperature charge ordering.

3. References

[1] Sumaiya, S.A., Liu, J. and Baykara, M.Z., *True Atomic-Resolution Surface Imaging and Manipulation under Ambient Conditions via Conductive Atomic Force Microscopy.* ACS Nano, 2022. **16**: 20086-93.

Investigating Topography Effects on Tribological Performance of Graphite Nanoparticles Deposited by Drop-Casting

Pires, J.A.[1)*], Salvaro, D.B.[1)] Klein, A.N.[1)], de Mello, J.D.B.[2)]

[1)] Department of Mechanical Engineering, Universidade Federal de Santa Catarina, Florianópolis, 88040-900, Brazil
[2)] Department of Mechanical Engineering, Universidade Federal de Uberlandia, Uberlândia, 38400 901, Brazil
[*]Corresponding author: julia.a.f@labmat.ufsc.br

1. Introduction

Solid lubricant nanoparticles can provide lubrication as an additive in oil-lubricant, impregnated in sintered material porosity, or deposited on the surface [1,2,3]. Their interaction with topography is a key point to nanolubricants performance since it defines how the nanoparticles will be available on the surface, and the predominant effects that will govern the lubrication process like shearing, rolling, polishing, and mending. [4]. This study evaluated the effect of topography on the tribological performance of carbide-derived carbon nanoparticles applied by drop-casting on the metallic surface.

2. Methodology

Cylindrical specimens (Ø=20mm h=15mm) of AISI 1020 steel were ground (flat surface) to obtain three different topographies (mesh 80, 600, and 1200). Then, carbide-derived carbon (CDC) nanoparticles were deposited on the surfaces by the drop-casting process. The roughness and particles distribution on the surface and its correlation with the topography were evaluated via optical interferometry (WLI) and SEM. Cylinder-on-flat (line contact) reciprocating tribological tests were carried out in two modes using the parameters in Table 1: i) scuffing resistance (incremental normal load of 7N each 10 min), ii) constant normal load of 14 N for 30 min to determine the friction coefficient and wear.

Table 1: Tribological test parameters

Stroke	10 mm
Frequency	2 Hz
Atmosphere	Ambient
Temperature	23 °C
Humidity	30%
Counter-body	AISI 52100 cylinder

Wear scars were analyzed by WLI, SEM, EDS, and Raman spectroscopy to quantify the wear and elucidate the wear mechanisms.

3. Results

The specimens' name is associated with the sandpaper used to produce the roughness, therefore the specimens 80, 600, and 1200 presented Sq values of 0.59, 0.07, and 0.04µm respectively. Figure 1 shows that the rougher surface induces a very low friction coefficient (0.07) and outstanding scuffing resistance followed by specimens 600 and 1200.

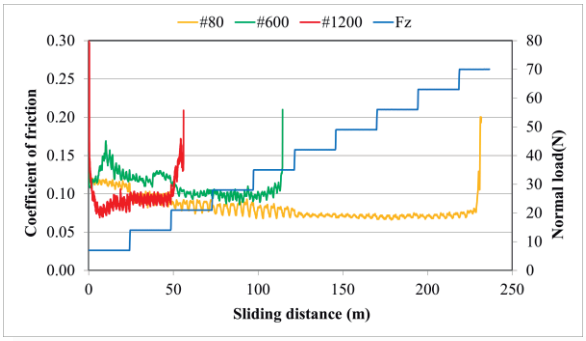

Figure 1: Typical results from scuffing resistance tests.

The rougher topography presents a reduced solid lubricant "available" in the contact at the beginning of tribological tests (0.05µm³/µm²) because the valleys work as reservoirs providing solid lubricant to tribological contact (Figure 2). Thus, graphite-rich tribolayers are formed enhancing the scuffing resistance. Additionally, in the constant normal load test, it was observed that the rougher surface displayed a lower friction coefficient of 0.09 followed by 1200 (0.12) and 600 (0.19) specimens.

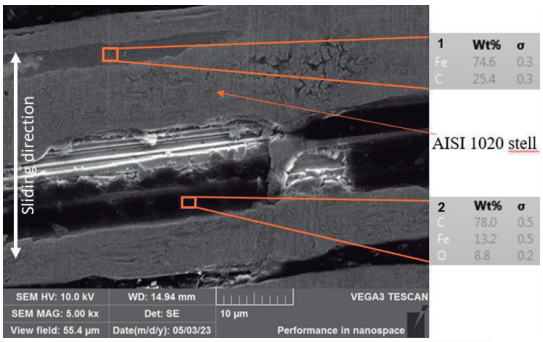

Figure 2: Wear mark on the specimen 80.

4. Conclusions

In contrast to the smoother surfaces (600 and 1200), the rougher surface exhibited higher scuffing resistance. This can be attributed to their ability to retain particles in the valleys as reservoirs, which contributes to the formation of benefic tribolayers.

5. References

[1] Bordignon, R; et al. https://doi.org/10.1007/s11249-018-1065-3.
[2] Binder, C; et al. https://doi.org/10.1016/j.carbon. 2017. 09 .036
[3] Salvaro, D. B; et al. http://dx.doi.org/10.1016/j. jmrt.20 15.10.008.
[4] Dai, W.; et al. https://doi.org/10.1016/j.triboint.20 16.05.020

Deterministic Asperity-Based Elastic-Plastic Rough Contact Model

Queiróz, J.C.[1)*] and Profito, F.J[1)]

[1)] Department of Mechanical Engineering, Polytechnic School of University of Sao Paulo, Sao Paulo, Brazil
*Corresponding author: jcqueiroz@usp.br

1. Introduction

Contact mechanics modelling of rough surfaces is still challenging due to the multi-scale nature of actual surface topographies and the consideration of inhomogeneous and nonlinear material behaviour, adhesion effect and damage evolution in advanced models. Furthermore, despite last decade's advances in modelling approaches, numerical methods and computation power, the computational effort required to predict the contact behaviour of rough surfaces is still prohibitive during usual engineering design processes [1-3]. Recently, Wen et al. [4] proposed an efficient asperity-based contact model involving morphological segmentation, geometrical fitting of asperities into ellipsoidal shapes, and elastoplastic material behavior. To enhance this model, we introduce a refined surface segmentation using a watershed algorithm controlled by the h-min transform to identify asperities accurately. Furthermore, we improve the asperity fitting process using elliptic paraboloid functions. These advancements enable efficient deterministic elastic-plastic contact simulations of rough surfaces.

2. Methodology

The segmentation process was compared and validated against the standard Wolf pruning methodology [5]. Figure 1 shows the result of a segmented region compared to the original view.

Afterwards, each asperity was fitted to an elliptic paraboloid function. Compared to the ellipsoidal shape used by Wen et al. [4] (see Figure 2), the new elliptic paraboloid fitting presents better metrics (e.g., *R², MSE and MAE*). Table 1 exhibits the average of these metrics for all asperities of the same surface.

Finally, according to the curvature radii of each asperity, it is possible to calculate the real contact area and contact pressure using a semi-analytic elastoplastic contact model with high accuracy and low computational cost compared with existing methods. Figure 3 shows the variation of the dimensionless contact pressure with the interference of a single asperity.

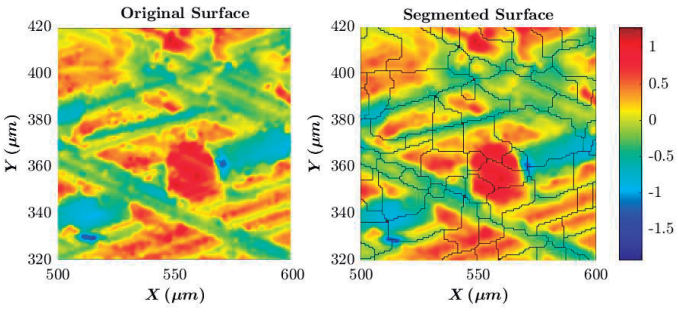

Figure 1. Morphological Segmentation result.

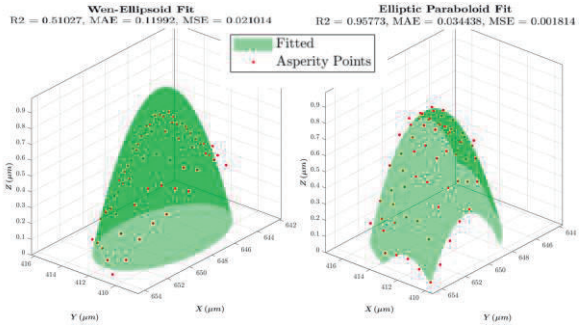

Figure 2. Asperity fitting comparison.

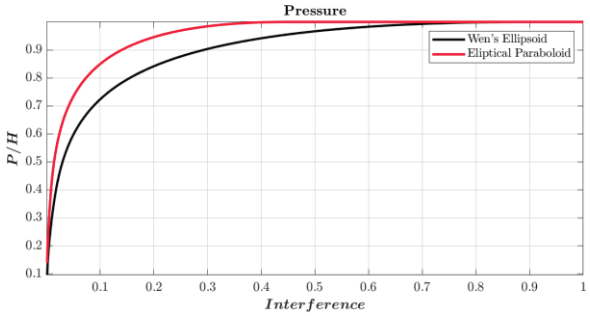

Figure 3. Development of dimensionless rough contact pressure.

Table 1. Fitting Metrics

Method	R²	MSE	MAE
Wen's Ellipsoid [4]	0.042	0.066	0.184
New Elliptic Paraboloid	0.808	0.012	0.078

3. References

[1]. Kogut L and Etsion I. A finite element based elastic–plastic model for the contact of rough surfaces. Tribol Trans 2003; 46: 383–390.

[2] Jamari J and Schipper DJ. An elastic–plastic contact model of ellipsoid bodies. Tribol Lett 2006; 21: 262–271.

[3] Wen, Yuqin, et al. "A new elliptical microcontact model considering elastoplastic deformation." *Proceedinof the Institution of Mechanical Engineers, Part J: Journal of Engineering Tribology* 232.11 (2018): 1352-1364.

[4] Wen, Yuqin, et al. "A reconstruction and contact analysis method of three-dimensional rough surface based on ellipsoidal asperity." *Journal of Tribology* 142.4 (2020): 041502.

[5] ISO 16610-85: 2013-02. "Geometrical Product Specifications (GPS)—Filtration—Part 85: Morphological Areal Filters: Segmentation (ISO 16610-85: 2013)." (2013).

Influence of Surface Texturing on Chrome-coated Cylinder Liners via Deterministic Mixed Lubrication Simulation

Silva, S. A. N.[1)*], Profito, F.J.[2)], Costa, H.L[1,3)]

[1)] Mechanical Engineering Department, Universidade Federal de Uberlandia, Uberlandia, 38408 144, Brazil
[2)]Mechanical Engineering Department, Universidade de Sao Paulo, Sao Paulo, 05508 030, Brazil
[3)] School of Engineering, Universidade Federal do Rio Grande, Rio Grande, 96083 040, Brazil
[*]Corresponding author: snunesilva@gmail.com

1. Introduction

The primary goal of this study is to evaluate if deterministic surface texturing with a pattern of dimples can improve the tribological performance of cylinder liners used in two-stroke engines. The liners investigated possess noticeable superficial porosity due their coating with hard chrome. Two types of surface finish are used: honing and deterministic texturing.

A deterministic simulation analysis of mixed lubrication is conducted. It utilizes the modified Reynolds equation, as suggested by Elrod-Adams, to calculate the scaled hydrodynamic pressure (HP) and scaled hydrodynamic shear stress (HSS). Additionally, the simulation employs the Li and Chen approach to assess the contact roughness model for Twin Land Oil Control Rings and obtain the asperity contact curves [1].

2. Surfaces

Figure 1 illustrates the texture of the honed surface (1.a), referred to as S_B, which is derived from a chrome coating, resulting in micro-surface porosities. After a conventional honing surface finishing step, S_B exhibits rather smooth regions (plateaus) and randomly distributed micro-cavities resulting from the pores. The second surface (1.b), denoted as S_O, initially shares a similar pattern with S_B and is subjected to a deterministic texturing process using micro-electrical discharges to create a pattern of deterministic dimples.

3. Results

Figure 2 presents the average results from the numeric simulations in terms of hydrodynamic pressure, hydrodynamic shear stress, asperity contact pressure and asperity shear stress for different lambda parameter values (Λ), varying from boundary to full film lubrication. It is evident that the SB surfaces exhibit higher hydrodynamic pressures in the range of $0 \leq \Lambda \geq 3$, as well as lower contact asperity pressure and contact shear stresses. This effect is achieved by physically removing the highest peaks through honing. In contrast, the S_O surface demonstrates lower HSS. This occurs because the reduced surface roughness minimizes flow disruptions and promotes smoother fluid movement, resulting in increased pressure. Similarly, a smoother surface can also lead to higher hydrodynamic shear stress, as the fluid experiences less resistance when flowing over a smoother surface. These observations imply that the S_B surface is well-suited for minimizing wear in the Top Dead Centre and Bottom Dead Centre regions, while a textured surface is recommended for the central region to reduce fuel consumption.

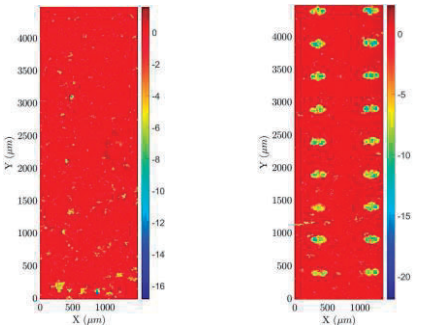

(a) S_B surface (b) S_O surface

Figure 1 - Textured surfaces

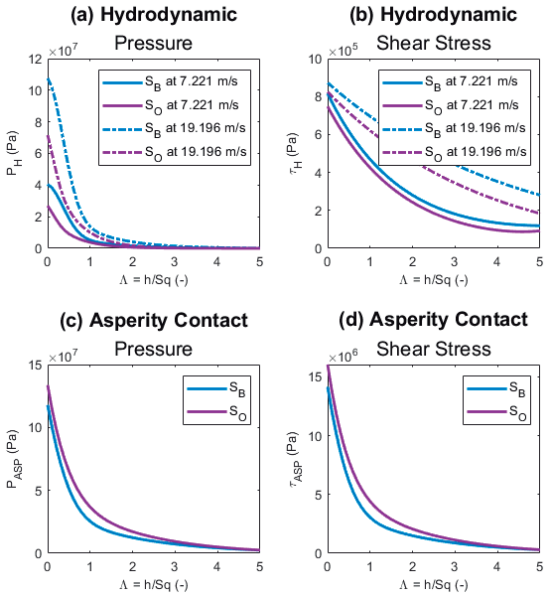

Figure 2 Deterministic simulation's results

4. References

[1] Profito, F.J., E. Tomanik, and D.C. Zachariadis *Effect of cylinder liner wear on the mixed lubrication regime of TLOCRs.* Tribology International, 2015. **93**: p. 723-732.

AI-Driven tribological approach applied to on-machine surface roughness prediction

Knoblauch, R.[1,2)*], El Mansori, M.[1,2)], Ghosh, S. [1)] and Corleto, C.[3)]

[1)] Arts et Metiers Institute of Technology, MSMP, HESAM Universite, Aix-en-Provence, France
[2)] Texas A&M Engineering Experiment Station, College Station, TX 77843, USA
[3)] Stil Marposs, Domaine Saint Hilaire, 595 Rue Pierre Berthier, Aix-en-Provence, France
*Corresponding author: ricardo.knoblauch@ensam.eu

1. Introduction

Manufacturing of precision parts plays a vital role in the global economy, and the integration of Artificial Intelligence (AI) into tribology, known as Triboinformatics, is a recent approach that can be used to better understand manufacturing processes. Through the sensorization of machine tools, one can obtain rich datasets to gain deeper insights into the machining process, chip formation, and cutting phenomena. With a final goal of driving a more sustainable manufacturing sector by reducing part scrapping due to machined surface quality issues, this work proposes the implementation of on-machine sensors for surface quality assessment, in order to acquire a database for developing a Machine Learning (ML) model to predict machined surface roughness considering tribological aspects involved in the cutting process.

Prediction of surface roughness in machining has been addressed in many works in the past decades, and recently AI models have been taking the place of former traditional methods such as simulation, statistical, and linear/polynomial regression methods. AI-based models of roughness prediction are described in the literature [1,2], but they cover only contact-type profilometers, they do not consider different cutting modes, nor tribological aspects of the cut.

Among various surface roughness measurement methods, the Chromatic Confocal (CC) exhibits particular advantages: non-contact, avoiding surface damage; good range (total roughness down to 0.1 µm); capability of measuring dimensions and texture; fairly rapid measurement speed, and significant easiness of integration into industrial machine tools [3]. Based on that, the CC was the measuring method selected to be applied on-machine in this work, to make the proposed approach more suitable for a future implementation in an industrial setting.

1.1. Objectives

The primary objectives are twofold: i) to investigate the effects of different cutting modes, namely up milling and down milling, on forces and surface roughness; ii) to leverage AI techniques, starting from feature selection (Principal Component Analysis and Correlation Matrices), followed by an ML prediction model, in order to elucidate the correlation between surface roughness and cutting mode.

2. Methodology

In this study, a mill-turn machine tool was equipped with a non-contact CC sensor CL1-MG210, and a Kistler dynamometer for active and normal force measurement in face milling of Aluminum 2017A, Figure 1 . In total, 250 cutting conditions were performed to generate a database for ML training.

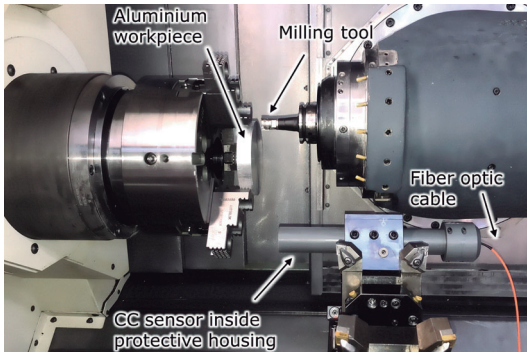

Figure 1 Experimental setup.

3. Conclusion

Experimental cuts were conducted under up and down milling, while on-machine force and surface quality data were recorded. The analysis focuses on the COF (Coefficient of Friction) to discern variations in chip formation between the two cutting modes, as up milling initiates chip formation with substantial friction and limited cutting depth, while down milling initiates chip formation at greater cutting depths, displaying lower initial friction. To gain deeper insights and interpret the data, ML models are trained for the prediction of surface roughness based on input cutting parameters, cutting forces, and COFs.

4. References

[1] Leco, M. and V. Kadirkamanathan, *A perturbation signal based data-driven Gaussian process regression model for in-process part quality prediction in robotic countersinking operations*. Robot. Comput. Integr. Manuf., 2021, **71**: p. 102-105.
[2] Kong, D., J. Zhu, C. Duan, L. Lu, and D. Chen, *Bayesian linear regression for surface roughness prediction*. Mech. Syst. Signal Process., 2020. **142**: p. 106-770.
[3] Minoni, U. and F. Cavalli, *Surface quality control device for on-line applications.* Meas. J. Int. Meas. Confed., 2008. 41: p. 774–782.

Friction and Wear Analysis: How to face new challenges.

Mohamadou DIEW, Dr.[1], Melinda Bullaro [1], Damien Khoo[1], Udo Volz, Dr. [1],

[1]Bruker Nano Surfaces and Metrology

To analyze and improve the tribological contacts through the design, the materials, the lubricant and /or surfaces, Tribologists deal in transportation but not only with many factors that can affect the contact friction, wear, and electrical behavior. Define the right material, coating, surface roughness, and lubricant with the properties allowing to have a great lifetime are a real challenge. Engineers need to design a representative test allowing to solve issues that was cheaper and reliable compared to a real bench test, less time consuming to build test and the easiest way to understand the tribological behavior of materials for all tribosystems. For this purpose, the Bruker TriboLab™ series are designed with various setups that enable a deep analysis of the Friction and Wear through materials, lubricants, and surface topography. With the ability of using different types of motions, loads, surface contacts, temperature, and ambient conditions, I will present TriboLab™ how useful is to reproduce the real tribosystems through lab scale sample and to characterize the wear using 3D Surface analysis.

Tribological characterization of laser cladding deposited stellite 6 coatings

Viridiana Humarán-Sarmiento [1,2)*], Juan Manuel González-Carmona [1)], Ángel-Iván García-Moreno[1)]

[1)] Centro de Ingeniería y Desarrollo Industrial, Av. Playa Pie de la Cuesta No. 702, Desarrollo San Pablo, C.P. 76125, Santiago de Querétaro, Querétaro, México.
[2)] Instituto Tecnológico Superior de Guasave, Carr. Internacional entronque a la Brecha S/N, Ej. Burrioncito, C.P. 81149, Guasave, Sinaloa, México.
[*]Corresponding author: v.humaran@posgrado.cidesi.edu.mx, viridiana.hs@guasave.tecnm.mx

1. Introduction

Nowadays, the use of additive manufacturing technologies is important to fabricate coatings with higher tribological performance in industrial processes and contribute to the reduction of energy consumption [1], [2]. The present work assess friction and wear tests on Laser Cladding coatings at room temperature for metal-mechanical applications. Coatings were cladd with different parameters (laser power, robot speed, and mass flow rate) of Cobalt-based powder metal (Stellite 6) on SS304 substrate and tribologically evaluated with a scratch test on zircon ball of 6mm. Wear rates and friction coefficients were obtained at 5000, 12500 and 20000 cycles, which will serve as output data to train a prediction model using supervised machine learning.

Keywords: Láser cladding, wear rate, coefficient of friction, stellite 6.

2. Materials and Methods

Part of the materials and methods used are shown. Figure 1 shows a sample of a coating scratched at different cycles. Table 1 shows the conditions and parameters of the friction wear study.

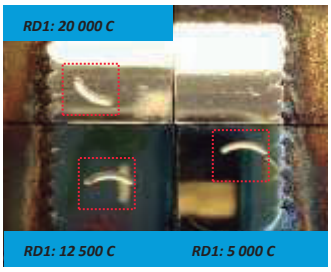

Figure 1 Sample RD1 with traces of wear

Table 1 Tribological conditions and parameters

Tribology conditions	
Aplication	Cutting die
Motion type	Reciprocating
Pair	Stellite 6
Counterpart	Zirconía/Itria (ZRO2(Y)), spheres of 5 mm
Lubrication	No
Parameters	***Value***
Load	10 N
Contact stress	1648.7 Mpa
L1 (5000 Cycles)	*Velocity:* 1,3203 cm/s *Distance:* 42,03 m
L2 (12500 Cycles)	*Velocity:*1,3203 cm/s *Distance:* 105,07 m
L3 (20000 Cycles)	*Velocity:* 1,3203 cm/s *Distance: 167,55* m
Angle	80 °
Radius	3,01 mm
Frequency	1 Hz

3. Results

Figure 2 shows a graph of the coefficients of friction obtained for 20000 cycles of the RD sample. Table 2 shows the numerical values of the wear rate and friction coefficient.

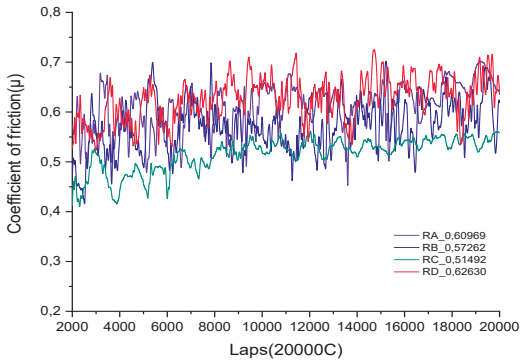

Figure 2 Coefficients of friction for samples RA, RB, RC, RD_20000 Cycles

Table 2 Wear rate and coefficient of friction

Sample	*Wear Rate (mm^3/Nm)*	*Coefficient of friction (μ)*
RA_5000	**3,94E-05**	**0,60238**
RA_12500	**1,33E-05**	**0,54323**
RA_20000	**1,02E-05**	**0,60969**
RB_5000C	**5,28E-05**	**0,47939**
RB_12500C	**1,82E-05**	**0,64453**
RB_20000C	**2,00E-05**	**0,57262**
RC_5000C	**6,03E-05**	**0,60281**
RC_12500C	**1,27E-05**	**0,59614**
RC_20000C	**1,29E-05**	**0,51492**
RD_5000C	**4,74E-05**	**0,53796**
RD_12500C	**2,15E-05**	**0,58964**
RD_20000C	**1,27E-05**	**0,6263**

4. References

[1] Anitesh Kumar, *An approach towards energy and material efficient additive manufacturing: Multi-objective optimization of stellite-6 deposition on SS304, (*2022), Optics and Laser Technology.
[2] Teng Wu, *Effect of Preheating Temperature on Geometry and Mechanical Properties of Laser Cladding-Based Stellite 6/WC Coating, (*2022), Materials.

Tribological behavior of duplex CrN/DLC and nanoscale multilayer DLC-W coatings at elevated temperatures

Funsho Olaitan Kolawole[1,2], Shola Kolade Kolawole[3], Newton Kiyoshi Fukumasu[4], Paulo Konrad Vencovsky[5], Danilo Assad Ludewigs[5], Roberto Martins de Souza[4], André Paulo Tschiptschin[1]

[1] Metallurgical and Materials Engineering Department, University of São Paulo, São Paulo, SP, Brazil
[2]Department of Materials and Metallurgical Engineering, Federal University, Oye-Ekiti, Nigeria.
[3]National Agency for Science and Engineering Infrastructure, Abuja, Nigeria
[4] Surface Phenomena Laboratory, Polytechnic School of the University of Sao Paulo, Sao Paulo, Brazil.

1. Introduction

Diamond-like carbon (DLC) coatings has been used due to their environmentally friendly behavior, inert, ultralow friction, mechanical (high hardness and elastic modulus) and excellent tribological properties (wear and friction) above room temperatures [1, 2–4]. However, there are challenges when been applied to automobile parts. The use of interlayer and metallic doping are the methods used to improve the adhesion properties of DLC coatings, which will in turn circumvent the problems related to moderate temperatures tribological behaviour of DLC. Different deposition methods and variation in deposition parameter, varies the properties of DLC. Hence, the need to study various deposition methods to produce DLC coatings that would overcome problems caused by adhesion of DLC on metallic substrate. Hybrid combination of these deposition method for depositing CrN/DLC and DLC-W is likely to produce coatings with excellent mechanical and tribological properties. The present research investigates the tribological behavior above room temperature of CrN/DLC and DLC-W coatings deposited on valve tappets using hybrid Physical Vapour Deposition (PVD) and Plasma Enhanced Chemical Vapour Deposition (PECVD).

2. Methodology

16MnCr5 920 HV martensitic valve tappets were coated in a hybrid (PVD) / (PECVD) reactor. Two coating systems were compared: duplex CrN/DLC and nanostructured multilayer DLC-W. Structural and mechanical characterization of the coatings were carried out by SEM, TEM, Raman spectroscopy and nanoindentation. Elevated temperatures reciprocating wear tests were carried out with a ball on plane configuration in an Optimol SRV® equipment, under dry condition at 25 ºC, 150 ºC, 200 ºC and 250 ºC. The testing conditions were 20 N load, 30 min, 10 Hz and a 2 mm stroke. The wear tracks were observed by SEM and EDS. The wear volumes were measured in a 3D – CCI - Taylor Hobson profilometer. The structure and mechanical properties inside the wear track were evaluated using Raman spectroscopy and nanoindentation respectively.

3. Results

The CrN/DLC coating has a duplex layer coating architecture, with an underlying 0.35-µm thick Cr adhesive layer, followed by a 0.75 µm CrN reinforcing layer and finally, a 1.85 µm thick DLC layer, total thickness of 2.95 µm. The DLC-W coating is preceded by a WC adhesion interlayer 0.58 µm. The DLC-W coating is 6 µm thick, shows a multilayer columnar structure with a 6.58 µm total thickness.

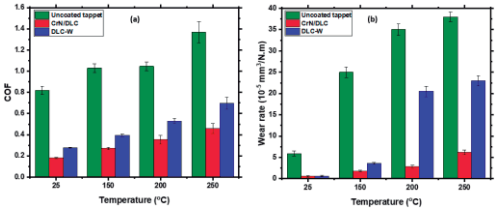

Figure 1 - Friction coefficients and wear rates for both coatings at 25, 150, 200 and 250°C.

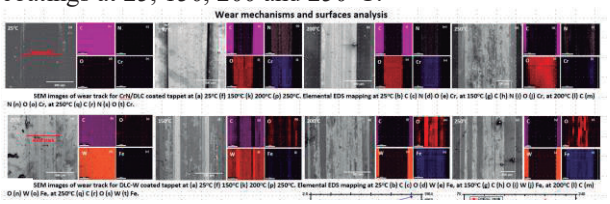

Figure 2 - SEM images and EDS mapping of the wear tracks of both coatings at 25, 150, 200 and 250°C.

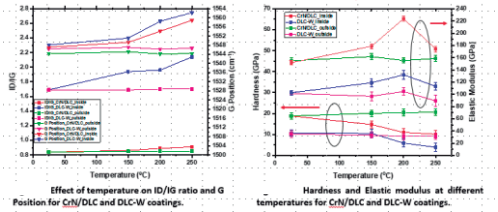

Figure 3 - Id/Ig ratio, hardness and reduced elastiuc module of both coatings as afunction of the tesing temperature.

4. Discussion

The obtained results are discussed for understanding the wear mechanisms acting during the reciprocating wear tests. The CrN/DLC coating presented the lowest wear rates during the sliding reciprocating tests at 25ºC. The wear rates increase with increasing temperature, but always remained lower in comparison with the DLC-W coating.

5. References

[1] K. Holmberg, P. Andersson, and A. Erdemir, "Global energy consumption due to friction in passenger cars," Tribol. Int., vol. 47, pp. 221–234, 2012, doi: 10.1016/j.triboint.2011.11.022.
[2] A. Erdemir and C. Donnet, "Tribology of diamond-like carbon films: Recent progress and future prospects," J. Phys. D. Appl. Phys., vol. 39, no. 18, 2006, doi: 10.1088/0022-3727/39/18/R01.
[3] J. Robertson, "Diamond-like amorphous carbon," Mater. Sci. Eng. R Reports, vol. 37, no. 4–6, pp. 129–281, 2002, doi: 10.1016/s0927-796x(02)00005-0.
[4] P. A. Dearnley et al., "Coatings tribology drivers for high density plasma technologies," Surf. Eng., vol. 26, no. 1–2, pp. 80–96, 2010,

Effect of heat input on ultrahard Fe-Cr-B-C-W-Mo-Nb hardfacing

Gramajo, J.[1)*], Gualco, A.[2)] and Svoboda, H.[3)]

[1)] Institute of Materials Science and Technology (ICyTM), Faculty of Engineering UNLZ, Buenos Aires Buenos Aires, Argentina
[2)] CONICET, Av. Godoy Cruz 2290, C.A.B.A., Argentina
[3)] GTSyCM3, INTECIN, Faculty of Engineering - UBA. Av. Las Heras 2214 (1427), CABA, Argentina
[*]Corresponding author: nahuel_jona@yahoo.com.ar

1. Introduction

Iron based multicomponents alloys containing niobium (Nb), chromium, (Cr), molybdenum (Mo), and tungsten (W) in combination with boron (B) and carbon have been designing for hardfacing application due to their high hardness and wear applications, using electric arc welding processes [1]. Heat input is controlled by electrical parameters and welding speed (WS). This last defines the productivity of hardfacing applications. High deposition rates, low dilutions and high hardness are the basic requirements to maximize application costs [2]. Some nanostructured alloy deposits were produced by this technique. Samples with lower dilution and higher cooling rates showed finer and harder structures. However, the information available on the welding of the new Fe-based multicomponent systems is scarce, so it is relevant to analyze the effect of heat input on the chemical composition, metallurgy, hardness and wear properties of the weld deposited metal.

In this work, single layer samples were made using between 4 and 7 beads with an overlap of approximately 50%. The consumable used was a tubular wire (Fe-16Cr-1C-4B-5W-4.2Mo-6Nb), deposited using semi-automatic welding process under gaseous protection of Ar-20%CO_2. The welding parameters used can be seen in Table 1, as well as the identification used.

Table 1 Welding Parameters

Sample	Voltage (V)	Current (A)	WS (mm/s)	Heat Input (kJ/m)
1	26	200	1,3	4.0
2.5	26	200	2,5	2.0
5	26	200	5	1.0
12	26	200	12	0.4

The microstructure was characterized on cross sections of weld deposits by X-ray diffraction and scanning electron microscopy. Dilution percentage was determined, and Vickers microhardness profiles (HV2) were made, as well as measurements on the different phases (HV 0,025). The abrasion wear tests were carried out in accordance with the ASTM G65-04 "Dry Sand / Rubber Wheel" standard, according to method A.

The microestructure was formed by elongated carboborides type $(FeCr)_2(BC)$, WC and a eutectic, which is formed by flat and globular carboborides of the type (FeCr)23(BC)6 and α'-Fe matrix. The increase of heat input (reducing welding speed) produced an increase in the size of the phases. The microhardness of the carboboride $(FeCr)_2(BC)$ was 1472 HV and the WC was 2032 HV. The average hardness values increased from 1050 (sample 1) to 1150 HV2 (sample 12).
Figure 1 shows the weight loss as a function of welding speed, obtained from the abrasion wear test.

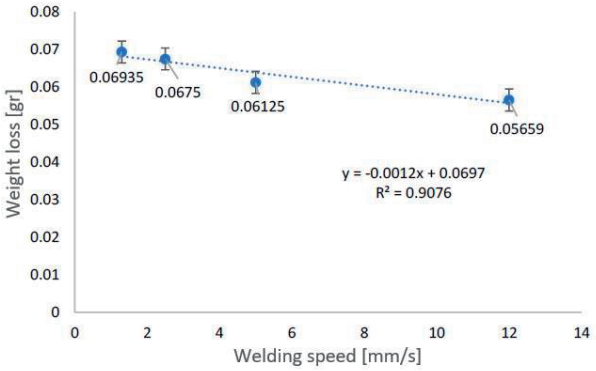

Figure 1 Weight loss vs welding speed

The samples that had the highest welding speed presented a 20% reduction in wear resistance compared to those with the lowest speed. This would be related to a greater number of hard phases and finer microstructures. Furthermore, it is interesting to observe that a large variation of the heat input (ten times) and the reduction of the deposited metal (layer from 12 mm to 5 mm in height) produced a slight change in the wear resistance.

2. References

[1] S. Merrick, D. Kotecki, et.al. "Materials and applications - Part 2. Welding Handbook". American Welding Society. 1998.
[2] G. Heath, "Nanotechnology and Welding – Actual and possible future applications". Proceedings of the CASTOLIN-EUTECTICSEMINAR, Brussels: Belgium, 2006: 25-35

Abrasive wear performance of tungsten carbide coatings

Xavier, F.A.[1)], Bordin, F.M.[1)*], Costa, E.C. [1)], Barcelos, M.C.S.[1)], Oliveira, L.L.[2)], and Bezerra, W.[2)]

[1)] Department of Mechanical Engineering, Universidade Federal de Santa Catarina, Florianópolis, 88040 900, Brazil
[2)] Jirau Energia, Porto Velho, RO, 20030 021, Brazil
[*]Corresponding author: f.m.bordin@posgrad.ufsc.br

1. Introduction

The most part of wear/erosions in hydropower turbines is a cavitation outcome. [1]. However, Madeira River in Brazil is one of the most erosive in the world, with high concentrations of abrasive silts, which greatly contributes to the erosion phenomena. Selection of appropriate coating materials is a compromise solution: in one side, materials selected to protect against cavitation must exhibit high ductility; in the other side, the materials must exhibit high hardness [2].

Due to the expressive erosive wear of the hydropower plant turbine blades, two commercial tungsten carbide-based coatings were selected for abrasive wear screening tests, as means to compare the performance of both coating materials using simple experiments.

2. Materials and methods

The experiments were performed according to the ASTM G65-16 (Rubber wheel/dry sand) test procedure D (6,000 revolutions – 30 minutes, 45 N load), using an inhouse built test machine. A standardized sand (SiO_2) was used as abrasive.

An AISI 306L stainless steel was used as substrate for the specimens. Coating A (Cobalt alloy, with W, C, Fe, Ni, Cr) and Coating B (WC Co Cr 86 10 4) were coated onto the workpieces by high velocity oxygen fuel thermal spray process. The samples were supplied with a 300 µm coating thickness. The cross-sectional microstructure of the samples is highlighted on Figure 1.

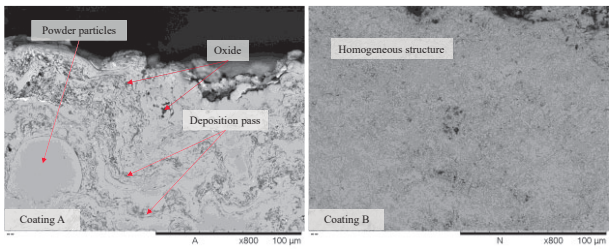

Figure 1 Microstructure of the tested coatings.

The results were evaluated in terms of average and behavior of the samples' wear rate. The profile of the cavity and texture of the wear track was also analyzed.

3. Results

The follow-up wear behavior can be observed in Figure 2. Coating A presented a higher wear rate, reaching the expected coating life in 12 minutes for all samples, whereas coating B reached the time limit for the samples without reaching substrate (highlighted in Figure 3 through the cavity profile).

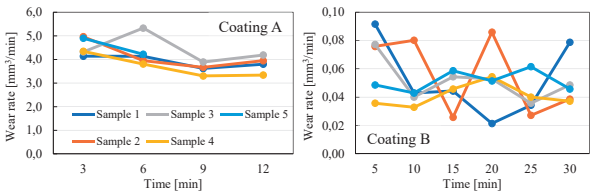

Figure 2 Wear rate within time intervals.

A higher wear rate is observed at first, due to the lower contact area leading up to higher contact pressures. As the contact area increases, wear rate reaches a threshold and stabilizes.

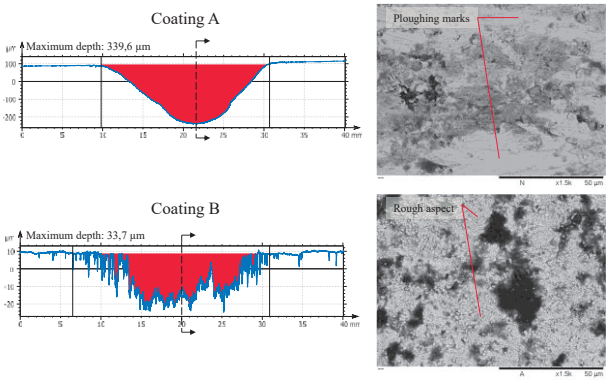

Figure 3 Wear track profiles and the resulting surface.

The wear tracks showcase the maximum depth of the wear track, induced by abrasive cutting.

4. References

[1] Kumar, K. and R.P. Saini, *A review on operation and maintenance of hydropower plants*. Sust. En. Tech. and Assess., 2022. **49**: 21 p.

[2] Szymanski, L., E. Olejnik, J.J. Sobczak, M. Szala, P. Kurtyka, T. Tokarski and A. Janas, *Dry sliding, slurry abrasion and cavitation erosion of composite layers reinforced by TiC fabricated in situ in cast steel and gray cast iron*. J. of Mat. Process. Tech., 2022. **308**: 15 p.

5. Acknowledgments

ANEEL
Agência Nacional de Energia Elétrica
Programa de Pesquisa e Desenvolvimento
JIRAU ENERGIA

Project regulated by ANEEL and developed in the scope of R&D of Jirau Energia S.A.

Tribological characterization of deterministic polyamide surfaces manufactured by additive and subtractive methods

Luis Miguel Ballesteros[1),2),3)*], David Cano[1)], Camilo Andrés García[1)], Laura Vanessa Giraldo[1)], Luis Felipe Jiménez [1)], Esteban Rave[2)], Sebastián Rudas[2)], Alejandro Toro[1)]

[1)]Tribology and Surface Group, Universidad Nacional de Colombia, Medellín, Colombia
[2)]Energy Research and Innovation Group, Institución Universitaria Pascual Bravo, Medellín, Colombia
[3)]Centro de Ingeniería y Desarrollo Industrial, Av. Playa Pie de la Cuesta No. 702, Desarrollo San Pablo, C.P. 76125, Querétaro, México
[*]Corresponding author: lmballesteroso@unal.edu.co

1. Introduction

The use of deterministic surfaces to control the contact conditions between sliding mechanical pairs has shown to reduce friction in dry [1] and lubricated conditions [2]. The present work compares the tribological behavior of deterministic surfaces manufactured by two different methods, namely 3D printing by fused filament fabrication and CNC micromachining (micro-CNC). Correlations among The geometrical descriptors of the surfaces, the surface finish of the manufacturing technique and the friction coefficient (COF) are discussed.

2. Materials and Methods

A set of samples was built on a Prusa Tairona i3 3D printer, equipped with 0.3 mm brass nozzle. The Nylon filament and the heating bed were kept at 245°C and 60°C respectively.

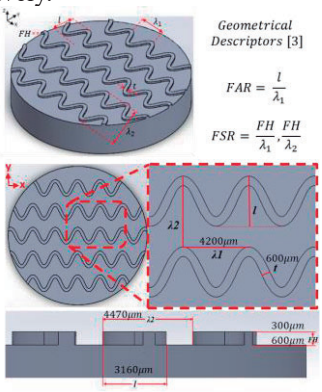

Figure 1 CAD design of textured surfaces.

On the other hand, the subtractive method consisted of CNC micromachining in a simultaneous CNC machining center (HAAS UMC750). The textures were fabricated on a Nylon bar using a V-shaped CNC engraving cutter (0.2 mm radius, 20°). The cutting and forward speed were set at 7000 RPM and 2000 mm/min respectively. The textured samples were subjected to an annealing treatment at 135 °C for 2 hours.

3. Results

Both manufacturing processes were suitable for fabricating deterministic surfaces with reduced COF in contrast to untextured samples. Micro-CNC provided the best tribological response due to repeatability and surface finishing.

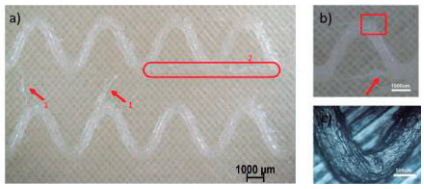

Figure 2 Patterns fabricated by 3D printing.

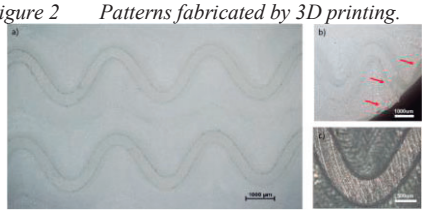

Figure 3 Patterns fabricated by micro-CNC.

Table 2 COF values measured in pin-on-disk tests.

Sliding Direction	3D Printing		Micro-CNC	
	FH 0.3	FH 0.6	FH 0.3	FH 0.6
Parallel	*0.21*	*0.24*	*0.20*	*0.19*
Lateral	*0.22*	*0.21*	*0.20*	*0.19*
Control	*0.28*		*0.26*	

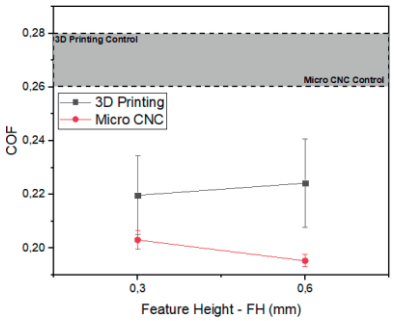

Figure 4 Comparison of COF in parallel sliding direction influenced by the manufacturing methods.

a) b)

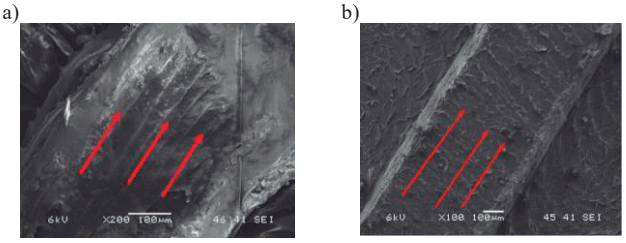

Figure 5. Abrasive Wear in surfaces, a) 3D printed, b) Micro-CNC.

4. References

[1] Y. Hong, P. Zhang, K.H. Lee, C.H. Lee, Friction and wear of textured surfaces produced by 3D printing, Sci China Technol Sci. 60 (2017) 1400–1406. https://doi.org/10.1007/s11431-016-9066-0.
[2] I. Etsion, Discussion of the paper: Micro CNC surface texturing on polyoxymethylene (POM) and its tribological performance in lubricated sliding (M.H. Cho and Sangil Park, Tribology International 44 (2011) 859–867), Tribol Int. 44 (2011) 1262. https://doi.org/10.1016/j.triboint.2011.05.024.
[3] H.A. Abdel-Aal, M. El Mansori, Tribological analysis of the ventral scale structure in a Python regius in relation to laser textured surfaces, Surf Topogr. 1 (2013). https://doi.org/10.1088/2051-672X/1/1/015001.

Microstructure and Wear Behavior of Austenitic Stainless Steel AISI 316L Produced by Rolled and Direct Metal Laser Sintering Methods

Tahanzadeh,S.[1)*], Seriacopi, V.[1,2)] Machado, I.F. [1)]

1) Polytechnic School of the University of São Paulo, São Paulo, 05508-030, Brazil
2) Mauá - Instituto Mauá de Tecnologia, São Caetano, 09580-900, Brazil

*Corresponding author: s.tahanzadeh@usp.br

1. Introduction

Additive manufacturing (AM) has become more prevalent in recent years. One of the AM technologies is Direct Metal Laser Sintering (DMLS), which allows for the layer-by-layer fabrication of metallic parts that produce a unique microstructure [1]. Austenitic stainless steels (316L SS) are suitable for various industrial applications because of their strength, corrosion resistance, and biocompatibility. The conventional approach for manufacturing 316L SS is expensive for complex shapes since their machinability usually needs to be higher [2]. In addition, wear and friction are critical factors in engineering parts. This work aimed to evaluate AISI 316L steel processed by DMLS and rolled using scratch tests.

2. Materials and Methods

2.1. Materials

This study investigated one rolled sample and two laser-sintered samples. The rolled 316L sample was purchased from a commercial company. At the same time, the additively manufactured components were produced using a commercial LPBF machine and 316L stainless steel powder supplied by LPW Ltd with an average particle size of 32 µm. ***Table 1*** shows the chemical composition of rolled part and 316L powder used for laser sintering.

Table 1 Chemical Composition (wt%)

	Cr	Ni	Mo	Mn	Si	Cu
Rolled	16-18	10-14	2.0-3.0	≤ 2.0	≤ 0.75	-
DMLS	18.88	11.75	2.06	1.32	0.80	0.53

2.2. Experimental Methodology

Scanning electron microscopy (SEM) and light optical microscopy carried out the material microstructural characterization. To analyze the wear performance, a single pass scratch test was conducted using a Bruker UMT-2 Tribometer at a constant velocity and distance (5mm) for 1 min with 20N of normal load at ambient temperature and humidity. Before the wear test, the samples were mechanically ground, polished, and ultrasonic cleaned. The 3D interferometry technique was used to analyze the profiles of the wear track and surface roughness.

3. Results

Figure 1 depicts the variation in COF (friction of coefficient) and scratch tracks; the rolled sample presented a higher COF. The 3D profilometry allowed us to find a removed volume of material during the scratch tests: 1.73×10^{-3} mm^3 for DMLS 190W, 2.30×10^{-3} mm^3 for DMLS 160W, and 2.90×10^{-3} mm^3 for rolled steel. The relative density of DMLS samples is about 97%, although the hardness is almost the same ($260HV_{0.5}$) for all the samples. The process impacted and can improve the Laser AM applications related to COF. On the other hand, the track features do not easily explain the higher COF and the higher wear of rolled sample because all of the samples are similar. Ploughing was the dominant mechanism. The differences between DMLS and rolled samples can be attributed to the manufacturing processes, resulting in differences in relative density and microstructures since the hardness does not present a significant variation. This preliminary work shows that a detailed microstructure characterization is required to explain the results found. Grain size and chemical composition should have affected the tribological performance.

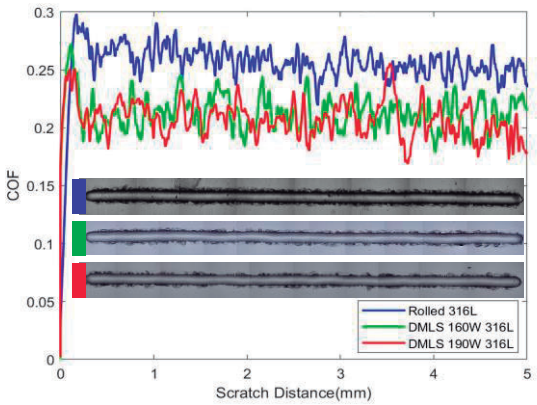

Figure 1 COF along with the scratch distance and wear track.

4. References

[1] Bordinassi, Éd Claudio, et al. *"Effect of hybrid manufacturing (am-machining) on the residual stress and pitting corrosion resistance of 316L stainless steel."* J. Braz. Soc. Mech. Sci. Eng. 44.10 (2022): 491.
[2] Özer, Gökhan, and Alptekin Kisasöz. *"The role of heat treatments on wear behaviour of 316L stainless steel produced by additive manufacturing."* Mater. Lett. 327 (2022): 133014

Phototribology: active control of friction by light in solid and liquid states

Perotti, B.L.[1)], Leidens, L.M[1)], Alvarez, F.[2)], Michels, A.F.[1)] and Figueroa, C.A.[1)*]

[1)] PPGMAT, Universidade de Caxias do Sul, Caxias do Sul-RS, 95070-560, Brazil
[2)] Instituto de Física *"Gleb Wataghin"*, Universidade Estadual de Campinas, Campinas-SP, 13081-970, Brazil
[*]Corresponding author: cafiguer@ucs.br

1. Introduction

Friction phenomenon is a ubiquitous manifestation of nature originated in the dissipation of energy after stochastic interactions of particles from two surfaces. There are several ways to set up the friction behavior of tribological systems by means of surface finishing, liquids and gases, all of them nonreversible processes. Thus, the active control of friction through external sources is a challenge in tribology. Electric and magnetic fields were proposed to control friction remotely [1]. It is a new paradigm in tribology where radiation fields can tune friction [2,3].

2. Experimental setups and results

In our case, we used a photoactive material (TiO_2) to active control of friction forces at the nanoscale as a function of the presence or absence of UV illumination (λ = 365 nm and variable luminous flux) by friction force microscopy (FFM) and quartz crystal microbalance (QCM). We could determine that the light can tune friction forces in a reversible, stable, reproducible and reliable way as shown in Figure 1 where two solid surfaces are in sliding contact (solid state). The UV light induces surface rearrangements of atoms in a similar way of those processes for degradation of organic molecules on activated TiO_2 surfaces. Indeed, the half-life of the pseudo-first order kinetics is roughly the same of those well stablished degradation processes of organic molecules in aqueous suspension with TiO_2 particles. Moreover, the reduction of friction under UV illumination follows a sigmoidal behavior with the luminous flux.

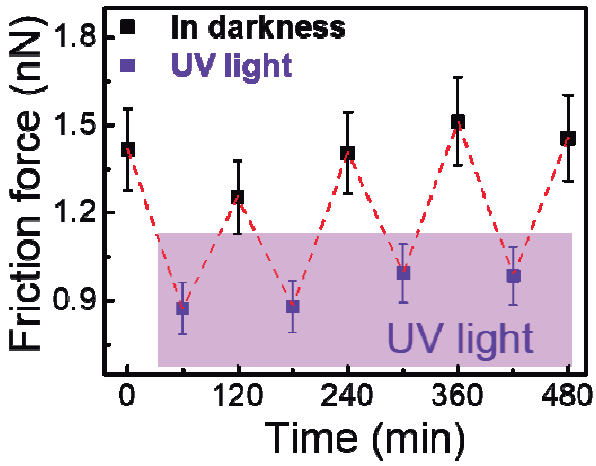

Figure 1 Photo-Frictional behavior of silicon tip on TiO_2 thin film.

The same effect is observed in liquid state where TiO_2 nanoparticles were photo-activated in aqueous suspensions. As can be seen in Figure 2, a higher(lower) frequency(resistance) is attributed to TiO_2 nanoparticles desorption from the QCM surface, which implies in lower friction. This behavior is attributed to a surface electrical potential change of TiO_2 nanoparticles due to UV absorption that modifies the lubrication properties of the nanofluid.

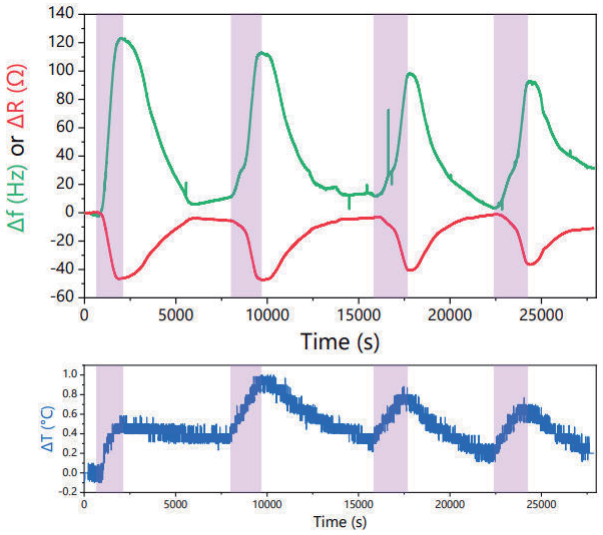

Figure 2 Photo-Frictional behavior of TiO_2 nanoparticles in aqueous suspension.

3. Conclusions

These findings contribute to a new conceptual framework in tribology where light may be defined as a fourth body and the integration of tribology with photonics and optoelectronics. Also, active control of friction in solid and liquid states may open new technological application in mechanical systems.

4. References

[1] Seed, C. M., B. Acharya and J. Krim, *QCM Study of Tribotronic Control in Ionic Liquids and Nanoparticle Suspensions*. Tribol. Lett., 2021, **69**: p. 1–12.
[2] Perotti, B. L., A. Cammarata, F. Cemin, S. R. Sales de Mello, L. M. Leidens, F. G. Echeverrigaray, T. Minea, F. Alvarez, A. F. Michels, T. Polcar and C. A. Figueroa, *Phototribology: Control of Friction by Light*, ACS Appl. Mater. Interfaces, 2021, **13**: p. 43746–43754.
[3] Sasaki, M., Y. Xu and M. Goto, *Control of friction force by light observed by friction force microscopy in a vacuum*. Appl. Phys. Express, 2017, **10**: p. 015201.

Effect of electric current flow on the coefficient of friction of exfoliated and reassembled graphite films measured in reciprocating linear sliding tests

Gonçalves, R.P.N.[1)*], Oliveira, O.J.C.[1)], Fukumasu, N. K. [1)], Tomanik, E. [1)], Galembeck, F.[2)], Souza, R.M. [1)] and Tschiptschin, A.P.[1)]

[1)] University of São Paulo, São Paulo, 05508 030, Brazil
[2)] University of Campinas, Campinas, 13083 970, Brazil
[*]Corresponding author: ronnypeterson@usp.br

1. Introduction

Graphene is a 2D carbon material with unique electrical, mechanical, and thermal properties. Over the years, methods have been developed to produce graphene, including exfoliation, chemical vapor deposition, and epitaxial synthesis. Recently, a new approach has been developed [1], which involves using a cellulose solution to disperse graphene particles that are then reassembled to create a graphitic nanomaterial with multifunctional properties such as high electrical conductivity, impermeability, and thermal resistance [2]. These materials adhere to substrates like wood and canvas and can potentially be used as fire retardants [3]. One promising application is in sliding contacts that conduct electrical current due to their high conductivity and low friction coefficient. This study assesses the coefficient of friction of exfoliated and reassembled graphite (ERG) films under electrical current.

2. Material and methods

Exfoliated and reassembled graphite (ERG) films on cellulose substrate were tested against a 10 mm SAE 52100 bearing ball. Samples were subjected to reciprocating sliding friction tests with a contact electrification system under different conditions: four voltage levels (0V, 2V, 4V, and 6V) and two current flowing directions (film-to-ball and ball-to-film) at an average load of 10N. Each test lasted 1200 seconds. The coefficient of friction data was collected, and optical microscopy was used to examine the balls after testing.

3. Results and discussion

Considering the entire test duration, Figure 1 suggests that the coefficient of friction (COF) decreases as the applied voltage increases. During the initial run-in period of all tests, there is a rapid decrease in the COF, which could be attributed to the transfer of ERG material onto the bearing ball, creating a lubricating film. However, after about 100 seconds, the COF begins to increase again, probably due to the degradation of the transferred film and the introduction of abrasive particles between the film and the ball.

Figure 2 shows optical micrographs of the transferred film on bearing balls collected after 1200 seconds. They confirm that ERG adheres to the ball's surface, changing the contact from graphite-steel to graphite-graphite, thus reducing the COF. In addition, it seems that increasing the applied voltage results in less material being transferred to the ball's surface, leading to a more homogeneous lubricating film. Degradation of the lubricating film after the tests can be seen.

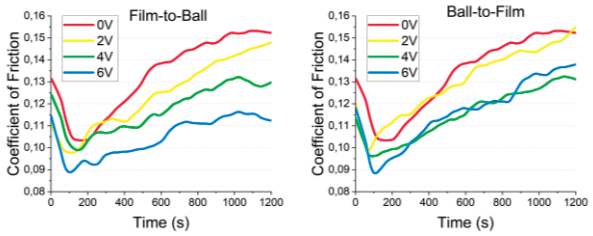

Figure 1 Coefficient of friction under different levels of voltage and current flow direction

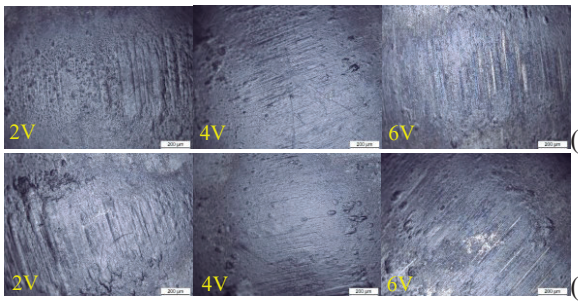

Figure 2 Optical microscopy of bearing balls surface collected after 1200 seconds for current flowing from (a) film-to-ball and (b) ball-to-film.

4. Conclusion

ERG films on cellulose substrate exhibit varying friction coefficients when exposed to electrical current flow during sliding against a hardened steel ball. COF initially drops as graphite transfers onto the ball but increases after 100 seconds, probably due to film degradation and the introduction of abrasive particles.

5. References

[1]Ferreira, E. S., Da Silva, D. S., Burgo, T. A. L., Batista, B. C., and Galembeck, F. *Graphite exfoliation in cellulose solutions*. Nanoscale, 2017. **9**(29): 10219-10226.

[2] Santos, L. P., Soares Da Silva, D., Ferreira Bertacchi, J. P., Moreira, K. S., Lima Burgo, T. A., Batista, B. C., Santos, J. Dos, De Paula, P. A., and Galembeck, F. *Multifunctional coatings of exfoliated and reassembled graphite on cellulosic substrates*. Faraday Discussions, 2021. **227**: p. 105–124.

[3] Santos, L. P., Da Silva, D. S., Morari, T. H., and Galembeck, F. *Environmentally friendly, high-performance fire retardant made from cellulose and graphite.* Polymers, 2021. **13**(15): p. 2400.

Tribological Performance of 410L Martensitic Stainless Steel Parts Manufactured by Laser Directed Energy Deposition

Sousa, J.M.S.S[1,2)*], Pereira, M.[1)], Cruz, J. R.[2)], Gutjahr, J.[3)], Thiesen Jr., A[2)] , Salvaro, D.B.[4)] and Binder, C.[4)]

[1)] Precision Engineering Laboratory - LMP, Federal University of Santa Catarina, Florianópolis, 88040900, Brazil
[2)] Senai Innovation Institute for Manufacturing Systems and Laser, Joinville, 89218153, Brazil
[3)] TWI Ltd. - Laser Additive Manufaturing, Rotherham, South Yorkshire, S6 5AY, United Kingdom
[4)] Materials Laboratory - LABMAT, Federal University of Santa Catarina, Florianópolis, 88040900, Brazil
[*]Corresponding author: jurandirmarcos37@gmail.com

1. Introduction

Martensitic stainless steels (MSS) possess high hardness, mechanical, and wear resistance. Applied in parts that suffer sliding wear (e.g. bearings, rails, ball valves) [1,2]. On-demand parts manufacturing and repair is possible with additive manufacturing by laser directed energy deposition (AM L-DED). However, MSS sensibility and L-DED thermal history can generate uneven microstructure [1]. Post heat-treatments are an alternative in this direction [2]. This work evaluates microstructure, mechanical, and tribological performance of AISI 410L MSS multilayers produced by AM L-DED in as-built and heat-treated conditions.

2. Materials and Methods

Hot-rolled AISI 410 MSS was the substrate. AISI 410L MSS (wt.% 12.8Cr, 0.8 Mn, 0.8Si, 0.7Ni, 0.02C, Fe-Bal.) gas-atomized powder (53-150 µm, Höganäs) was the feedstock. L-DED system used was the RPMI 535®, coupled to a 3000 W Yb fiber laser source (IPG®). A design of experiments (DoE) to AM L-DED parameters selection was performed: spot size Ø=2.54 mm, powder feedrate F=30 g/min, laser power P=1800 W, travel speed S=635 mm/min, hatch spacing HS=1.93 mm, and layer height LH= 1.22 mm. Two samples (25×25×25 mm) were manufactured for microstructure (OM optics and SEM-EDS scanning electronics) and Vickers microhardness, and 2 samples (Ø16×40 mm), later machined in Ø16×10 mm disks, for tribological test. Half of AM L-DED samples were annealed at 1050 °C, water quenched, and tempered at 600 °C then air cooling. Based on AISI 410L applications, ASTM G99 ball-on-disk sliding test (10 mm wear track radius, 10.0 N load, 0.5 m/s sliding speed, and 1000 m sliding distance) was chosen. It was analysed wear rate of disks and balls (optical interferometry), friction coefficient (COF, load cell), wear surfaces and debris by SEM.

3. Results

DoE AM L-DED parameters produced layers free from defects. Multilayers showed Archimedes density close to the AISI 410L powder (7.67 - 7.74 g/cm^3). As-built microstructure (Figure 1a) displayed columnar growth with different orientations, due to low C-content feedstock and L-DED fast cooling. Grain boundaries second-phases showed lath-martensite and higher Cr and Mn-contents in EDS (Figure 1b and f). Heat-treatment provided recrystallization (Figure 1c), dissolving molten pool contours and refining grains. SEM confirmed grain boundaries second-phases only in as-built condition (Figure 1b). In heat-treated one (Figure 1d), there was a microstructure recovery. Average as-built microhardness was 232±32 HV (Figure 1f) [1]. Fe-matrix displayed 170 HV and 240 HV at grain boundaries. Heat-treatment decreased that to 207±10 HV. Regarding substrate (190±5 HV), both AM L-DED conditions showed higher microhardness.

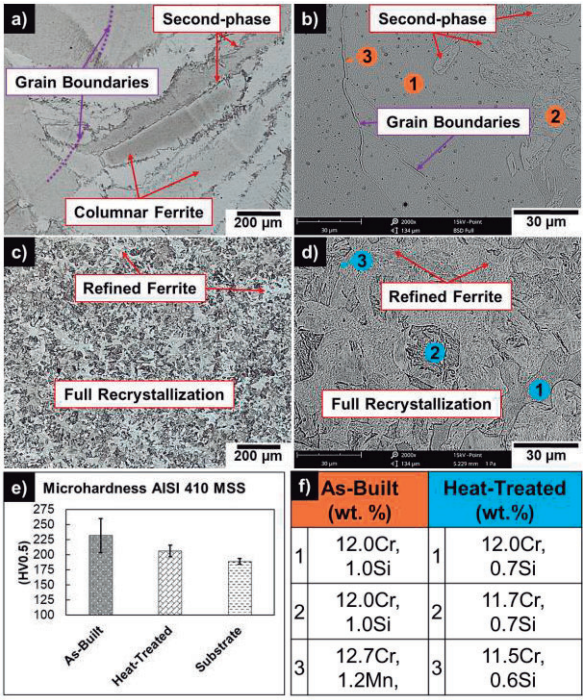

f) As-Built (wt. %)		Heat-Treated (wt.%)
1	12.0Cr, 1.0Si	1	12.0Cr, 0.7Si
2	12.0Cr, 1.0Si	2	11.7Cr, 0.7Si
3	12.7Cr, 1.2Mn,	3	11.5Cr, 0.6Si

Figure 1 AM L-DED 410L MSS samples features.

Different AM L-DED conditions will presumably show differential wear rates and dominant wear mechanisms in the pin-on-disk tribological test (to be conducted). As-built heterogeneous microstructure will influence the body/counterbody contact dynamics, during the ball displacement over Fe-matrix and second-phases at grain boundaries. COF should likewise showed higher oscillations in as-built condition. It is expected that heat-treated increase tribological performance regarding as-built condition [1,2].

References

[1] Lai, Q., Abrahams, R., Yan, W., Qiu, C., Mutton, P., Paradowska, A., Soodi, M. and Wu, X., *Influences of Materials, Parameters and Heating on Laser-Cladded Rails.* J. of Mat. & Proc. Tech., 2019. **263:** p. 1-20.

[2] Meura, V., Pacheco, J., Veiga, M., Rabelo, A., Silva, L., Milan, J. and Costa, C., *Effect of Post-Heat Treatment on Tribological Performance of AISI 410L Processed by L-DED.* Prog. In Add. Man., 2023. **8:** p. 1-11.

Effects of coconut fruit fiber and Oyster seashell concentration and porosity on the impact energy and absorption of friction linings

Eziwhuo S. J. and Ossia C. V.

Department of Mechanical Engineering, University of Port Harcourt, Port Harcourt, Nigeria.

Correspondence Email: engrsje1985@gmail.com

1. Introduction

The manufacturing of friction linings using asbestos fibres poses a challenge due to its nature of Carcinogenic. Some researchers applied natural fibres to replace carcinogenic asbestos fibres in brakepad production using organic agricultural wastes [1-4]. Palm kernel shells have equally been used as a substitute for asbestos brakepads [5, 6]. The use of coconut fruit fibre combined with oyster seashells as raw material for brakepad production has not been reported. The effect of different combinations of this raw material on the porosity and impact strength will be investigated and compared with commercial (control) brakepad (CBP) sample.

2. Materials and Methods

Materials used include: (a) Oyster seashell OSS (*Magallana-Gigas L.*) (Figure 1), (b) coconut fruit fiber CFF (*Coir L.*) (Figure 2), (c) epoxy resin (binder), (d) Cu (abrasive), (e) hardener (catalyst), and (f) graphite (friction modifier). These were used to develop the friction materials in Figure 3 by compression moulding and curing at elevated temperatures.

The brakepad specimens were developed and processed based on a 4 factors, 3-levels L27 $(4)^3$ Box-Behnken design (BBD) for the purpose of optimising the process parameters involved. The factors were: concentration of coconut fruit fibre (CFF) in the reinforcement materials, curing temperature (T_c), molding Pressure (P_m), and curing time (C_t). To give equal weights to the factors, coding equations were applied to obtain coded variables for concentration of coconut fruit fiber X_1, molding pressure X_2, curing temperature X_3, and curing time X_4 which are expressed as equations (1) – (4), respectively.

$$X_1 = \frac{C_{CFF} - 50}{50} \quad (1)$$

$$X_2 = \frac{P_m - 11.25}{1.32} \quad (2)$$

$$X_3 = \frac{T_c - 150}{30} \quad (3)$$

$$X_4 = \frac{C_t - 120}{60} \quad (4)$$

The evaluation criteria utilized to assess the developed brakepads and control sample were impact energy and absorption (in water and SAE 20W50 oil medium).

Figure 1: Oyster sea shell (Magallana-Gigas L.)

Figure 2: Grounded coconut fruit fiber (Coir L.)

Figure 3 Developed brakepad materials samples after curing

3. Results and Discussions

3.1 Impact energy

The impact energy test results (Figure 5) was modeled as in equation (5) with a coefficient of determination R^2-value 0.8793.

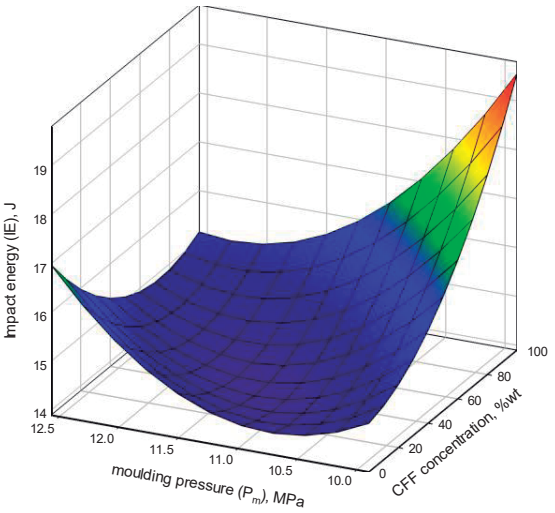

Figure 5: Effect of molding pressure and CFF concentration on impact energy

The impact energy tests (ASTM E23-23a) results of the developed brake pad samples were 14.01J *(S2222)* ≤ IE ≤ 18.99J *(S2121)* which were comparable to the impact energy of the CBP (16.89N). The impact energy for the commercial brakepad (control) sample was 16.89J.

$$IE = 14.24333 - 0.69083X_1 - 0.54167X_2 + 1.6025X_1X_2 + 0.994167{X_1}^2 + 1.370417{X_2}^2 \quad (5)$$

3.2 Absorption

The absorption characteristics of the developed friction materials in water medium based on weight loss measurement (24h ASTM D570-22) are shown in Figure 6. Expectedly, the materials exhibited higher absorption in hot water (gray) than cold water (cyan). This is attributable to pores expansion with heat application.

The water absorption properties were modeled as equation (6) and (7) for cold water and hot water absorption, respectively.

$$A_{cw} = 0.2949 - 0.005683X_1 + 0.007142X_2 + 0.01605X_1X_2 - 0.000067{X_1}^2 + 0.005721{X_2}^2 \quad (6)$$

Hot water absorption model obtained is equation (7)

$$A_{Hw} = 0.4421 + 0.0019X_1 + 0.001917X_2 - 0.02755X_1X_2 + 0.003221{X_1}^2 - 0.00543{X_2}^2 \quad (7)$$

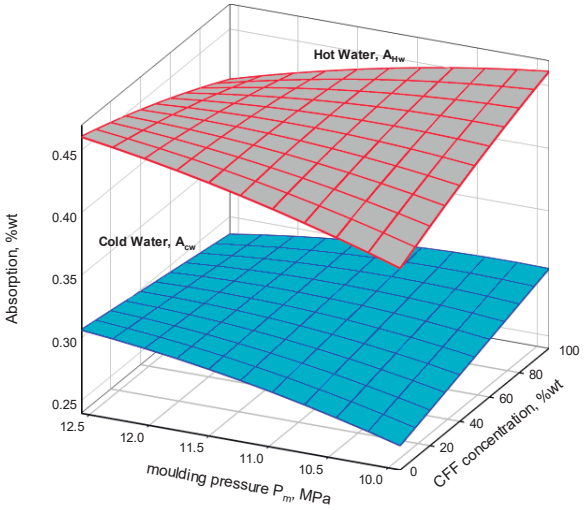

Figure 6: Effect of moulding pressure and CFF concentration on water absorption at T_c = 150°C, and C_t = 120min

Oil absorption results after 24h soaking in the oil was modeled as obtained in equation (8).

$$A_o = 0.3628 - 0.00667X_1 + 0.00405X_2 - 0.0174X_1X_2 - 0.003{X_1}^2 - 0.03571{X_2}^2 \quad (8)$$

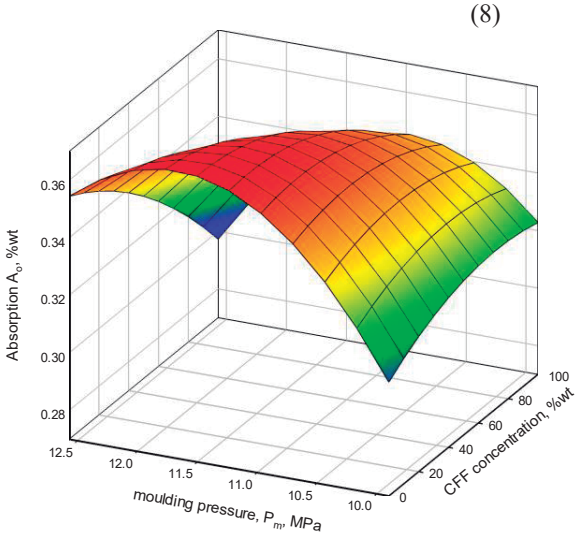

Figure 7: Effect of moulding pressure and CFF concentration on oil absorption at T_c = 150°C, and C_t = 120min.

4. Conclusion

The uneven shape of the reinforcement material particles size creates pores in the matrix structure. Lesser particle size creates tougher structural links and less pore sizes. The characterization (impact energy and absorption) of the resulting samples decreased by means

of decreasing pore sizes. Oil absorption of the developed samples showed $0.3012 \leq A_o \leq 0.4411$ comparable to 0.3799 for the CBP, while water absorption results showed $0.2756 \leq A_{CW} \leq 0.339$ and $0.4012 \leq A_{HW} \leq 0.4798$ for cold and hot water absorption, respectively. These were comparable to CBP results of 0.3116 and 0.4412, for cold and hot water, respectively.

References

[1] C.H. Achebe, J.L. Chukwuneke, F.A. Anene, "A retrofit for asbestos based brake pad employing palm kernel fiber as the base filler material". *Proc IMechE, Part L: J Materials: Design and Application 2019*; 233: 1906–1913.

[2] S.T Kholil, A. Dwiyati, Sugiharto, I. W. Sugita, "Characteristics composite of wood powder, coconut fiber and green mussel shell for electric motorcycle brake pads". ǁ in *Journal of Physics: Conference Series, 2019,* 1–6.

[3] G.S. Krishnan, L. G. Babu, R. Pradhan, S. Kumar, "Study on Tribological Properties of Palm Kernel Fiber for Brake Pad Applications." *Material Research Express* 7: 1–7. https://doi.org/10.1088/2020-1591/ab5af5

[4] C.V. Ossia, A. Big-Alabo, E.O. Ekpruke, "Effect of grain size on the physicomechanical Properties". *Advances in Manufacturing Science and Technology, AMST* 44(4), 2020, 135–144. https://doi.org/10.2478/amst-2019-0023

[5] J. Abutu, S.A. Lawal, M.B. Ndaliman, R.A. Lafia-Araga, O. Adedipe, I.A. Choudhury, "Production and Characterization of Brake pad developed from Coconut shell reinforcement material using Central Composite Design". *SN Applied Sciences,* 1:18/2019.

[6] S.J. Eziwhuo, T. Joseph, "Performance Evaluation of Non-Edible Vegetable Seed Oil as Cutting Fluid in Metal Turning Operation". *World Journal Of Engineering Research & Technology WJERT,* 2020, 6(4) 354-366.

Relationship between mechanical properties and galling resistance of API grade steels

Abdelnabe, J.P.[1)2)*], Prieto, G.[1)2)], Crespo, M.I. [2)] and Tuckart, W.R.[1)2)]

[1)] IFISUR, CONICET-UNS, Bahía Blanca, CP8000, Argentina
[2)] Engineering Department, Universidad Nacional del Sur, Bahía Blanca, CP8000, Argentina
[*]Corresponding author: juan.abdelnabe@uns.edu.ar

1. Introduction

Galling is a severe adhesive type of damage that commonly occurs in the oil and gas industry due to the harsh conditions that the materials are subjected to.

The aim of this study was to determine the relationship between the mechanical properties of API and proprietary steel grades for Oil Country Tubular Goods (OCTG) applications and their galling resistance by means of cross-cylinder tests.

It was found that toughness correlates inversely with the galling occurrence in these steels.

2. Materials and Methods

Both API and proprietary steel grades, namely L80, P110, T95, and TN125 HC steel grades were used in this work. Tensile and hardness tests were performed to assess their mechanical properties. Both the tensile specimens and the cylinders to perform tribotests (ϕ 10 mm) were machined from actual casing and drilling elements.

To avoid variations in the results, samples were polished with abrasive paper until reaching predefined values of arithmetical mean roughness (Ra), skewness (Rsk), kurtosis (Rku) and mean roughness depth (Rz) [1].

Cross-cylinder tests were conducted with a continuously varying load ranging between 70 and 170 N and a sliding distance of 30 mm at 0.5 mm/s (Fig. 1a). Wear tracks were analyzed using optical, confocal and scanning electron microscopy. COF versus load was plotted for each test and the average COF was calculated.

The severity of galling was assessed following the method proposed in [2]. The galling events were classified into four groups -minor, moderate, major and severe events (Figs. 1b)- and a galling score (GS) was calculated for each tribopair. Higher values of GS indicate higher severity of wear in the material.

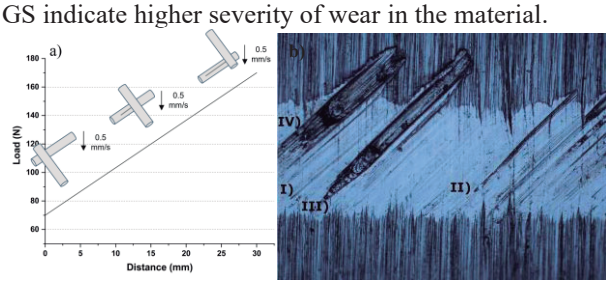

Figure 1 a) Cross-cylinder test conditions, b) I) minor, II) moderate, III) major and IV) severe galling event

3. Results and discussion.

As can be seen in Fig. 2, sudden increases in the COF register, correlate with galling events. However, an analysis of the COF register is not enough to determine the galling resistance of a tribopair and the whole tested surface must be assessed using microscopy techniques.

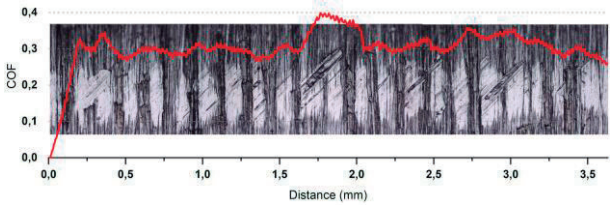

Figure 2 Overlapping of the COF curve over the wear track

L80 versus P110 steel grade test summed a total of 282 galling events and 1089 points for GS, showing the worst response. Instead, L80 versus TN125HC tribopair had the least GS, with a total of 141 events and 301 points.

All tribopairs showed an inverse relationship between GS and toughness. As the value of toughness decrease, the material is more prone to gall (Fig. 3). Particularly when pairing different steels, performance depends on the toughness of the harder one.

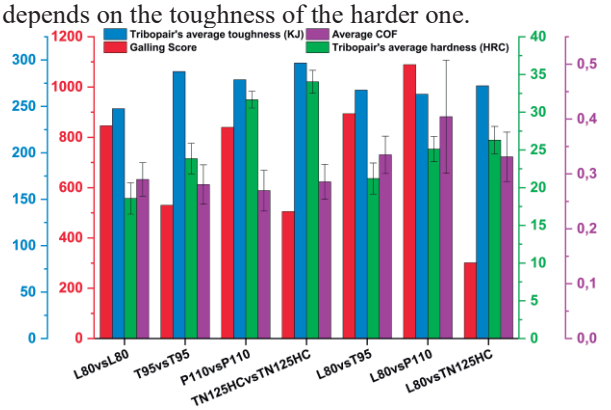

Figure 3 Mechanical properties and tribological behavior of the tribopairs

4. References

[1] Sedlaček, M., Podgornik, B., & Vižintin, J. *Correlation between standard roughness parameters skewness and kurtosis and tribological behaviour of contact surfaces*. Tribology International, 2012. **48**: p. 102–112.

[2] Budinski, K. G., Budinski, S. T. *Interpretation of galling tests*. Wear, 2015. **332–333**: p.1185–1192.

Development of a graphic tool for rail corrugation assessment in a commercial Metro line

Sebastián Gómez[1*)], Valentina Mejía-Gallón[1)], Margarita Echeverri[1)],A. Restrepo-Martínez[1)], A. Toro[1)], J. F Santa.[1)]

[1)]Universidad Nacional de Colombia, Sede Medellín
[*]Corresponding author: segomezd@unal.edu.co

1. Introduction

Railway systems play a crucial role in densely populated cities, and their efficient operation heavily relies on the tribological performance of the tracks [1]. One significant tribological challenge encountered in these systems is rail corrugation, a periodic surface anomaly caused by the complex interactions between the track and train wheels. Corrugation not only leads to increased maintenance costs but also results in wear, structural damage and elevated noise levels [2]. In this study, a graphic tool was developed to quickly diagnose the corrugation of a commercial metro line by processing the data from the longitudinal profile of the tracks. The findings from this research will contribute to the development of effective maintenance strategies and the optimization of tribological performance in railway systems, enhancing their reliability, durability and safety.

2. Materials and methods

Corrugation measurements were conducted using a rail grinding machine in one commercial line of a metropolitan transportation system [3]. Raw data were extracted from the rail grinding machine software and processed with a Python interface that facilitated automated data segmentation and analysis. The quality of the track was evaluated according to ISO 3095 standard using one-third octave bands and comparing the results with the measurements taken by the Corrugation Analysis Trolley (CAT), which is a dedicated device for the assessment of longitudinal profile of rails. Figure 1 depicts the methodology used for corrugation analysis.

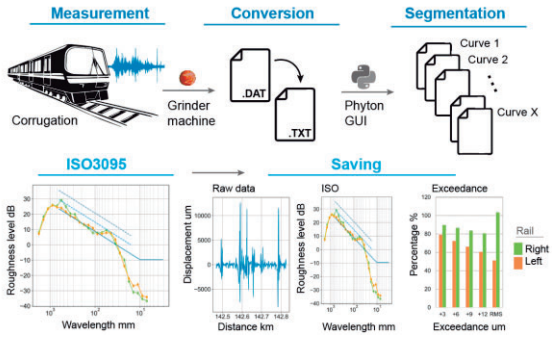

Figure 1 Methodology for corrugation analysis

3. Results and discussion

A heatmap analysis was conducted to plot the severity of the corrugation damage of the track according to ISO3095 standard, as shown in Figure 2. The heatmap categorized the sections based on their corrugation levels. Sections exceeding +12dB over the ISO3095 standard were marked in red, indicating a critical state, while sections between ISO3095 limit and +12dB were marked in yellow. Sections within the accepted values of the standard were marked in green. Out of 80 analyzed segments, 15% exceeded the critical 12 dB threshold, indicating a critical state. Sections between S9-S10 and S12-S13 had critical states for both left and right rails in the ascending direction but were cautionary (yellow) in the descending direction. In the descending direction, the left rail between S5 and S8 exhibited significant corrugation, surpassing the 12 dB threshold. Similar patterns were observed in the curved segment between S7 and S8 for both directions, with the left rail exceeding limits due to tight curves.

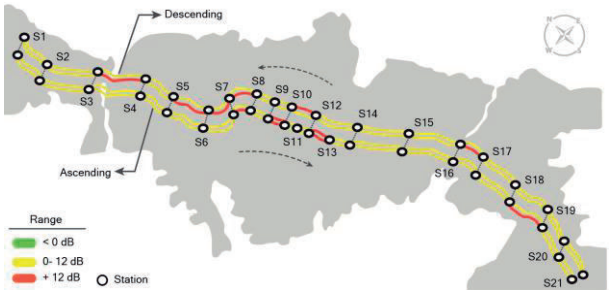

Figure 2 Heatmap for the corrugation of Line A

4. Conclusions

A graphic tool was developed for fast assessment of rail corrugation in a commercial railway. The map allows identifying areas with corrugation and fatigue defects, which in turn can be related to the dominant wear mechanisms and dynamical loads caused by the wheel-rail interaction. Further research and analysis focused on identifying and mitigating the causes of corrugation in specific sections - particularly tight curves - will contribute to the development of effective strategies for track maintenance and ensure the smooth and reliable operation of metro systems.

5. References

[1] S. L. Grassie, *Rail corrugation: advances in measurement, understanding and treatment*. Wear, vol. 258, no. 7, pp. 1224–1234, Mar. 2005, doi: https://doi.org/10.1016/j.wear.2004.03.066.

[2] R. Lewis and U. Olofsson, *Wheel-Rail Interface Handbook*, 1st ed. Elsevier, 2009, pp. 349–351.

[3] European Committee for Standardization, Railway applications—Track—Acceptance of works—part 3: Acceptance of reprofiling rails in track, EN 13231-3:2012 (E), 29 Feb 2012.

Tribological response of ceramics by linear scratch test

Magnol, R.V.[1) 2)*] Pretti, A.F. [1)] Strey, N.F.[1)] Scandian, C.[1)]

[1)] Tribology, Corrosion and Materials Laboratory – TRICORRMAT, Department of Mechanical Engineering, Federal University of Espírito Santo – UFES, [2)] Instituto Federal do Espírito Santo – IFES.
Vitória, 29075 910, Brazil
[*]Corresponding author: renanvmagnol@gmail.com

1. Introduction

Unlike the general situation where multiple abrasives come into contact with the surface of the material to be worn, the scratch test is performed with a single hard particle, which facilitates the understanding of the tribological responses of the material (friction and wear mechanisms). Additionally, it is possible to control parameters of the severity of the contact, such as the geometry of the hard particle. [1]
The aim of this study is to investigate the response of different ceramic materials to scratching, analyzing the influence of normal load and the geometry of the hard particle through tests with Vickers and Rockwell diamond indenters.

2. Methods

Scratch tests were performed on various ceramic materials such as alumina, zirconia, ZTA, silicon carbide and boron carbide using two types of diamond indenters, Vickers and Rockwell C. The equipment used for the tests was the CETR-Bruker APEX Universal Microtribometer. The data acquisition frequency for normal load and coefficient of friction was 50 Hz.

The edge of Vickers indenter was parallel to the scratch direction, with progressive increasing of normal load, ranging from 0.2 to 5.2 N, and a minimum length of 5 mm. As for the Rockwell indenter tests, the load range was from 2 to 52 N or 2 to 102 N, in cases where achieving a higher degree of fracture was not possible with 52 N.

The wear mechanisms were analyzed by optical microscopy. The hardness of the ceramics was measured using Vickers Hardness method with 1 kgf load. The fracture toughness was obtained through the Vickers indentation fracture toughness test applying the Evans and Charles equation (1) [2]:

$$KI_{IC} = 0.16 H_V a^{0.5} \left(\frac{c}{a}\right)^{-1.5} \quad (1)$$

3. Results and discussion

As can be seen in the table 1, brittle materials exhibited higher friction coefficients. This is likely due to the tendency of severe cracking in these materials, as can be observed in Figure 1, comparing the scratch response of silicon carbide (K_{IC} = 3.2 Mpa.m$^{1/2}$) and zirconia (K_{IC} = 7.8 Mpa.m$^{1/2}$).
We can also observe that in the Rockwell indenter tests, there was a greater difference in the coefficient of friction among the studied materials and also a lower mean friction compared to the Vickers tests. This is possibly due to the spherical shape of the indenter tip, which leads to a progressive increase in the attack angle with the normal load and also to a less severe stress field, achieving extensive fracture as well as higher friction only at higher loads. This is not the case with the Vickers indenter, which is sharp and has a fixed attack angle, resulting in higher contact severity and also higher friction.

Table 1 – Maximum Friction Coefficient registered on the scratch tests with Vickers and Rockwell indenters and mechanical properties of the samples

Material	Vickers	Rockwell	K_{IC}	HV1
Alumina 96%	0.40	0.22	4.71	1374
Alumina 99%	0.45	0.24	4.77	1798
ZTA	0.38	0.24	5.09	1317
Zirconia	0.40	0.18	7.75	1248
Silicon Carbide	0.50	0.65	3.2	2725
Boron Carbide	0.75	0.70	3.18	2596

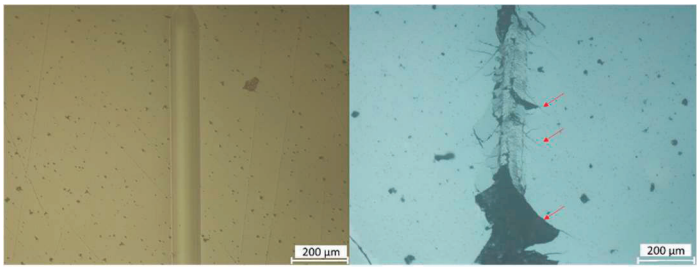

Figure 1 - Response to Rockwell scratch of Zirconia (left) and Silicon Carbide (Right). Note: the red arrows indicate cracking and material detachment.

4. References

[1] Desa, O., & Bahadur, S. (1999). Material removal and subsurface damage studies in dry and lubricated single-point scratch tests on alumina and silicon nitride. Wear, 225, 1264-1275.
[2] Evans, A.G., & Charles, E.A. (1976). Fracture toughness determinations by indentation. Journal of the American Ceramic society, 59(7-8), 371-372.

PEEK contact temperature sliding against brass, alumina and PEEK

Camporez, R.M.[1)*], Strey, N.F.[1)] and Scandian, C.[1)]

[1)] Tribology, Corrosion and Materials Laboratory - TRICORRMAT, Department of Mechanical Engineering, Federal University of Espírito Santo, Vitória, 29075-910, Brazil
[*]Corresponding author: rubsonmc@gmail.com

1. Introduction

During sliding, almost all energy dissipated by friction, within and around the real contact area, is in the form of heat and is responsible for the increase in temperature in the contacting bodies. It is known that the temperature influences the tribological behavior, especially of polymers, as they have low thermal diffusivity and a low melting point. Thus, it becomes important to know the contact temperature (T_c) under operating conditions to prevent damage and premature wear. To predict T_c, a mathematical model based on the work of Kennedy, Lu, and Baker [1] was used. However, evaluating the T_c of polymeric materials is a challenging task, given that thermal conductivity, one of the most important variables in calculating T_c, is highly dependent on chain ordering, temperature itself, and pressure [2].

2. Methods

2.1. Materials

Dimensions and properties of commercially available samples of alumina, brass and PEEK were used, according to the geometries shown in Figure 1, that represent the pin-on-disc configuration.

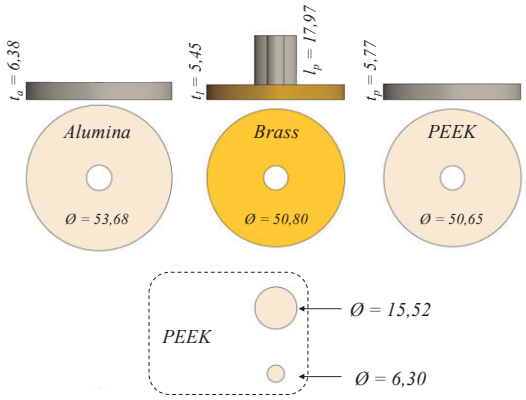

Figure 1 Geometries and dimensions of the sample. Note: dimensions in mm.

2.2. Contact temperature

Based on Kennedy, Lu and Baker model [1], the energy dissipated by friction defined as the rate of heat energy generated per unit area, q_{total}, is determined by the product of real contact pressure, coefficient of friction, and sliding speed ($q_{total} = \mu P v$).

The q_{total} generated at the interface does not flow equally to both bodies, being $q_{total} = q_1 + q_2$, where q_1 and q_2 are the heat fluxes flowing to body 1 and body 2, respectively. This information is necessary to predict the T_c, which is expressed as follows, $T_c = T_{amb} + \Delta T_{ss} + \Delta T_f$, where T_{amb} is the ambient temperature, ΔT_{ss} is the nominal temperature rise in steady state and ΔT_f is the flash temperature rise.

The mathematical modeling of the pin and disc depends on the boundary conditions applied. For the pin, only heat conduction was considered, whereas for the disc, heat conduction and convection were taken into account. The heat source area is defined as the real contact area between the bodies.

3. Results and discussion

The real contact area, necessary for calculating the q_{total}, was calculated from the surface topography of the pin and disc extracted from a three-dimensional surface analyzer. Contact temperature was calculated for PEEK-PEEK, PEEK-alumina and PEEK-brass pairs in pin-on-disc configuration. The results obtained by the mathematical model show that the T_c is strongly influenced by the sliding speed and the normal load, as shown in Figure 2, and no significant differences were observed between the diameters of the pin.

The PEEK-brass pair had a lower T_c than the PEEK-alumina pair, due to the difference in thermal diffusivity of alumina and brass, the higher thermal diffusivity of brass (approx. 3 times greater than that of alumina) allows for greater heat dissipation. For the PEEK-PEEK pair, not shown in the graph, T_c values greater than 1000 °C were observed, indicating a limitation of this model for polymeric pairs.

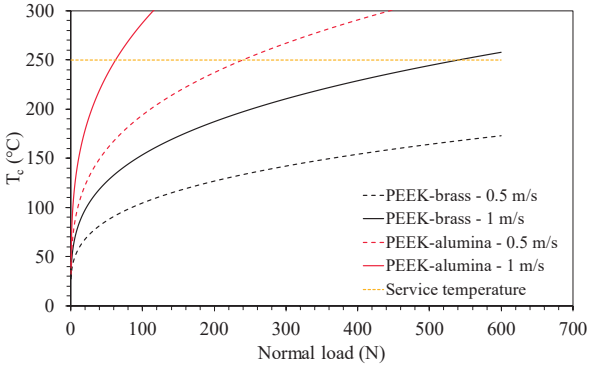

Figure 2 Contact Temperature for pin-on-disc configuration.

4. References

[1] F.E. Kennedy, Y. Lu, I. Baker, *Contact temperatures and their influence on wear during pin-on-disk tribotesting*, Tribol Int. **82** (2015) 534–542.

[2] DAWSON, A.; RIDES, M.; NOTTAY, J. The effect of pressure on the thermal conductivity of polymer melts. Polymer Testing, Elsevier, v. 25, n. 2, p. 268–275, 2006.

Effect of NaCl Concentration on The Stainless Steels Tribocorrosion

De Mendonça, A.S.[1)*], De Mello, J.D.B.[1)]

[1)] College of Mechanical Engineering, Federal University of Uberlândia, Uberlândia, 38400 901, Brazil
[*]Corresponding author: arthur.s.m@labmat.ufsc.com

1. Introduction

The chloride content can influence the corrosive behaviour of the systems involved. Depending on the application, the Cl concentration in the environment can present significant variation. Even the salinity in marine environments varies according to atmospheric and ecosystem parameters [1]. Marine machinery and other applications exposed to high humidity environments, such as orthopaedic and dental implants are examples of tribocorrosive systems with varying Cl^- concentrations [2]. The present work aimed to study the effect of NaCl concentration in the stainless steel tribocorrosion.

2. Methodology

The methodology was based on sliding wear, pure corrosive and tribocorrosion tests, aiming to evaluate the mechanical and electrochemical mechanisms separately. Tests were performed in four different media, distilled water (sliding wear tests) and three different NaCl solutions, 0.05 %, 1.78 % and 3.56 % (corrosion and tribocorrosion tests). The tested specimens were made of AISI 304 and AISI 410 stainless steels and, for comparative purposes, carbon steel ASTM A36. Zirconia balls (ϕ = 5 mm, Sq = 0.05 µm) were used, as counter body, in the sliding and tribocorrosion tests. The electrochemical parameters analysis was made through the potentiodynamic curves, friction coefficient by the triboscopy technique, degradation and wear rates by gravimetry and surfaces morphological analysis by SEM.

3. Results

Figure 1 shows all materials' average friction coefficient in the sliding and tribocorrosion tests. Friction coefficient tended to decrease with increased NaCl percentage. In these cases, the corrosion products acted as lubricants, reducing the friction coefficient.

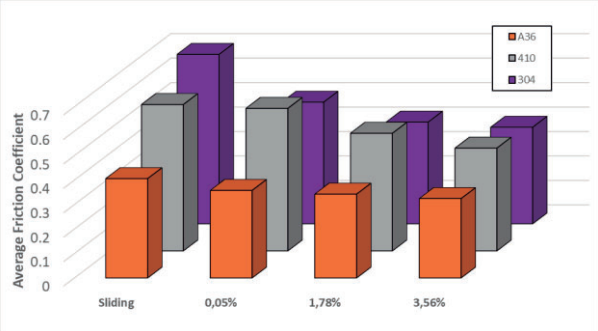

Figure 1 Average friction coefficients for sliding and tribocorrosion tests.

Figure 2 compares the sliding and tribocorrosion tests' average friction at 3.56 % NaCl in the same graph with the corresponding potentiodynamic curve. The sliding contact increases the current density during the tests due to the impact of the direct contact on the passive layer. The tribocorrosion friction coefficient shows lower values when compared to sliding. When the potentiodynamic curve enters the anodic regime, friction coefficient values drop, indicating the lubricant action from corrosion products.

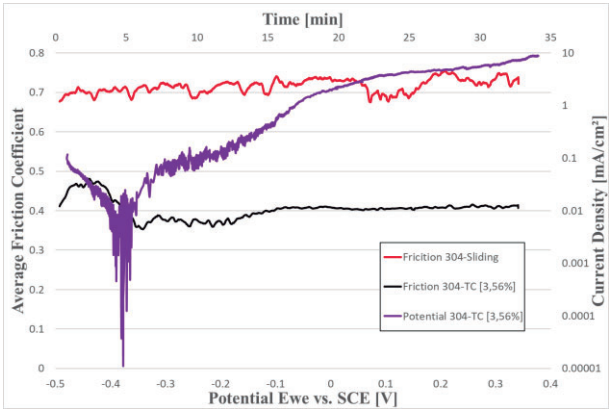

Figure 2 Mean friction coefficient and the corresponding potentiodynamic curve in the sliding and tribocorrosion test. 3.56 % NaCl

4. Conclusions

The increasing NaCl concentration tended to increase the tests' degradation rate, induced more severe corrosion, pitting formation and increased the metal dissolution. In addition, the higher chloride content caused a change in the prevalence of degradation mechanisms. In the stainless steel, greater chloride content led to narrower passive zones in the potentiodynamic curves.

5. References

[1] Von Der Ohe, C. B., R. Johnsen, N. Espallargas, *Premature failure of riser tensioner piston rods exposed to offshore splash zone operation – status and review of critical multidegradation factors*. NACE 2009, **9199**. 2009.

[2] Ponthiaux, P., F. Wenger, D. Drees, J. P. Celis, *Electrochemical techniques for studying tribocorrosion processes*. Wear, v. 256, **5**, p. 459–468, 2004.

Improvement of wear resistance of a lean duplex stainless steel through low temperature plasma nitriding

Dib, J.*, Strubbia, R., Gómez, B., Hereñú, S.

Instituto de Física Rosario, CONICET, ESP2000, Rosario, Santa Fe, Argentina
*Corresponding author: dib@ifir-conicet.gov.ar

1. Introduction

Lean duplex stainless steels (LDSS) emerged as a competitive duplex stainless steel (DSS) where Ni is partially replaced by small additions of lower cost alloying elements such as Mn and N. They have exceptional mechanical and corrosion resistance properties, making them suitable for diverse industries [1]. Nevertheless, for some service conditions the wear resistance of LDSS needs to be improved without affecting the corrosion resistance.

Plasma nitriding (PN) is a surface modification process used to enhance hardness, and wear and corrosion resistance, leading to an upgrading of the tribological performance. PN is a glow discharge process that introduces nitrogen into the surface of a metal, which subsequently diffuses into the material [2]. This work aims to cover the knowledge gap about the effects of PN on the sliding wear behavior of LDSS.

2. Materials and methods

The studied material is a LDSS (LDX 2101), received as cold-rolled 3 mm thickness plate with 2B surface finish [3]. This condition is referred as as-received (AR).

PN treatments were carried out in a DC-pulsed reactor, at 250 °C for 6 hours. A 25% N_2 - 75% H_2 atmosphere at a pressure of 4 torr and a 700 V square wave with 500 Hz frequency was used.

X-Ray diffraction (XRD) and roughness measurements were carried out before the tribological tests. Microhardness profiles along depth were performed using a Knoop indenter.

Dry sliding tests were carried out with ball-on-disc tribometer, using discs of LDX 2101 and 10 mm diameter aluminium oxide (Al_2O_3) balls. The applied load was 10 N and the sliding speed was 0,035 m/s. Different sliding distances (20, 100, 500 and 1000 m) were studied. Each test was repeated three times to ensure repeatability. During the tests the friction coefficient was continuously measured. Samples were ultrasonically cleaned and then weighted before and after the tests. Volume losses were calculated by dividing the weight loss by the density of the material and then, average wear rates were calculated according to [4].

Wear tracks were observed in a scanning electron microscope (SEM) equipped with energy dispersive spectroscopy (EDS).

3. Results

Figure 1 illustrates the XRD diffractograms of LDX 2101 prior and after PN. The results indicate the formation of expanded austenite (γ_N) and ferrite (α_N) after the treatment. Precipitation of detrimental CrN that decreases the corrosion resistance is not detected. Furthermore, reflections corresponding to the original phases are still present. Similar findings were also reported by Pinedo et al. [5].

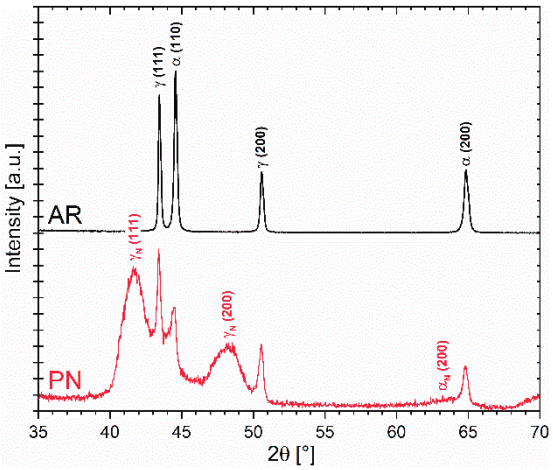

Figure 1 – XRD of AR and PN LDX 2101

Table 1 shows the average wear rates of AR and PN LDX 2101. In AR samples the wear predominantly takes place during the initial sliding stage. Moreover, all the nitrided samples exhibit lower wear rates than AR ones. This last fact is related to the supersaturated solid solution of nitrogen expanded phases, (γ_N) and (α_N), formed during PN process that increase the hardness pronouncedly.

Table 1 Average wear rates $\times 10^{-5}$ *[mm³ / N m]*

Condition	20 m	100 m	500 m	1000 m
AR	42.15	16.86	6.49	3.70
PN	Neglig.	9.73	2.59	2.20

4. References

[1] R. Francis and G. Byrne, *Duplex Stainless Steels—Alloys for the 21st Century,* Metals, 2021, **11 (5)**, 836.
[2] H. Aghajani, and S. Behrangi. *Plasma Nitriding of Steels*. Springer International Publishing. 978-3-319-43068-3, (2017).
[3] D. Cochrane, "Guide to Stainless Steel Finishes," Euro Inox, 2005.
[4] S. Syahrullail and N. Nuraliza, *Effects of Different Load with Vary Lubricant on the Friction Coefficient and Wear Rate Using Pin on Disk Tribometer*, AMM, 2016, **819**, p 495–498.
[5] C.E. Pinedo, L.B. Varela, and A.P. Tschiptschin, *Low-Temperature Plasma Nitriding of AISI F51 Duplex Stainless Steel*, Surf. & Coat. Tech., 2013, **232**, 839–843.

Data automation for wheel-rail contact evaluation

Lopes, M. V. M.[1)*], de Lima, V. A.[1)], Machado, I.F.[1)], de Souza, R.M.[1)], F.J.[1)],Profito, F.J.[1)], Fukumasu, N.K.[1)] and Driemeier, L.[1)]
[1)] Escola Politécnica, Universidade de São Paulo,
São Paulo, 05508-030, Brazil
[*]Corresponding author: modsval@usp.br

1. Introduction

According to Jamshidi et al. [1] and Andrade [2], the increase in train traffic loads has changed the lifespan of the railways. Therefore, developing methodologies to improve the monitoring and maintenance of structures are among the main concerns to prevent accidents and diminish costs in railway operations. Artificial Intelligence (AI) is the most promising among the several approaches. However, one of the bottlenecks faced by AI researchers is the need for a large volume of data for training, whether from experimental measurements or computer simulations.

Within the scope of numerical simulations, several answers that bring information about the wheel-rail tribo-system can be achieved based on stresses, strains, and contact pressure analysis and, consequently, the type of damage that will be predominant in the system. The work conducted by Magel [3] proposes a metric that allows classifying the type of contact between the wheel and the rail. According to the author, conformal and closely conformal contacts favor wear damage, whereas non-conformal contacts will promote rolling contact fatigue (RCF) damage.

2. Objectives

The objective of this study is to propose the automation of a computer simulation that uses the Finite Element Method (FEM) for the calculation of stresses, strains, and contact pressure, as well as for the determination of the type of damage (wear or rolling contact fatigue) that will be predominant in the wheel-rail contact. The analysis combines different geometric profiles of wheels and rails to obtain a database that can be used to train AI models or provide a basis for various statistical analyses.

3. Methodology

The virtual model used to evaluate the contact between wheel and rail profiles consists of a simplified 2D representation of a wheelset under tangent traffic conditions, which was modeled in Abaqus software in a quasi-static simulation (Figure 01).

To automate the model, a Python script was developed that can access and execute the Abaqus tools through the command lines present in the code. The code makes it possible to import the wheel and rail geometries, define the boundary conditions, perform the simulations, and extract the results automatically from the software.

Figure 1 : 2D Virtual Model.

4. Results and Discussions

After the code execution, it was possible to perform 5454 simulations of different cases and obtain their respective results (Figure 02). The simulation execution and the extraction of the results took about 54 seconds, resulting in approximately 82 hours to generate the proposed database.

The von Mises stresses in the simulations varied between 287.15 MPa and 900 MPa, where only 4% of the cases presented some plastic deformation. The contact pressure varied between 287 MPa and 1985 MPa. Furthermore, 68% of the cases presented contacts whose predominant damage would be wear, while 32% presented contact fatigue as predominant damage.

5. Conclusions

The automation proposed by this work assisted in the development of a database that can provide information about wheel-rail contact through the variation and combination of geometric profiles.

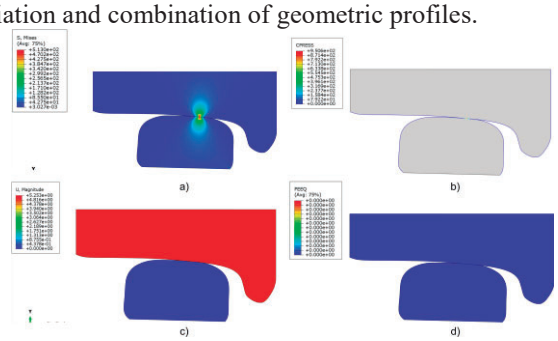

Figure 2 : Results obtained by Abaqus simulation where: a) is the von Mises stresses, b) the contact pressure, c) the displacement of the geometry and d) the equivalent plastic strain.

6. References

[1] JAMSHIDI, A. et al. *A decision support approach for condition-based maintenance of rails based on big data analysis*. Transportation Research Part C: Emerging Technologies, 2018. **95**: p. 185 – 206.
[2] ANDRADE, A. R. et al. *A Bayesian model to assess rail track geometry degradation through its life-cycle*. Research in Transportation Economics, 2012. **36**, p. 1-8.
[3] MAGEL, E. E. et al. *Control of Rolling Contact Fatigue of Rails*. 2002.

The impact of high chromium cast iron modified with niobium and boron on abrasive wear assessed by industrial tests under different severity conditions

Lima, M.M.[1)*], Godoy, C. [2)], Scal, M.W.[3)], Oliveira, C. [2)] and Bueno, M. [2)]

[1)*], Vallourec Research Center Brasil
[2)] Department of Metallurgical and Materials Engineering, Federal University of Minas Gerais - UFMG, Brazil
[3)] MScal Steelmaking Consulting Co., Brazil
*Corresponding author: marilia.lima@vallourec.com

1. Introduction

The austenite (γ) destabilization heat treatment aims to get the highest hardness through a martensite (α')-based microstructure with low retained austenite in white cast iron (WCI). Computational Thermodynamic (CT) is a good tool to define the austenitization temperature and equilibrium phases. With enough time, at high temperature, the equilibrium chemical composition is reached, the solid solution elements get the minimum value, increasing Ms temperature (thermodynamic factor for γ-α' transformation). Depends on the cooling rate a low γ content can be obtained in a martensitic matrix with secondary carbides (M_7C_3 and $M_{23}C_7$) – kinetic factor [1]. This study aims to clarify that not only alloy microstructure and hardness influence the wear resistance, but also that the same alloy may have different responses to wear when subjected to varying severity conditions.

2. Methods

The abrasion resistance was obtained through industrial tests in an iron ore transfer chute and a belt feeder conveyor. X-ray diffraction (XRD), OM, and SEM analyses were used to detect phases and microstructure. A destabilization treatment at 1020ºC for 2 h was carried out followed by air quenching and tempering at 250ºC for 2h. A high severity occurred in the transfer chute: transport rate of 1180 ton/h, speed of 3.0 m/s and a drop height of 12 m after 75 operating days. A low severity took place in belt feeder: transport rate of 2834 ton/h, speed of 0.5 m/s and with no drop height after 57 operating days. Based on the eutectic composition of 25%Cr and 2.8%C, four different WCI were designed: WCI, Nb-WCI, B-WCI, and NbB-WCI.

3. Results and Discussion

The WCI showed a eutectic microstructure with carbides surrounded by martensite and with austenite occupying the available space between these phases. The Nb addition leads to NbC precipitates at a temperature higher than eutectic promoting a hypoeutectic microstructure. According to CT the addition of B causes M_2B (M=Cr,Fe) formation at the eutectic temperature leading to a hypereutectic microstructure. These structural aspects are fundamental in abrasive wear resistance [2]. All Nb-B modified alloys have just martensite and no remaining austenite. Eutectic alloys showed greater wear resistance at high severity and hypereutectic alloys showed better performance at low severity tests, faced with different severities in industrial tests.

The distinct chemical compositions explain the microstructure variation in the materials (Fig.1a-d). B-WCI contain large primary carbides, B nitrides, and Fe-B carbides, whereas WCI retains austenite that contributes to the lowest wear rate under greater severity conditions (Fig.2a,b). On the other hand, NbB-WCI with a hypereutectic microstructure exibits the same effect but under less severe conditions in the Belt Feeder (Fig.2c,d). It is worth noting that even though the hardness of different alloys varies in a narrow range, these microstructural differences play a crucial role in their performance.

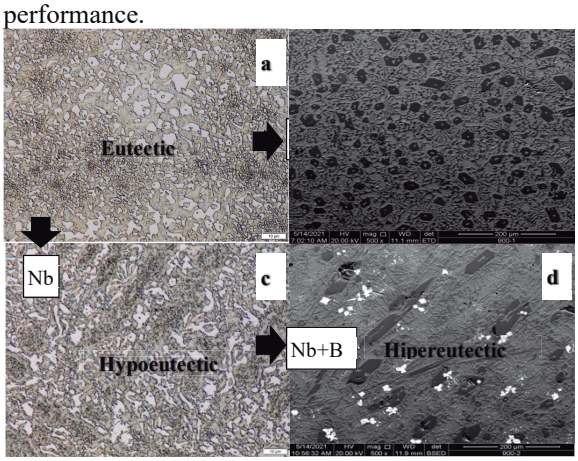

Fig.1: Microstructure: (a)WCI, (b)B-WCI, (c) Nb-WCI, and (d) NbB-WCI.

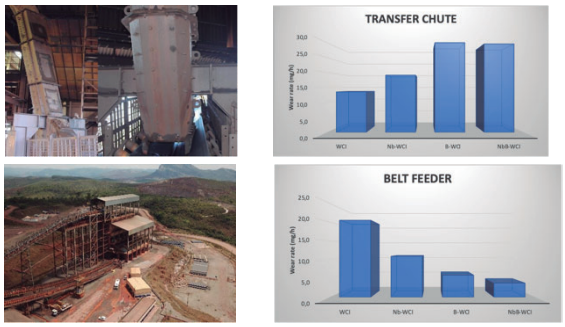

Fig 2: Wear Rate of alloys in industrial equipment.

4. Conclusions

An alloy responds differently to wear when subjected to different severities of industrial applications on mining process. Equal microstructures subjected to different severities lead to different responses in wear rate.

5.References

[1] Albertin E., Beneduce F., Matsumoto M. and Teixeira, I., *Optimizing heat treatment and wear resistance of high chromium cast irons using computational thermodynamics*. Wear, 2011. **271**: p.1813–1818.

[2] Pintaude G., Bernardes, F.G., Santos, M.M., Sinatora A., Albertin E., Mild and severe wear of steels and cast irons in sliding abrasion.Wear, 2009. 267: p. 19–25.

Thermally sprayed oxide-based coatings for tribological interfaces at high-temperature

Mayer, A.R.[1)*], Ettouil, F.B. [1)] , Moreau, C.[1)] , and Stoyanov, P.[2)]

[1)] Department of Mechanical, Industrial & Aerospace Engineering, Concordia University, Montreal, Quebec, Canada
[2)] Department of Chemical and Materials Engineering, Concordia University, Montreal, Quebec, Canada
[*]Corresponding author: andre.mayer@mail.concordia.ca

1. Introduction

Next-generation gas turbine engines are expected to operate at higher temperatures in order to achieve higher efficiencies. More specifically, a higher turbine inlet temperature, as shown in Figure 1, will increase the temperature of the surrounding components. Consequently, this can create challenges related to the employed materials in the engines. Oxide-based coatings present the required chemical and mechanical properties demanded to fulfill the need for new surfaces in more demanding conditions. In particular, some oxides have shown excellent lubricity and capability as solid lubricants at elevated temperatures [1]. Additionally, suspension plasma spray (SPS) is a process that can spray submicron powder, making the manufacturing of coatings with dense morphology possible. Therefore, this study aims to develop new oxide-based coatings by SPS.

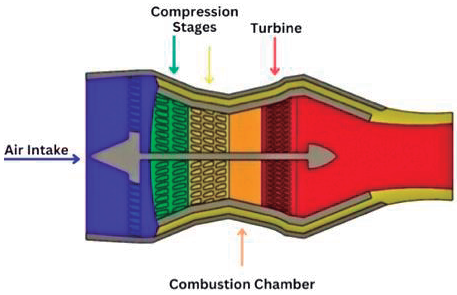

Figure 1 - Aircraft jet engine stages.

2. Materials and Methods

CoCrO coatings were sprayed using a Mettech's Axial III plasma spray system. An ethanol-based suspension containing 10% of solid content was used as feedstock. Tribology tests were performed using a TRB³ tribometer (Anton Paar TriTec SA, Switzerland). The parameters are shown in Figure 2.

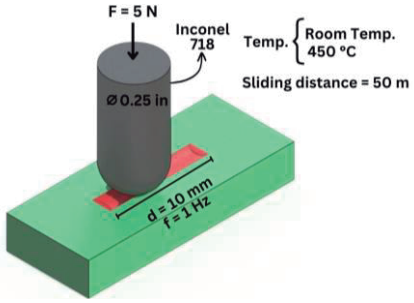

Figure 2 – Pin-on-flat parameters.

3. Results

CoCrO coatings with dense morphology were achieved, as shown in Figure 3. The coefficient of friction is shown in Figure 4 for the room temperature and at 450°C. The friction coefficient is lower for the tests performed at elevated temperature compared to that of the tests performed at room temperature. This behavior is consistent with prior literature for Co-based oxides, when the friction decreases by increasing temperature [2].

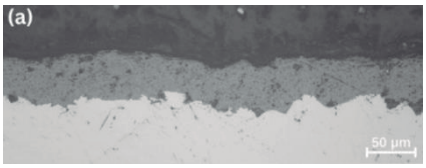

Figure 3 - Cross-section image of the oxide coating.

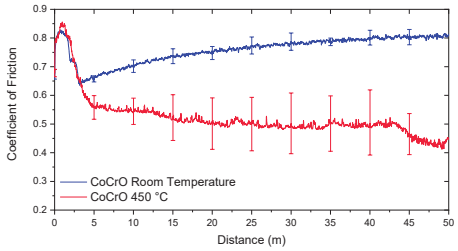

Figure 4 - Coefficient of Friction at room temperature and 450 °C.

4. Conclusions

Thermally sprayed CoCrO coatings have shown a substantial decrease in the coefficient of friction by increasing the temperature. Low wear rate at higher temperatures alongside the low coefficient of friction, makes this new family of coatings a possible candidate to solve problems related to the next generation aircraft engines.

5. References

[1] M. B. Peterson, J. J. Florek, and R. E. Lee, "Sliding Characteristics of Metals at High Temperatures," *E Trans.*, vol. 3, no. 1, pp. 101–109, Jan. 1960, doi: 10.1080/05698196008972392.

[2] M. B. Peterson, S. J. Calabrese, S. Z. Li, and X. X. Jiang, "Paper I (ii) Frictional properties of lubricating oxide coatings," in *Tribology Series*, Elsevier, 1990, pp. 15–25. doi: 10.1016/S0167-8922(08)70237-2.

Study of the effect of duplex treatments of nitrocarburizing and deposition of DLC films doped with nitrogen and silicon on the tribological properties of M2 steel

Danelon, M. R.[1)*], Manfrinato, M. D.[2), 3)] and Rossino, L. S.[2), 3)]

[1)] Department of Materials and Metallurgical Engineering, University of São Paulo - USP, São Paulo, Brazil
[2)] University of São Carlos – UFSCar – Sorocaba Campus, Sorocaba, Brazil
[3)] Sorocaba Technological College, FATEC-So, Sorocaba, Brazil
[*]Corresponding author: miguel.danelon@usp.br

1. Introduction

Duplex treatments consist of a combination of superficial treatments to improve the tribological properties of materials when compared to those treated individually [1]. A well-known duplex treatment is a combination of nitrocarburizing with DLC film, which promotes the formation of a ceramic compound layer and an amorphous carbon film, respectively. This work aims to study the effect of duplex treatment (nitrocarburizing+DLC) of silicon-doped and nitrogen-doped DLC on the wear resistance of AISI M2 steel.

2. Materials and Methods

Plasma treatments were carried out using a pulsed-DC power supply. A plasma ablation cleaning was performed with a gas mixture of 80%Ar-20%H2 for 1h. Plasma nitrocarburizing was performed with a gas mixture of 80%N2-15%H2-5%CH4 at 450ºC, a gas flow of 750sccm for 6h. DLC, NDLC, and Si-DLC films were deposited with a gas mixture of 90%CH4-10%Ar, 70%CH4-30%N2, and 90%CH4-8%Ar-2%HMDSO respectively, with a gas flow of 30sccm, for 2h. Duplex treatments were a combination of nitrocarburizing and DLC films with different doping. To evaluate the tribological properties of treatments, wear tests by fixed ball were performed, with a load of 8N, rotation of 158rpm, and different sliding distances, in which were evaluated the wear volume in function of the sliding distance and the coefficient of friction in the function of the test time. Wear volume was calculated according to equation 1, where b stands for the diameter of the crater and R is the radius of the sphere.

$$V = \frac{\pi b^4}{64R} \quad \text{for b <<<R} \qquad (1)$$

3. Results and Discussion

It was possible to observe that every treatment had a better wear resistance than the base material. However, the duplex treatment of nitrocarburizing + DLC-Si film presented the lowest wear volume, due to the combination of hardness in the depth of the compound layer and stabilization of sp^3 hybridizations promoted by the Si-DLC film.

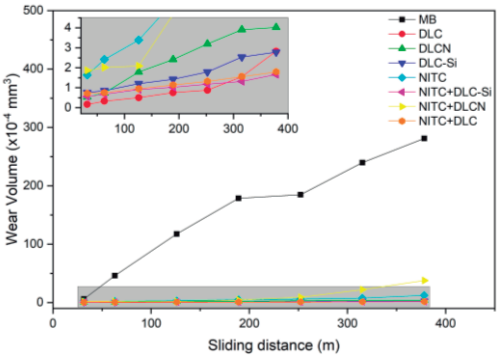

Figure 1 – Wear volume by sliding distance

The coefficient of friction of samples has presented the interaction between nitrocarburizing and DLC films and the low coefficient of friction of DLC films, due to the lubricity of the film. It is also possible to observe that duplex treatments present a rapid increase in the coefficient of friction, due to the complete wearing of the film, where the coefficient of friction relies on the nitrocarburizing layer.

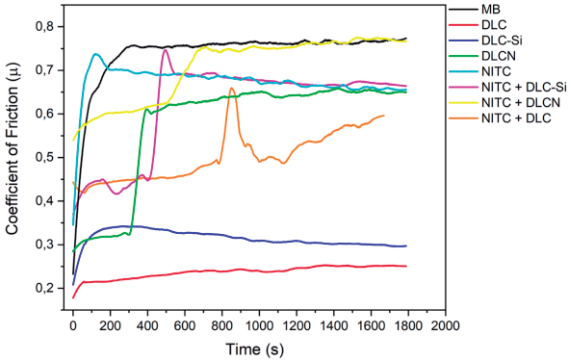

Figure 2 – Coefficient of friction as a function of the time of the test

4. Conclusions

To summarize, the combination of nitrocarburizing and DLC films has shown a great synergy and was able to improve the wear resistance of AISI M2 steel.

5. References

[1] Tschiptschin, A. P. *Duplex Coatings.* Encyclopedia of Tribology. Springer US, 2013. p. 794 – 800.

A wear map for the scratch behavior of Fe-Cr-C hardfacing

Colaço, F.H.G.[1)] and Pintaude, G.[2)*]

[1)] Department of Mechanical Engineering, Instituto Federal de Santa Catarina, Jaraguá do Sul, 89254 430, Brazil
[2)] Department of Mechanical Engineering, Universidade Tecnológica Federal do Paraná, Curitiba, 81280-340, Brazil
[*]Corresponding author: pintaude@utfpr.edu.br

1. Introduction

Fe-Cr-C hardfacings are well-recognized as a wear-resistant alternative for many components. Their performance depends on the microstructure and the interaction with the tribosystem. This tribological response was previously reported elsewhere for microabrasion tests [1]. Considering the possibility of employing these hardfacings in more aggressive environments, one can use the intense contact pressures in a scratch test. The possibility of building maps of scratch resistance was recently demonstrated in the literature [2] but without considering microstructural features.

Based on this possibility, this investigation presented a wear map for different kinds of microstructures, applying progressive loads during the scratching test.

2. Experimental procedures

Fe-Cr-C coatings were deposited by the newly developed FCDW-GTAW technique [1] to verify abrasion performance on a macroscopic scale. Four coatings were deposited on the AISI 1020 steel substrate by combining the tubular wires: Fe-Cr-C (3.34C; 27.0Cr; 0.31B), Fe-Cr-C-Nb (3.4C; 17.8Cr; 3.0Nb), Fe-Cr-C-Mo-Nb (4.56C; 19.0Cr; 6.1Mo; 0.7V; 1.53W; 5.5Nb) and Fe-Cr-C-Mo-Ti (2.0C; 6.5Cr; 1.1Mo; 6.0Ti). The combination of these wires resulted in a hypoeutectic microstructure with niobium and titanium carbides, with an average hardness of 650 $HV_{0.3}$. The hypereutectic microstructures were formed by different niobium contents, with microhardness ranging from 820 to 1020 $HV_{0.3}$. The mean free path matrix (MFP) was calculated by Equation 1, where Vf is the volume fraction of carbides, and NL is the average number of linear interceptions by carbides.

$$MFP = (1 - Vf)/Nl \quad (1)$$

Linear scratching tests, based on the ASTM-G171 Standard, were carried out applying progressive load between 20 and 180N in a diamond indenter with HRC geometry, with a tip radius of 200 µm, without lubrication and with a constant displacement speed of 0.17 mm/s. The coefficient of friction was measured using the load sensors of the CETR-UMT equipment. The widths of scratches were determined using a non-contact interferometer.

3. Results and Discussion

The wear map for hypoeutectic and hypereutectic microstructures is shown in Figure 1. For hypereutectic microstructures (blue), the scratch width increases with the applied load but tends to stabilize. In contrast, the behavior of the hypoeutectic microstructure curve (red) does not show a plateau tendency. This behavior can be associated with the matrix's resistance to deformation as the load increases. The austenite is predominant in the hypoeutectic microstructure; it deforms more than the eutectic matrix of the hypereutectic microstructure during the interaction with the indenter.

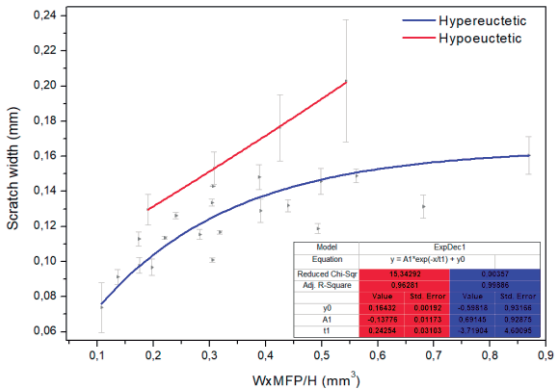

Figure 1 Scratch resistance map based on applied load (W), mean free path (MFP), and hardness (H) of hypoeutectic (in red) and hypereutectic (in blue) coatings.

4. Conclusion

We build a wear map based on scratch testing for different microstructures of Fe-Cr-C hardfacings. The effect of the mean free path on the scratch resistance of the hypereutectic microstructure is limited by the hardness of the matrix.

5. References

[1] Colaço, F.H.G., Pintaude, G. *Wear Regimes of Fe–Cr–C Hardfacing Alloys in Microscale Abrasion Tests*. Tribol Lett, 2022. **70**: p. 47. https://doi.org/10.1007/s11249-022-01590-7

[2] Kada, S.R., de Vaucorbeil, A., Fabijanic, D. and Barnett, M.R. *Work hardening and the scratch resistance of Ni–Co alloys using a rapid prototyping approach*. Wear, 2022, **510**, p.204493. https://doi.org/10.1016/j.wear.2022.204493

Influence of Polyethylene Glycol addition on the deposition and tribological performance of cobalt coatings prepared via cathodic plasma electrolytic deposition.

Romero, M.C.[1)*] ; Mello, V.[1)] ; Cunha, A.[2)] and Scandian, C.[1)]

1) Department of Mechanical Engineering, Federal University of Espírito Santo, Brazil,
2) Department of Physics,
Vitória, 29047 105, Brazil
*Corresponding author: manu.curbani@gmail.com

1. Introduction

Plasma electrolysis is a hybrid process that combines conventional electrolysis and atmospheric plasma processing. It is an emerging technology, firstly demonstrated in 1960's, with potential use in commercial scale for cleaning and coating due to its low cost, high adhesion to substrate, high deposition rates and environmental compatibility [1].
Cobalt is known as a wear and corrosion resistant material. It has high hardness, biocompatibility and unique magnetic properties that allows its use in microelectronics, sensor technology and in critical applications in industry and in defense [2]. In this study, the influence of PEG addition on deposition mechanism of Cobalt coating through CPED was investigated.

2. Materials and Methods

A CPED device was developed for preparing the coating. A graphite (99.9% purity) plate is used as the anode while the AISI 304 austenitic stainless-steel sample is used as the cathode. Both, anode and cathode are connected to the power supply by a metallic joint and were placed inside an ABS polymer holder to avoid contamination of the electrolyte with other metals and to bound the deposition area. A high-speed camera was used to monitor bubbles evolution. The electrolyte was composed by CoSO4.7H2O (25 g/l), H2SO4 (60 g/l), different contents of PEG (0, 0.75, 1.5 and 2.5 g/l), known as 0, 3, 6 and 10% of PEG. For CPED process, the voltage was directly increased to 85 V and held for 3 min.
Ball-on-plate sliding tests were done on a PLINT TE67 tribometer (Phoenix Tribology Ltd) using the deposited sample as the plate (body) and a 11 mm AISI 52100 ball as the counter-body. The applied normal load was 500 N, the sliding frequency of 3 Hz and stroke length of 2.5 mm. Test duration was 30 min.
Field emission scanning electron microscope (FESEM, FEI-Inspect F50) was used to investigate the morphology of both, surface and cross-section. Energy dispersive spectroscopy (EDS) was carried out to analyze the composition of the coatings. The topography of the coatings was assessed by an 3D optical profilometer (S Neox, Sensofar). The X-ray diffraction (XRD, Rigaku) measurements were performed for identifying phases present. Besides, grain size was estimated using Scherrer's equation. Wetting angle measurements were carried out using water and synthetic polyalphaolefin (PAO) oil. In order to evaluate de adhesion of the coating with the substrate, scratch tests were done using a Universal Macro-Tribometer Apex CETR-Bruker, in the linear scratch configuration.

3. Results and discussion

Figure 1 shows the current-voltage characteristic curves of the different studied electrolytes. It can be observed that PEG addition reduced the current density overall and delayed the occurrence of arcing regime (current rise in higher voltages). PEG increases the viscosity of the electrolyte, hindering the migration of the bubbles formed on the cathode surface towards the electrolyte. Besides, PEG is known to increase adsorption of gas on cathode surface. Thus, vapor sheath needed to form plasma discharge is more easily formed due to bubbles entrapment to the surface, decreasing ipeak. Images taken by the HSC camera during deposition process help to better understand bubbles formation and coalescence. When bubbles implode, a current peak is observed, due to the momentaneous contact of the conductive electrolyte with the sample surface. At this moment, cobalt ions are accelerated toward the surface, forming the deposit. Thus, a correlation between density of current peaks and thickness was established.
PEG increased electrolyte viscosity, reducing bubble expansion and implosion severity, then, decreasing surface roughness. However, PEG addition did not alter hardness, nor friction and wear.
Nanocrystalline cobalt coating with high hardness and FCC metastable phase was formed. It showed 2 times wear reduction compared to the substrate AISI 304.

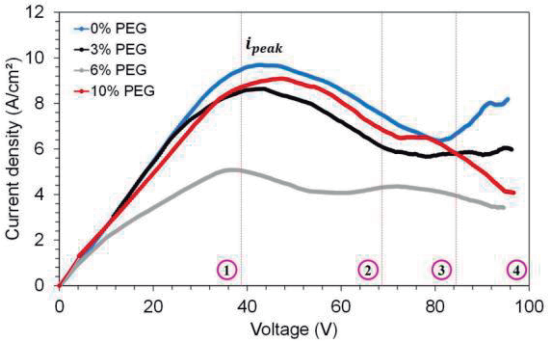

Figure 1 - *Current density - Voltage characteristic curves for 0%, 3%, 6% and 10% PEG samples*

5. References

[1] Yerokhin, A. L. et al. (1999). Plasma electrolysis for surface engineering. Surf. and coat. tech. 122(2-3), 73-93.
[2] Mahdavi, S., & Allahkaram, S. R. (2013). Characteristics of electrodeposited cobalt and titania nano-reinforced cobalt composite coatings. Surf. and Coat. Tech., 232, 198-203.

Effect of Plasma Nitriding on Resistance to Microwear and Fatigue of AISI 321 Stainless Steel

Manfrinato, M.D.[1,2)*], Almeida, L.S.[2)], Móron, R.C.[3)], Florêncio, O.[1)], Rossino, L.S.[1,2)] and Kiauga, A.M.[1)]

[1)] PPGCM UFSCar, Universidade Federal de São Carlos, Sorocaba, 18052-780, Brazil
[2)] Department of Materials, Fatec Sorocaba, Sorocaba, 18013-280, Brazil
[3)]Tecnológico Nacional de México Campus Tlalnepantla, Tlalnepantla de Baz ,54070, México
[*]Corresponding author: marcos.manfrinato@fatec.sp.gov.br

1. Introduction

AISI 321 stainless steels have excellent corrosion resistance, which is why they are used in metallic expansion joints, pipelines for oil cracking, and chemical reactors [1]. However, they have low resistance to wear and fatigue. To increase resistance to wear and fatigue, thermochemical plasma nitriding treatments are used [2]. The objective of this work is to verify the effect of the nitriding temperature on the formation of the layer and its relationship with the resistance to fatigue and abrasive microwear.

2. Materials and Methods

AISI 321 austenitic stainless steel was used in the form of a 15 mm diameter bar. The fatigue specimens were machined according to Figure 1. The specimens of microwear were used 15 mm diameter and 13 mm thickness. The fatigue and microwear specimens were sanded (120, 220, 320, 400, 600, 1200, 2000, and 2500) and polished with alumina with a grain size of 0.5µm.

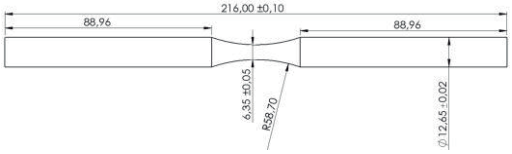

Figure 1 Fatigue specimens with dimensions in mm.

Plasma nitriding was performed with a gaseous mixture of 80%vol.N2 and 20%vol.H2 for 6 hours at temperatures of N400°C and N500°C. To characterize the layer formed, X-ray diffraction was carried out.

The abrasive microwear tests were carried out with a load of 8N, 150RPM, a ball with a diameter of 25.4mm of AISI 52100 steel quenched and tempered with a hardness of 60HRC and time of 10 and 20 minutes. To determine the volume removed, equation 1 was used.

$$V = \frac{\pi b^4}{64r} \quad (1)$$

3. Results and Discussions

The N400°C and N500°C specimens have a layer of 21µm (and surface microhardness of 1035HV) and 47.1µm (and surface microhardness of 1180HV), respectively. The base metal has a microhardness of 255HV. Figure 2 presents the XDR and the presence of expanded austenite is observed at N400°C and N500°C there is CrN and γ'-Fe4N. Figure 3 presents the fatigue results from rotational flexion.

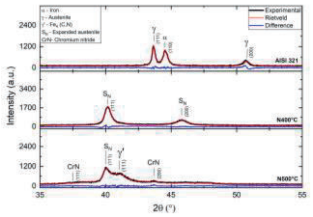

Figure 2 XRD patterns of the as-received and nitrided samples

Figure 3(a) shows the SN curve and it is observed that the increase in the fatigue limit for N400°C and N500°C were 44.73% and 25.31% respectively, about the base metal.

Figure 3(b) shows the volume removed during the abrasive microwear test. The N400°C treatment has the lowest volume removed due to the expanded austenite layer formed in the nitrided layer.

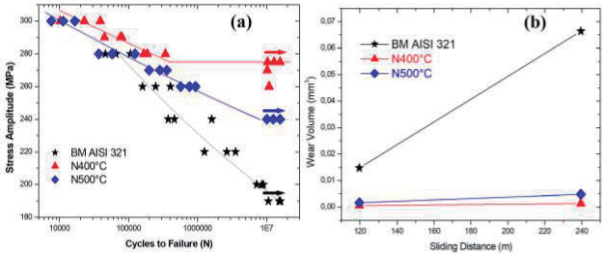

Figure 3 (a) SN curve and (b) volume wear.

4. Conclusion

The expanded austenite layer formed at N400°C produces a higher fatigue limit (380MPa) and greater resistance to abrasive microwear. The N500°C treatment presents the formation of CrN, which is very hard and has low ductility. In this way, cracks in rotational flexion and wear produce hard fragments that intensify the volume removed.

5. References

[1] El-Rahman, A.M.A. *An investigation on the microstructure, tribological and corrosion performance of AISI 321 stainless steel carbonitrided by RF plasma process*. Surf.& Coat. Tech, 2010, **205**, p. 674-681.
[2] Stinville, J.C,. et. al. *Plasma nitriding of 316L austenitic stainless steel: Experimental investigation of fatigue life and surface evolutions.* Surf & Coat. Tech., 2010. **204**: p. 1947-1951.

Abrasive wear of polymer coatings for sustainable energy generation

Xavier, F.A[1)], Bordin, F.M.[1)*], Costa, E.C. [1)], Barcelos, M.C.S.[1)], Oliveira, L.L.[2)], and Bezerra, W.[2)]

[1)] Department of Mechanical Engineering, Universidade Federal de Santa Catarina, Florianópolis, 88040 900, Brazil
[2)] Jirau Energia, Porto Velho, RO, 20030 021, Brazil
[*]Corresponding author: f.m.bordin@posgrad.ufsc.br

1. Introduction

The interest in sustainable energy generation predicts that 25% of all new energy production will be focused on hydropower plants [1]. Thus, it is mandatory that the technology applied to protect the turbine blades is effective and sustainable.

In the past few years, the application of carbide coatings (WC-Co-Cr, VC, etc.) by thermal spray, welding, or adjacent coating processes is being replaced by time and energy-efficient polymeric (epoxy resin) coatings, as an alternative with lower service life. Therefore, this study showcases the wear resistance and behavior of polymeric coatings applied for turbine blade protection.

2. Materials and methods

The experiments were performed according to the ASTM G65-16 (Rubber wheel/dry sand) test procedure D (6,000 revolutions – 30 minutes, 45 N load). A standardized sand (SiO_2) was used as abrasive.

An AISI 306L stainless steel was used as substrate for the specimens. Coating A (epoxy resin embedded with spheric and irregular silicon carbide particles) and coating B (epoxy resin embedded with irregular particles silicon carbide particles) were applied to the substrate material, with an average thickness of 600 µm.The cross-sectional microstructure of the samples is highlighted on Figure 1.

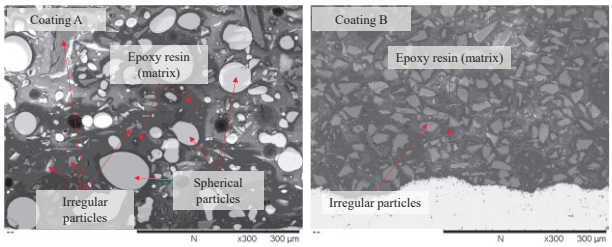

Figure 1 Microstructure of the tested coatings.

The results were evaluated in terms of average and behavior of the samples' wear rate, calculated by the adjusted volumetric loss (AVL). The profile of the cavity and texture of the wear track was also analyzed.

3. Results

The follow-up wear behavior can be observed in Figure 2. Both coatings illustrated a similar behavior and magnitude: a sharp decrease within the first seconds of testing, reaching a constant wear rate halfway through the coatings' life. The higher wear rate observed at first is due to the lower contact area leading up to higher contact pressures; as the contact area increases, wear rate reaches a threshold and stabilizes.

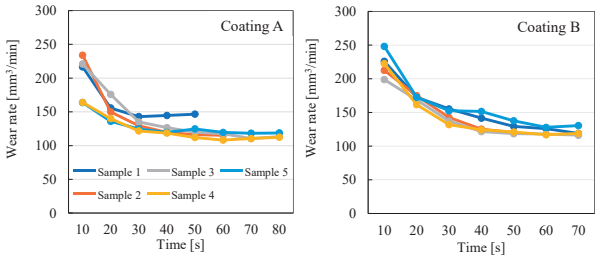

Figure 2 Wear rate along time intervals.

There is no statistically significant difference between the two coatings, as the erosion of the matrix is the main wear mechanism, even though the microstructure is different in both particle shape and distribution. This is also observed in the wear track longitudinal profile, highlighted in Figure 3.

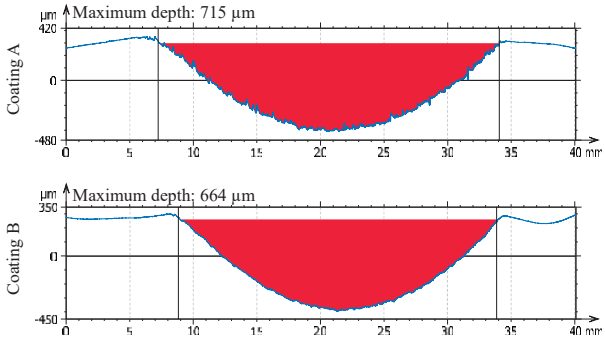

Figure 3 Wear track profiles and the resulting surface.

4. References

[1] Hauer, C., B. Wagner, J. Aigner, P. Holzapfel, P. Flödl, M. Liedermann, M. Tritthart, C. Sindelar, U. Pulg, M. Haimann, B.O. Donnum, M. Stickler, H. Habersack. *State of the art, shortcomings and future challegens for a sustainable sediment management in hydropower: A review*. Renew. & Sust. En. Rev., 2018: **98**, pp. 40-55.

5. Acknowledgments

Project regulated by ANEEL and developed in the scope of R&D of Jirau Energia S.A.

Electric Vehicle Traction Motor Bearing Tribology

- Damage Assessment and Mitigations

Gnanamoorthy R* and G V Balakrishna

Department of Mechanical Engineering
Indian Institute of Technology Madras
Chennai 600036, India

*Corresponding author: gmoorthy@smail.iitm.ac.in

Electric mobility from various energy sources will reduce air pollution and noise, as traction motors replace internal combustion engines in modern mobility. Bearings are the critical elements in the traction motors and decide the overall performance of the vehicles and passenger comfort. The rolling element bearings used in the motors experience electrical loads in addition to mechanical loads and fail prematurely. Understanding the contact characteristics under combined loading in individual contacts rather than full-bearing testing will assist in understanding the micro mechanisms of failure. An in-house developed tribo-testing device that simulates the ball-on-disk contact under the influence of an electromechanical environment is used in the current investigations. Our research focuses on understanding the effect of electric current, voltage, load, and speed on the damage to lubricant and bearing steel using the developed simulator. Mitigation measures are also discussed.

Compatibility assessment of PAO and POE with PA6 for potential EVs application

Bernardo Tormos[1], Adbeel Balaguer [1] Enrique Gimenez[2]
1) CMT – Motores Térmicos, Universitat Politècnica de València, Valencia, Spain.
2) Instituto de Tecnología de Materiales, Universitat Politècnica de València (UPV), Valencia, Spain
*Corresponding author: abalrey@mot.upv.es

1. Introduction

In the context of developing fluids for battery electric vehicles and given the fast-paced growth of e-mobility powertrains, it is important to ensure the compatibility of fluids with standard electric motor components beforehand. Incorporating an electric motor into the powertrain results in a variety of nonmetallic materials being in contact with the lubricant [1]. The objective of this study was to assess the material compatibility between two synthetic base oils and a hard plastic through an immersion test. The goal was to determine and compare the effects of both fluids on the physical and mechanical behavior of the polymer in order to assess their potential to be used in immersion cooling applications. The loss mass, hardness tensile strength, and ultimate strain, before and after exposure to the fluids, were examined.

2. Materials and methods

At the moment of this research, there is no standard for this particular application; some suggestions to study the material compatibility between fluids and plastics have been proposed in the SAE Information Report J3200 [1]. The method used in this study was based on a modification of ASTM D7216 standard and D638 for the tensile measurements. The effects of the test oils on the polymer were determined by measuring the changes in mass, hardness, and tensile properties resulting from the immersion test.

The base oils evaluated were polyalphaolefin (PAO4) and polyolester oil (POE). Polyamide (PA6), a polymer with repeating units linked by amide bonds, was selected as hard plastic. This engineering thermoplastic has a number of automotive applications such as engine covers, battery trays, and electrical connectors.

The PA6 samples were immersed in the test oil for a duration of 168 hours at a constant temperature of 120°C. Five rectangular samples with dimensions of 50x25x2 mm^3 were used to evaluate the mass loss and hardness. Both properties were measured before and after exposure in each specimen to calculate the percentage change in each case. The hardness was measured using the Shore D hardness tester. Regarding tensile strength, five tensile test specimens (type I, ASTM D638) were used for each immersion test, For comparative purposes, samples without immersion treatment were also tested.

3. Results

Table 1 presents the variations in the physical properties of the PA6 after the immersion test, compared to the pre-immersion measurements. Immersion significantly alters the polymer properties. Contact with PAO reduced the ductility by 94.89%. However, contact with POE resulted in only a 29% decrease. Analyzing the stress-strain curves (see Figure 1), the three groups of samples are observed: (1) specimens in contact with PAO, (2) specimens in contact with POE, and (3) control specimens, PA6 that did not come into contact with any fluid. The curve behavior for group 2 of samples closely resembles the typical behavior of PA6 without any contact with a fluid, indicating that POE has a lesser impact on plastic properties. Both fluids decrease the sample mass by approximately 2%, suggesting the removal of associated polymer components. Additionally, both fluids increase material hardness, with PAO showing the greatest increase of 6 points.

Table 1 PA6 physical property changes due to contact with the fluids by immersion test

	In contact w/PAO4		In contact w/POE oil	
Evaluated physical property	***Change***	***SD***	***Change***	***SD***
Mass	-1.90 %	0.03	-2.27%	0.03
Shore D hardness	6	0.84	4	0.46
Tensile strength	9.95%	4.66	19.79%	0.59
Ultimate strain	-94.89%	1.73	-29.00%	3.87

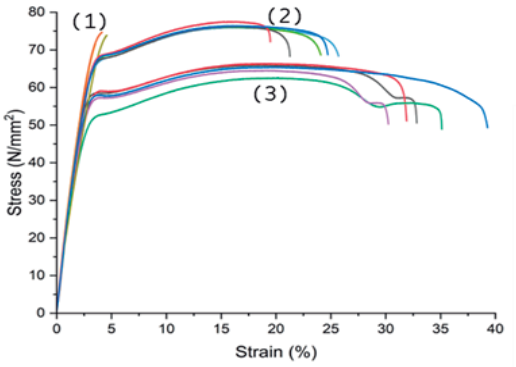

Figure 1 Strain- stress curve for the samples

4. Conclusion

Based on the results of this study, it is evident that when comparing the effects of both fluids on the polymer, POE has a lesser impact on the material properties. This suggests that polyolesters are more favorable candidates as base oils for the development of fluids intended for battery electric vehicles. Further research and validation are recommended to ascertain the long-term effects and optimize the formulation for optimal performance and durability in electric vehicle systems.

5. References [1] SAE J3200 *Fluid for automotive electrified drivetrains.* (2022). SAE International. https://doi.org/10.4271/j3200_202210.

6. Acknowledgments GVA grants for the hiring of predoctoral research personnel, CIACIF/2021/241.

How can tribology help the energy transition?

Costa, H.L[1,2,4)], Souza, R.M. [2,3)], de Mello, J.D.B. [2,4,6)], Pintaude, G.[2,5)], Binder, C. [2,6)], Scandian, C. [2,7)], Alves, S.M. [2,8)], Cava. S.S. [2, 9)]

[1)] Surface Engineering Group, Universidade Federal do Rio Grande, Rio Grande, 96203-900, Brazil
[2)] National Research Institute on Green Tribology for the Energy Transition (INCT CT-Trib)
[3)] Surface Phenomena Laboratory, Universidade de São Paulo, Brazil
[4)] Tribology and Materials Laboratory, Universidade Federal de Uberlândia, Uberlândia, Brazil
[5)] Universidade Tecnológica Federal do Paraná, Curitiba, Brazil
[6)] LabMat, Universidade Federal de Santa Catarina, Florianópolis, Brazil
[7)] Laboratory of Tribology, Corrosion and Materials, Universidade Federal do Espírito santo, Vitória, Brazil
[8)] Universidade Federal do Rio Grande do Norte, Natal, Brazil
[9)] Ceramics Group, Universidade Federal de Pelotas, Pelotas, Brazil
[*]Corresponding author: henaracosta@furg.br

1. Introduction

Humanity is experiencing a critical moment that requires a complete paradigm shift through a radical energy transition. According to the targets established in the COP26 report, to rescue the planet's climate and guarantee its sustainable development, two strategic themes are the mobility sector and the generation of clean and renewable energy. In transport, electric vehicles should gradually replace internal combustion engines, but this transition will occur at different rates in different regions. Heavy vehicles used in sea and air transport are difficult to electrify. Thus, the use of low or zero carbon biofuels is a key technology in this transition, as well as other technologies such as fuel cells and innovative solutions for the reuse of waste. However, there are technological bottlenecks for the application of the various technologies proposed in the transport sector. In the generation of clean energy (wind, hydroelectric, thermochemical generators, etc.), the tribology of the mobile components involved, the proposition of tribological solutions and the environmental impact of technologies are fundamental points that need to be addressed for a successful energy transition.

2. The National Research Institute on Tribology for the Energy Transition (INT CT-Trib)

Faced with the enormous challenges associated with the energy transition, TriboBr created an integrated and multidisciplinary national network that uses tribology as a tool to contribute to the solution of the. This knowledge generation ecosystem encompasses the most eminent groups of tribology, from the extreme south to the northeast of the country, bringing together researchers in tribology, materials science, physics, chemistry, biochemistry and environment to foster strong interaction with the productive sector. The approval of the creation of a national research institute (INCT) on Green Tribology Towards the Energy Transition (CT-Trib) is fundamental to develop new solutions in lubricants, materials and surface engineering for the mobility and energy of the future. CT-Trib is focused on identifying and acting on the main tribological challenges arising from current technologies, which will guide research for tribological optimization of new sustainable solutions.

3. Methodological contexts

CT Trib works on several fronts, all with strong industrial partnerships, based on three main visions: *i.* understanding of tribological phenomena based on laboratory experiments, simulations at different scales, collection and interpretation of results obtained in the field; *ii.* development of alternatives in terms of products and processes to solve tribological problems of interest to the Institute and its network of relationships; and *iii.* assessment of the environmental impact of technologies and inputs developed by CT Trib. From this set of visions, some of these fronts guide the objectives and activities.
In the mobility sector, CT Trib focuses mainly on the optimization of tribological systems (material / lubricant / surface engineering / additives) for engines with low-emission forms of propulsion. With regard to automotive vehicles, three fronts are worth mentioning: 1. Tribological challenges associated with electric vehicles; 2. Low carbon fuels, for which it is necessary to clearly identify the main challenges arising from current technologies, creating systematic information and an extensive database of friction, wear and degradation of current low carbon fuels. These data should guide the investigation of, for example, how new fuels, fuel blends and/or fuel additives can affect the tribological behavior of engines and what tribological solutions can be applied. 3. Innovative solutions, including for example carbon neutral fuels, fuel cells of the future and new solutions using waste recycling. 4. Database of tribological challenges associated with biodiesel. 5. Engines powered by low and zero carbon fuels; and 6. development of new materials to reduce weight and increase the durability of vehicles. 7. Tribological challenges in the generation of clean electricity (wind, hydroelectric, solar and thermochemical generators from waste).
CT-Trib vision involves the strengthening of partnerships with companies that develop projects aimed at the energy transition, as well as fostering new industrial partnerships, creating an innovation ecosystem that attracts investments aimed at reducing pollutant emissions and cooling global warming.

Exploring the Potential of Ti3C2TX MXene as a Lubricant Additive: Topography Evolution and Performance under Boundary Lubrication

Franzosi, D.[1)*], Profito, F. J[1)]., Rosenkranz, A.[2)] , Souza, R.M.[1)]

[1)]Department of Mechanical Engineering, Universidade de São Paulo, São Paulo, Brazil
[2)]Department of Chemical Engineering, Biotechnology and Materials, FCFM, University of Chile, Santiago, Chile
[*]Corresponding author: davi.franzosi.oliveira@usp.br

1. Introduction

Lubricant additives are developed to enhance lubricant performance and mitigate unwanted interfacial phenomena, such as friction, wear, corrosion and oxidation [1]. One promising option in lubricant additive research involves utilizing 2D materials that can promote friction reduction and improve wear resistance in many lubricated tribosystems. Among these materials, MXenes, which are carbides and nitrides of transition metals [2], have gained attention. A recent study has demonstrated the significant role of MXenes in reducing friction [3]. Notably, unlike other 2D materials, the friction reduction provided by MXenes does not seem to be significantly altered by the number of layers present [4]. This study aims to examine the impact of Ti3C2TX MXene on the coefficient of friction (COF) and wear under boundary lubrication conditions to determine its suitability as an additive in engine oil. Differently from a previous study [3], this paper will investigate the tribochemistry of MXenes in boundary conditions.

2. Methodology

Tribological tests were conducted using an SRV tribometer under reciprocating sliding motion using a base oil (PAO) and a fully-formulated low-viscosity engine oil (FF). The concentration of MXenes in each test is shown in Table 1.

Table 1 Concentration of MXenes

Oil	MXene Concentration
PAO	0% ; 0,05% ; 0,1% ; 0,2%
FF	0% ; 0,05% ; 0,1% ; 0,2%

Friction was evaluated using SRV data, in terms of the cycle average COF and peak-to-peak COF. The test conditions are shown in Table 2.

Table 2 Test procedure

Test Variables	Correspondent Values
Preload	50N
Normal Load	150N
Oscilattion Frequency	10Hz
Ocilattion amplitude	5mm
Temperature	90°C
Duration	60 min

3. Results

In order to assess the effect of MXenes on wear, the surface roughness of the tested samples was measured using 3D optical interferometry before and after (Fig.1) tests.

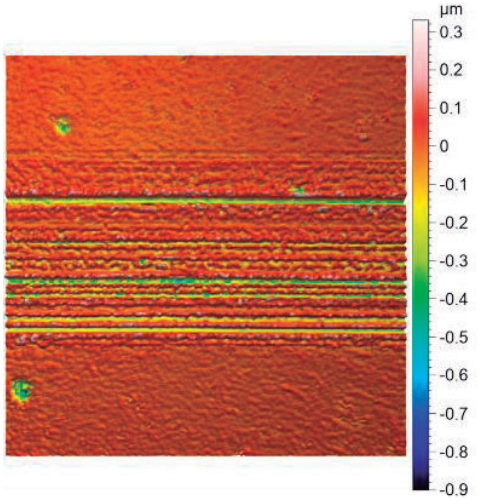

Figure 1 0W20 Wear Track Topography

The topography measurements allowed the evaluation of the evolution of the surface topography, including the statistical parameters and the mean curvature radius of the asperities.

In addition to the surface roughness analysis, the tested surfaces were chemically characterized using Raman spectroscopy and Scanning Electron Microscopy (SEM) with Energy-Dispersive X-ray Spectroscopy (EDS). These analyses were conducted to verify the potential formation of MXenes tribofilms on the surfaces. Results have indicated that the concentration plays a major role in COF values. The results of this study will be compared to previous results with graphene, to check how two different nanoparticles works.

4. References

[1]A.K. Rahid, M. khalid, et al., in Tribology International 2016, 103, 504-515.
[2] Y. Gogotsi, B. Anasori, in ACS Nano 2019, 13(8), 8491-8494
[3], G. Boidi, J.C.F de Queiróz, F.J. Profito, A. Rosenkranz. in ACS Applied Nano Materials 2023, 6(1), 729737.
[4] P. Serle, M. Hamidinejad et al., et al..in Nano Letters, 2022 22(8), 3356-3363.

Influence of Dimple Texturing on Coefficient of Friction of Piston Ring–Cylinder Liner Conjunction

Luz, F.K.C.[1)] *, Costa, H.L.[1)] Profito, F.J.[2)] and Santos, M.B.[3)]

[1)] Laboratory of Surface Engineering, Federal University of Rio Grande, Rio Grande – RS, 96203-900, Brazil
[2)] Surface Phenomena Laboratory, University of São Paulo, São Paulo - SP, 05508-030, Brazil
[3)] Department of Mechanical Engineering, Federal University of Uberlandia, Uberlandia, 38408-100, Brazil
*Corresponding author: felipekevin.fkcl@furg.br

1. Introduction

This study utilizes a deterministic numerical model to investigate the mixed lubrication performance of textured piston ring–cylinder linear conjunction in internal combustion engines. The model considers rough contact mechanics, cavitation effects, and texturing features on the cylinder surface. The obtained results provide insights into the lubrication behaviour of textured contacts under mixed lubrication conditions.

2. Materials and Methods

2.1. Numerical model

The numerical model proposed in [1] employs a modified $p-\theta$ Reynolds equation (Eq. 1) to calculate the fluid pressure, where ρ and μ are the lubricant density and viscosity, respectively, h is the local lubricant gap that account for surface roughness deterministically, U is the sliding velocity of the contacting surfaces, p_H is the hydrodynamic pressure, and θ is the lubricant film fraction associated with the fluid film cavitation effect.

$$\frac{\partial}{\partial x}\left[\frac{\rho h^3}{12\mu}\frac{\partial p_H}{\partial x}\right]+\frac{\partial}{\partial z}\left[\frac{\rho h^3}{12\mu}\frac{\partial p_H}{\partial z}\right]=\frac{\partial}{\partial x}\left[\theta\rho h\frac{U}{2}\right] \quad (1)$$

The hydrodynamic shear stress is calculated using Eq. 2:

$$\tau_H=\frac{h}{2}\frac{\partial p_h}{\partial x}+\mu\theta\left(\frac{U}{h}\right) \quad (2)$$

The rough contact model utilizes the Hertz theory for elastic contact to calculate the contact pressure at each asperity between the piston liner surface and the admitted smooth and rigid ring surface. The contact shear stress is calculated as a proportion of the contact pressure as $\tau_{ASP}=\mu_{bl}p_{ASP}$, where μ_{bl} is the boundary coefficient of friction provided from experimental data.

The calculation for the overall friction coefficient of the contact is written in Eq. 3.

$$\overline{COF}\ (\Lambda)=\frac{\tau_H(\Lambda)+\tau_{ASP}(\Lambda)}{p_H(\Lambda)+p_{ASP}(\Lambda)} \quad (3)$$

2.2. Surface characterization

The surface of the honed cylinder liner undergoes a virtual texturization process that generates spherical pockets, called dimples, with a diameter of 200 µm and a depth of 3 µm. The textured area density was varied, resulting in surfaces with 20%, 30%, and 50% textured area to evaluate the influence of dimples on the friction coefficient. The topography of the virtually textured cylinder surfaces was sliced into segments of 1000 µm, and a finite volume mesh with 376 x 251 nodes was generated to solve Eq. 1 numerically. The ring is assumed to be rigid and smooth, and its dynamic effects are neglected.

2.3. Simulation parameters

The parameters used for the numerical simulation are summarised in Table 1.

Table 1 Simulation parameters

Sliding velocity ($\boldsymbol{U}$)	2,82 m/s
Dynamic Viscosity ($\boldsymbol{\mu}$)	4 cSt
Density ($\boldsymbol{\rho}$)	0,82 g/cm^3
Elastic Modulus ($\boldsymbol{E_s}$)	120 GPa
Elastic Modulus ($\boldsymbol{H}$)	420 HV
Boundary Coefficient of Friction ($\boldsymbol{\mu_{lb}}$)	0,14

3. Results

The dimples have proven to be beneficial for the cylinder liner surface, showing a reduction in the friction coefficient for all three textured area densities investigated (see Figure 1). Among them, the 20% textured area demonstrated the best perform.

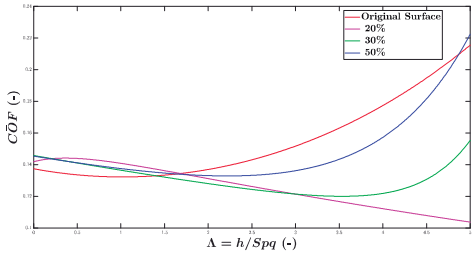

Figure 1 – Coefficient of friction

4. References

[1] F.J. Profito, E. Tomanik, D.C. Zachariadis, Effect of cylinder liner wear on the mixed lubrication regime of TLOCRs, Tribology international, 93 (2016) 723-732.

Wear Coefficient Determination of Heterogeneous Microstructures using Numerical Simulation and Machine Learning

Lima, A.O.[1)*], Souza, R.M[1)] and Machado, I.F.[1)]
[1)] Polytechnic School of the University of São Paulo, São Paulo, 05508-030, Brazil
[*]Corresponding author: arnaldo_olima@usp.br

1. Introduction

Estimating the wear coefficient in heterogeneous microstructures presents a challenge due to the complex microstructure and the variation of mechanical properties at different length scales [1][2]. This study integrates experimental tribological tests, numerical simulations, and machine learning algorithms to investigate the wear of a heterogeneous microstructure, such as that shown in Figure 1a. Experimental scratch tests and numerical models were used to evaluate the wear coefficient in a heterogeneous material. At the same time, machine learning algorithms such as Artificial Neural Networks, Random Forest, and Robust Linear Regression were employed for data analysis.

2. Experimental, numerical, and machine learning procedures

Experimental tests were conducted using a Bruker Inc. UMT-2 tribometer. The tests were performed in cycles, in which the indenter (Rockwell C tip) scratched the surface in both forward and backward directions. The selected cycles were 1, 5, 10, 20, 30, and 40. The wear tracks were subsequently analyzed and characterized using scanning electron microscopy (SEM) with a Jeol JSM 6010-LA and a Coherence Correlation Interferometry (CCI) device from Taylor Hobson.

The numerical models were developed using the Abaqus software with the 3D explicit module (Figure 1b). The models incorporated the same indenter geometry and experimental test configurations. Within the Abaqus environment, a heterogeneous microstructure was constructed, consisting of three phases: graphite, carbides, and matrix (Figure 1a).

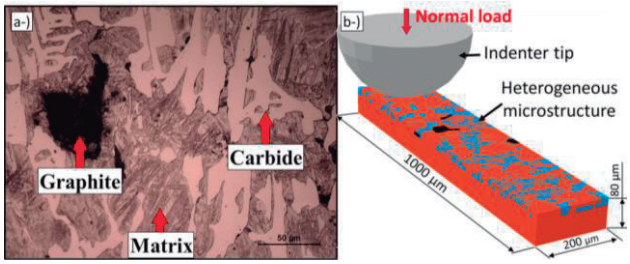

Figure 1a: Heterogeneous microstructure. b- Numerical 3D model.

The database was built using a combination of experimental and numerical results. Three different distinct machine learning algorithms were employed:

- **Artificial Neural Network** (ANN): The architecture consisted of two hidden layers, each with eight neurons. The activation function used is *ReLu*.
- **Random Forest** (RF): The algorithm used the *Sklearn* library and the *RandomForestRegressor* function.
- **Robust Linear Regression** (RLR): The algorithm used the *statsmodels* library with the RLM function and the Huber-T estimator to mitigate outliner effects.

During the model evaluation step, the model's accuracy and mean absolute error (MAE) were measured on the test set.

3. Results

Figure 2 presents the results of the wear coefficient obtained from both experimental tests and numerical models. The coefficient is influenced by the applied load and the number of cycles, showing increased stability as these parameters increase.

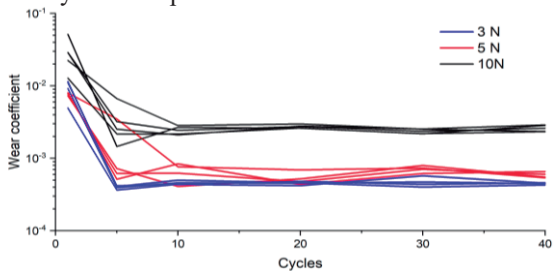

Figure 2 - Wear coefficient by cycles numbers

Figure 3 shows a comparison of the results obtained by applying machine learning methods to the test data. The MAE values obtained were 2.61E-6, 1.72E-3, and 1.42E-3 for ANN, RF, and RLR, respectively. The closer the points are to the red diagonal line, the better the predictive model performs. A lower MAE value indicates a better approximation and improved method performance.

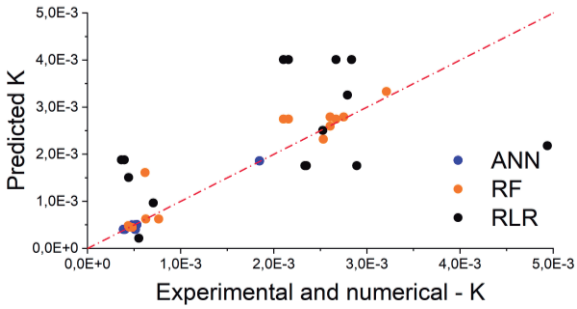

Figure 3- Comparison of real and predicted K

4. Conclusions

In this work, the prediction of the wear coefficient using machine learning algorithms was analyzed from experimental and numerical database results.

The neural network exhibited the best approximation to the experimental and numerical results.

It was verified the effectiveness of machine learning algorithms in modeling wear behavior and providing valuable insights for engineering applications.

5. References

[1] Seriacopi, V., et al., *Mechanical behavior and abrasive mechanism mapping applied to micro-scratch tests on homogeneous.* Wear. 2020. **450-451**. 203240.
[2] Aydin, F. and Durgut, R.*Estimation of wear performace.*Trans. Non. Me. Soc. China, 2021. **31**.

A Novel Nonlocal Wear Model for Assessing the Tribological Performance of Journal Bearings

Blanco-Rodríguez, J.[1)*], Porteiro, J.[1)], Profito, F. J.[2)]

[1)] CINTECX, Universidade de Vigo, Lagoas-Marcosende s/n, Vigo, 36310, Spain
[2)] Department of Mechanical Engineering, Polytechnic School of University of Sao Paulo, Sao Paulo, Brazil
[*]Corresponding author: javier.blanco.rodriguez@uvigo.gal

1. Introduction

Journal bearings are critical components of many engineering systems that require optimal performance and durability. Wear modelling is a powerful tool that can help predict and explain the wear behavior of bearings under various operating conditions. It can also help detect and address excessive wear issues that may compromise the reliability and longevity of bearing systems. This enables improved design and material selection for bearings that withstand high thermal-mechanical loads, detrimental misalignment, and transient operation effects. Moreover, wear modelling can also help tailor optimal bearing designs to reduce frictional losses, enhancing system efficiency and reducing energy consumption. In this work, we present an integrated simulation approach to evaluate the synergistic effect of low-viscosity lubricants and ultralow friction coatings on the tribological performance of engine components. A new wear model based on a nonlocal averaging method is developed to overcome the mesh size dependency of wear predictions. The model is validated by comparing the simulation results with experimental data from [1,2]. The model is then used to investigate the friction and wear behaviour of an Al bearing with a DLC-coated journal in a connecting rod assembly.

2. Methodology

A novel wear model is developed by extending the simulation approach used by [3] to account for steady-state wear depth prediction in the experimental apparatus and procedure shown in Figure 1. In the proposed model, several subroutines are elaborated to improve the wear simulation of transient conditions. First, a predictive time step algorithm establishes each iteration's steady state step of wear. Subsequently, a nonlocal averaging method enhances the wear area prediction and reduces the mesh dependency on results.

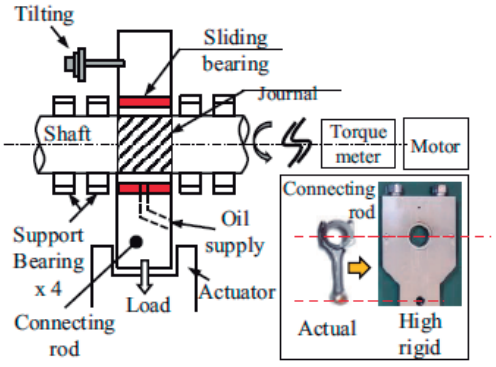

(a)

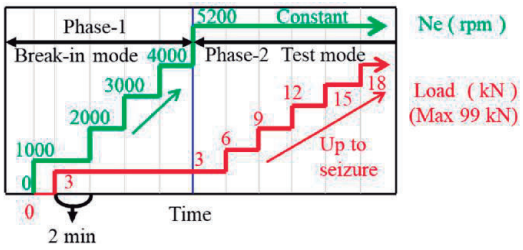

(b)

Figure 1 – (a) Experimental apparatus and (b) test procedure used to validate the wear model [1, 2].

This averaging method is based on weighting functions and the influence area per node. Therefore, correctly selecting these two elements of the method is critical to predicting a realistic wear zone and strongly depends on the application.

3. Results

Results from the experimental tests of [2] will be used as a benchmark to validate the proposed wear model (see Figure 2). Measurements of axial bearing profiles will be used to calibrate the simulation model, and then wear assessment will compare predicted wear load and wear depth for the experimental procedure. Furthermore, a lubricant selection procedure will be presented to determine which lubricant suits this application better as a function of friction losses and wear.

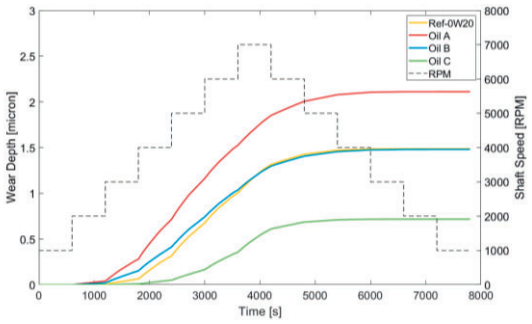

Figure 2 – Wear Assessment

4. References

[1] Ogihara H.; Iwata T. et al. The effects of DLC-coated journal on improving seizure limit and reducing friction under engine oil lubrication. International Journal of Engine Research. 2022;23(8):1267-1274.
[2] Iwata, T.; Oikawa, M. et al. Excellent Seizure and Friction Properties Achieved with a Combination of an a-C:H:Si DLC-Coated Journal and an Aluminum Alloy Plain Bearing. Coatings 2021, 11, 1055.
[3] Profito F.J. On the development of advanced techniques for mixed-elastohydrodynamic lubrication modelling of journal and sliding bearing systems. 2015.

Prediction of Friction Torque and Kinematics of Tapered Roller Bearings with detailed Multibody Simulation

Wingertszahn, P.[1)], Koch, O.[1)*]

[1)] RPTU University of Kaiserslautern-Landau, Kaiserslautern,
Chair of Machine Elements, Gears and Tribology (MEGT)
Gottlieb-Daimler-Straße, 67663 Kaiserslautern, Germany
*Corresponding author: oliver.koch@rptu.de

1. Introduction

As part of the general trend towards CO2 reduction, preload forces in adjusted bearing arrangements are being reduced as far as possible to minimize frictional losses in rolling contact. A one-sided load or, in the case of an O arrangement, heating of the overall system can lead to axial operating clearance, which significantly influences the operating behavior of one or both bearings. Especially in applications where the bearing is subjected to low loads and lack of lubrication during its life cycle and the rollers are relatively large and heavy, there is an increased sliding component in the rolling element motion. In combination with rapid speed and load changes, the risk of slip-induced bearing damage increases. These operating conditions occur, for example, in wind turbines.

2. Multibody Simulation

Since more than 20 years a multibody simulation tool is developed at the MEGT. The general workflow is shown in figure 1.

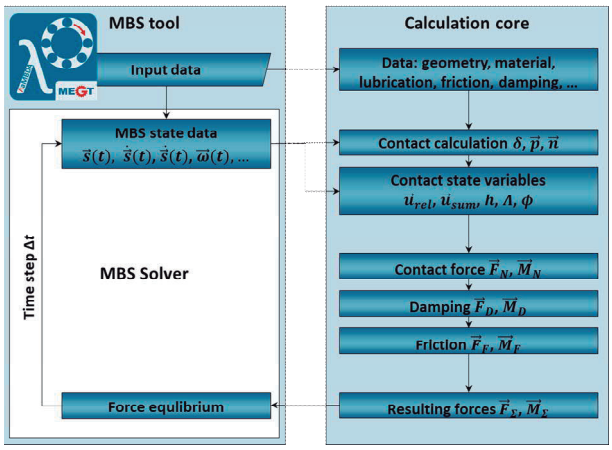

Figure 1 Flow chart of contact force calculation between rolling elements and ring raceways

For highly accurate prediction of the bearing friction the consideration of solid and lubricant friction is mandatory. Figure 2 shows the principles of the friction model. For tapered roller bearings in particular the friction in the contact between the rolling element end face and the inner ring rip is of importance. To cover this contact in good manner a cell model [1] has been developed which allows a much better calculation of the contact pressure in comparison to the usual used model according to Hertz (Figure 3) and which computation time is suitable for a multibody simulation [2].

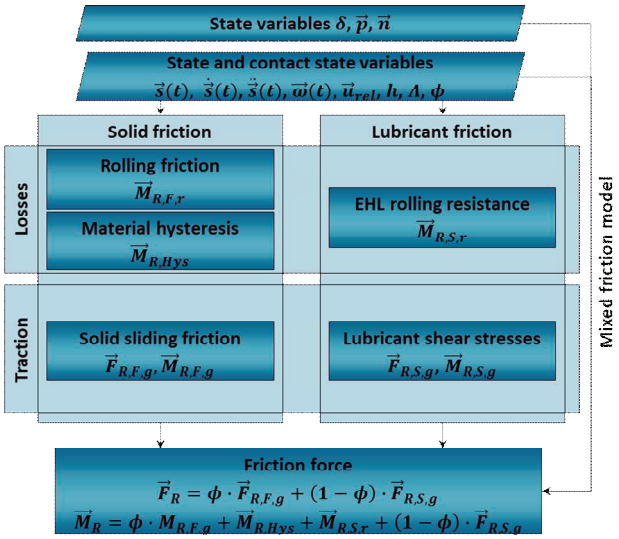

Figure 2 Sequence of friction calculation for lubricated contact between rolling element and raceway

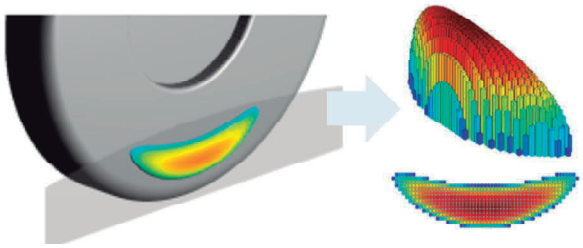

Figure 3 Contact area and pressure distribution of the rib contact

A lot of validation work has been carried out for critical operating conditions of tapered roller bearings. It can be shown that especially the modelling of the churning losses has a significant impact on the prediction of the kinematics and therefore surface damage characteristic values.

3. References

[1] Kiekbusch, T.: *Strategien zur dynamischen Simulation von Wälzlagern.* PhD-Thesis, Technische Universität Kaiserslautern, 2017, Maschinenelemente und Getriebetechnik Berichte Bd. 23/2017, ISBN 978-3-95974-043-2.

[2] Wingertszahn, P., Atalay, O., Sauer, B., Koch, O.: *Modelling geometrical raceway deviations of roller bearings in multi-body simulation and analysis on its effects in experiment*. Orlando 15.-19. May 2022, 76th Annual Meeting & Exhibition (STLE) 2022

Effects of Highly Dynamic Rotational Cycles on Radial Shaft Seals with Dust Lip

Silva, L.M.C.[1)*], Stiemcke, Y.[1)], Thielen, S.[1)] and Koch, O.[1)]

[1)] Chair of Machine Elements, Gears and Tribology (MEGT), Rheinland-Pfälzische Technische Universität Kaiserslautern-Landau,
Kaiserslautern, 67653, Germany
[*]Corresponding author: lenine.silva@rptu.de

1. Introduction

The incidence of applications involving shafts with dynamic reciprocating shaft movements has witnessed a significant increase. For example, positioning robots carry out their tasks at extremely high rotational speeds and accelerations, often accompanied by frequent changes in direction. However, the impact of these oscillations on seals remains unknown. In practical applications, mineral oil has been found in undesirable situations such as in groceries [1] [2]. Previous studies have hinted at a potential relationship between highly dynamic oscillation in rotary shafts and the build-up of vacuum pressure in the intermediate room between the dust lip and the sealing lip of a radial shaft seal (IR) [3]. Therefore, this study aims to bridge this knowledge gap by investigating the performance of a radial shaft seal operating under unsteady rotary oscillation.

2. Materials and Methods

To comprehensively explore various operational scenarios and assess the influence of each parameter variation on sealing performance, a series of trials was designed. These trials were conducted using a specialized test bench capable of replicating the unsteady rotation patterns typically encountered in positioning robots. Throughout each trial, precise pressure measurements were obtained directly from the IR between lips.

2.1. The High Acceleration Test Bench

The high acceleration test bench of the MEGT is used to reproduce the operating conditions of a dynamic application. The test bench consists of two cells to which two highly dynamic motors are coupled. Each cell consists of a metallic housing with a main shaft supported on two bearings and is fully filled with oil. To conduct the seals tests, the cells are sealed with two elements per open side: one test shaft and one test seal.

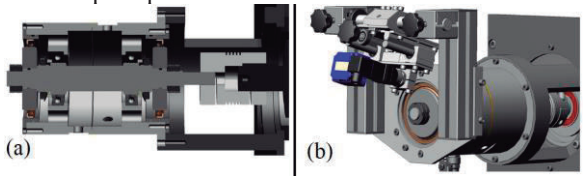

Figure 1 Cross-section of the test cell of high acceleration test bench (a), test cell with mounted pressure sensor (b)

In addition, a prick device was developed to measure the pressure in the IR. This device is attached to the front side of the cell. It can be adjusted in the vertical plane as well as in the pitch angle. In addition, a pressure sensor is mounted on a linear guide, which can be moved by turning a hand wheel. This platform is used to pierce the dust lip with the aid of a surgical needle (see Fig. 1).

2.2. Test Procedure

The tests were realized varying the parameters of Table 1: (*i*) the acceleration at the sealing contact; (*ii*) the angle of shaft oscillation; and (*iii*) the degree of greasing in IR (between the lips).

Table 1 - Parameter variation for each test

Parameter	Setting		
Cycle	Triangular Curve		
Acceleration / m/s²	80	160	240
Oscillation Angle / °	5	10	15
Grease in IR / %	30	50	70

3. Results and Conclusions

The measured pressure was important to determine not only the lowest pressure in the radial seal but also the volume of air extracted from the IR.

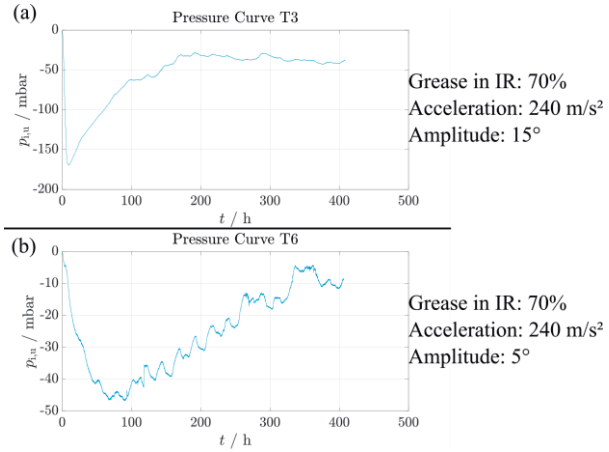

Figure 2 Curve representation of the pressure in the space between the main lip and the dust lip during the Test 3 (a) and 6 (b).

4. References

[1] Foodwatch, „Mineralöle in Lebensmitteln - Ergebnisse des foodwatch-Tests,“ *Foodwatch Test,* 2015.

[2] EFSA Panel on Contaminants in the Food Chain (CONTAM), „Scientific Opinion on Mineral Oil,“ *EFSA Journal,* p. 185, 2012.

[3] S. Thielen, „Reibverhalten und Dichtfunktion von Radialwellendichtringen bei instationärer Wellendrehzahl . Forschungsvorhaben 784 I,“ Forschungsvereinigung Antriebstechnik e.V. (FVA), IGF-Nr.: 18870 N, Abschlussbericht, FVA-Heft Nr. 1355,“ 2019.

COMPARATIVE SLIDING WEAR BEHAVIOR OF A PEARLITE AND A TEMPERED UPPER BAINITE MICROSTRUCTURES

Souza, S.S.[1] Pereira, H.B.[1], Tressia, G.[2], Centeno, D.M.A.[3], Lima, A.O[1]; Alves, L.H.D.[5] and Goldenstein, H.[1]

[1] Department of Metallurgical and Materials Engineering, Universidade de São Paulo, São Paulo, 05508-030, Brazil
[2] Vale Institute of Technology, Ouro Preto, Brazil
[3] Metallurgical Processes Laboratory, Instituto de Pesquisas Tecnológicas, São Paulo, 05508-901, Brazil
[4] Federal University of Juiz de Fora, Minas Gerais, 36036-900, Brazil
*Corresponding author: hgoldens@usp.br

1. Introduction

The wear resistance of steel railroad wheels is affected by a complex combination of mechanical properties and ultimately by the morphologies and distributions of the phases composing the microstructure, i.e., the microconstituent (e.g., pearlite, upper bainite, ausferrite and tempered martensite). For microstructures obtained with a specific microconstituent, the wear resistance usually increases linearly with increasing hardness. This relationship is described by the Archard equation [1]. However, the wear resistances of microstructures obtained from different microconstituents cannot be compared only based on hardness [1, 2].

The aim of the present work is to give further contributions to the question explored in Kalousek [2], Chaves [3], Bavaresco [4] and many others: for the same steel chemical composition, which microconstituent present the best combination of tribological properties for application in heavy haul wheels?

Table 1 presents the chemical composition of the cast steel wheel from which samples were obtained for this study.

Table 1: Studied steel chemical composition

C	Mn	Si	Cr	Mo	Ni	B
0,721	0.746	0.614	0.203	0.079	0.026	0,0003

A pearlite (357+-8Hv0.3) and a tempered upper bainite (370+-10Hv0.3) microstructures were obtained, by heat treating samples in a quenching dilatometer. Masoumi [5] gives details of the procedure. Tribological studies used pin-on-disc sliding wear experiments; sliding wear parameters were: 100 N and 300 N of normal load, 1 hour, dry, without debris removal and 25 mm of radial distance. The pins were 4 mm in diameter and the counter bodies were made of a quenched and tempered AISI H-13 steel (600+-10 Hv30). The coefficients of friction (COF) were calculated as the average of the values between 2000s and 3600s, as done by [6]. More details about the pin-on-disc configuration used are given by [5, 6].

Figure 1a presents the tribological results. Figures 1b and 1c present, respectively, the pearlite and tempered upper bainite microstructures studied. The slightly softer pearlite microstructure presented better wear resistances for both conditions tested. These results evidence the influence of carbide morphology upon the tribological behavior. The greater surface to volume ratio of the cementite in the pearlite seems to favor its work hardening capacity, leading ultimately to higher sliding wear resistance [2]. The COF values were indistinguishable between the studied microstructures for each load studied. But the values decreased with increasing load. This phenomenon is attributed to the greater presence of oxides at higher loads which inhibit the metal/metal contact and was also seen by [6].

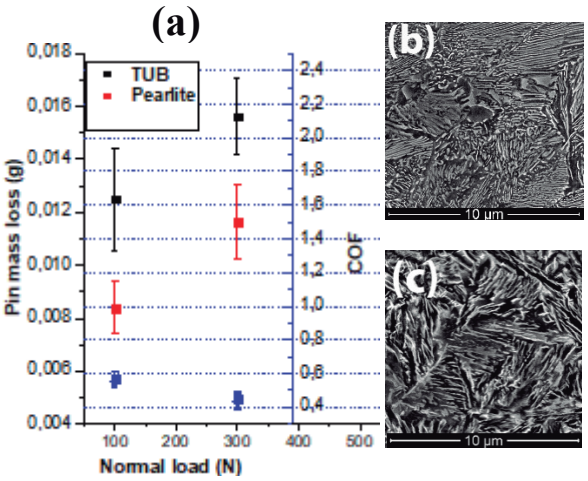

Figure 1: (a) Pin mass losses and COF as a function of load for the different microstructures; (b) pearlite and (c) tempered upper bainite.

2. References

[1] Hutchings, I; shipway, P. 2017. Tribology: Friction and Wear of engineering Materials. Butterworth-Heinemann.
[2] Kalousek, J; Fegredo, D.M; Laufer, E.E. 1985. The wear resistance and worn metallography of pearlite, bainite and tempered martensite rail steel microstructures of high hardness. Wear. 105(3):199-222.
[3] Chaves, A. P. G. 2021. Relação entre a microestrutura e a resistência ao desgaste na pista de rolamento de rodas ferroviárias em suas múltiplas vidas. 168 f. Tese (Doutorado em Ciências) – Escola Politécnica, Universidade de São Paulo, São Paulo.
[4] Rezende, A.B; Fonseca, S.T; Fernandes, F.M; Miranda, R.S; Grijalba, F.A.F; Farina, P.F.S; Mei, P.R. Wear behaviour of bainitic and pearlitic microstructures from microalloyed railway wheel steel. Wear. v.456-457. 2020.
[5] Masoumi, M., Tressia, G., Centeno, D.M.A. *et al.* Improving the Mechanical Properties and Wear Resistance of a Commercial Pearlitic Rail Steel Using a Two-Step Heat Treatment. *Metall Mater Trans A* **52**, 4888–4906 (2021).
[6] Tressia, G; Pereira, J.I; Penagos, J.J; Bortoleto, E & Sinatora, A. Effect of in-service work hardening on the sliding wear resistance of a heavy haul rail in the gauge corner. Wear. 482, 2021.

Evaluation of the micro-scratch resistance in different directions of a directionally solidified high chromium cast iron

Bergami, L.B[1)*], Lima, A.O.[1)], Albertin,E[2)], Machado, I.F.[1)] ,Souza, R.M.[1)]

1) Department of Mechanical Engineering, University of São Paulo, SP, Brazil
2) Institute for Technological Research – IPT, São Paulo, SP, Brazil
*Corresponding author: leandrobergami@usp.br

1. Introduction

This study employed a scratch test technique in micro-scale to assess the micro-scratch resistance of a directionally solidified high chromium cast iron (HCCI). This type of material was chosen due to its exceptional wear resistance properties, primarily due to the significant content of rod-like chromium-rich carbides. In respect of the orientation of this phase, studies [1,2] have indicated that the wear resistance of this material may change depending on the direction of the scratches in relation to the long exes of the carbides. The main objectives of this research are to compare scratches made in three different directions in terms of the lateral force and depth of the groove and to evaluate their aspects. Different from a previous study [2], micro-scale scratches were able to investigate the action of a single abrasive particle under loads in the mN range.

2. Materials and Methods

Samples of eutectic high chromium cast iron with 3.0 wt% C, 25.3 wt% Cr, directionally solidified and heat-treated at an austenitization temperature of 1100 °C were scratched using a Berkovich diamond indenter [2]. The tests were performed with a progressive normal force, starting in 0 mN up to 100 mN. The other test parameters are the test time, of 60 seconds, and the scratch length, of 300 µm. Throughout the tests, information regarding groove depth and lateral force is acquired in real-time. For each scratch direction, three scratches were performed. Scanning electron microscopy was used to examine the scratched surfaces.

3. Results and discussion

Figure 1 depicts the microstructure with examples of scratches performed in each direction. Firstly, in Figure 1a, we observe a groove on the basal plane of the carbides, which corresponds to a transversal direction relative to the long axis of the carbides (TR). Secondly, in Figure 1b, as the indenter moves across the HCCI surface, it strikes the carbides at an angle close to 90° with respect to the long axis of the carbides. This direction can be referred to as parallel-orthogonal direction (PA-OR). The third direction is shown in Figure 1c, where a scratch parallel to the long axis of the carbides is visible. Figure 2 displays results obtained during the tests. In terms of the lateral force, Figure 2a exhibits no notable differences in the curves. However, the results for groove depth, illustrated in Figure 2b, clearly indicate that the curve in the PA-PA direction exhibited significantly high values. This finding aligns with the results reported in Bergami et al. [2], where macro-scratches were realized, and the PA-PA direction exhibited groove depth substantially higher compared to the other directions. Nonetheless, the reasons for micro-scratches are different. While in macro-scratches the surface hardness and the wedge formation in front of the tip explained this phenomenon, here the responsible mechanism seems to be the contact of the indenter with the carbides. In TR and PA-OR directions, carbides greater than the width of the scratch partially blocked the passage of the tip, forcing it to move upwards, which in turn reduces the depth and width of the scratch.

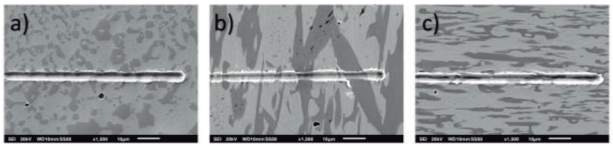

Figure 1 The end of scratches a) transverse (TR), b) parallel-orthogonal (PA-OR) and c) parallel-parallel (PA-PA) direction.

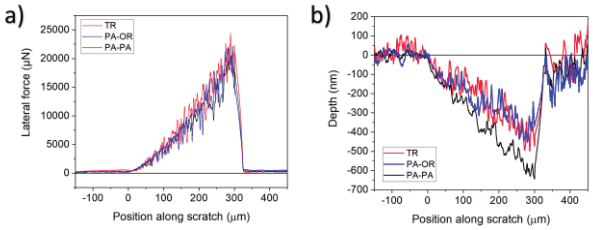

Figure 2 Curves of a) lateral force and b) depth of the grooves

4. Conclusions

Scratches were observed in three different directions in a HCCI directional solidified. The finding suggests that when the scratch is parallel to the long axis of the carbides, the resulting groove tends to be deeper compared to scratches in other directions. This phenomenon arises from the reduced ability of the carbides to partially block the scratch.

5. References

[1] Hawk JA, Dogan ÖN. Effect of carbide orientation on abrasion of high Cr white cast iron. Wear. 1995;189:136–42.

[2] Bergami LB, Lima AO, Venturelli BN, Machado IF, Albertin E, Souza RM. Effect of carbide orientation during single scratch test in directionally solidified and heat-treated high chromium cast irons. Wear. 2023.

Soft Tribology and Rheology of Functional Soy Yogurts Supplemented with Prebiotics

Cardoso, B.B.[1,2)], Gomes, J.S.[1,2)], Vieira, J.M.[1,2)], Rodrigues, R.[1,2)], Abreu, C.S.[2,3,4)], Gomes, J.R.[2,3)*], Silvério, S.C.[1,2)] and Rodrigues, L.R.[1,2)]

[1)] Centre of Biological Engineering (CEB), Universidade do Minho, Campus de Gualtar, 4710-057 Braga, Portugal
[2)] LABBELS – Associate Laboratory, Braga/Guimarães, Portugal
[3)] Center for Microelectromechanical Systems (CMEMS), Universidade do Minho, 4800-058 Guimarães, Portugal
[4)] Physics Department, Porto Superior Engineering Institute, ISEP, 4200-072 Porto, Portugal
[*]Corresponding author: jgomes@dem.uminho.pt

1. Introduction

Functional foods can be defined as food products that provide health benefits beyond basic nutrition. They are usually enriched or fortified with bioactive ingredients such as probiotics, prebiotics and flavonoids. However, the development of functional foods faces several challenges due to the high expectations of consumers in terms of taste, texture and healthiness.

2. Methods

Different new dairy-alternative functional yogurts were produced through the fermentation of soy milk supplemented with prebiotics (epilactose, lactulose, raffinose and inulin). A plain yogurt was made without the addition of prebiotics and a commercial soy yogurt was considered as reference sample.

Texture analysis was performed by compression tests at 30% strain. Firmness, stickiness and Young´s modulus were determined by the highest peak force measured during compression, the negative peak load and the slope of the first linear interval of the compression curve, respectively.

Rheological analysis was performed at 25 ºC in a HR-1 rheometer equipped with a stainless-steel cone-plate geometry (∅60 mm, 2º angle, truncation 64 μm). Flow curves were obtained by an up–down–up step program to assess rheological properties within the linear viscoelastic domain. A frequency sweep (from 0.1 to 10 Hz) at 0.5% strain was performed to evaluate the viscoelastic properties of the yogurts.

The tribological characterization of the yogurts was carried out using a reciprocating ball-on-plate contact geometry to study their frictional properties. A stainless-steel ball (Ø10 mm), purposed to represent the palate, was subjected to a reciprocating sliding motion on a polydimethylsiloxane (PDMS) disc mimicking the human tongue surface. The experiments were performed with constant stroke length (8.5 mm), applied load (1 N) and maximum speed of 40 $mm.s^{-1}$ for 60 s. The maximum (CoF_{max}) and average (CoF_{av}) values of the friction were evaluated. In addition, a ball-on-plate contact geometry with relative circular motion of the ball was used to obtain *Stribeck* curves for the different yogurts and identify typically observed lubrication regimes for food samples. Later experiments were done with constant load (1 N) and increasing speed (25 - 200 $mm.s^{-1}$) during 60 s. The CoF was plotted as a function of the sliding speed to obtain look-alike *Stribeck* curves.

3. Results and Discussion

Texture parameters suggested that the addition of prebiotics did not promote significant textural changes on the yogurt´s matrix, compared to plain samples, as no significant differences were found in either, firmness, stickiness or young´s modulus.

Rheological data showed that the addition of prebiotics did not increase the viscosity, agreeing with the firmness results. The functional yogurts showed no relevant differences in the rheological parameters, but the epilactose loaded yogurt exhibited the higher consistency index. This characteristic may be important for palatability providing a more pleasant mouthfeel and swallowing process.

Reciprocating sliding tests revealed no major differences between the different samples in terms of CoF_{max}, which may indicate that the initial mouthfeel promoted by functional yogurts could be similar to the commercial one in terms of oral sensation, suggesting good consumer acceptance. Contrarily, CoF_{av} values for functional yogurts were significantly lower than the commercial sample. This could represent a softer mouthfeel attained following initial tribological interaction between the samples and oral tissues, which could facilitate swallowing and appeal to the consumers. Moreover, the yogurt containing epilactose has the lowest CoF_{av} value, highlighting that this prebiotic is suitable for incorporating in functional yogurts with expected good acceptance by the consumers. *Stribeck* curves for the different yogurts revealed a perceptible variation in friction within the studied speeds, indicating different lubrication regimes. However, the epilactose loaded yogurt showed no perceptible changes concerning the lubrication regimes and denoted the lowest CoF of all analyzed systems, which could be relevant for palatability and a more pleasant mouthfeel. In conclusion, soft tribology combined with rheology has demonstrated that functional soy yogurts supplemented with prebiotics could potentially have good commercial acceptance characteristics.

Acknowledgements: This work was supported by FCT national funds, under the national support to R&D units grant, through the reference projects UIDB/04436/2020, UIDP/04436/2020, UIDB/04469/2020 and UIDP/04469/2020. Cardoso, B.B., acknowledges her doctoral grant (SFRH/BD/132324/2017) from FCT.

Effect of potential on the friction coefficient and wear of the Co-Cr-Mo alloy in Ringer´s lactate solution

Silva, R.N.A.[1)], Soares, R. [2)], Neto, R. [2)], Vieira, A. [3)], Radi, P.A. [3)], Santos, M. [1)], Viana, F [2)] and Vieira, L. [3)*]

[1)] Department of Materials Engineering, University of the State of Amazonas – UEA, 69050-020, Brazil
[2)] Department of Metallurgical and Materials Engineering and Mechanical Engineering, Faculty of Engineering, University of Porto - FEUP, 4200-465, Portugal.
[3)] Research and Development Institute (IP&D), University of Paraiba Valley (UNIVAP), 12244-000 S. J. dos Campos, SP, Brazil
*Corresponding author: lucia.vieira@univap.br

1. Introduction

Cobalt-chromium-based alloys have been developed and employed in high-demanding medical applications [1], such as the knee and hip, due to their excellent ability to maintain mechanical properties and biocompatibility over long periods. Co-Cr-Mo alloy castings or forged with 28% Cr and 6% Mo could be divided into two orders according to carbon content: i) low carbon alloys (C content < 0.05 %) - present a homogeneous structure and alloys and ii) high carbon (the content of C > 0.15 %) - characterized by carbides precipitation [2]. The first casting was produced without applying electromagnetic stirring casting (EMS) for comparison. The others were submitted to different EMS frequencies for 15 min. In these three foundries, the applied EMS frequencies were 15 Hz, 75 Hz, and 150 Hz. This paper investigates the effects that may occur in a Co-Cr-Mo alloy submitted to different potential and to tribocorrosion tests in a Ringer's lactate solution, like biomedical conditions. The Co-Cr-Mo alloy is a passive alloy that spontaneously forms a protective oxide layer. This study was performed after the Co-Cr-Mo was submitted to EMS.

2. Experimental

The tribocorrosion behaviour of the Co-Cr-Mo alloy samples was evaluated through different potential and OCP evolution in static and dynamic modes in a Ringer's lactate solution. The friction and wear were also evaluated according to the applied potential on passive and cathodic voltages.

3. Results and discussion

Fig. 1 shows the evolution of OCP before, during, and after tribocorrosion tests on bare samples immersed in Ringer´s solution at room temperature. It is possible to observe in Fig. 1 that, in static mode, the OCP of sample A1 have a much lower value than other samples, indicating the formation and consumption of the passive layer (the potential recovery corresponds to the film passivation). This abrupt drop may mean breaking the oxide film on the sample surface or damaging the passive protective film. By the time the sliding (rubbing) starts, there is a decrease in the OCP in all samples, with greater emphasis on sample A1. Sample A1 has the highest decrease value of OCP. A significant reduction in OCP when the rubbing started at -0.16 to -0.45 V and returned to -0.16 V. This result shows that in this concentration, there is a tendency to remove the passive layer. The A2 (-0,19 to -0.42 V) sample behaved similarly to samples A1 and A4 and returned to -0.17 V. The least propitious corrosion is sample A3, the average value is -0.36 V. When the rubbing started -0.14 to -0.36 V and returned to -0.14 V and recovered gradually, thus showing more excellent resistance from this surface about corrosion. These results can be initially associated with the size of the reduced grains by EMS.

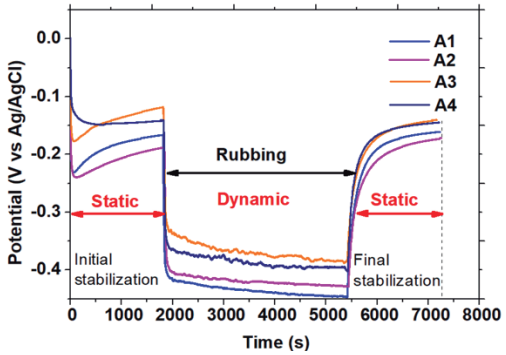

Figure 1 Evolution of open circuit potential (OCP vs Ag/AgCl) values during tribocorrosion tests in the samples A1, A2, A3 and A4

4. Conclusion

Tribocorrosion results showed that in the dynamic mode with OCP, the samples A2, A3, and A4 with reduced grains showed a lower corrosion tendency concerning the sample (A1) without EMS application. Among the material tested in this study, the A3 sample gave the lowest friction coefficient 0.34±0.15 in Ringer´s solution and the lowest material loss, compared with A1. In this case, the carbides in the grain interstices can be responsible for the A3 sample result.

5. References

[1] Aherwar A, Patnaik A, Bahraminasab M. Effect of Molybdenum Content on Structure and Properties of a Co-Cr Biomedical Alloy. *J Mater Eng Perform* 2019; 28: 6340–6353.
[2] Mischler S, Muñoz AI. Wear of CoCrMo alloys used in metal-on-metal hip joints: A tribocorrosion appraisal. *Wear* 2013; 297: 1081–1094.

Influence of Particle Size and Porosity on The Tribological Behaviour of Vacuum-Impregnated Sintered Steel

Araya, N.[1-2)*], Neves, G.O.[2-3)], Binder, C.[3)], Klein, A.N. [3)], de Mello, J.D.B.[3-4)].

[1)] Department of Materials Engineering, Concepcion University, Concepción, 4070 386, Chile
[2)] Department of Mechanical Engineering, Bio Bio University, Concepción, 4081 112, Chile
[3)] Department of Mechanical Engineering, Santa Catarina Federal University, Florianópolis, 88040 900, Brazil
[4)] College of Mechanical Engineering, Uberlandia Federal University, Uberlandia, 38400 901, Brazil
[*]Corresponding author: nicolasiaraya@udec.cl

1. Introduction

Porosity is a common trait of sintered components produced by conventional powder metallurgy techniques. For sintered moving parts, pores at the surface are undesired but unavoidable [1]. This paper presents the opportunity of using this residual porosity to stock solid lubricant, so they can provide solid lubrication during the motion of the component, improving its wear resistance and the overall efficiency of the mechanical systems where they are being used. Vacuum-impregnating sintered components with solid lubricant is an attractive technique to take advantage of this residual porosity and obtain self-lubricating sintered components.

2. Experimental procedure

In this work, sinter-hardened Astaloy CRL + 0.6 wt.% C steel was produced by the press and sinter technique, as summarized in Table 1.

Table 1 Processing conditions for the sintered steels produced in this work.

Compaction pressure, MPa	Sintering temperature, °C	Atmosphere
200	1100	Ar-5 vol.% H_2 1 slpm
400	1100/1200	
600	1100	

Then the samples compacted at 400 MPa were vacuum impregnated with 1.10, 6.01 and 21.07 µm graphite particles, while the rest of the specimens were impregnated only with 1.10 µm graphite. The scuffing resistance and wear rates of the resulting composites were studied using dry sliding reciprocating ball-on-flat tests with a 10 mm diameter AISI 52100 ball, a 10 mm stroke and a 2 Hz frequency. The wear scars were analysed using scanning electron microscopy, white light interferometry and Raman spectroscopy.

3. Results and Discussion

Figure 1 shows the influence of particle size and porosity on the coefficient of friction and wear rates. The tribological behaviour of the system is dependent on both the graphite particle size and the porosity of the sintered steel. Smaller graphite particles provide better lubrication due to the slow release from the pores during the sliding process [2]. On the other hand, while the friction coefficient remained the same for all the porosities, the wear rates were linked to the mechanical resistance of the samples (which drops with porosity and increase with sintering temperature) rather than the number of lubricant reservoirs available.

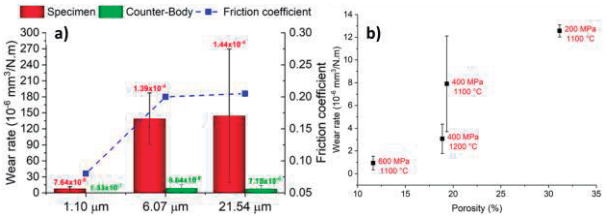

Figure 1 a) Influence of the particle size on the wear rates and COF of the tribosystem and b) Influence of the porosity on the wear rate of the tribosystem.

4. Conclusions

The main conclusion of this work is that the wear rate and friction coefficient of the system are proportional to the particle size of graphite due to it being slowly released from the pores (because small particles have low flowability). On the other hand, the wear rate of the system and scuffing resistance of the system both increase with porosity because pores act as both lubricant reservoirs and stress risers.

5. References

[1] B. Dubrujeaud, M. Vardavoulias and M. Jeandin, *The role of porosity in the dry sliding wear of a sintered ferrous alloy.* Wear, 1994. **174(1-2) 155-161.**
[2] L. Rappoport et al., *Slow Release of Fullerene-like WS2 Nanoparticles from Fe-Ni Graphite Matrix: A Self-Lubricating Nanocomposite.* Nano Lett., 2001. **1(3)**: 137-140.

Production of Biolubricant by the Enzymatic Esterification of Ricinoleic Acid with TMP

Monteiro, R.R.C.[1)], de Luna, F.M.T.[2)], Cavalcante Jr, C.L.[1)], Fernández-Lafuente, R.[2)] and Vieira, R.S.[1)*]

[1)] Department of Chemical Engineering, Universidade Federal do Ceará, Fortaleza, 60455 760, Brazil
[2)] Department of Biocatalysis, Instituto de Catálisis y Petroleoquímica, Madrid, 28049, Spain
[*]Corresponding author: rodrigo@gpsa.ufc.br

1. Introduction

Biolubricants are produced from renewable feedstocks, with a special interest for non-edible oils (e.g., castor oil) [1]. Overall, biolubricants have been produced by the chemical modification of vegetable oils, aiming to improve their physio-chemical and/or tribological properties [2]. On the other hand, enzymes (e.g., lipases) may be employed to biologically modify vegetable oils under milder reaction conditions and high selectivity/specificity [2]. Among lipases, Eversa Transform 2.0 (ETL, for short) was primarily designed to modify vegetable oils with short-chain alcohols to produce biodiesel; however, ETL is a potential biocatalyst to modify vegetable oils with fatty alcohols and polyols (e.g., trimethylolpropane – TMP) [3].

Herein, ricinoleic acid (the major fatty acid of castor oil) was esterified with TMP by ETL to produce a biolubricant. The reaction conditions [biocatalyst content, molar ratio (ricinoleic acid/TMP), temperature and time] were screened by an orthogonal array.

2. Methodology

2.1. Screening

An experimental advanced design by the Taguchi method with a standard L9 orthogonal array was used to examine four factors at three levels to screen the esterification of ricinoleic acid with TMP catalyzed by ETL (Table 1). The reactions were carried out in an orbital shaking incubator (150 rpm). Statistica® 10 software was used for experimental design and statistical analysis.

2.2. Product characterization

The conversion of ricinoleic acid into TMP esters was accompanied by a reduction in the acid number. The viscosity index of the raw material (ricinoleic acid) and product (TMP esters) were determined according to standard methodology.

3. Results and Discussion

As depicted in Table 1, the highest conversion (73.99%) of ricinoleic acid and TMP catalyzed by ETL was observed in experiment 4. Nevertheless, the optimal S/N ratio obtained was 37.98, which suggests that the best levels for each parameter are N3 (15 v/m%) for biocatalyst content, N1 (3:1) for molar ratio (ricinoleic acid/TMP), N2 (50 °C) for temperature, and N3 (72 hours) for reaction time, resulting in a predicted conversion of 75.18% and an experimental conversion of 75.03%. Temperature was the independent variable that most influenced the process. The activity of ETL increases with increasing temperature up to 35 °C and thereafter remains constant up to 50 °C. Any increase in temperature after 50 °C results in a decrease in enzymatic activity.

Table 1 L9 orthogonal array for screening

Run	B	MR	T	t	C
1	5	3:1	40	24	25.08
2	5	4:1	50	48	40.69
3	5	5:1	60	72	36.63
4	10	3:1	50	72	73.99
5	10	4:1	60	24	46.51
6	10	5:1	40	48	24.04
7	15	3:1	50	48	67.12
8	15	4:1	40	72	35.22
9	15	5:1	60	24	42.98

B: Biocatalyst content; **MR**: Molar ratio (ricinoleic acid/TMP); **T**:temperature (°C); **t**: Time (h) and **C**: Conversion (%).

The product of the esterification of ricinoleic acid with TMP catalyzed by ETL was characterized according to the viscosity index to use it as a biolubricant. TMP esters have a viscosity number of 94.81. Generally, polyol esters have a lower viscosity index and are mainly used as hydraulic fluids.

4. Conclusions

In general, ETL is a potential enzymatic biocatalyst to produce biolubricants from the esterification of ricinoleic acid with TMP. Among the variables studied, temperature is the independent variable that has the greatest influence on the conversion.

5. References

[1] Nyholm, N., Espallargas, N., *Functionalized carbon nanostructures as lubricant additives – A review*. Carbon, 2004. **201**: p. 1200–1228.

[2] Mendes, A. A., Soares, C. M. F., Tardioli, P. W., *Recent advances and future prospects for biolubricant base stocks production using lipases as environmentally friendly catalysts: a mini-review.* World J. Microbiol. Biotechnol., 2023. **39**: p. 25-38.

[3] Monteiro, R. R. C., *et al*., *Liquid lipase preparations designed for industrial production of biodiesel. Is it really an optimal solution?* Renew. Energ., 2021. **164**: p. 1566–1587.

Investigation on the improvement of tribological resistance of UHMWPE GUR 1020 by application of a DLC film on argon and oxygen etched surfaces

Kapps, V.[1)*], Maru, M.M[1)], Simão, R.A[2)], Archanjo, B.S[1)], Buthers, E.L[1)] and Achete, C.A.[1)]

[1)] Materials Metrology Division, National Institute of Metrology, Quality and Technology - Inmetro, Duque de Caxias, 25250 020, Brazil
[2)] Department of Metallurgical and Materials Engineering, Federal University of Rio de Janeiro, Rio de Janeiro, Brazil
[*]Corresponding author: vkapps@inmetro.gov.br

1. Introduction

In this work, investigation on the surface improvement of ultra-high molecular weight polyethylene (UHMWPE), medical grade GUR 1020 resin, was performed through coating the polymer with a DLC film by plasma-enhanced chemical vapor deposition (PECVD) technique. Previous surface etching, using Ar and O_2 plasma, was performed in order to introduce some polar groups into the chains of the polymer [1]. The produced surfaces were evaluated through microscratching tests.

2. Methods

Non-crosslinked UHMWPE GUR 1020 plates of (24×24×5) mm (n=18) were obtained from a 70 mm diameter bar. The plates (n=12) were polished and etched with O_2 (n=6) and Ar (n=6) plasma (50 W, 1×10^{-1} mbar, (195±10) V bias voltage) for 180 seconds, under 2.0×10^{-3} mbar system pressure and 13.56 MHz RF power supply. DLC coating was deposited by PECVD ((20±2) °C, 1800 seconds) with methane as working gas, with a film thickness of (610±37) nm (n=18), measured by contact profilometry (Taylor Hobson, PGI 830). Scratches of 2 mm length were performed with 5 mN to 20 mN linearly increasing normal load at 0.3 mN/s rate (CETR, UNMT1, 12.5 µm radius diamond tip, FL0380 load sensor). Failure mechanisms were observed through helium-ion scanning microscopy (Orion, Carl Zeiss) at 8×10^{-7} torr, 0.6 pA and 30 kV. Contact angle measurements and confocal Raman spectroscopy were performed to evaluate the wettability and the integrity of the DLC film in the specimens.

3. Results and Discussion

Figure 1a shows the contact angle in three different fluids for the control and for both etched polymer surfaces. Notable decrease is seen after etching; it was associated to the creation of polar functional groups on the surface [2, 3]; however, there was not exactly a direct relationship to the scratch resistance by looking to the scratching depths in Figure 1b for O_2 and Ar etched surfaces. On the other hand, all the performed surface modifications led to increase the tribological resistance, of about 42% in general, compared to the unmodified UHMWPE (control). Surface etching only, with Ar or O_2, resulted in marked improvement. The best alternative was the DLC film applied on the O_2 plasma etched surface (O_2+DLC column), with 51% of improvement considering the depths of 51 µm and 25 µm (t-test, 95%). Interestingly, the DLC film did not produce significant effect (t-test, 95%) when the film was applied on the Ar etched surface, while the film on the O_2 etched surface had the depth decreased by 15% (t-test, 95%), from 29 µm to 25 µm. In the HIM images of Figure 2, near the end of the scratch, the higher contrast within the scratch track in the DLC deposited on the Ar etched surface demonstrates superior tribological resistance of the DLC film applied on the O_2 etched surface. Raman analyses confirmed the presence of the DLC film on the scratched area in both specimens.

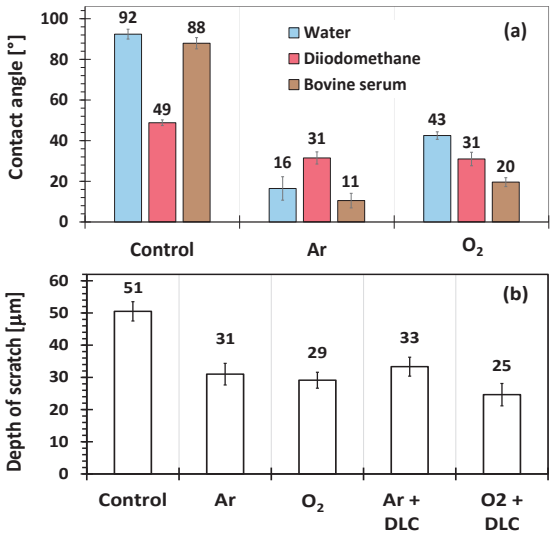

Figure 1 a) Contact angle in UHMWPE with and without etching. b) Maximum scratch depth in the surface modified specimens, compared to the unmodified one (control).

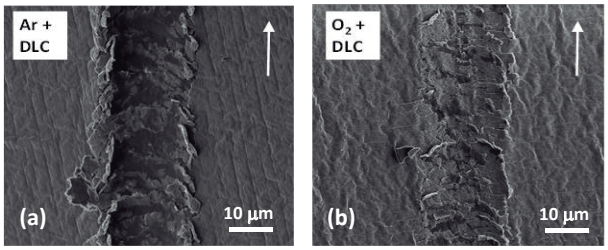

Figure 2 HIM images of the scratched area of DLC coated UHMWPE previously etched with plasma of Ar (a) and O_2 (b). Arrow: scratching direction.

4. References

[1] Spyrides, S.M.M et al., *Mechanism of oxygen and argon low pressure plasma etching on polyethylene (UHMWPE)*. Surf. & Coat. Tech., 2019, **378**: 124990.

[2] Liu, H. et al., *Surface modification of ultra-high molecular weight polyethylene (UHMWPE) by argon plasma*. App. Surf. Sci., 2010. **256**: p. 3941–3945.

[3] Liu, H. et al., *The mechanical properties of the ultrahigh molecular weight polyethylene (UHMWPE) modified by oxygen plasma*. Surf. & Coat. Tech., 2011, **205**: p. 2697-2701.

Importance of data acquisition rate selection for reliable evaluation of resistance to friction of tribomaterials

Kapps, V.[1)*], Maru, M.M.[1)] and Achete, C.A.[1)]

[1)] Materials Metrology Division, National Institute of Metrology, Quality and Technology - Inmetro, Duque de Caxias, 25250 020, Brazil
[*]Corresponding author: vkapps@inmetro.gov.br / vanessakapps@gmail.com

1. Introduction

The objective of this work is to demonstrate that friction coefficient (COF) values obtained from reciprocating sliding tests can be significantly affected by the selected data acquisition rate. The intrinsic variable kinematics promoted by the reciprocating motion may origin variable friction phenomena along the stroke length, more or less intensified depending on the tested pair of materials. Having this in mind, it can be argued that depending on the chosen data acquisition filter size, it is likely that relevant information about friction of the tribossystem is eliminated from the computation of COF [1]. This fact can critically impact the reliability for materials screening through reciprocating sliding tests and indicates that care should be taken to consider the optimum data rate for accurate comparison between results from different materials and/or test conditions.

2. Methods

Dry reciprocating ball-on-plate sliding tests were carried out (UMT Tribolab, UMT software version 1.136.257F05) with non-crosslinked GUR 1050 UHMWPE plate specimens running against 10 mm chromium steel balls, in a 10 mm stroke length. COF under oscillation frequencies of 1 Hz and 5 Hz were compared under 15 N normal load tests. COF data were recorded during the test time. The data acquisition rates varied, in which the average values of COF were acquired at 10, 20 and 100 data/second.

3. Results and Discussion

Figures 1 and 2 present the COF data obtained from the tests at 1 Hz and 5 Hz, simultaneously with the position at the stroke length (-5 mm to +5 mm), along a window of two test cycles. Figures 1a and 1b are related to the data acquired at 10 data/second, for 1 Hz and 5 Hz tests. Given the different oscillation frequencies in the tests, the amount of data obtained per cycle was quite different, of 10 and 2 data/cycle, respectively, meaning that data were extracted from different positions in the stroke length. This makes any comparison between both COF erroneous. The same happens by using 20 data/second acquisition rate (Figures 1c and 1d), but with less extent. The optimum data acquisition rate should be balanced considering an equal amount of data obtained per cycle test, in order to compare the COF resulting from same positions along the wear track.

In the case of the performed tests, 20 data per second and 100 data per second are the optimum acquisition rates, respectively for 1 Hz and 5 Hz test conditions, as seen in Figure 2, which are related to 20 data per cycle. As conclusion, selecting reciprocating tests for screening materials and/or investigating the effect of testing conditions on friction, the same number of data acquired per cycle is a priority for improved reliability of the obtained results.

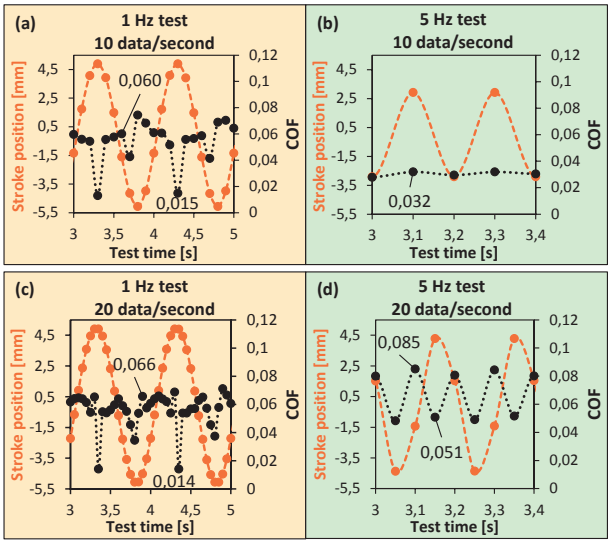

Figure 1 COF data obtained in two cycles, from 1 Hz (a, c) and 5 Hz (b, d) tests, extracted at acquisition rate of 10 (a, b) and 20 (c, d) data per second.

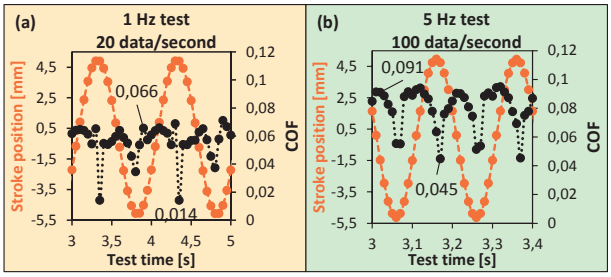

Figure 2 COF data obtained in two cycles from 1 Hz (a) and 5 Hz (b) tests, extracted at acquisition rate of 20 (a) and 100 (b) data per second.

4. References

[1] Matz, S., and R. Grönqvist, *Comparing two methods of data collection for walkway friction measurements with a portable slip meter and a force platform*. Saf. Sci., 2004. **42**: p. 483-492.

Effect of plasma nitriding temperature on wear resistance of Hadfield steel

Danelon, M.R.[1)], da Silva, J.V.P.[3)], Almeida, L.S.[2)], Rossino, L.S.[2,3)], Manfrinato, M.D.[2,3)*]

[1)] Department of Materials and Metallurgical Engineering, University of São Paulo - USP, São Paulo, Brazil
[2)] PPGCM UFSCar, Federal University of São Carlos – Sorocaba Campus, Sorocaba, Brazil
[3)] Sorocaba Technological College, Sorocaba, Brazil

[*]Corresponding author: marcos.manfrinato@fatec.sp.gov.br

1. Introduction

Hadfield-type austenitic manganese steel is used in situations of high mechanical stress and wear resistance [1] and to improve wear resistance the thermochemical treatment of plasma nitriding is the most recommended because, since they are carried out at low temperatures and short times [2]. Nitrided layer is formed by a composite and diffusion layer, being responsible for increasing the resistance to abrasive wear and corrosion resistance in steels [2]. This work aims to evaluate the resistance to abrasive microwear with a fixed ball of manganese steel-type Hadfield plasma nitrided at different temperatures.

2. Materials and Methods

The austenitic manganese steel Hadfield used in this work has a chemical composition in percentage by weight of 1.15% C, 12.5% Mn, 2.2.5% Cr, 0.86% Si, and 0.02% P. Test specimens were prepared in dimensions of 25mm in width by 25mm in length and 13mm in thickness at Fatec Sorocaba. The specimens were sanded and polished according to the ASTM E3-18 standard. Plasma nitriding was at N400°C, N450°C, and N550°C for 2h in a gas mixture of 80%N_2 and 20%H_2. The specimens were cut perpendicular to the treatment surface to measure the thickness of the layer formed with the aid of SEM/EDS

Fixed sphere abrasive microwear tests were carried out with a load of 8N, 150RPM using a sphere of 25.4mm in diameter made of AISI 52100 steel quenched and tempered with a hardness of 60HRC. The test times were 2, 5, 10, 15, 20, 25 and 30 minutes. The tests were carried out with a polished sphere and a sphere etched with 20% Nital. The wear volume during the test is calculated by measuring the diameter of the cap and the volume removed is obtained according to Equation 1.

$$V = \frac{\pi b^4}{64R} \quad \text{for b <<<R} \qquad (1)$$

3. Results and Discussions

Figure 1 shows the micrography of the composite layer (P1 and P2) and the diffusion layer (P3 and P4) with a thickness of 8.5 ± 1.2µm and a microhardness of 765HV. For N450°C. N400°C produced a layer of 3.5 ± 0.6µm and 674HV and N550°C 20.8 ± 1µm and 965HV. Figure 2 shows the amount of wear per distance covered. For the sphere without attack, it was observed that there was a greater loss of volume for the nitrided and untreated material. Sample N400°C has presented a thin compound layer that breaks and produces wear debris during the wear test, intensifying the wear volume both for etched and polished spheres, as shown in Figure 2.

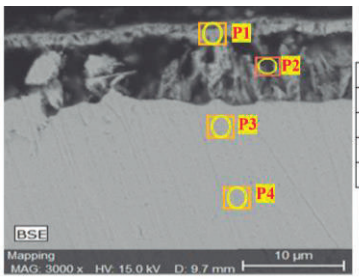

	%Fe	%Mn	%N
P1	82,61	14,90	2,45
P2	87,91	9,34	2,75
P3	86,21	13,42	0,37
P4	85,39	14,44	0,17

Figure 1 - SEM/EDS for N450°C.

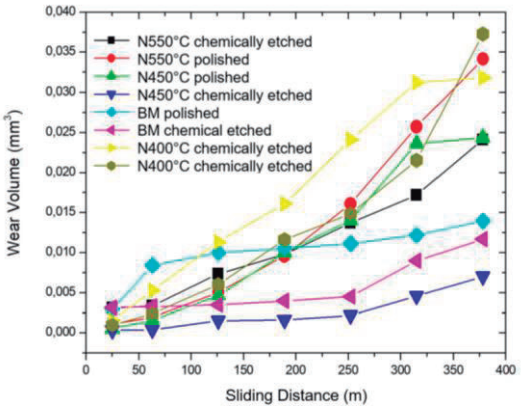

Figure 2 - Graph of wear volume by sliding distance.

4. Conclusions

Plasma nitriding at 450°C showed greater resistance to abrasive wear for the severe test with the etched ball.

5. References

[1] Venturelli, B.N. *Efeito do refino do tamanho de grão pela adição de Hf nas propriedades mecânicas de tração e impacto do aço Hadfield* [dissertação]. São Paulo: Universidade 'de São Paulo, Escola Politécnica; 2018

[2] Danelon, M.R., et. Al. *Study of the effect the plasma ionic nitriding parameters in wear resitance of SAE 1020 steel used in forming die*. Rev. Bras. Apl. Vac, 2020, 39, 2, p. 142-155.

Increased energy efficiency in iron ore milling, changing lubricant from mineral oil to synthetic oil

Campos, D. M.[1)*], Silva, R.M.[2)] and da Costa, A.R.[3)]

[1)] REDEMAT/UFOP, Eng. Mec. Ouro Preto, Brazil
[2)] Consultor, Eng. Mec. M.Sc.
[3)] REDEMAT/UFOP – Eng. Met.; D. Sc. - Professor Titular da Escola de Minas
REDEMAT/UFOP, Praça Tiradentes, 20, Centro – CEP: 35400-000 Ouro Preto, Minas Gerais, Brasil.
[*]Corresponding author: mota600@hotmail.com

1. Introduction

The article presents the results of performance analysis studies of three types of lubrication in tests an equipment in an iron ore mining processing plant. The operating parameters of two ball mills drive speed reducers were monitored. The tests were carried out with mineral-based lubricant and two types of synthetic-based lubricant oil from two different suppliers.

Currently, the search for energy efficiency is a major challenge for the industrial sector [1]. Water crises, measures against global warming, reduced availability of energy resources points to implement new technologies aimed at reducing losses and increasing the efficiency of processes. This economy is very relevant for the company in question, being a current demand from the industry to increase the efficiency of its assets by reducing energy consumption.

2. Methodology

Mining industry equipment is exposed to severe operating conditions. The milling stage demands high consumption of electricity to drive the ball mills, directly impacting production costs (Figure 1). The increase in the energy efficiency of the mill drive reducers provides a reduction in the consumption of electricity per ton produced, making the operation more sustainable.

An alternative for reducing power losses is the application of lubricants with more energy efficient technology. Synthetic oil technology based on polyalphaolefin (PAO) present in the oils and its balanced additives allows minimizing the energy consumed during lubrication regimes compared to mineral base oil [2].

Two suppliers of mineral oils were selected to carry out the tests, called Supplier A and Supplier B. The same test procedure was carried out for the two companies that manufacture and distribute the lubricants.

This work was premised on carrying out a test which consisted of replacing mineral oil by synthetic oils in the mill's reducers. During the work, the parameters of interest were monitored (energy consumption, operating temperature of the speed reducer components, oil contamination, etc.) before and after the application of the new oil, subsequently evaluating the changes detected.

Figure 1. View of an industrial ball mill.

3. Conclusion

The study carried out allowed to prove that the replacement of mineral type lubricating oil by synthetic types allowed an increase in the energy efficiency of large electric motors. The measurements of the operating parameters of the speed reducer of a ball mill for iron ore processing proved that there was a reduction in energy consumption: for the oil from Supplier A there was a reduction of 1.04% and for Supplier B 1.22%. This reduction is equivalent to savings of 513,162 kW per year, making it possible to supply around 280 family homes per year, considering the average consumption of brazilian families. The estimated gain considering the average values of kWh for the industrial sector is around R$ 351 thousand reais per year, and this gain can be maximized if replicated to other similar equipment, reaching a gain of R$ 1.4 million reais per annum.

4. References

[1] COSTA, A. R.; Tribology applied to mining – Concepts and Applications; First ed. Fontenele Editions São Paulo – SP - 2021.

[2] DE VAAL, P.L., BENADE, H., Energy-efficient and environmentally-conscious industrial lubrication, Department of Chemical Engineering, University of Pretoria, 2019.

Effect of Glass Fiber Concentration in PA Based Composites Tribology

De Mendonça, A.S.[1)*], Michelotti, A.C.[2)], Binder, C.[1)], Klein, A.N.[1)], Salvaro, D.B.[1)], De Mello, J.D.B.[1)]
[1)] Departamento de Engenharia Mecânica, Universidade Federal de Santa Catarina, Florianópolis, 88040 900, Brazil
[2)] ZEN S.A. Indústria Metalúrgica, Brusque, Brazil
[*]Corresponding author: arthur.s.m@labmat.ufsc.com

1. Introduction

The use of fiber-reinforced polymers composites in mechanical applications is a promising option to replace traditional materials due to their low weight, strength-to-weight ratio and cost-effectiveness, with polyamide (PA 66) being one of the most used polymers in the automotive industry, glass fiber (GF) is the most employed reinforcement due to their availability and low cost [1-2]. The present work aimed to study the influence of GF content in the tribological performance of PA 66-based composite.

2. Materials and Methods

Cylindrical specimens were produced by powder injection molding using commercial PA reinforced with different GF content identified as GF1, GF2 and GF3. The specimens mechanical properties were evaluated by tensile testing according to ATMS D638 and dynamic mechanical analysis (DMA). Reciprocating cylinder-on-flat wear tests were performed (UMT-3MO CETR® tribometer) with the parameters presented in Table 1 to evaluate the effect of frequency and time in the tribosystems friction coefficient. Samples of commercial EPDM rubber were used as counter-body aiming to simulate actual conditions from automotive industry. Tests were performed with the GF1, GF2 and GF3 specimens.

Table 1: Tribological tests parameters

Config.	Stroke (µm)	Frequency (Hz)	Load (N)	Time (min)
1	3	2	30	30
2	3	4	30	30
3	3	4	30	60
4	3	8	30	60

In order to evaluate the influence of GF content in the wear, similar tribological tests were carried out in configuration 4. The worn volume of rubber was measured by gravimetry, while the wear of specimens was quantified by white light interferometry (WLI) along with MountainsMap® post processing. Additionally, the wear marks (rubber and specimen) were analyzed via SEM-EDS.

3. Results

As expected, the addition of GF improves the composites mechanical properties. Figure 1 presents the typical friction coefficient (COF) evolution from the tests described in Table 1. The results showed that higher oscillation frequencies induce lower COF. Surprisingly, the amount of GF did not influence these results. Differences in COF can be attributed to higher energy dissipation in the contact leading to higher local temperature, consequently, softening the composite matrix.

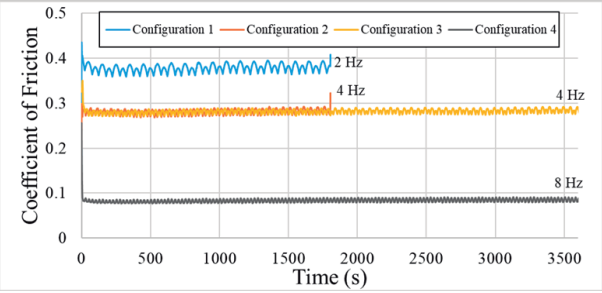

Figure 1: GF3 samples typical friction coefficient evolution.

Figure 2 presents a typical topography of the specimens before and after tribological tests which is possible to see that the topographic parameter Sq reduces significantly after the tribological work (from 2.05 µm to 1.08 µm). It can be explained due to the prominent peaks removing, plastic deformation of polyamide, and the deposition of material from counter-body on the specimen surface, characterized by the presence of Zn on the specimens wear marks. The rubber wear rates are very similar, independently of the GF content (around $16.73 \pm 1.50 \times 10^{-8}$ $mm^3mm^{-1}N^{-1}$). However, It was observed a slight increase in the mean wear to GF concentration.

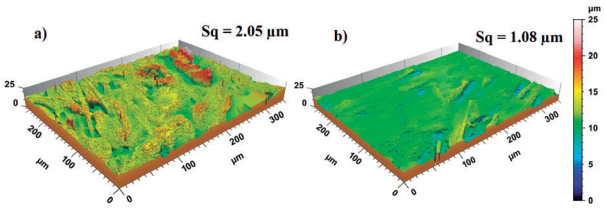

Figure 2: Topographical images from a GF3 sample a) before and b) after the test.

4. Conclusions

The GF concentration does not affect the COF, in fact, the oscillation frequency strongly influences this parameter, in which 8 Hz induces COF around 0.08. The wear of composites is as mild as to promote topography smoothing. However, adding GF slightly increases the counter-body (rubber) wear rate.

5. References

[1] Singh, P. et al., *Characterization of wear of FRP composites: A review*. Materials Today, **64**. 2022.
[2] Sarfraz, M. et al., *Recent developments in the manufacturing technologies of composite components and their cost-effectiveness in the automotive industry A review study*. Composite Structures, **266**. 2021.

Evaluation of point contact areas and contact pressure distribution between railway sleeper and ballast: field measurements and FEM modeling

Jales, E.S.[1,2], and Bortoleto, E.M.[2]

[1] Department of Civil Engineering, Universidade Federal de Ouro Preto, Ouro Preto, 35400 000, Brazil
[2] Instituto Tecnológico Vale, Ouro Preto, Ouro Preto, 35400 000, Brazil
*Corresponding author: erivaldo.jales@aluno.ufop.edu.br

1. Introduction

The complexity of research on railroads steel sleepers, especially when it comes to simulating the contact between the sleepers and the ballast, is further increased, mainly because the dealing with U-shaped laminated profile, which have distinct mechanical and geometric properties compared to prismatic sleepers. According to [1], there is an increase in the pressure zone primarily under the rail seat for prismatic sleepers. The interface between the sleeper and the ballast compromises several track aspects, such as lateral resistance, pullout, and load distribution. The present study focused on analyzing the contact aspects between steel sleepers bottom surface and ballast particles, and the effects on contact pressure distribution.

2. Methodology

Two steel sleepers samples, used in a heavy haul railway during six months, were randomly selected. Surfaces presented oxidation marks on the underside, indicating the area in contact with ballast particles (Figure 1). The complete image of 2,1m long sleeper bottom side was obtained by combining multiple images of smaller regions, covering the entire area in contact with the ballast. The relationship between the contact areas and the sleeper bottom face total area was obtained as a function of sleeper length, and considering the ballast particle average diameter, an equivalent contact model could be proposed.

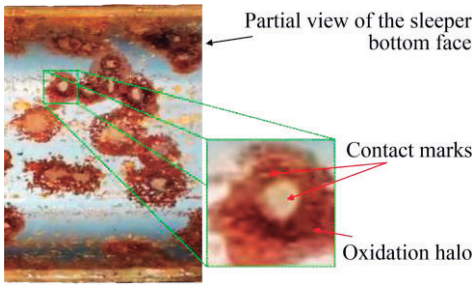

Figure 1 Contact marks and oxidation halos.

This model was implemented using FEM, and real steel sleeper geometry obtained by means of 3D laser scanning. Symmetry was considered [2], and it was sufficient to simulate one-half sleeper, applying contour constraints. Orthogonal cylinders were designed in order to represent the interaction between sleeper and ballast, considering the same contact area per sleeper length and the same number of measured contact marks. (Figure 2).

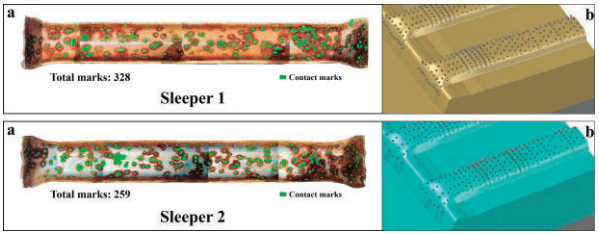

Figure 2 a) Identification of contact marks, and b) Ballast simplification.

Three models were developed: the first one considered a continuum interface between sleeper and ballast, while second and third models considered the methodology based on area equivalent cylinders. Therefore, a 190MPa static load on top of rail was applied.

3. Results

According to field measurements results, only a small percentage (6.3% and 6.1%) of the horizontal contact projection area of the underside of the analyzed sleepers came into direct contact with the ballast particles. The variation of ballast in the models did not result in differences in rail gauges, but did lead to a slight variation in rail laying angle. Consequently, using the proposed approach, based on 'area equivalent cylinders', resulted in a more concentrated vertical displacement on the rail seat, reduction of stress peaks, and, better distribution of Von Mises stress.

4. Conclusions

The simulations using 'area equivalent cylinders' approach resulted in bi-trapezoid distribution of stress in ballast, while the models with continuous ballast presented stress concentrated under the rail seat.

5. References

[1] Zakeri, J.A.; Sadeghi, J. *Field investigation on load distribution and deflections of railway track sleepers*. Journal of Mechanical Science and Technology Springer, v. 21, n. 12, p. 1948, 2007.
[2] Kukulski, J.; et. Al. *Finite element method in assessing strength properties of a railway surface and its elements*. Symmetry. 11.p. 1014, 2019.
[3] Abadi, T. Effect of sleeper and ballast interventions on rail track performance. PhD thesis, University of Southampton, 2015.

Rough Contact Models for Multibody Tribodynamics Simulation of Crank–Connecting Rod–Piston Mechanisms: A Critical Assessment

Nascimento, I.V.[1)*], and Profito, F.J.[1)]

[1)] Department of Mechanical Engineering, Polytechnic School of University of Sao Paulo, Sao Paulo, Brazil
[*]Corresponding author: isaacvnascimento@usp.br

1. Introduction

Current technological demands associated with stricter environmental legislation have caused changes and impacts on the design of mechanical components operating under high thermal-mechanical loads and subjected to complex multiphysics phenomena that affect their performance and durability [1]. For example, the crank-connecting rod-piston-cylinder mechanism in internal combustion engines and reciprocating compressors experience friction, wear, and lubrication effects at the revolute joints. To design and optimize such components in a context of rapid advancement of potential tribological solutions (*e.g.*, new materials and surface engineering techniques and low-viscosity lubricants), engineers need accurate and fast simulation tools that can capture the tribodynamic behaviour of the system under realistic working conditions. Particularly in the cases of systems working in mixed lubrication conditions, current simulation tools often rely on simplified rough contact models that do not account for the elastoplastic deformation and roughness of the contact surfaces, leading to inaccurate predictions of the contact forces and stresses. Therefore, there is a need for more realistic models that can represent the mixed lubrication regime and the rough contact mechanics in a computationally efficient way. In this context, the present study sought to analyze the tribodynamic behaviour of a crank-connecting rod-piston-cylinder mechanism with lubricated joints operating under mixed lubrication conditions. Different elastoplastic rough contact models are used to calculate the contact forces, and a comparative critical analysis is performed to evaluate the influence of the contact model on the main system operational parameters.

2. Methodology

The present work proposes a multibody tribodynamics model for crank-connecting rod-piston-cylinder mechanisms that fully couples the tribological phenomena at the lubricated joints with the constraints and motion equations derived using the Lagrange approach [2]. A Reynolds-based mixed lubrication model with mass-conserving cavitation is used to calculate the hydrodynamic loads [3], and different elastic and elastoplastic statistical rough contact models are used to compute the asperity contact loads. Figure 1 shows the simulation workflow of the proposed numerical framework.

3. Results

The current results indicate that significant differences in the joints' performance parameters and the overall dynamic behaviour of the crank-connecting rod-piston-cylinder mechanism studied were observed depending on the rough contact model used. In particular, this behavior was verified mainly in the connecting rod–piston joint (see Figure 2) when considering geometrically identical clearance revolution joints.

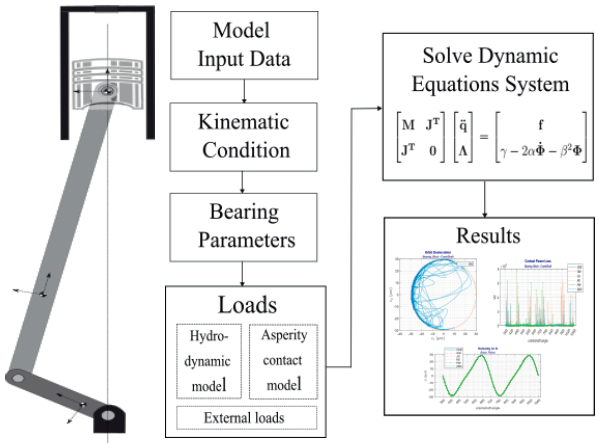

Figure 1 – Schematic of the mechanism and simulation workflow.

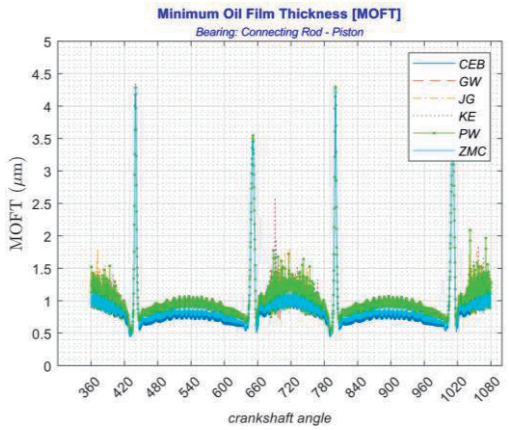

Figure 2 – Minimum oil film thickness for the different rough contact models.

4. References

[1] Allmaier, G., Offner H. *Current challenges and frontiers for the EHD simulation of journal bearings: a review*. SAE Technical Paper Series, SAE International, 2016.
[2] Flores, P. *Kinematics and dynamics of multibody systems with imperfect joints*. In: Lecture Notes in Applied and Computational Mechanics. Springer, 2008.
[3] Profito, F.J., Zachariadis, D.C., Dini, D. *Partitioned Fluid-Structure Interaction Techniques Applied to the Mixed-Elastohydrodynamic Solution of Dynamically Loaded Connecting-Rod Big-End Bearings*. Tribology International **140**, 105767, 2019,

Effect of Reinforcement with Nanosheets of MXenes ($Ti_3C_2T_x$) on the Compressive and Wear Resistance of Structural Concrete

Silva, C.A.[1)], Gonçalves, M.R.F.[1)] , Rosenkranz, A.[2)] Costa, H.L.[1,3)] *

[1] Universidade Federal de Pelotas, Graduate Program on Materials Science and Engineering, Rua Gomes Carneiro 1, Porto, Pelotas, RS, Brazil, ORCID 0000-0002-2925-9935 (CAS); ORCID 0000.0001.6834-8546 (MRFG); ORCID 0000-0002-0412-4436

[2] University of Chile, Department of Chemical Engineering, Biotechnology and Materials, Avenida Beauchef 851, Santiago, Chile, ORCID 0000-0002-9006-1127.

[3]Universidade Federal do Rio Grande, School of Engineering, Av. Itália km 8, Bairro Carreiros, Rio Grande, RS, Brazil.

* Corresponding author: henaracosta@furg.br, +55 53 999922424

1. Introduçtion

Concrete is a leading composite material for structural use in buildings. MXenes are new two-dimensional (2D) materials that are very promising for applications as lubricants in machine bearings due to their layered structure and physical-chemical characteristics (Fig. 1). Wear is an important pathological manifestation in civil construction, as it can influence the durability of structures. In an attempt to evaluate the effect of using MXenes as reinforcement of concrete surfaces, with regard to abrasion and fretting resistance, concrete specimens were formed with the addition of 0.02%wt. of MXenes.

2. Metodology

In this work, part of the cement was replaced by 0.02% of functionalized MXenes. Conventional concrete, with MXenes and coated with MXenes (Fig. 2) were molded. They were tested in sliding situations with small displacements (fretting) and in terms of its resistance to abrasion. In the abrasion tests, rubber-wheel tests used sand with grain sizes of 50 and 100 grit following two standard procedures from ASTM G65-00 (2001): “A” for more severe wear and “B” for lighter wear. In fretting wear, two speeds were used: 0.2 mm/s and 2 mm/s for 5 minutes and 30 minutes of tests.

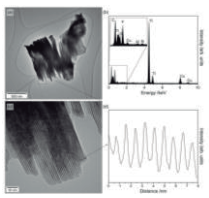

Figure 1 *HR-TEM of the $Ti_3C_2T_x$ nanosheets. Adapted from (Rosenkranz, Grützmacher et al. 2019).*

Fig. 3 shows the behavior of the coefficient of friction versus time for the samples in the condition v = 0.2 mm/s and test time of 5 minutes. Fig. 4 shows the samples without and with MXenes from the abrasion tests.

Figure 2 *Dispersion of the nanosheets: (a) ultrasound; (b) dispersion in water; (c) mixing of the dispersion into the concrete.*

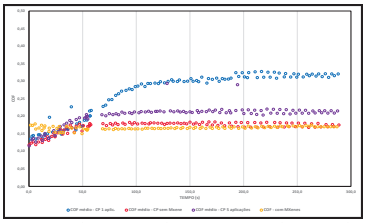

Figure 3 *COF Evolution with tests time during the fretting tests; v=0,2 mm/s, test duration = 5minutes.*

After the abrasion tests, the surface of the samples without MXenes showed more wear when compared to the concrete surface with the addition of 0.02% of MXene in the concrete mass.

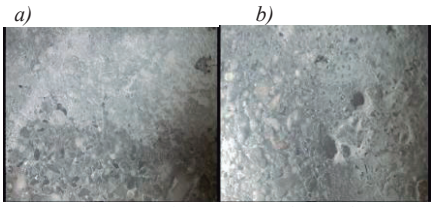

Figure 4 *Optical images of the worn surfaces aftr the abrasion tests: a) concrete e b) concrete with MXenes.*

3. References

[1] Rosenkranz, A., Grützmacher, P. G., Espinoza, R., Fuenzalida, V. M., Blanco, E., Escalona, N., Gracia, F. J., Villarroel, R., Guo, L., Kang, R., Mücklich, F., Suarez, S., & Zhang,Z. (2019). *"Multi-layer Ti3C2Tx-nanoparticles (MXenes) as solid lubricants – Role of surface terminations and intercalated water."* Applied Surface Science, *494*: 13–21.

[2] ASTM G65-00. (2001). *Standard test method for measuring abrasion using the dry sand/rubber wheel apparatus.* ASTM International, West Con-shohocken.

Image processing for automatic wear track measurements

Valente, C.A.G.S[1)*], da Silva, C.H[1)]

[1)] Department of Mechanical Engineering, Federal University of Technology - Paraná, Curitiba, 81280 340, Brazil
[*]Corresponding author: caiovalente@alunos.utfpr.edu.br

1. Introduction

Data collection and processing may be one of the most time-consuming steps in scientific works. One way to improve the efficiency of this process is through computational automation. In the case of wear track width measurement, it's common to test hundreds of samples, generating thousands of images which often must be measured manually. Image processing techniques can be used to evaluate worn surfaces, both quantitative and qualitatively [1]. In this work, we developed a simple yet effective solution to measure wear track widths on images obtained via optical microscopy, using a Python script associated with the image processing library OpenCV (Open Source Computer Vision).

2. Methods

Polymer composite specimens were subjected to sphere-on-flat linear reciprocating wear tests under different sliding speeds and normal loads. Optical microscopy surface images were obtained with 50x magnification, with 2048×1532-pixel resolution, from three different equidistant sites through the length of wear tracks. Those images were measured manually by a trained operator, generating the mean widths for each track (M_{manual}). The same images were then measured using the Python package cv2, which wraps the OpenCV library, scanning the images and generating a curve graph for each color intensity on the image (Figure 1).

For each pixel in the images, a vector represents the intensity of red, blue and green colors. The graph for the color intensity is generated by taking the vector sum on each line and plotting each color separately. To determine the wear tracks limits, an image segmentation technique called thresholding was used [2], thus partitioning the image in worn and unworn regions (respectively above and below threshold). The threshold was calculated using the blue channel, by iteratively minimizing the quadratic deviation (σ) given by Eq. (1), where N is the number of images (N=48) and M_{auto} is the mean width for the i-th image for each iteration of threshold value.

$$\sigma = \sqrt{\frac{\sum_{i=1}^{N}(M_{auto} - M_{manual})_i^2}{N-1}} \quad (1)$$

3. Results and Discussion

Sample code and datasets are available at <https://github.com/caio-valente/TriboBR2023_Image-processing>

We found that, for the wear tracks used in this work, the threshold of 87.3% of average intensity gives the minimum quadratic deviation (11.6 µm). Considering the average width was 369.9 µm, the coefficient of variation (using the deviation from Eq. (1)) is only 3.1%.

It's important to point out that the time spent to measure each image varies within the range of a few minutes. On the other hand, the automated process takes only a few milliseconds per image, depending on the hardware used. Estimating the average time to measure one image equal to 1 minute, manually, and 10 ms when automated, this method can save over 16.5 hours of work for each 1000 images processed.

This algorithm relies on the vertical orientation of the wear tracks respective to the image. Thus, it must be noted that alignment errors when taking the pictures can lead to errors in the measurements. This can be solved by adjusting the script to find the right orientation prior to the measurements. However, this was not under the scope of this work, as the errors obtained were considerably low.

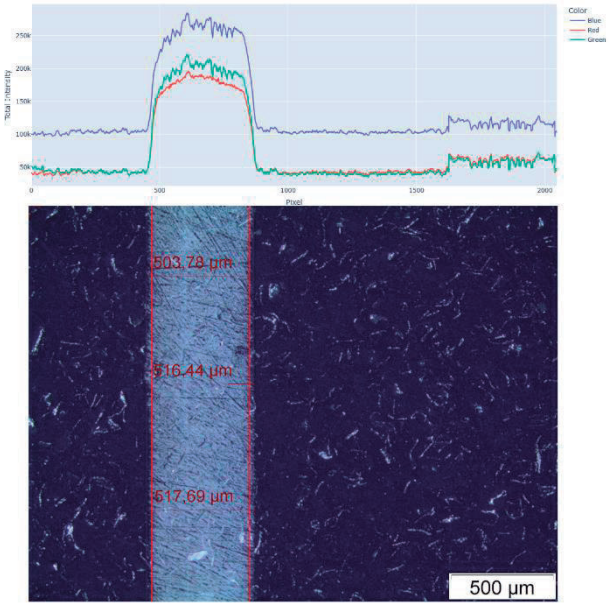

Figure 1 Worn surface (bottom) and calculated color intensity (top).

4. References

[1] Shashikala, T.D., Sunitha, S.L. and S. Basavarajappa, *Quantification of worn surface using digital image processing.* Tribology International, 2022. **176**: 107864.

[2] Gonzalez-Arias, C., Viafara, C.C., Coronado, J.J. and F. Martinez, *Automatic classification of severe and mild wear in worn surface images using histograms of oriented gradients as descriptor.* Wear., 2019. **426-427, Part B**: p. 1702– 1711.

Effects of Surface Texturing of Sheet Metal Forming Tools in Strip Drawing Tests

Silva, R.S.[1)*], Angélica Paola, Diego Tolloti, Felipe Luz, João Henrique, Costa, H.L[3)]

[1)] Postgraduate program in mechanical engineering, Federal University of Rio Grande, Rio Grande, 96.203-900, Brazil
[2)] Engineering School, Federal University of Rio Grande, Rio Grande, 96.203-900, Brazil
[*]Corresponding author: renan.s.silva@hotmail.com

1. Introduction

In metal forming, the surface behavior to control friction, reduce lubricant consumption and ensure good surface finishes has gained attention in many studies, due to the high stresses involved in the contact between the tool and the workpiece. Surface texturing is one of the techniques with potential to control friction and reduce tool wear. Several techniques can be used to create textures: laser texturing, texturing using abrasive jets, photochemical texturing, electrochemical machining and some others [1].

In this research, the texturing technique used was photochemical texturing, with the purpose of evaluating the benefits of surface texturing in sheet metal forming tools subjected to strip-drawing friction tests [2].

2. Methodology

Two texturing techniques used was: photochemical texturing. The photochemical texturing technique is widely used in the electro-electronics industry, where a photosensitive resin is used to protect the surface regions where the material will not be removed by subsequent chemical attack. The application of the resin is carried out at high rotation to ensure uniform and fine spreading (Figure 1a). Subsequently, the mask containing the desired geometric pattern is inserted on the surface of the tool with the resin, and then exposure to UV radiation is performed (Figure 1b) so that polymerization occurs in the region affected by the radiation. The resin is taken to another solution that will remove part of the exposed resin and the piece, now with the mask, will be ready to receive the chemical attack (Figure 1c).

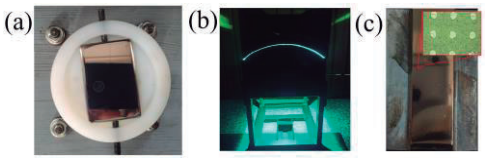

Figure 1 (a) example of a tool with a thin layer of photosensitive resin; (b) UV attack chamber; (c) cathode with textures

Subsequently, strip drawing tests were performed on textured and non-textured tools. The tools were pressed against the plates with a force of 5000 kgf which were pulled at a constant speed of 100 mm/s for a time of 5 s.

3. Results and Discussions

The friction tests (Figure 2) showed that the textured tools had a lower tribological behavior than the tests carried out by the non-textured tools. The main hypothesis debated by the research work was the lack of hardness of the tested tools. The textures could contribute to the increase of pressures in the contact regions leading to the adhesion of textured tools.

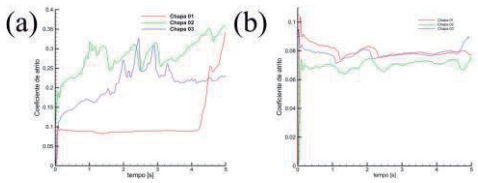

Figure 2 (a) Tool test with texture and; (b) tool test without texture

4. Conclusions

The texturing carried out on the surfaces of the tools did not show behavior that could benefit the tribological behavior of the forming tools. These results show the need to carry out future friction tests on tools with harder surfaces. In this way, it will be possible to verify if the texturing for the application in question presents benefits that outweigh the harms.

5. References

[1] Costa, H.L. and Hutchings, I.M., *Some innovative surface texturing techniques for triboligical purposes*. Institutions of Mechanical Engineers, 2015.
[2] Souza, J.H., *New Design Approaches for sheet Metal Forming Dies Using Polymeric Materials*, 2008, Institut für Umformtechnik der Universität Stuttgart.

Study of Adherence evaluation the feasibility of using stainless steel coated with a film of TiO2 in the treatment of sanitary effluents

Silva, M.G.P[1)*], Merlo, R.B[1)], Machado, A.A[1)], Segreto, E. [1)],

Marques, V.E.C.[1)*], Manfroi, L.[2)], Vieira, A.[1)], Doria, A.C.O.[1)], Almeida, F.S.[1)], Pereira, A.L.J.[3)], Marques, F.C.[3)], and Lúcia Vieira[1)]

[1] Instituto de pesquisa e desenvolvimento, Universidade do Vale do Paraíba (IP&D/UNIVAP), São José dos Campos, SP, Brazil; vagner.eduardo@agnet.com.br; angela.vieira@univap.br; ane.doria@univap.br; lucia.vieira@univap.br
[2] Instituto Tecnológico Aeroespacial (ITA), São José dos Campos, SP, Brazil; andreljp@ita.br
[3] Universidade Estadual de Campinas Instituto de Física "Gleb Wataghin", Campinas, SP, 13083-859, Brazil; marques@ifi.unicamp.br

* Correspondence: vagner.eduardo@agnet.com.br; Tel.: +5511980332066

1. Introduction

The treatment of unsanitary water is essential to guarantee the access of safe water to millions of people. A lot of techniques used to treat contaminated water are described by Seul-yi and Park (2013)[1], but to date, the most advantageous technique reported is the decomposition of organic materials due to photocatalytic properties, specially from Titanium dioxide (TiO_2) [2][3]. Titanium dioxide (TiO_2), or titania, is a chemically and biologically inert semiconductor that appears in three allotropic forms: anatase, rutile and brookite [4]. Most research on photocatalysis has focused on anatase and rutile TiO_2 films. The most thermodynamically stable phase at all temperatures and the most common natural form of TiO_2 is rutile, but anatase TiO_2 films are more efficient photocatalysts than rutile TiO_2 films [4].

2. Methodology

The 304 stainless steel (AISI 304) was used as substrate in this study, samples with 10 mm diameter and 1 mm thickness was cleaned first with propanone in the ultrasonic bath for 15 min, then isopropanol ultrasonic bath for 15 min, and ultrapure water ultrasonic bath for 15 min. The samples surface was dried before placing it in the ALD chamber reactor. The ALD reactor used to deposit TiO_2 film was a Beneq Oy TFS-200 (Helsinki – Finland) with automated system and in thermal operating mode. Titanium tetrachloride ($TiCl_4$), purchased from Sigma Aldrich with 99.95% purity, were used as titanium precursor; as oxygen precursor and oxidizing agent, ultrapure water (H_2O) was used; the precursors were kept at a constant temperature of 24 ºC and no carrier gas was used. The deposition occurred in a set of 3 thousand cycles at 300 °C; in each cycle a $TiCl_4$ pulse of 250 ms was performed; and then 1 second purge; a 250 ms of H_2O pulse; and again a purge of 1 second. For background atmosphere control and purge gas the nitrogen (N_2) was used, with a purity of 99.998%, in a constant flow of 250 sccm.

3. Test Results

Scratch Test Results - Samples will be characterized.

SEM and AFM images of the TiO_2 thin film deposited on AISI 304 can be seen in Figure 1. The film densely covered the substrate with nanometric particles evenly distributed on AISI 304 surface, with maximum surface grain sizes of ~40 nm and RMS of roughness measured 11,27 nm. The thin film is smooth and does not show the formation of agglomerates or cracking.

Figure 1 – SEM and AFM images of TiO_2 thin film deposited on AISI 304.

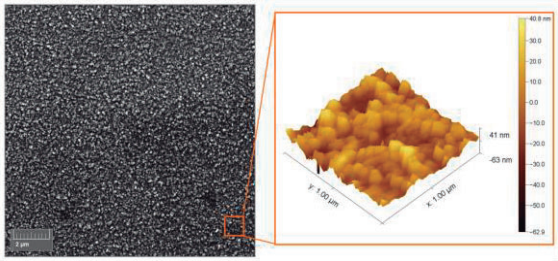

Source: the author

The Raman spectra of TiO_2 film in Figure 2 shows the representative peaks identified near to 148, 244, 399, 455, 518 and 640 cm^{-1}, these peaks indicate that the crystalline phase of the film is mostly anatase, corresponding to its representative peaks near 152, 400, 522 and 642 cm^{-1}, as also shown by Hardcastle (2011)[20] and Evans and Sheel (2007)[21].

Figure 2 – Raman spectra of TiO_2 film deposited on AISI 304 substrate compared to anatase specter.

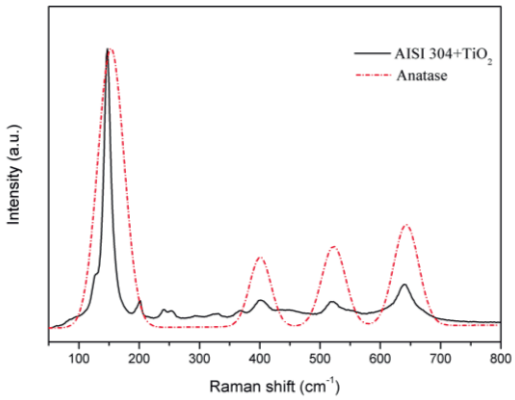

Source: the author

4.Conclusions

The atomic layer deposition of TiO_2 film, via $TiCl_4$ and H_2O cycles produces uniform, smooth and homogeneous film on AISI 304 surface. The film deposited is especially composed of anatase evenly distributed in the film, as showed by Raman diffraction results.

*5.*References

[1] Q. Seul-yi and S. Park, "Review of TiO 2 photocatalyst for water treatment applications," *J. Ind. Eng. Chemestry*, vol. 19, no. 6, pp. 1761–1769, 2013.

[2] M. Grao, M. Ratova, C. C. Amorim, R. B. P. Marcelino, and P. Kelly, "Crystalline TiO2 supported on stainless steel mesh deposited in a one step process via pulsed DC magnetron sputtering for wastewater treatment applications," *J. Mater. Res. Technol.*, vol. 9, no. 3, pp. 5761–5773, 2020.

[3] M. Urbonavicius, S. Varnagiris, S. Sakalauskaite, E. Demikyte, S. Tuckute, and M. Lelis, "Application of Floating TiO 2 Photocatalyst for Methylene Blue Decomposition and Salmonella typhimurium Inactivation," *Catalyst*, vol. 11, no. 794, pp. 1–12, 2021.

[4] J. Zheng, S. Bao, Y. Guo, and P. Jin, "TiO2 films prepared by DC reactive magnetron sputtering at room temperature: phase control and photocatalytic properties," *Surf. Coat. Technol.*, vol. 240, pp. 293–300, 2014.

Reduction of mechanical energy dissipation in hierarchical titanium coatings

Teixeira, J.V.U[1)], Santos, A.A.[1)], Capelin, G.R.[1)], Pintão, C.A.F. [1)] and Lisboa-Filho, P.N.[1)*]

[1)] Materials Science and Technology Program, Department of Physics, School of Sciences, UNESP—São Paulo State University, Bauru 17033-360, SP, Brazil
[*]Corresponding author: paulo.lisboa@unesp.br

1. Introduction

Titanium and its alloys are used widely in several fields, with a focus on biomedical applications as hard tissue substitutes, including implants and prostheses [1]. This versatility is attributed to its noble mechanical properties, low young modulus, low density, corrosion resistance, and biocompatibility [1].

Many approaches have been proposed to improve both tribocorrosion and mechanical wear. In recent research, Santos and coworkers [2] provide tribological and electrochemical protection in titanium substrates with the electrodeposition of titanium oxide (TiO_2) and calcium phosphate (CaP) layers.

Despite the findings in the previous tribocorrosion investigation, the effect of coatings protection against wear must be evaluated. In this context, the present research aims to investigate the energy dissipation due to wear in wet and dry conditions.

2. Materials and Methods

Four samples were prepared using metallographic techniques until 1200 mesh with silicon carbide sandpaper and etched with Piranha solution for 2 hours. The samples were coated with titanium oxide and calcium phosphate (CaP).

The coated samples were produced by electrochemical methods, with TiO_2 sample produced in chrono-potentiostats configuration, with 1.0 V applied for 30 minutes on the titanium sample against Ag/AgCl electrode, and platinum rod as a counter electrode. Furthermore, the reaction was performed in a solution of 10% H_2O_2, being the sample named Ti/TiO_2.

In a similar configuration, CaP was deposited on titanium by chronoamperometry in $CaCl_2$ + $(NH_4)_2PO_4$ solution at a pulsed arrangement with 30 seconds of power on, with -1.5 V. In addition, 60 seconds of power off was repeated ten times to form the CaP layer. The obtained samples were named Ti/CaP and Ti/TiO_2/CaP.

The wear characterization was performed in wet and dry conditions, with phosphate buffer solution in wet environment and air in dry environment. The experiment was performed with an alumina ball as a counterpart using a load of 1.5 N for 180 seconds. The recorded data provided instant power in both conditions, which was further converted into accumulated energy according to reported by Santos and coworkers [2]. Additionally, the 2D profile of wear track was obtained with confocal microscopy.

3. Results and discussion

The results presented in Figure 1 demonstrated that the proposed coatings could perform effective protection against wear damage. The protective coatings function as a lubricating surface when they are in contact with an alumina counterpart. This lubricating effect occurs not only in wet conditions, where it affects both mechanical and electrochemical behavior but also in dry conditions.

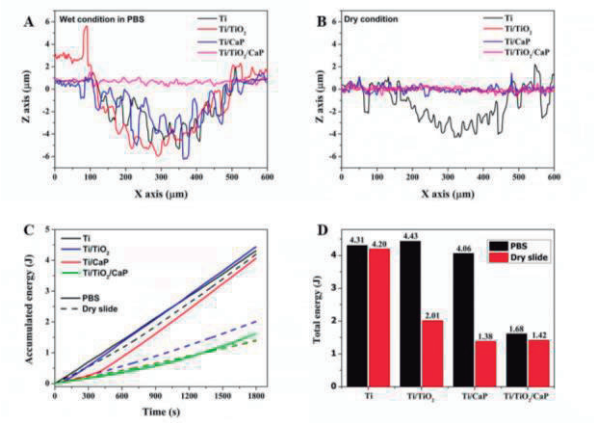

Figure 1 Wear track of samples in PBS (A) and dry condition (B). Accumulated energy (C), and Total energy (D).

The Ti/TiO_2/CaP sample demonstrates a more noticeable effect in both scenarios wet and dry, as seen in the similar depth of the wear track (Fig. 1 A and B) and it can also be observed in the accumulated energy derivative from friction during the experiment (Fig. 1C). When comparing the total energy, it is evident that all coatings reduce dissipated energy in dry conditions, while the TiO_2/CaP coating shows effective in both wet and dry conditions.

4. Conclusion

Based on existing literature knowledge, the results indicate that the electrodeposition of TiO_2/CaP effectively protects titanium substrates. This coating can be used in internal environments to reduce wear damage during tribocorrosion or in external applications to minimize friction. Consequently, it can increase the lifetime of titanium products such as scalpels and orthoses.

5. References

[1] W. NICHOLSON, John. *Titanium alloys for dental implants: A review*. Prosthesis, 2020. **2**: p. 11.
[2] SANTOS, Adriana et al. *A Tribological Investigation of the Titanium Oxide and Calcium Phosphate Coating Electrochemical Deposited on Titanium*. Metals, 2023 **13**: p. 410.

Study on the tribological behavior of new titanium alloys for biomedical applications

Santos, A.A.[1)], Teixeira, J.U.V.[1)], Fonzar, C.A.P.[1)], Correa, D.N.[1)] Pinto, B.O.[1)] Grandini, C.R.[1)] and Lisboa-Filho, P.N.[1)*]

[1)] Materials Science and Technology Graduate Program, São Paulo State University, Bauru - SP, 17033360, Brazil.
*Corresponding author: paulo.lisboa@unesp.br

1. Introduction

In the study of tribology, multiple factors such as friction force, plastic deformation, hardness, applied load, and energy dissipation are considered as they collectively influence the wear behavior of materials [1]. Energy dissipation, particularly the measurement of frictional resistance during surface movement, plays a critical role in comprehending and assessing the wear resistance performance of biomaterials [1]. A study introduced an innovative method to isolate pure wear and provided a detailed explanation of the involved wear mechanisms [2]. Additionally, another research indicated that an increase in hardening resulted in higher friction coefficients, and abrasion was identified as the primary observed mechanism in the samples [3].

2. Materials and Methods

After the processing of the Ti-15Zr and Ti-15Zr-5Mo (%wt.) alloys, metallographic techniques were employed to achieve the desired surface finish. Moreover, microhardness tests were conducted to establish a correlation with the coefficient of friction (COF). Thus, friction tests were performed using a tribometer. Subsequently, volume measurements were obtained using confocal topography. Equations (1) and (2) were then utilized to calculate the volume loss and wear rate, respectively. In these equations, *Vm*, *Rm*, *Am*, *Wr,* and *ET* represent the average volume loss (mm^3), average radius (mm), average area (mm^2), wear rate ($mm^3 \cdot N^{-1} \cdot m^{-1}$), and total energy ($N \cdot m$), respectively [4].

$$Vm = 2 \cdot \pi \cdot Rm \cdot Am \quad (1)$$

$$Wr = \frac{Vm}{ET} \quad (2)$$

3. Results and discussion

The microhardness results, in Table 1, indicate that the addition of alloying elements and phase precipitation contributed to an increase in hardness. Specifically, the inclusion of Zr in pure titanium (Ti-CP), and Mo in the Ti-Zr alloy led to further enhancements in microhardness.

Table 1 Microhardness and coefficient of friction.

Samples	Microhardness	COF
Ti-CP G4	201.21 ± 5.80	0.38 ± 0.07
Ti-15Zr	241.84 ± 9.32	0.52 ± 0.07
Ti-15Zr-Mo	292.24 ± 7.63	0.48 ± 0.05

The COF for pure titanium displayed approximate values compared to the developed alloys. Furthermore, the binary alloy exhibited a higher volume loss, while the ternary alloy necessitated more energy to remove material during the friction process, likely due to its increased hardness. Overall, both the binary and ternary alloys demonstrated comparable performance when considering the error bars indicated by the wear rate results, as showed in Figure 1.

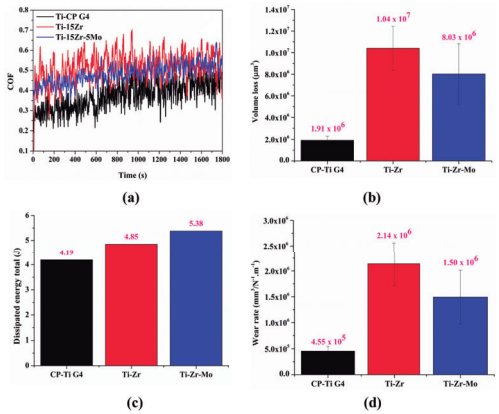

Figure 1 (a) coefficient of friction. (b)Volume loss. (c)Dissipated total energy. (d)Wear rate.

4. Conclusion

The study findings indicate that the developed alloys exhibited excellent performance, showing similar COF values to commercially used pure titanium in orthotic applications. This suggests that the alloys have the potential to be viable alternatives to pure titanium, offering comparable frictional properties while potentially providing additional advantages due to their specific composition and unique characteristics.

5. Acknowledgments

CAPES. FAPEAM. FAPESP. CDMF.

6. References

[1] Santos, A. et al., *A Tribological Investigation of the Titanium Oxide and Calcium Phosphate Coating Electrochemical Deposited on Titanium*. Metals.2023.**13**.
[2] Núñez, Y. et al., *The effect of plasma nitriding on the synergism between wear and corrosion of SAF 2205 duplex stainless steel*, Ind. Lubr. and Trib. 2020. **9**, 1117.
[3] Berton, E. et al., *Transitional behavior in sliding wear of martensitic layer obtained with SHPTN process on AISI 409 steel*. Surf. Topogr.: Metrol. Prop. 2022. **10.**
[4] Santos, A. et al., *Ti–15Zr and Ti–15Zr–5Mo Biomaterials Alloys: An Analysis of Corrosion and Tribocorrosion Behavior in Phosphate-Buffered Saline Solution*. Materials. 2023, **16**, 1826.

Tribological Characterization of Nanoporous Anodized Anodic Alumina Coatings for Biomedical Applications

Pieretti, E.F.[1,2)*], Correa, O.V[1)] , Neves, M.D.M.[1)], Oliveira, M.C.L.[2)], Antunes, R.A.[2)] and Pillis, M.F.[1)]

[1)] Institute of Energy and Nuclear Research (IPEN/CNEN), 05508-000, São Paulo, Brazil
[2)] Federal University of ABC, 09210-580, Santo André, Brazil
[*]Corresponding author: eurico.pieretti@ipen.br

1. Introduction

Biomaterials surfaces need to be adequate to the function they perform; for this reason, the importance of studying surface finish increases as design requirements grow, regarding geometry and precision requirements in biomedical devices. These biomaterials are subject to several types of premature failure, such as wear, fatigue, micro movements, particle detachment and degradation, which may generate the need for new interventions [1]. Anodizing is an electrolytic passivation process used to increase the thickness of the natural oxide layer on the surface of metal parts. Due to good biocompatibility, regular arrangement of nanopores, ease of control of nanopore diameter, large specific surface area, low cost, good thermal stability and absence of toxicity, anodic aluminum oxide has been studied. The geometric arrangement of nanopores makes it possible to use alumina as a mold for the synthesis of several nanostructures that have many advantages in advanced application areas due to their unique chemical, physical, mechanical, and optical properties. The aim of this work was to evaluate the tribological behavior of anodized aluminum alloys specimens using ball cratering wear tests.

2. Materials and methods

The tribological behavior of samples of aluminum alloy AA6061 anodized in oxalic acid solution (C2H2O4) and sulfuric acid (H2SO4) at three immersion times: 1 h, 2 h, and 4 h was evaluated. Prior to the anodization stage, the samples were electrolytically polished in a solution of perchloric acid and ethanol. For comparison reasons, pristine surfaces were also evaluated. Atomic force microscopy was also used to evaluate samples roughness and topography. The wear tests were carried out during 10 min, solid spheres of 52-100 chrome steel, with 2 mm in diameter, were used as counter-bodies.

3. Results

There is a tendency towards an increase in friction force values according to the use of the surface anodizing treatment of aluminum AA6061. Only the sample anodized in sulfuric acid for 1 hour of immersion showed a slight drop in this value, in relation to the standard reference sample, as shown in Figure 1.

4. Conclusions

The results indicated that the tribological behavior is influenced by the anodized layer process parameters, and the wear rate is dependent of the normal force and the roughness of each sample. Therefore, it is necessary to constantly advance research on the use of nanoporous anodic alumina coatings on the surfaces of biomaterials.

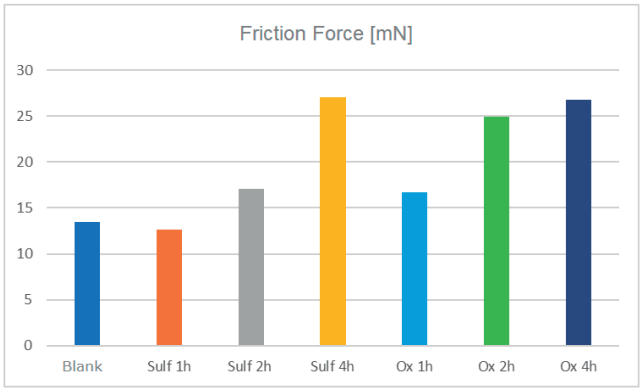

Figure 1 Friction force for blank and anodized surfaces.

5. References

[1] Pieretti, E.F., E.J. Pessine, O.V. Correa, W. Rossi, M.D.M. Neves, *Effect of Laser Parameters on the Corrosion Resistance of the ASTM F139 Stainless Steel*, Int. J. Electrochem. Sci., 2015. **10**: p. 1221 – 1232.

Laboratory evaluation of tribological performance of biodegradable grease with magnetite nanoparticles coated with stearic acid for wheel/rail interface

Ferrer, B.P. [1], Zuin, A. [1]*, Cousseau, T.[1),3)], Tayer, P. [1] and Biazon, L.[2]

[1] Department of Mechanical Engineering, Universidade Tecnológica Federal do Paraná, Curitiba, 81280 340 , Brazil
[2] Department of Mechanical Engineering, University of Sheffield, Sheffield, S10 2TN, UK
[3] The Centre for Bulk Solids and Particulate Technologies, The University of Newcastle, Newcastle, Callaghan NSW 2308, Australia
*Corresponding author: brunopferrer@hotmail.com

1. Introduction

Grease lubrication is a process used to control the coefficient of friction (CoF) at the interface between wheel flange/rail gauge corner in heavy-haul railways, aiming to improve wear rates, lateral forces in curves, and fuel economy [1]. The present study focuses on the evaluation of comparing CoF and wear of a biodegradable rail grease containing magnetite nanoparticles coated with stearic acid (MagNP) with eleven others rail greases. This evaluation is conducted through pure sliding sphere-on-disc tribological tests with abundant lubrication, simulating the contact between the wheel flange and the rail gauge corner [2]. The effect of MagNP in oil formulations has shown that: i) maintained lower and more stable CoF values; ii) reduced wear marks; iii) improved the deposition of oil additives on the contact surface [3].

2. Materials and Methods

The tribological tests were performed using a sphere-on-disc configuration with abundant lubrication. The test specimens consisted of i) polished AISI 52100 chrome steel spheres (d=10 mm, 848 HV20), ii) pearlitic steel discs (353.9 ± 11.8 HV20, Sq= 0.6 to 1 µm). A load of 50 N was applied, resulting in a Hertzian pressure of 1.150 MPa at the initial contact. The tests were conducted at a 32°C, 0.5 ms^{-1}, relative humidity above 30%, during 3600 s and a total distance traveled 1800 m.

Twelve greases were evaluated, including one specially formulated grease (IcE460+MagNP) prepared from a commercial biodegradable grease (IcE460). The IcE460+MagNP grease has 0.5% in mass of MagNP in powder. The coated MagNP is readily attracted to a magnet and easily dispersed in oil. The size of 95% of the dispersed MagNP was estimated using dynamic light scattering and shows a value of 17 ± 3 nm. A white light interferometer was used to measure the wear of the spheres and a 2D-profilometer was used to measure the wear of the tracks in discs. The CoF was obtained by tribometer software.

3. Results and Discussion

The IcE460+MagNP grease exhibited the lowest CoF (0.063 ± 0.006), which was 17.1% lower than the grease with the second-best performance (SulCaE58, 0.076 ± 0.001) and a 36.3% reduction compared to its base grease (IcE460, 0.099 ± 0.001). The IcE460+MagNP grease showed the lowest total volume wear (1.93E-02 ± 1.28E-2 mm^3), which was 70.0% lower than its base grease (IcE460, 6.43E-2 ± 1.98E-2 mm^3) and 37.9% lower than the grease with the second-best performance (SulCaE58, 3.11E-02 ± 1.31E-2 mm^3).

MagNP as an additive significantly influenced the performance enhancement in terms of both CoF and wear, as it effectively altered the lubricant's mechanism of action, resulting in distinct changes in the wear patterns observed. In contrast to the irregular and non-circular wear marks observed on the spheres subjected to the other grease formulations (Figure 1a), the utilization of IcE460+MagNP grease yielded a remarkable wear pattern characterized by a uniformly worn circular mark. This wear pattern deviation was accompanied by the presence of fine particles surrounding the wear mark (Figure 1b). These findings showed the potential of MagNP as an additive in rail grease formulations.

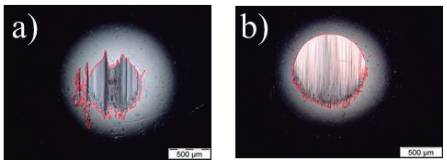

Figure 1 - Micrograph of the worn sphere tested with (a)IcE460 grease *and (b) IcE460+MagNP grease*

4. References

[1] Sroba, P. et al. *Canadian Pacific Railway's 100% effective lubrication initiative.* In: Proceedings of the Presentation for AREMA 2001 Conference & Exhibition, Chicago, Illinois. 2001. p. 9-12.
[2] Ferrer, B. P. et al. *Rail grease formulation effect on its tribological performance under pure sliding conditions*. Tribology Transactions, v. 66, n. 1, p. 104-116, 2023.
[3] Zuin A, Cousseau T, Sinatora A, Toma HE. *Lipophilic magnetite nanoparticles coated with stearic acid: A potential green and low cost way to improve thermal stability and tribological properties of fully formulated low viscosity engine oils*. Tribol Int 2020;106209.

Friction and wear of graphene-based polymer nanocomposites for dental applications

Beltrami, L.V.R.[1)], Gamba, T.O.[2)], Adami, C.R.[2)], Piazza, D.[1)], Zattera, A.J.[1)] and Farias, M.C.M.[3)*]

[1)] Postgraduate Program in Engineering of Processes and Technologies, University of Caxias do Sul, RS, Brazil
[2)] Postgraduate Program in Health Science, University of Caxias do Sul, RS, Brazil
[3)] Postgraduate Program in Materials Science and Engineering, University of Caxias do Sul, RS, Brazil
[*]Corresponding author: mcmfarias@ucs.br

1. Introduction

Contact between the tooth, remaining hard particles from food, toothbrushing, muscular forces, nature of saliva and eating habits of patient are the main factors that cause significant tooth damage due to wear. Lack of control and prevention of severe tooth wear can lead to oral disorders, including orofacial pain, reduced masticatory function, impaired orofacial aesthetics, and malocclusion or occlusion disharmony [1, 2]. Materials used for dental restorations have suffered changes to provide the most suitable clinical treatment to the patients and also to reduce tooth wear. The usage of composite-based materials has significantly increased recently on account of their good aesthetics and ability to bond to tooth structures. Adding micro- and nano-filler to polymer composites has been one of the current practices to enhance their mechanical and wear resistance. The use of graphene-based materials in dentistry has become popular because of their large surface area, low bulk density, and facility for chemical modification [3]. The aim of this study was to evaluate the friction and wear behavior of a resin added with graphene nanoplatelets (NGPs) produced by 3D printing for dental applications.

2. Experimental

To develop of the graphene-based polymer nanocomposites, graphene nanoplatelets (0.125, 0.25, and 0.5 wt%) were incorporated into a commercial resin. Reciprocating sliding tests were conducted in a ball-on-plate geometry using a Bruker UMT Tribolab tribometer. Polished plate samples of the graphene-based polymer nanocomposites and pure resin were loaded against alumina balls with a diameter of 6.35 mm. In order to simulate the oral conditions, reciprocating sliding wear tests were conducted in artificial saliva solution and in dry conditions. The wear experiments were conducted under a normal load of 30 N, using a 1 Hz sliding frequency and 4 mm stroke length. The duration of each test was 3600 s. The average values of the friction coefficient of the steady-state stage, wear volume, and specific wear rate were obtained from three repetitions of the wear tests. The volume removed by wear of the composite materials was determined with the aid of a Bruker CountourGT-I 3D optical profilometer. The specific wear rate (k, $mm^3/N.m$) of the tested materials was quantified according to the Archard equation for sliding wear [4]. Wear mechanisms were identified by morphological and chemical analysis of the wear tracks using a field emission scanning electron microscope equipped with an energy-dispersive X-ray spectroscopy detector.

3. Results and main remarks

Figure 1 shows the evolution of the friction coefficient for all the tested materials against alumina. Friction evolution was characterized by a running-in period with a pronounced increase in friction coefficient followed by a most steady stage.

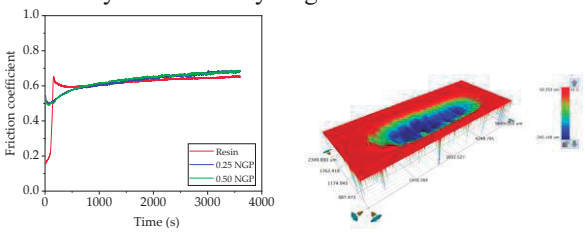

(a)

Figure 1 (a) Evolution of the friction coefficient along the sliding time. (b) 3D profile of the wear track of the 0.25 wt% NGPs composite

Graphene additions produced no significant changes in friction coefficient during the reciprocating sliding tests conducted in dry conditions. The wear resistance of graphene-based polymer nanocomposites decreased compared with the resin sample. Analyses of microstructure, mechanical properties, processing parameters, and wear mechanisms can help to elucidate the tribological response of the nanocomposites.

4. References

[1] Lee, A., He, H., Lyons, K. and Swain, M.V. *Tooth Wear and Wear Investigations in Dentistry*. J. Oral Rehabil., 2012, **39**: 217–225.
[2] Carvalho, A., Pinto, P. Madeira, S., Silva, F.S., Carvalho, O. and Gomes, J.R. *Tribological Characterization of Dental Restorative Materials.* BioTribol., 2020, **23**: 100140.
[3] Scarano, A., Orsini. T., Carlo, F., Valbonetti, L. and Lorusso, F. *Graphene-Doped Poly (Methyl-Methacrylate) (PMMA) Implants: A Micro-CT and Histomorphometrical Study in Rabbits.* Int. J. Mol. Sci., 2021, **22**:1441.
[4] Archard, J.F. Contact and Rubbing of Flat Surfaces, J. Appl. Phys., 1953, **24**: 981–988.

Biotribological Characterization of Laser Textured Ti6Al4V Produced by Addictive Manufacturing

Pieretti, E.F.[1,2)*], Oliveira, M.C.L.[2)], Antunes, R.A.[2)], Ribeiro, M.S.[1)] and Neves, M.D.M.[1)]

[1)] Institute of Energy and Nuclear Research (IPEN/CNEN), 05508-000, São Paulo, Brazil
[2)] Federal University of ABC, 09210-580, Santo André, Brazil
[*]Corresponding author: eurico.pieretti@ipen.br

1. Introduction

Implantable medical devices used in human body as well as for dental purposes require biocompatibility with the surrounding tissues and organs, biomechanical strength and corrosion resistance. The body fluids constitute a hostile environment for the implant, which is also subjected to various loads. The implant can release particles due to corrosion, corrosion associated with fatigue, and even friction against implantable components, bones or other body parts. By coming into contact with body fluids, these particles can be placed in locations far from the removed source causing complications to the patients. Interaction between metallic implants and the human body can be affected by numerous factors such as the structure of the metal surface, its mechanical properties, size and shape. When in contact with the body tissues after implantation, metallic devices affect the intensity of stresses to which the whole human body is subjected the implant as well. Wear and corrosion processes are additional effects arising from the interaction between metallic biomaterials and the body tissues [1]. The micro-scale abrasion test (or ball-cratering wear test) is a practical method to analyze the wear resistance of biomaterials. The ball-cratering wear test has gained large acceptance at universities and research centers and is widely used in studies focusing on the abrasive wear behavior of different materials. Tests in micro and nano tribometers are used to investigate small regions and thin layers of different surfaces. The aim of this work was to evaluate the tribological behavior of Ti6Al4V textured by pulsed Ti: Sapphire laser, using ball-cratering wear tests.

2. Materials and methods

The tribological behavior of Ti6Al4V samples was assessed by wear tests conducted in a nanotribometer (Anton Paar - model NTR^2). The tests were performed in the air, at 25° C, with counter-body of chrome steel 52-100 rotating ball shape, 2 mm in diameter, during 10 minutes, with normal force of 100.0 mN, distance equivalent to 2.4 m, and scan speed of 4.0 cm.s^{-1}. Both laser-textured and pristine material were evaluated. Prior to the texturization stage, the samples were electrolytically polished in a solution of perchloric acid and ethanol.

3. Results

This work also analyzed the evolution of the friction coefficient by nanotribometer wear tests of the surfaces of these biomaterials with laser texturing treatment comparing with the blank specimen (without treatment). No direct relationship between wear volume and friction coefficient was observed, i.e., the highest value of wear volume was not related to the higher value of coefficient of friction. For the laser textured surfaces, Figure 6, the values of friction coefficient obtained were lower than those obtained in the samples without treatment by the laser beam (blank).

The friction coefficient values for the untreated specimen showed a rapid increase in the beginning of the test, and practically stabilized as the surface becomes less rough. In the case of the Ti6Al4V laser textured samples, the friction coefficient decreases primary, reaching a stabilization period up to the end of the running test. The variation of the coefficient of friction as a function of the test time was studied by Huang et al. [2]. They verified this effect on tribological properties in Ti6Al4V alloys with and without coatings ("laser clad"), for a running time of 3500 seconds in different rotation frequencies, at the end of the tests they verified that the coefficient of friction for the coatings was always inferior to the substrate.

4. Conclusions

The results indicated that the tribological behavior is influenced by the surface finishing parameters, and the wear rate is dependent of the normal force and the roughness of each sample. Therefore, it is necessary to constantly advance research on the use of femtosecond pulsed laser coatings on the biomaterial's surfaces produced by addictive manufacturing techniques.

5. References

[1] Anderson, J.M., *Biological response to materials*, Annual Rev. of Mater. Res., 2001. **31**: p. 81-110.
[2] Huang, C., Zhang, Y., Vilar, R., Shen, J., *Dry sliding wear behavior of laser clad TiVCrAlSi high entropy alloy coatings on Ti-6Al-4V substrate*, Mater. and Des., 2012. **41**: p. 338-343.

Quantification of powder evaporation for optimization of coating deposition by plasma spray

Castro, F.D.[1)*], Fonseca, M.G [1,2)], Collares, M.P.[2)] and Costa,H.L[1,2)]

[1)] Universidade Federal de Pelotas, Graduate Program in Materials Science and Engineering, RS, Brazil
[2)] Universidade Federal do Rio Grande – FURG, Rio Grande, RS, Brazil
[*]Corresponding author: fran.dias.castro.fd@gmail.com

1. Introduction

Plasma spray is a very versatile technique for coating deposition since it allows deposition of virtually any material or composite without excessive heating of the substrate. When using powder particles in the coating deposition process, powder evaporation may occur [1]. Evaporation causes significant mass loss and can be detrimental to the formation of coatings. Therefore, the focus of the research was to quantify the evaporation that serves as a subside in optimizing the deposition of plasma spray coatings.

2. Experimental procedure

The plasma torch was built at the Surface Engineering Laboratory, Universidade Federal do Rio Grande (FURG). The plasma spray system consists of a direct current source (responsible for generating and maintaining the electric arc), high frequency source (breaking the dielectric barrier of the plasma gas), control unit (responsible for controlling the flow of plasma, outlet and inlet temperatures and gas mixing), powder feeder. The powder used was calcined alumina (Al_2O_3) powder with 99.3% purity and a size distribution of 44 µm, 74 µm, 149 µm. The processing parameters used were primary gas flow Argon (70 SLPM), secondary gas flow Hydrogen (3.5 SLPM), current of 320 A. The flow rate of the powder varied from 0.57 to 3.39 g/min and the carrier gas rate was 1.66 SLPM. The maximum operating voltage is 55 V. Therefore, knowing the current and voltage, the power is approximately 17.6 kW.

3. Model development

Based on equations from the literature, we developed an analytical model to quantify evaporation during plasma spray deposition. When the particle interacts with the plasma, it is necessary to define an equilibrium equation to match the heat exchange between the plasma and the particle to quantify the evaporation. Assuming that the temperature variation inside the particle is zero and rewriting the equation as a function of the injected mass we obtained:

$$\dot{m}_e = \frac{4\pi\left(\sqrt[3]{\frac{3}{4\pi\rho_p}m}\right)^2}{L_e}\left[h\,(T_\infty - T_s) - \varepsilon\sigma_s T_s^4\right] \quad (1)$$

where h is the convective heat transfer coefficient, T_∞ is the temperature of the plasma outside the boundary layer, T_s is the surface temperature, r_p is the radius of the temperature surrounding the particle, ε is the emissivity of the particle, σ_s is the Stefan-Boltzmann constant, $\dot{m}_e$ is the evaporated mass rate and L_e the latent heat of evaporation.

4. Results and discussions

The experiment carried out to quantify evaporation lasted one minute varying the powder feed rate. During the process, some particles do not penetrate the plasma jet, remaining in the reservoir below the torch. This material was collected and weighed to define what powder was lost. Therefore, the relationship to determine the mass of evaporation was:

$$m_s = m_i - m_c \quad (2)$$

where m_s is the total evaporated mass, m_i is the mass injected into the plasma jet and m_c is the collected mass. The values of the rates obtained using equations 1 and 2 are shown in Table 1.

Table 1 Evaporation of particles

Powder Feed	m_s (g/min)	$\dot{m}_e$(g/min)
0.57	0.16	0.27
1.02	0.30	0.33
2.24	0.68	0.43
3.39	0.46	0.50

Comparing the evaporation rate values obtained using the theoretical model and the experimental values, there is a decrease in evaporation when the injected mass increases, but the amount of collected mass increases. Therefore, the amount of dust that entered the plasma was less. The reasons for this phenomenon may be linked to the drag flow and torch power. Regarding the flow rate, for the higher feed rate, the ideal would be a proportional carrier gas flow rate to ensure that the particles penetrate the plasma. Estimating the power needed to completely evaporate the 3.39g would require 79 kW, but the torch provided a power of 17 kW influencing the evaporation. In this way, to obtain the ideal optimization of the coating process, the available power must be greater than 17.6 kW for materials such as alumina and the drag flow must guarantee the immersion of the particles.

5. References

[1] FAUCHAIS, Pierre L.; HEBERLEIN, Joachim VR; BOULOS, Maher I. Thermal spray fundamentals: from powder to part. Springer Science & Business Media, 2014.

Determination of Lubricant Film Thickness Using Ultrasonic Reflection

Piovesan, A.S.[1,2)*], Costa, H.L..[1,2)], Tatzgern, F.[3]

[1)] Universidade Federal do Rio Grande, School of Engineering, Rio Grande, RS, Brazil
[2)] Universidade Federal de Pelotas, Graduate Program on Materials Science and Engineering, Pelotas, RS, Brazil
[3)] Austrian Center for Competence on Tribology (AC2T), 2700 Wiener Neustadt, Austria
*Corresponding author: alvaro.piovesan@furg.br

1. Introduction

The presence of lubricant oil between tribological pairs aims to ensure the lubrication and separation of the involved surfaces. Determining the thickness of this layer is critical for component performance and integrity to be controlled. Techniques based on the principle of the reflection of ultrasonic waves have been widely used for the measurement of lubricant film thickness [1].

Different approaches and mathematical models considering the wave behavior in the lubricant layer can be employed to measure its thickness. The type of application, the tribo-pair geometry and range of thickness investigated should be considered for the choice of method [2].

In this work it is studied the relationship between the reflection coefficient, R, and the acoustic properties of four different lubricating oils in obtaining the film thickness between two stationary plates that make up an experimental measurement system.

2. Experimental method and materials

A typical three-layer system was assembled for the tests. One drop of oil was deposited between two stainless steel plates separated by two standard steel gauges with a thickness of 10 µm fixed at the ends of the face of the lower plate. A Table 1 shows the acoustic properties of the oils and steel plates used.

Table 1 Acoustic properties of the materials

	Speed of sound, c (m/s)	Acoustic impedance, z (MRayl)	Density, ρ (kg.m³)
PAO 4 Oil	1450	1.19	820
15W40 Oil	1413	1.25	882
SAE-30 Oil	1409	1.24	881
ISO VG46 Oil	1405	1.22	868
Steel Plates	5883	45.4	7700

The ultrasonic waves were generated by the excitation of a piezoelectric sensor, with a central frequency of 14 MHz, fixed on the upper plate and connected to a function generator (pulser) and an oscilloscope (receiver). A Labview interface was created for signal acquisition and processing.

Through the information contained in the signal returned the spring model was used to calculate the values of film thickness. In this model the behavior of the oil layer is governed by its stiffness, defined by R. Considering the values of R and the acoustic characteristics of the materials the film thickness was obtained through Equation 1.

$$h = \frac{\rho c^2}{\pi f z'}\left(\frac{R^2}{1-R^2}\right) \quad (1)$$

Where ρ is the density of the liquid, c is the speed of sound in the lubricant, z' is the acoustic impedance of the materials on each side of the fluid and f is the center frequency of the ultrasonic sensor.

3. Results and discussion

The film thickness values closest to the reference show R further away from 1. However, it was verified the existence of limits to where this condition is true. Table 2 shows the film thickness values measured at the central frequency of 14 MHz together with the reflection coefficient for each of the four lubricants.

Table 2 Film thickness to 14 MHz

	Reflection coefficient, R	Film thickness (µm)
PAO 4 Oil	0.9814	11.35
15W40 Oil	0.9798	10.65
SAE-30 Oil	0.9802	10.80
ISO VG46 Oil	0.9796	10.24

To complement the research and confirm the accuracy of the measurement system adopted, two other models based on the frequency response of the reflected signals should be added to the work.

The sequence of this study comprises the application of the principles of ultrasonic wave reflection to analyze the growth of tribofilm formed in lubricating oils in the presence of anhydrous and hydrated ethanol. For this the system presented must be adapted to a tribometer.

4. References

1. P. Dou, Y. Jia, T. Wu, Z. Peng, M. Yu, & T. Reddyhoff, *High-accuracy incident signal reconstruction for in-situ ultrasonic measurement of oil film thickness*. Mechanical Systems and Signal Processing, 2021. **156**, 107669.
2. P. Dou, Y. Jia, P. Zheng, T. Wu, M. Yu, T. Reddyhoff, & Z. Peng, *Review of ultrasonic-based technology for oil film thickness measurement in lubrication*. Tribology International, 2022. **165**, 107290

Effect of Plasma Nitriding Pressure on Micro-abrasive Wear of AISI 316 l Austenitic Stainless Steel

Almeida, A.F., Cáceres, J.A.S. and Franco Jr, A.R
Propemm, Instituto Federal do Espírito Santo – campus Vitória
Vitória, 29040-780, Brazil
Corresponding author: antoni-almeida@hotmail.com

1. Introduction

Stainless steels have been widely used since the beginning of the 20th century, due to their lower density compared to other special nickel alloys, as well as adequate mechanical strength, higher elastic modulus, rigidity and good corrosion resistance. AISI 316L austenitic stainless steel is the main of these material class, initially used to replace noble alloys.

Components or parts of this steel are used in devices and equipment in various industry segments, among which we can mention: chemical, oil and gas, agricultural, food, pharmaceutical and nuclear [1]. Due to the high resistance to corrosion, biocompatibility with the human organism and adequate values of mechanical resistance according to the processing.[2]

2. Material and Procedures

Samples of 32 mm in length, 20 mm in thickness were cut from a 316 L stainless steel bar and embedded in Bakelite, where submitted to conventional metallographic preparation including griding and polishing with alumina. Subsequently, samples were extracted from Bakelite and subjected to plasma nitriding at 6 h and 400 °C, varying pressure from 1.6 to 2.3 mbar.

Micro-abrasive wear tests were carried out using a device type “free ball” CSM CALOWEAR with an AISI 52100 martensitic steel ball, 25.4 mm in diameter, with a hardness of 990 ± 40 HV.[3] The rotation of the drive shaft, which makes the sphere move, was set at 180 rpm, the applied load was 0.27 N. As abrasive, it was used a paste consisting of silicon carbide (SiC), with particles of from about 7 µm at concentration of 100 mg/cm³ and with approximately 40 drops per minute.

Nitrided layers were observed using light microscopy and scanning electron microscopy (OM/SEM).

3. Results and Discussion

After plasma nitriding, on surface of the 316L stainless steel samples, occurs the formation of a thin layer, as was verified. When comparing the layer produced by the 1.6 mbar pressure through that layer produced at 2.3 mbar, it is possible observe a small variation in layer thickness. However, the samples presented after micro-abrasive wear tests no significant variation in the wear coefficients. It is inferred that small variation on the pressure will result in not appreciable variation on the wear resistance of the stainless steel.

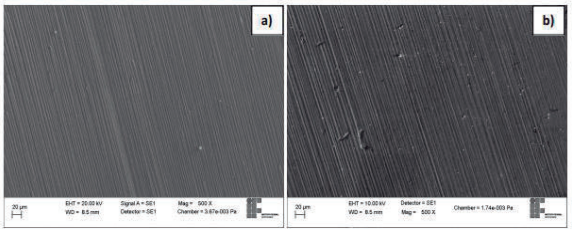

Figure 1: Wear surface of AISI 316L steel: (a) non-nitrided and (b) plasma nitrided after micro-abrasive weartests performed under normal load of 0.3N and SiC slurry.

4. Conclusion

Increasing nitriding pressure from 1.6 to 2.3 mbar did not promote significant variations on the thickness and the microstructure of layers formed on top of 316L stainless steel. New experiments using both lower or higher pressures should be carried out to analyze the effect of the plasma sheath covering the sample surface and consequently on the wear resistance of the material.

5. References

[1] LIANG, W. et al. The wear and corrosion properties of stainless steel nitride by low pressure plasma-arc source ion nitriding at low temperatures. Surface and Coatings **Technology**, v. 130, n. 2–3, p. 304–308, 2000.

[2] ARAÚJO, F.O. de. et al. Nitretação a Plasma de Aço Inoxidável Austenítico AISI 316: Uniformidade da Camada Nitretada. Revista Brasileira de Aplicações de Vácuo, v. 26, n. 1, p. 31–35, 2007.

[3] ARCHARD, J. F. Contact and rubbing of flat surfaces. Journal of Applied Physics, v. 24, n. 8, p. 981–988, 1953.

Effect of the Nitrogen Content used in the Plasma Nitriding Atmosphere on the Abrasive Wear Resistance of AISI H13 Hot Work Tool Steel

Lima, E.P., Franco Jr, A.R and Caceres, J. A. S.
Propemm, Instituto Federal do Espírito Santo – campus Vitória
Vitória, 29040-780, Brazil
Corresponding author: edsonpinheirolima@gmail.com

1. Introduction

Among the tool steels, the AISI H13 for hot working is one of the most used in making casting molds and forging dies. These tool steels are used in such applications must be able to withstand continuous mechanical and thermal stresses [1].
Seeking to improve the tribological properties, other materials and several surface hardening techniques have been developed and are being increasingly employed in industries. Surface hardening allows a combination of high surface hardness and a relatively toughness core, which includes mechanical, heat and thermochemical treatments [2].

2. Material and Procedures

Samples were obtained by cutting small pieces of an AISI H13 tool steel plate, resulting in samples approximately 30 mm long, 15 mm wide and 5 mm thick.

Subsequently, the samples were submitted to heat treatments of austeniziting, quenching and tempering. Samples were heated to 1050°C and kept at this temperature during 30 minutes for their complete austenitization. Then the samples were removed and cooled quickly in water with agitation.

After quenching, the samples were tempered at a temperature of 550°C for 2 hours and subsequentially cooled in air until room temperature.

The thermochemical treatment of plasma nitriding was performed in a pulsed plasma nitriding reactor model SDS Thor NP 300. Samples were submitted to the following nitriding conditions: temperature of 500°C, time of 5 hours, in different gas mixtures with 5% N_2 and 95% H_2, 10% N_2 and 90% H_2, 20% N_2 and 80% H_2.

Wear tests were performed using a CSM CALOWEAR "free ball" micro-abrasion apparatus with a 25.4 mm diameter AISI 52100 martensitic steel ball, with a hardness of 990 ± 40 HV. The rotation of the drive shaft, which causes the sphere to move, was set at 150 rpm, the applied load was 0.27 N. As abrasive, a slurry consisting of silicon carbide (SiC), with particles of size of about 5 µm at a concentration of 100 mg/ cm³ and with approximately 30 drops per minute.

3. Results and Discussion

The response to micro-abrasive wear were analysed after micro-abrasive wear tests performed during 1 h. The wear coefficient of the non-nitrided material is equal to $0.93x10^{-12}$ m^2/N [3].
It is possible to observe in table 1 that all treatment conditions presented greater abrasive wear resistance in relation to the non-nitrided material.

Table 1 Microbrasive wear coefficient of nitrided layers at 500°C as a function of N_2 potential and nitriding time

Coefficient of wear of the nitrided layer, k, $m^3/N.m(x10^{-12})$	
Composition of the Gaseous Mixture	k (average)
5% of N_2 and 95% of H_2	1.74
10% of N_2 and 90% of H_2	2.04
20% of N_2 and 80% of H_2	1.99

Figure 1 compares the three nitriding conditions in respect to the micro-abrasive wear coefficient. Using 10% of N_2 led to the most satisfactory result when compared to the others nitriding conditions, as this condition offered the lesser lost of material.

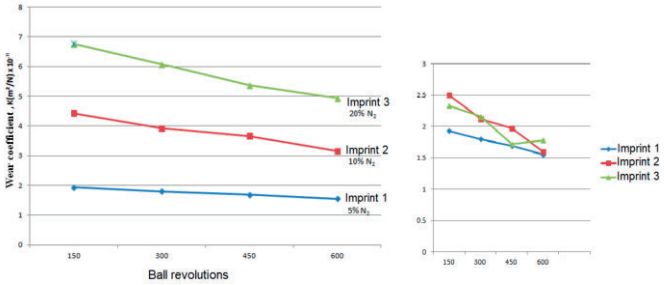

Figure 1: Micro-abrasive wear coefficient of the AISI tool steel as a function of the nitrogen content used in the gas atmosphere of plasma nitriding.

4. Conclusion

It is possible to observe that the lowest wear rate occurs with 10% N_2, as the wear is around 2.04. With 5% N_2 is 1.74 and with 20% N_2 1.99. Thus, the best condition is with diffusion zone that is, when nitrided with 10% N_2.

5. References

[1] Vilares, Metals S.A. *VH13 hot working steels. Villares tool steels.* [S.l.], 2012.
[2] Côco, L. A. *Influence of argon addition on plasma nitriding of AISI H13 steel. 107 p. Dissertation (Master's Degree) — PROPEMM: IFES, Vitoria, Brazil, Vitoria, Brazil, 2013.*
[3] Melado, A. C. *Influence of plasma nitriding parameters on the microabrasive wear resistance of AISI H13 tool steel. 118 p. Dissertation (Master's Degree) — PROPEMM: IFES, Vitoria, Brazil, 2011.*

Simulation-based Optimization of Fluid Distribution for Enhanced Grinding Performance

Costa, S.M.[1,2,3)*], Pereira, M. [4)], Ribeiro, J.E.[3,5)] and Soares, D.[1,2)]

[1] Center for Microelectromechanical Systems (CMEMS), University of Minho, 4800-058 Guimarães, Portugal;
[2] LABBELS – Associate Laboratory, 4710-057 Braga, Portugal;
[3] Centro de Investigação de Montanha (CIMO), Instituto Politécnico de Bragança, 5300-253 Bragança, Portugal;
[4] CF-UM-UP, Centro de Física das Universidades do Minho e Porto, 4710-057 Braga, Portugal;
[5] Instituto Politécnico de Bragança, Campus de Santa Apolónia, 5300-253 Bragança, Portugal;
*Corresponding author: scosta@dem.uminho.pt

1. Introduction

Grinding fluids play a crucial role in removing heat and debris during grinding processes. Their distribution directly affects the grinding results, particularly in reaching the contact zone between the wheel and workpiece [1]. Our study introduces a novel approach utilizing wheels with internal channels to distribute grinding fluid from the center of the wheel to the workpiece, aiming to reduce the air barrier phenomenon [2] and to control heat generation in the grinding zone. Through computational simulations, the fluid's distribution and spreading were evaluated through different internal cooling channel configurations. The findings offer valuable insights into enhancing fluid distribution strategies for optimizing cooling systems design in grinding operations.

2. Materials and methods

The ANSYS Workbench software was utilized to construct the geometric and mesh models of the channel structure, which were later imported into the FLUENT software to conduct simulations. Four structures were studied, with different channel diameters (Ø = 1 or 1.5 mm), number of channels (32 or 22) and orientations (θ = 0° or 15°, figure 1a). The area of the region immediately before the contact zone (with fluid velocity <0.1 m/s; non-wetted area - NWA) were measured to assess the fluid's efficacy in reaching the work zone (Figure 1b). A smaller NWA signifies a greater ability of the fluid to reach the work zone effectively.

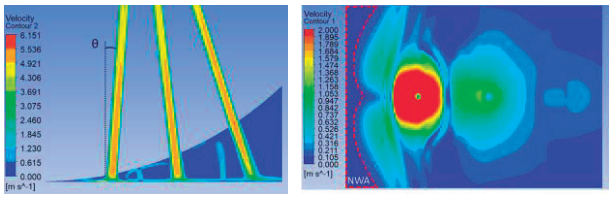

(a) (b)

Figure 1 Fluid velocity profile obtained at the medium plane of channels (a) and workpiece interface (b).

3. Results and discussion

Figure 1a and 1b visually depicts the phenomenon of neighboring channel interference in the fluid spreading process from the closest channel to the contact zone. It is evident from the illustration that only the immediate neighboring channel manifests interference, while other neighboring channels do not have a noticeable impact on the fluid flow and spreading behavior.

Figure 2 presents the NWA evolution varying the outflow per channel. In general, an exponential growing trend in NWA is observed as flow rate decreases. Under reduced flow rate grinding, a reduction of ~40% in the NWA was observed from the "22 channels, Ø = 1.5 mm, θ = 0°" configuration when compared to the "32 channels, Ø = 1 mm, θ = 15°" setup.

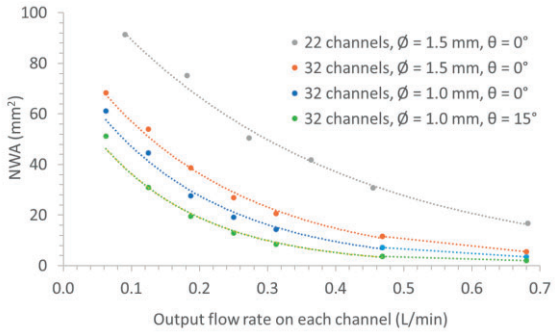

Figure 2 Non-wetted area as a function of outflow per channel.

4. Conclusions

The findings reveal that configurations with higher number of channels, smaller diameter and oriented channel reduces (~40%) the NWA. Furthermore, as the flow rate surpasses 0.3 L/min, the maximum lubricated areas tend to stabilize.

5. References

[1] Sieniawski, J. and K. Nadolny, *Experimental study into the grinding force in surface grinding of steel CrV12 utilizing a zonal centrifugal coolant provision system.* J Engineering Manufacture**,** 2016. **232**: p. 394 – 403.
[2] Peng, R., J. Tong, X. Tang, X. Huang, and K. Liu, *Application of a pressurized internal cooling method in grinding inconel 718: Modeling-simulation and testing-validation*. Int. J. Mech. Sci., 2021. **189**: 105985.

6. Acknowledgments

This work was supported by Portuguese FCT, under the reference project UIDB/04436/2020 (CMEMS center/LABBELS Associate Lab.); a PhD grant reference 2021.07352.BD, funded by FCT/MCTES (PIDDAC), granted to CIMO (UIDB/00690/2020 and UIDP/00690/2020), and SusTEC (LA/P/0007/2020).

Evaluation of parameters of an analytical solution for the surface temperatures of the pin-on-disk tribological test

Uliana, M.L.[1)], Ferreira, G.B. [1)], Camporez, R.M. [1)], Scandian, C. [1)], Strey, N.F.[*1)]

[1)] Tribology, Corrosion and Materials Laboratory – TRICORRMAT , Department of Mechanical Engineering, Federal University of Espírito Santo - UFES, Vitória, 29075-910, Brazil
[*]Corresponding author: nathan.strey@ufes.br

1. Introduction

Considering that the behavior of tribosystems is dependent on the temperature of the materials, the development of efficient models for predicting it, mainly on the contact surface, is therefore of fundamental importance. The objective of this study is to implement an analytical solution of contact temperature in the classic pin-on-disk test developed by Laraqi et al. [1], and to optimize the number of terms of the infinite series, and the grid used to plot the results.

2. Methods

The model by Laraqi et al. [1] proposes an analytical solution for temperature distribution in the pin-on-disk tribosystem. Starting from energy balance for cylindrical coordinates, the physical model considers the pin as a semi-infinite thin cylindrical rod with unidirectional heat conduction along the longitudinal axis, wall convection, steady-state conditions, negligible radiation and frictional heat generation only in the contact area. For the cylindrical disk, assumed as semi-infinite, three-dimensional heat conduction, surface convection, negligible radiation and frictional heat generation only in the contact area are considered.

Thus, with the pin fixed and the disk rotating at a constant angular speed, a uniform heat flux is generated at the contact interface. The analytical solution for the disk temperature distribution is given by Equation 1 [1].

$$T_d(r,\theta,z) = \frac{q_d a^2}{h_d b^2} + \frac{2q_d a}{b}\sum_{m=0}^{\infty}\sum_{n=1}^{\infty}\frac{\varepsilon_m(\beta_n b)J_1(\beta_n a)J_m(\beta_n e)J_m(\beta_n r)}{[(\beta_n b)^2 - m^2]J_m^2(\beta_n b)\delta} \times \cos[m\theta - \psi - zn\cos(\phi)]\, e^{-zn\cos(\phi)} \quad (1)$$

The disk temperature distributions were evaluated for the pair $Fe_{30}Ni_{20}Mn_{25}Al_{25}$ pin (r = 4.75 mm, k = 8.3 W/(m·K), h = 1 μW/(m²·K)) sliding over a zirconia disk (r = 50 mm, k = 2.0 W/(m·K), h = 14.23 W/(m²·K)), at speeds of 0.1 (μ = 0.351) and 1.0 m/s (μ = 0.416) [2]. The number of terms m and n (where $m = n$, for simplicity) evaluated in each summation was varied between 1 and 200. Calculations were performed on an Intel(R) Core(TM) i7-1165G7 CPU @ 2.80 GHz processor with 16 GB of DDR4-4266 RAM, using MATLAB R2021a.

3. Results and Discussions

Figure 1 shows the temperature distributions of disks, in a polar grid with 10,000 points, for $m = n = 5$ and $m = n = 200$. With the increase of the sliding speed, there is the development of a larger heat drag, and the region of maximum temperature is closer to the trailing edge of the contact area between pin and disk. The nominal contact temperatures found in this work matches closely what was obtained by Kennedy, Lu and Baker [2].

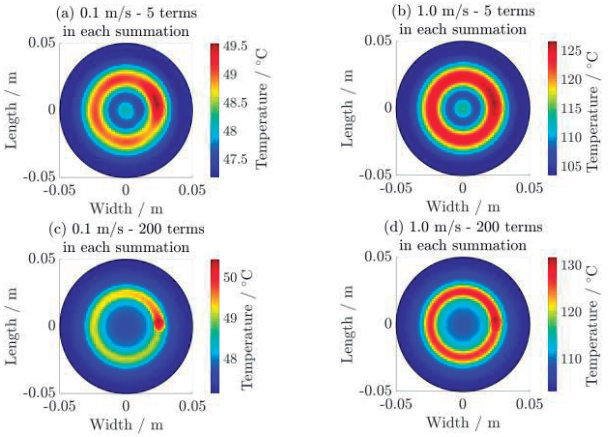

Figure 1 Temperature distributions of disks. The black circle represents the contact area.

Figure 2 shows that the number of terms where the maximum temperature of the disk stabilizes is 30. Using 200 terms resulted in a variation of only 0.2 % in the maximum temperature of the disk, while the computation time increased from 13 to 344 min.

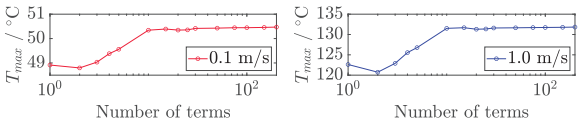

Figure 2 Effect of number of terms in T_{max}.

The model proves to be useful for obtaining the temperature distribution in the pin-on-disk test, and 30 could be an optimal number of terms (m and n) in each summation to reduce the computational effort, and still obtain reliable results. The next step is to compare the temperature distributions of the model with experimental results obtained via infrared thermography.

4. References

[1] Laraqi, N., et al. *Temperature and division of heat in a pin-on-disc frictional device—exact analytical solution*. **Wear** 266.7-8 (2009).

[2] Kennedy, F.E., Lu, Y., and I. Baker. *Contact temperatures and their influence on wear during pin-on-disk tribotesting*. **Tribology International** 82 (2015).

Influence of vapor on the next generation gas turbine engines

Castilho, Bruno C. N. M. de[1,2], Saikat, I.M.[1], Mayer, A. [2], Moreau, C.[2] ,Hazlett, M. [1] ,Stoyanov, P.[1]*
[1] Department of Chemical and Materials Engineering, Concordia University, Canada,
[2] Department of Mechanical, Industrial and Aerospace Engineering, Concordia University, Canada;
*Corresponding author: pantcho.stoyanov@concordia.ca

1. Introduction

The aerospace industry has been focusing on reducing emissions and improving gas turbine performance and efficiency during flights. One of the promising trends in this industry is the use of sustainable aviation fuel (SAF), which consists of several different compositions and approaches towards a more sustainable flight [1]. Among those, the use of hydrogen comes as a promising choice, considering the high energy output it can provide [2]. Some industries, such as automotive, have tried to implement hydrogen in their engines, with limited success [3].

Nevertheless, several challenges on the use of hydrogen as a fuel remain unanswered. One of them is how the materials currently being used on gas turbine engines will be affected with the combustion of hydrogen. In this study, some preliminary tests were performed under atmospheric and vapor-rich conditions at room and elevated temperature to determine how nickel-based superalloys will react when exposed to humid conditions.

2. Materials and Methods

Inconel 718 samples were tested under ambient conditions (40% humidity) and vapor-rich conditions using an TRB3 tribometer (Anton Paar, Austria), with a load of 5 N against Inconel 718 and alumina counterfaces under reciprocating conditions (1 Hz, 5000 cycles, 10mm wear track).

During the tests, a humidifier was adapted to the tribometer with the vapor flow directly aimed at the wear track. A humidity sensor, coupled to the tribometer, indicated the measured humidity throughout the test.

The friction coefficient was recorded by the equipment and averaged by each cycle. Meanwhile, the wear rate was calculated by measuring several cross-sectional profiles with a confocal microscope. Post-test analysis was performed with a scanning electron microscope (SEM – SU3500, Hitachi, Japan) equipped with an energy dispersive spectrometer (EDS – Oxford, UK).

3. Preliminary results

Figure 1 shows a scan of the worn surface of an Inconel 718 sample under ambient condition (left) and vapor-rich condition (right) at room temperature against alumina counterface. The wear track is significantly deeper under ambient conditions, indicated by the blue contour in the center of the track. Meanwhile, a shallow wear track is observed for the sample tested under vapor. It is hypothesized that, in such conditions, water got adsorbed at the surface of the alumina, creating a thin lubricating film that helped reducing the wear during the tests.

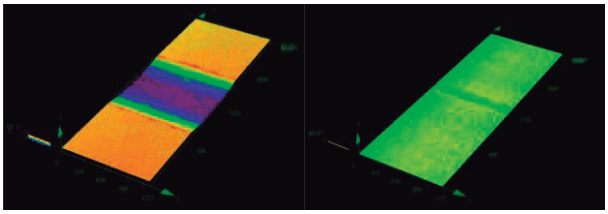

Figure 1 Comparison of surface profilometry after wear test between ambient (left) and vapor-rich (right) conditions

These results indicate that the lubricious film formed during the test on the sliding of alumina under vapor-rich conditions was effective in reducing the wear rates of the sample.

4. References

[1]Shahriar Md. F., Khanal, A. *The current techno-economic, environmental, policy status and perspectives of sustainable aviation fuel (SAF)*, Fuel **325**, 2022: 124905.
[2] Yusaf T., Mahamude, A.S., Kadirgama , K., et al. *Sustainable hydrogen energy in aviation – A narrative review,* Int. J. Hydrog. Energy, in press, 2023.
[3] Bakker, S. *The car industry and the blow-out of the hydrogen hype,* Energy Policy **38** , 2010 : p.6540-6544

Numerical Simulation of the Tribological Behavior of Hybrid Textured Surfaces (Stochastic Texturing + Honing) of Textured Cylinder Liners of Two-Stroke Engines

Oliveira, E.Y.G.[1)*], Silva, S.A.N.[2)], Costa, H.L.[1),2)] and Profito, F.J.[3)]

[1)] School of Engineering, Universidade Federal do Rio Grande
Rio Grande, 96203 900, Brazil
[2)] School of Mechanical Engineering, Universidade Federal de Uberlândia
Uberlândia, 38410 337, Brazil
[3)] Polytechnic School, Universidade de São Paulo
São Paulo, 05508 010, Brazil
* Corresponding author: eltondeoliveira96@gmail.com

1. Introduction

Plateau honing is widely used to reduce friction and wear in internal combustion engines by creating a surface topography composed of relatively smooth plateaus (good load support) and an array of cross-hatched grooves (lubricant reservoirs). Li *et al.* performed numerical and experimental analysis for a lubrication model for the piston/cylinder tribosystem to optimize friction [1]. This work aims to optimize honing patterns for texturing the surfaces of two-stroke engine cylinder liners mathematically simulated to be superimposed on a random texture resulting from a hard chrome plating process.

2. Methodology

Real liner surfaces were measured by optical interferometry. First, they were analysed the commercial software MountainsMap® to remove shape distortions, undulations and unmeasured points on the surface. Then, in the SurFAT program, developed by the Surface Phenomena Laboratory (LFS) from the University of São Paulo (USP), the sample was subdivided into several slices of 200 µm, perpendicular to the stroke direction.
The SurfLUB software, also developed by LFS/USP, simulated lubricant film thickness, averages of hydrodynamic and contact pressures of asperities, and cavitation. Virtual honing patterns were superimposed on the treated surfaces to evaluate the effects of crossing angle (α), groove depth and width (d_p and w), and groove density (d_e) on the lubrication and friction of the liners (*Figure 1*)

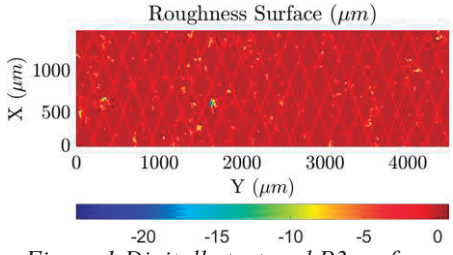

Figure 1 Digitally textured P3 surface

3. Results and discussion

Figure 2 exemplifies the results for the simulations obtained using different crossing angles. The results show that although the grooves reduce the hydrodynamic shear stress, it also reduces the hydrodynamic pressure, so that the effect is a slight in increase in friction with the honing grooves. After all the simulations, the best results were found for $\alpha = 40°$, $d_e = 0.15$, $w = 15\ \mu m$ and $d_p = 1.5\ \mu m$.

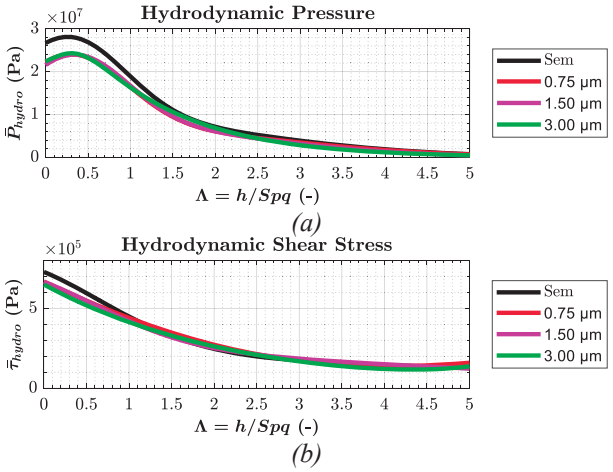

Figure 2 Average values for (a) hydrodynamic pressure and (b) hydrodynamic shear stress of P3 sample for every groove depth

4. Final considerations

Despite honing surface technique being widely used in the automotive industry, the simulations suggest that in this case the grooves would not improve tribology, probably because it already had a stochastic texture resulting from the previous hard chrome deposition.

5. Acknowledgments

This work was funded by the Academic Master's Program for Innovation of the National Council for Scientific and Technological Development - CNPq.

6. References

[1] Li, T., Lu, X., Ma, X., Xu H., Jiao, B., and Zou, D., *Numerical and experimental analysis of the honing texture on the lubrication performance of piston ring–cylinder liner tribosystem*, Tribology Transactions, 2019. **62**: p. 991-1006.

Opportunities to produce and operate waste-based lubricants

Nunes, I. dos S.[1)*], Trindade Jr., P. M.[1)], Murray, H.L.C.[1)] and Kessler, F.[1)]

[1)] National Institute of Science and Technology – Tribology, Federal University of Rio Grande, Rio Grande, 96203 900, Brazil
[*]Corresponding author: isaac.eq@gmail.com

1. Introduction

Considering the necessary reduction of the global warming and emissions to protect the planet, a true transition to a green energy platform will only occur with the establishment of a complete supply chain that is also green. Despite this, one of the major technological difficulties with green-based lubricants is that they are particularly vulnerable to oxidation compared to petroleum-based ones.

In another way, the use of post-consumer polymers remains largely unexplored, requiring efforts in scientific development. Producing lubricants from this waste presents a new route to avoid nonrenewable oil extraction. Transforming post-consumer polymers into lubricants requires an initial degree of oxidation. Polymer chain degradation reaction yield better results in the presence of catalysts, which operates more efficiently when the material contains oxygenated groups [1]. It means that the material that has been exposed to weathering for a longer period has a greater potential. Also, polymer degradation with photo-oxidation can saturate the material surface with oxygen [2]. Using UV lamps and simple chemical reagents, like glycerol and bicarbonate, these reactions are favoured. Thermal process catalyses are also employed, although require more energy to convert.

To produce waxes, a patent [3] from depolymerized mixed polyethylene presented uses of pressures ranging from 0.345 to 2.414 MPa and temperatures between 300 and 600ºC. Wastes were preheated and melted before being fed into the reactor, and degradation was catalyzed by different metals supported on ceramic material ([Fe-Cu-Mo-P]/Al_2O_3).

Another invention was registered [4] for a continuous system for wax production from polyethylene waste, with the same pre-treatment already reported [3]. In this case, operational parameters ranged from 325 to 450ºC, with residence times of 1 to 120 minutes, using 1 to 12 reactors connected in series. Different feed material composition results in waxes with melting points ranging from 40 to 65ºC, 65 to 85ºC, 86 to 105ºC, and 106 to 140ºC.

Another patent presented the production of high-speed chain lubricating grease containing a blend of microcrystalline wax and polyethylene [5]. However, the document does not specify that the source of wax was from depolymerization.

This work presents the possibility of the destination of polymer residues to produce wax. Despite this, these proposals require high temperatures and/or pressures for depolymerization. In this way, it is possible to investigate the use of green chemicals at low temperatures and atmospheric pressure to obtain these products. Furthermore, the cited inventions do not provide data on the use of the obtained waxes in lubricant compositions or their testing. Then, there is a novel possibility to evaluate performances when in mechanical structures.

2. References

[1] Fox [1] Zhang, Y *et al. The effects of atomic oxygen and ion irradiation degradation on multi-polymers: A combined ground-based exposure and ReaxFF-MD simulation*.
Polym. Degrad. Stab., 2022. **205**:110134.
[2] Moharir, R.; Kumar, S. *Structural characterization of LDPE films to analyse the impact of heavy metals and effect of UV pre-treatment on polymer degradation*. J. Clean. Prod., 2021. **298**: 126670.
[3] Kumar, A.; Kumar, P. *Processos para converter resíduos de polietileno misto para produzir ceras e graxas através de despolimerização catalítica e processos para converter grânulos primários de polietileno para produzir ceras e graxas através de despolimerização catalítica*, BR 112013001058-4 B1, 29 set. 2020.
[4] Gil, A.; Dimondo, D.; Rybicki, R. *Sistema para tratamento contínuo de material polimérico reciclado*, BR 112018013600-0 B1, 29 mar. 2022.
[5] Jie, C. *High-speed chain lubricating grease and preparation method thereof*, CN 102965178 B, 15 oct. 2014.

The role of manufacturing-induced texture on the tribological performance of cold work tool steels

Lopes, A.P.O.[1,2)*], Almeida, D.T. [2)], Johnson, S.M. [3)], D'Oliveira, A.S.C.M. [3)], Murray, H.L.C [4)], Scheuer, C.J.[1)]

[1)] Technology and Mechanics of Materials Group, Universidade Federal de Santa Maria (UFSM), 97105-900, Brazil.
[2)] Bruning Tecnometal Ltd., 98280-000, Brazil.
[3)] Surface Engineering Group, Universidade Federal do Paraná (UFPR), 81530-000, Brazil.
[4)] Surface Engineering Group, Universidade Federal do Rio Grande (FURG), 96203-900, Brazil.
*Corresponding author: angelica@bruning.com.br

1. Introduction

In recent years, the concept of life cycle assessment of products has gained increasing significance in the academic and technical realms. Environmental impacts and the costs associated with product disposal have received greater emphasis within this context [1]. Consequently, maximizing product durability has emerged as an imperative strategy. In this scenario, heightened industry competitiveness have driven the need to extend the lifespan of production tools. This objective is achieved by effectively managing the tools' failure mechanisms, with emphasis on controlling friction and wear processes [2].

Thus, over the past decades, the operational conditions of forming tools have increasingly become more severe. Therefore, enhancing tribological performance has become imperative. In this regard, one of the proposed solutions involves the production of microtextures on the tool surfaces, aiming to modify the contact and lubrication conditions [3]. Several surface texturing operations have been proposed and it effectiveness demonstrated. However, the introduction of a new manufacturing procedure into the production route of such tools further burdens the manufacturing process, resulting in increased product costs.

Considering the above, the objective of this study was to assess the impact of microtextures resulting from tool manufacturing operations on the tribological performance of two types of tool steels, one with 2.0% and the other with 0.8% carbon by weight.

2. Materials and Methods

As part of the experimental investigation, two rolled steels, labeled as 2% and 0.8% wt. C steels, were utilized as tool substrates. The test tools underwent identical manufacturing processes to the production tools employed in the factory. Initially, the tools were machined into the desired geometry, then hardened to achieve a hardness of 58±1 HRC, and subsequently subjected to heat treatment and a fine finishing operation. This processing ensured that the test tools possessed the same topographical characteristics as the tools used in the actual production process.

A 3.0 mm thick hot-rolled steel (0.15% wt C) was selected as the raw material for the workpiece (sheet), and it was in the pickled and oiled surface condition. To ensure consistency, all test specimens were obtained from the same steel coil, thereby eliminating variations in quality.

The tribological evaluation of the two tool substrates was performed using the strip drawing test, as described in reference [4]. The tests included applying contact pressures of 290, 340, and 420 MPa at a stretching velocity of 100 mm/s. Each test involved stretching up to 20 sheets. A commercial lubricant commonly used in sheet forming operations was employed as an intermediary between the tool and the sheet.

The tools were analyzed using SEM and CLSM to assess their characteristics before and after testing. The sheets underwent evaluation using a stereomicroscope, and their topographical features were determined using a contact profilometer. The tribological behavior was evaluated based on friction and wear coefficients, as well as the wear mechanism.

3. Results and discussion

Figure 1 visually depicts the fabricated tool surfaces of the 2% and 0.8% wt. C steels, observed through SEM, prior to conducting the strip drawing test. A distinct pattern of textures resulting from the manufacturing process is evident. While the manufacturing marks have a similar profile, each material responds differently to the machining process. Marks on the 2% wt. C steel indicate deeper tool penetration and the presence of adhesive traces, indicating material smearing. Conversely, marks on the 0.8% wt. C steel display shallower tool penetration and grooves with lateral projection of deformed metal. This divergence in response is attributed to the dissimilar characteristics of the materials: the 2% wt. C steel demonstrates superior abrasion resistance, while the 0.8% wt. C steel exhibits higher toughness and resistance to adhesive wear.

Figure 2 shows a comparison of the average values of friction and wear coefficients developed by both tools. It can be observed that both materials exhibit similar tribological behavior regarding the evolution of friction and wear coefficients with increasing contact pressure, as the friction coefficient increases in both cases. However, when analyzing the values of both the friction and wear coefficients, it is evident that for all evaluated contact pressure conditions, the values observed for the tool produced from the 0.8% wt. C steel were consistently about 40% higher than those of the tool produced from the 2.0% wt. C steel. This behavior is related to the microstructure of each material, specifically the size of the carbides precipitated within it. In this case, the larger carbides precipitated in the microstructure of the 2.0% wt. C steel provide better anchoring to the metallic matrix, reducing its wear.

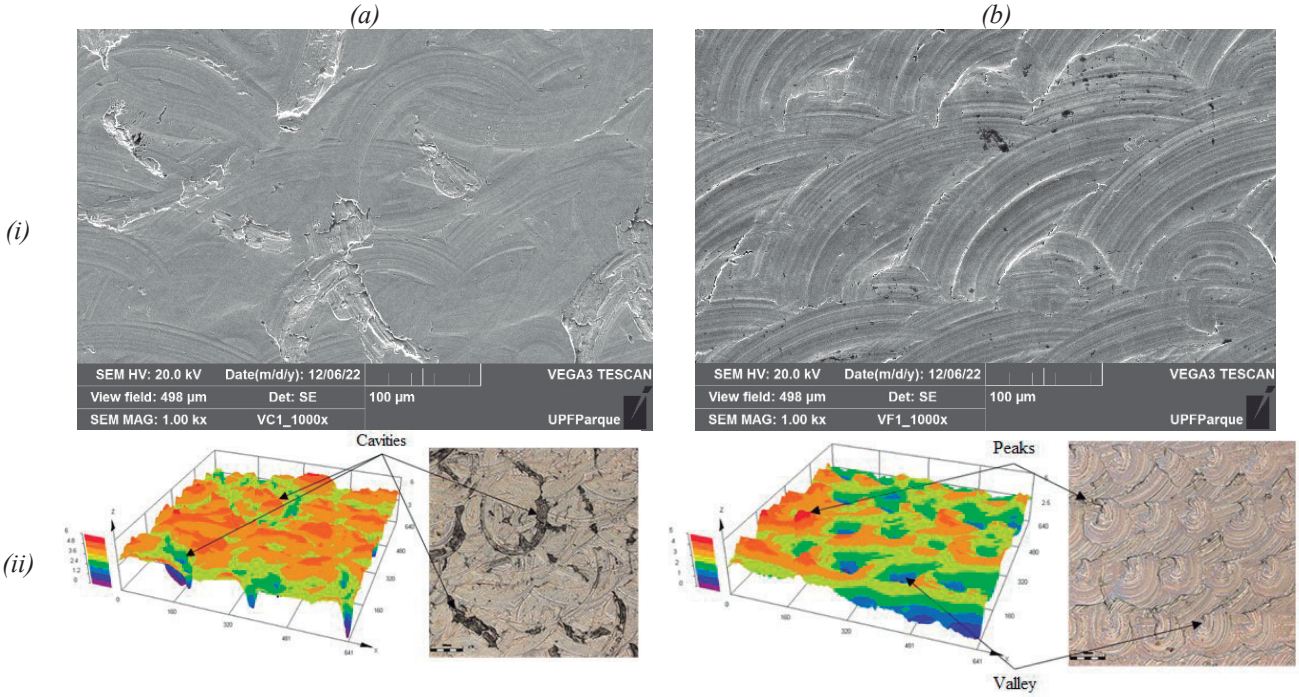

Figure 1 (i) SEM and (ii) CSLM micrographs of the surface of tool steels with (a) 2.0 and (b) 0.8% wt. C, before testing.

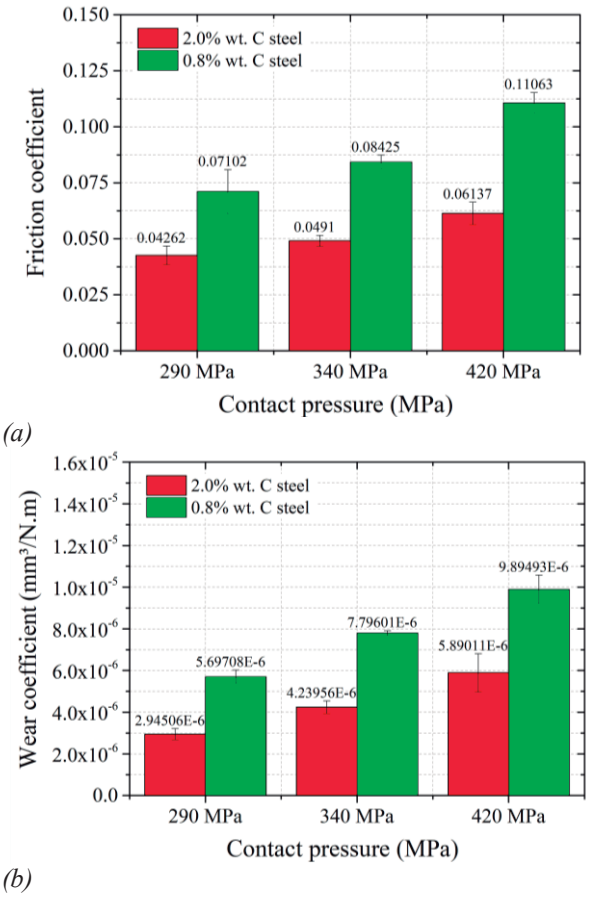

Figure 2 Dependence of the (a) friction and (b) wear coefficients of the test tool materials

Figure 3 displays the surface morphology of the tools produced from the 2.0% (a) and 0.8% wt. C (b) steels after conducting the strip drawing test on 20 sheets, using a contact pressure of 340 MPa and a sliding velocity of 100 mm/s. Comparing the images, it is evident that the 2.0% wt. C steel exhibits a wide and deep groove along the sliding direction of the sheet, accompanied by adhesive marks and material detachment. Conversely, the surface of the 0.8% wt. C steel shows a higher density of smaller and narrower grooves, as well as prominent signs of adhesion indicating material smearing and deposition. In the case of the 2.0% wt. C steel, it is believed that the observed groove was formed by a carbide detached from the metallic matrix, which underwent friction between the tool and the advancing sheet. For the 0.8% wt. C steel, a transferred layer of material from the sheet fills the valleys of the tool's surface roughness through adhesion. The higher density and smaller size of the grooves in this case are possibly attributed to the geometric nature of the debris detached from the sheet material. It is assumed that these material particles do not adhere to the tool but are displaced during the tool-sheet contact, experiencing work hardening and causing grooving on the tool surface as the sheet advances.

In addition to the microstructure effect, this behavior can also be justified in terms of the microtexture effect resulting from the manufacturing operation on the contact mechanics and lubrication. It is hypothesized that the cavities generated during the machining process in the 2% steel (Figure 1*a*) act as lubricant reservoirs, where the lubricant remains locally trapped in these irregularities, supporting the contact load even under high-pressure conditions. As the load increases, the lubricant film may rupture or the "trapped" lubricant may flow due to the relative movement between the sheet and the tool, leading to increased contact between their surfaces and consequently higher friction and wear coefficients.

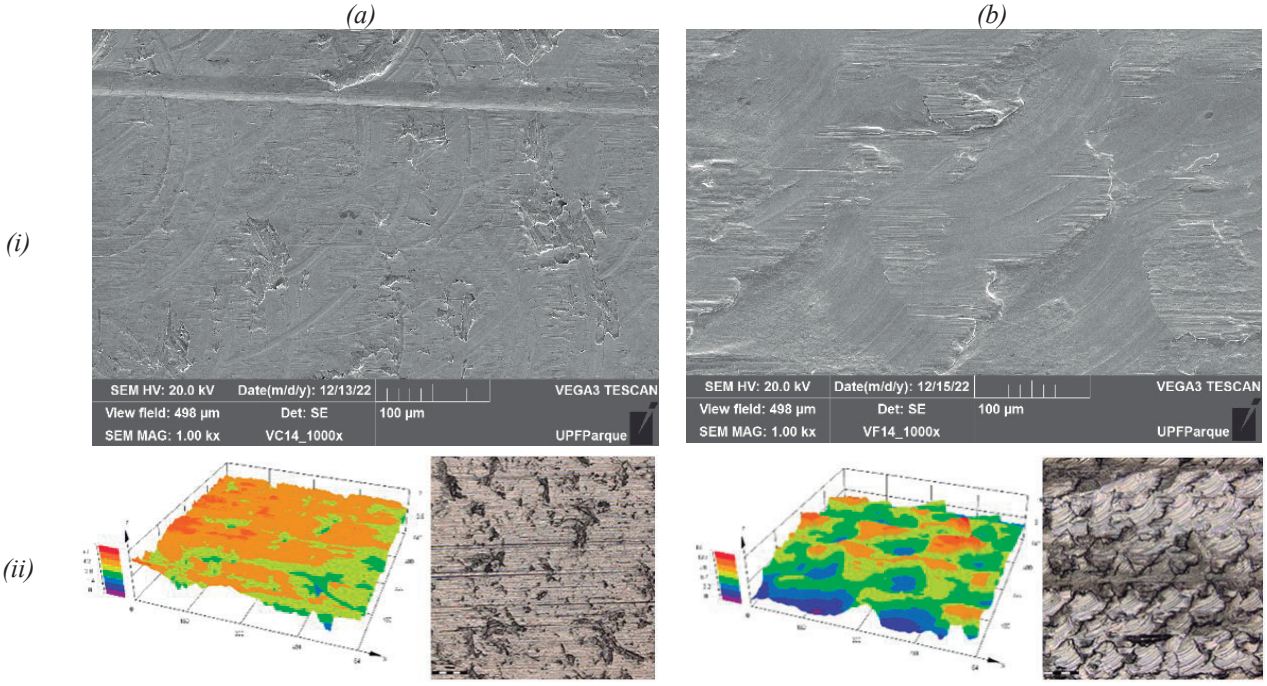

Figure 3 (i) SEM and (ii) CSLM micrographs of the surface of tool steels with (a) 2.0 and (b) 0.8% wt. C, after testing.

The analysis of surface roughness parameters for both test tools after the strip drawing test (Figure 4), reflects the differences on it tribological behavior. The 2.0% wt. C steel exhibited a significant reduction in the Sa, Sq, Sp, and Sv parameters compared to its initial condition, indicating a relatively smoother surface. On the other hand, 0.8% wt. C steel showed a slight increase in these values, indicating a rougher surface. The maximum valley depth (Sv) for 0.8% wt. C steel significantly increased after the test, doubling its initial value, indicating a greater number of grooves on its surface. However, the Ssk value increased for 0.8% wt. C steel, indicating an increase in the number of peaks (positive values), while it slightly decreased for 2.0% wt. C steel (due to the partial filling of valleys by material transfer from the sheet). The kurtosis values (Sku) for 2.0% wt. C steel decreased, indicating a flattening of the roughness peaks.

Photomacrographs of the sheets were obtained after the strip drawing test (*Figure 5*) to illustrate the influence of the tool material on the tribological system. Comparative analysis of the tested sheets using the tool steels with 2% and 0.8% wt. C reveals that in the former case, there is virtually no wear on the sheet, while in the latter case, wear grooves are clearly visible. This confirms a greater transfer of material from the sheet to the tool made of 0.8% wt. C steel. Figure 6 presents roughness values (Ra, Rz, and Rpk) measured on the cross-sectional and longitudinal sections of sheets stretched over tools made of 2% and 0.8% wt. C steels. The results show that the sheet stretched over the 0.8% wt. C steel tool exhibits higher roughness, while the sheet stretched over the 2.0% wt. C steel tool shows a smoothing effect, with post-test roughness lower than the original sheet. Furthermore, the Ra, Rz, and Rpk values measured on the longitudinal plane of the sheets are statistically equivalent to each other.

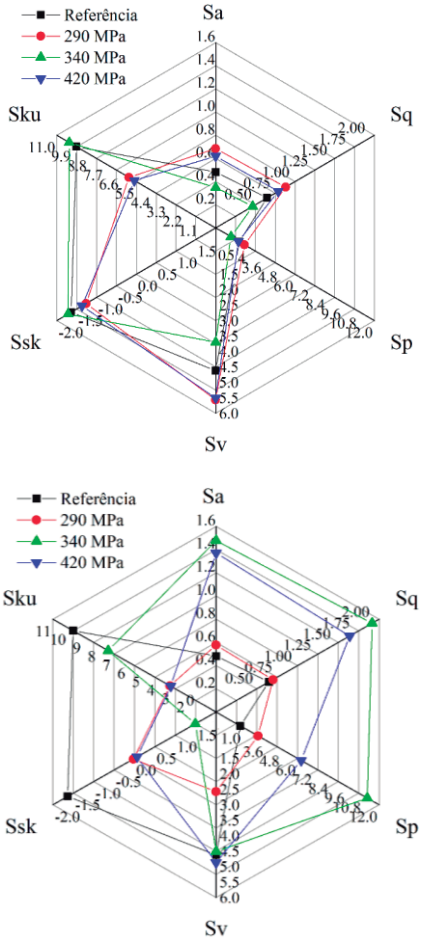

Figure 4 3D surface roughness parameters of the tools tool steels with (a) 2.0 and (b) 0.8% wt. C, before and after the test

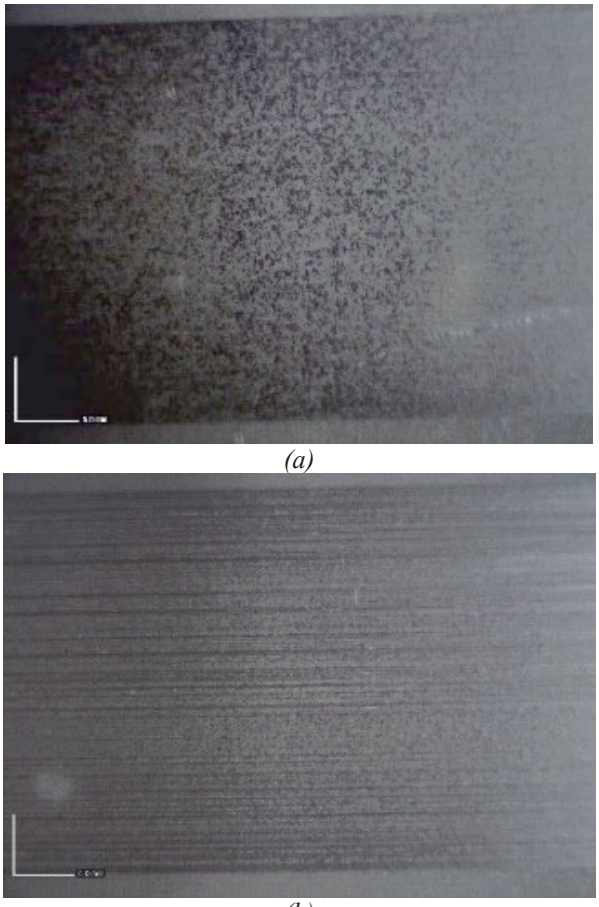

(a)

(b)

Figure 5 Photomacrograph of the sheets surface after test for the steel tools with (a) 2.0% and (b) 0.8% wt. C.

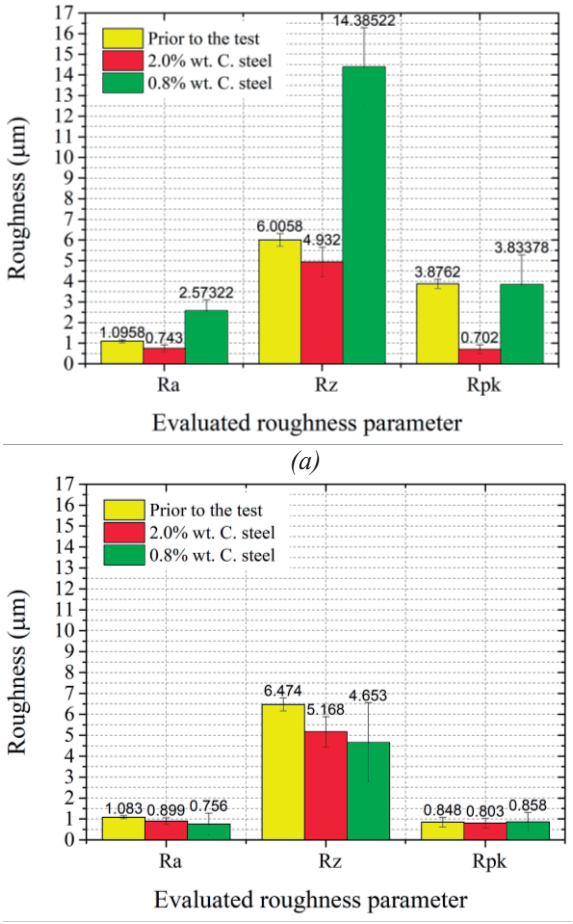

(a)

(b)

Figure 6 2D roughness parameters measured on the (a) cross-sectional and (b) longitudinal planes of the sheets stretched over the tools made from 2.0% and 0.8% wt. C steels, before and after the test.

4. Conclusions

- The surface texture of the tools, resulting from their finishing operations, varies from one material to another and has an impact on their tribological performance;
- The tribological tests showed that the 2.0% wt. C steel exhibits a lower coefficient of friction and lower wear coefficient when compared to the 0.8% wt. C steel under the test conditions;
- The characterization of the wear track produced in both tool steels indicates that the 2.0% wt. C steel is more prone to abrasion wear, whereas the 0.8% wt. C steel has a greater tendency to undergo adhesive wear;
- The 3D roughness parameters measured on the tools surface after the test indicate that the one produced from the 2.0% wt. C steel appears smoother compared to its initial condition, while the one produced from the 0.8% wt. C steel shows a rougher surface;
- The macrographic characterization of the sheets after the stretching test showed that those stretched over the 2.0% wt. C steel tool do not exhibit any visible signs of wear to the naked eye, while those tested using the 0.8% wt. C steel show clearly visible wear grooves;
- The 2D roughness measurements performed on the cross-sectional plane of the tested sheets indicate a higher roughness of the sheet after being stretched over the 0.8% wt. C steel tool, and a lower roughness in the sheet stretched over the 2.0% wt. C steel tool. The measurements taken on the longitudinal plane of the sheets show that there is no difference in the values of the sheets stretched over the different tool materials.

5. References

[1] F. Ardente, F. Mathieux. Environmental assessment of the durability of energy-using products: method and application. J. Clean. Prod., 2014. **74**. p.: 62–73.

[2] A. Arslan, et. al. Surface Texture Manufacturing Techniques and Tribological Effect of Surface Texturing on Cutting Tool Performance: A Review, Crit. Rev. Solid State Mater. Sci, 2016. p.: 1–35.

[3] M. Calandri, et al. Laser surface texturing of pvd coatings applied to sheet forming dies for stainless steel. La Metall Ital, 2016. **3**. p.: 27-35.

[4] A.F. Tavares, et al. Effect of transfer layers on friction and wear mechanisms in strip drawing tests of commercially coated forming tools. Wear, 2021. **476**. p.: 203733.

Influence of carbon content on the hardness and microstructure of different stainless steels hardenable by surface laser remelting

Almeida, L.K.A.[1)*] Labiapari,W.S.[2)] and Koga,G,Y.[1)]

[1)] Department of Materials Science and Engineering, Universidade Federal de São Carlos, São Carlos, 13565 905, Brazil
[2)] Aperam South America, 35180 222, Timoteo, Brazil.
[*]Corresponding author: lucaskaa@estudante.ufscar.br

1. Introduction

Hardenable or martensitic stainless steels are characterized by the formation of martensite after a heat treatment cycle [1]. The microstructure formation in this material type gives it a high hardness and mechanical resistance and consequently also provides a high resistance to wear [2].

This work will remelt stainless steels surface with different carbon contents and compare them with their quenched and annealed condition in terms of hardness and microstructure.

2. Materials and Methods

Table 1 shows the steels used and their respective chemical compositions. The samples for remelting were cut to dimensions, 20 X 20 mm, and the thickness was 3 mm. Subsequently, they were sanded using the following sequence P120, P220, P320, P600 sandpaper and then sandblasted with a shot blast until the entire surface was opaque. The remelting was carried out in a fiber laser in OmniSint-160 model equipment. The power used was 300 W at a speed of 250 mm/s. The distance between lanes was 75 µm. The hardness for all conditions were measured using a Shimadzu microhardness meter integrated with a C.A.M.S system (computer assisted microhardness system) following the ASTM E92 standard.

Optical microscopy (OM) and scanning electron microscopy (SEM) were used for microstructural characterization of the different conditions.

Table 1 - Chemical composition the samples (% weight)

Samples	Fe	Cr	C	Mo	Si	Mn
410	Bal.	11	0,03	-	1	1,5
420A	Bal.	12	0,30	0,48	1	1
420D	Bal	12	0,18	0,50	1	1
498	Bal	14	0,45	0,53	1	1

3. Results

Figure 1 shows the remelted layer thickness for each sample. In figure 1 it is observed that stainless steel 410 provided an equiaxed columnar growth of the ferritic microstructure rejecting solute to the grain boundary. The others samples presented a highly refined microstructure, it is observed the martensite formation as well as that austenite retained in addition to the presence of delta ferrite. The SEM image (fig 1e) shows the morphology and cell size obtained for 498 stainless steels.

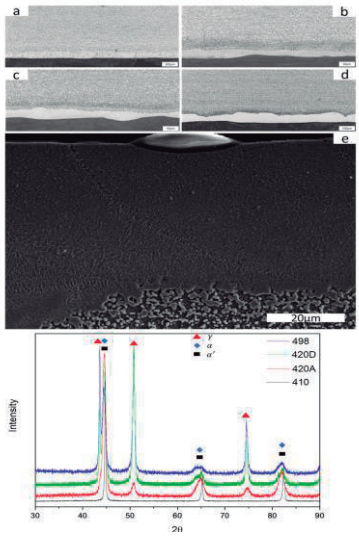

Figure 1: Microstructure and XRD remelt zone 410(a), 420A(b), 420D(c), 498(d). SEM image the remelted zone in 498 (e).

Table 2 shows the hardness for each sample in its respective condition. It is observed that the refuted sample provided hardness equal to or greater than the quenched samples, being able to infer that the resistance to abrasion of this one can be equal or better than the quenched condition.

Table 2 - Hardness sample according to condition

Sample	Dureza ($HV_{0,5}$)		
	Annealed	Quenched	Remelted
410	206±7	318±15	193±6
420A	190±4	585±20	700±24
420D	198±10	497±21	510±25
498	202±2	622±17	525±21

4. References

[1] ASTM A240 Standard Specification for Chromiumand Chromium-Nickel Stainless Steel Plate, Sheet, and Strip for Pressure Vesselsand for General Applications. 2022.

[2] George Krauss. Principlesof Heat Treatmentand Processing of Steels. American Society for Metals, Metals Park, Ohio, 1990

The behavior of annealed and quenched AISI 410 steel in sliding wear tests

Silva, R.G.[1)*], Labiapari, W.S[2)] and Koga, G.Y.[1)]

[1)] Department of Materials Science and Engineering, Universidade Federal de São Carlos, São Carlos, 13565 905, Brazil
[2)] Aperam South America, Timóteo, 35180 222, Brazil
[*]Corresponding author: rinaragregorio@estudante.ufscar.br

1. Introduction

The main characteristic of AISI 410 stainless steel (SS) is to combine resistance to abrasion and corrosion, which is why the consumption of these steels has been increasing in recent years [1].

The factors responsible for this fact were the increase in demands for this steel in the rail transport and sugar-alcohol sectors, where this material is applied in conditions that involve different types of wear and water [2]. This work investigates the tribological behavior of this material in the annealed and quenched condition in sliding abrasion.

2. Materials and Methods

Microsclerometry tests were performed with the Micro Combi Tester (MCT3) Step 500 equipment from Anton Paar in the Physical Methods Laboratory at Aperam South America to identify the different treatment conditions behavior of the samples in the risk test, analyzing the friction coefficient, penetration depth and elastic return. An indenter of 100 micrometers was used. The tests load was 10 N and the distance was 3 mm in length. Samples of AISI 410 annealed and quenched were investigated in triplicate.

Scanning electron microscopy (SEM) and confocal microscopy were used for wear micromechanisms investigation and to find the worn volume. Subsequently, the wear rate was calculated using the Archard equation.

$$\varphi = \frac{Vtot}{(LFn)} \quad (1)$$

3. Results and Discussion

3.1. Microsclerometry

The annealed sample had the lowest average friction coefficient, 0.32, with minimum and maximum values, 0.3 and 0.34. The quenched sample had the highest average friction coefficient, 0.36, with minimum and maximum values, 0.25 and 0.53. Peaks are found with higher values for the friction coefficient followed by valleys for the tempered condition. This variation may be related to the wear mechanism that these samples presented, micro-chipping, as it is a more fragile and brittle material.

The annealed condition has a greater penetration depth, 12 µm, compared to the quenched condition, 9.6 µm. This difference between the conditions may be due to the annealed material having a higher ductility. It manages to deform more without fracturing. Quenched samples, on the other hand, are more fragile and brittle, suffering less deformation.

The elastic return for the annealed condition was 7.45 µm, greater than the quenched condition, 4.86 µm. This issue is related to the elasticity modulus of the material (Young's modulus). More brittle metals break more easily without the elastic phase occurring.

3.2. Wear micromechanisms

In the annealed condition, the predominant wear mechanism was micro-grooving, fig. 1a, in which plastic deformations occur without matter loss, generating a groove with consequent formation of frontal and lateral material moved accumulations, because it is a softer and more ductile material. In the quenched condition, fig. 1b, the marble mechanism was micro-grooving, but it also presented the micro-chipping wear mechanism, as it is a more fragile and brittle material.

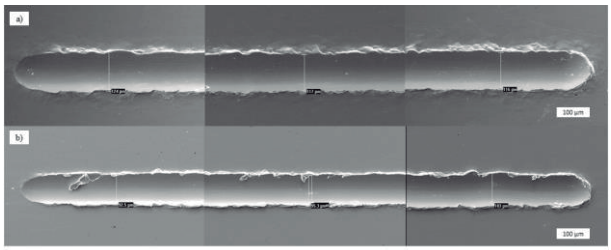

Figure 1 – Scratches performed in the SEM of 410 SS. a) Annealed. b) Quenched.

3.3. Wear rate

Table 1 shows the values of the dimensional wear rate (φ) obtained in the tests.

Table 1 – Dimensional wear rate [$mm^3(Nm)^{-1}$]

Condition	Mean	Standard Deviation
Annealed	5.1×10^{-3}	5.35×10^{-5}
Quenched	2.45×10^{-3}	2.74×10^{-4}

The test results showed a higher wear rate for the annealed condition, due to being a softer material compared to the quenched one. Therefore, quenched samples have greater scratch resistance compared to annealed samples.

4. References

[1] Krauss, G, *Steels: Processing, Structure and Performance*. 2ed. ASM International, 2015.
[2] Labiapari, W., S. Alcântara, C., M. Costa, H., L. De Mello, J., D., B, *Stainless Steel as an antiwear material for the bio-fuel industry*. Wear, 2013. **302**: p. 1536-1545.

Particle Abrasivity of Perlite Determined under Microscale Abrasion Testing

Marchiore, M.C.[1)], Benegra, M. [1)*] and Pintaude, G.[1)]

[1)] Academic Department of Mechanics, Universidade Tecnológica Federal do Paraná, Curitiba, 81280-340, Brazil
[*]Corresponding author: marjorieb@utfpr.edu.br

1. Introduction

Perlite is a semi-crystalline material of volcanic origin, composed mainly of anorthite and quartz [1]. It is used in the filtration of enzymes due to its high porosity and mechanical resistance. However, they can cause extensive wear in mechanical components. Understanding how these particulates wear the surfaces is essential for improving the durability and performance of components. This study aims to characterize the abrasiveness of perlite using microscale abrasion tests.

2. Methods

This investigation characterizes the perlite abrasivity using microscale abrasion testing. The particulate was dissolved in distilled water for a 5% wt solution. The material selected for wearing is the 316L stainless steel, sanded to 600 mesh, because it is found in filtration processing. To establish a pattern of wear coefficients and mechanisms, a standard diamond slurry usually employed for the cratering ball test was used under the same testing conditions.
The testing variables were selected based on previous studies developed at Surface and Contact Lab/UTFPR, which avoid excessive wear of rotating ball [2]. For the investigated tribological pairs, the steady-state regime was reached after 20 min testing time. The wear coefficients (k) were calculated using Equation (1):

$$k = d^4/ (128\ t\ n_B\ F\ R^2) \quad (1)$$

Where, d is the diameter of crater, t is the testing time, n_B is the ball rotation, F is the applied force, and R is the ball radius.
The morphology of abrasives was described in scanning electron microscope (SEM), as well as the wear mechanisms after microscale abrasion tests.

3. Results

Perlite particles caused a wear coefficient about three times higher than that of diamond solution, as shown in Table 1.

Table 1 Average wear coefficients determined under microscale abrasion tests for 20 min testing

Abrasive	Wear coefficient (10^{-10} mm^3/Nm)	Standard Deviation
Diamond slurry	4.5	± 1
Perlite 5%	13	± 3

This difference was due to the bimodal size distribution of perlite, which has much larger particles than diamond (Figure 1). Besides, the wear mode was described as a mix of cutting and deformation, mainly due to the irregular shape of perlite particles, contrary to those described after tests with diamond slurry, which showed very straight scratches.

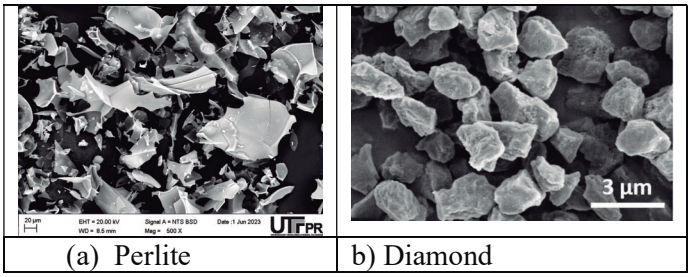

(a) Perlite | b) Diamond

Figure 1 SEM images of used abrasives: a) perlite, and b) diamond.

4. Conclusions

The bimodal size distribution of perlite is a relevant variable in defining its abrasivity. Even larger particles were found in a smaller proportion, they were enough to cause a wear in 316L stainless steel almost three times higher than the determined using a pattern diamond solution.

5. References

[1] Terzić A, Stojanović J, Andrić L, Miličić L, Radojević Z. *Performances of vermiculite and perlite based thermal insulation lightweight concretes*. Science of Sintering. 2020. **52(2)**: 149-162.
[2] Rovani, A.C., Rosso, T.A. and G. Pintaude, *On the Use of Microscale Abrasion Test for Determining the Particle Abrasivity.* J. Test. Eval., 2021. **49(1)**: https://doi.org/10.1520/JTE20180576.

Evaluation of Abrasive Wear Resitance of FeMnCr Coating on ASTM A128 grade C Steel

Rossino, L.S.[1,2], Farias, F.W.G.[2],Vacchi, G.S.[3], Teodoro, M.R.[2], Pereira, H.B.[4] and Manfrinato, M.D.[1,2]*

[1] PPGCM UFSCar, Universidade Federal de São Carlos, Sorocaba, 18052-780, Brazil
[2] Department of Materials, Fatec Sorocaba, Sorocaba, 18013-280, Brazil
[3] Department of Materials, Fatec Sertãozinho, Sertãozinho, 14170-120, Brazil
[4] Department of Metallurgical Engineering and Materials, Polytechnic School of USP, São Paulo, 05508-030, Brazil
*Corresponding author: marcos.manfrinato@fatec.sp.gov.br

1. Introduction

The manganese steel alloy known as Hadfield steel is generally used in applications that need wear and impact resistance, for example, mining. It is commonly composed of 1.2%C and 13%Mn and has a metastable austenitic structure that hardens quickly by deformation when subjected to repeated impacts, through the so-called hardening process [1]. During the manufacturing process or mining use, Hadfield steel parts wear out and need to be reconditioned. Normally, the coated electrode welding process is used. The objective of this work is to weld the FeMnCr coating and verify its resistance to wear on the rubber wheel.

2. Materials and Methods

Manganese steel ASTM A128 grade C was used in the format of specimens with dimensions of 100mm wide by 250mm long and 10mm thick. The buttering welding was carried out with tubular wire KDT Tub 4370 (DIN EN 14700) with a diameter of 2mm, DC+ voltage with 27V, 280A, and a welding speed of 180mm/min. The filling was carried out using ASME SFA-5.21 FeMnCr wire, 1.6mm in diameter, DC+ voltage with 26V, 270A, and welding speed of 210mm/min. 2 filling passes was performed.

Rubber wheel abrasive wear tests were conducted using ASTM G65-2021 procedure B. In this procedure B the load applied is 130N with 2,000 rpm of wheel rotation frequency maintaining the flow of the abrasive an AFS 50/70 sand of granulometry 212 µm to 300 µm with 350g/min. The time variation was used for the tests, with 2 specimens of each condition (without welding and welded) made every 10 minutes up to 60 minutes of testing in total and 1 specimen of the two conditions (without welding and soldier) during 30 minutes until reaching 60 minutes.

3. Results and Discussion

Figure 1 shows the results obtained from abrasive wear with a rubber wheel. It is observed that the mass loss increases with the increase of the test time. Tests carried out every 10 minutes show less weight loss than those carried out every 30 minutes. It is observed that the specimens welded with the ASME SFA-5.21 FeMnCr cored wire coating showed greater mass loss than the specimens without welding in all tested conditions. Figure 2 shows the measurement of the wear surface for (a) with weld and (b) BM

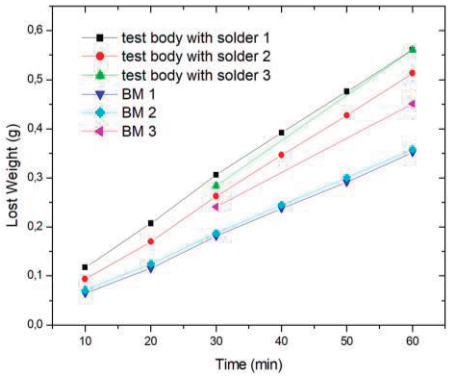

Figure 1 Loss weight in function of time testing

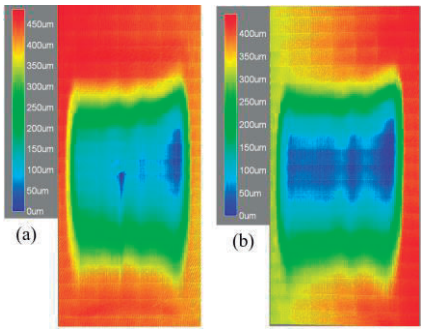

Figure 2 wear surface (a) with solder and (b) BM

The welded specimens showed a higher wear rate than the non-welded specimens, as shown in Table 1.

Table 1 Wear rate

	Wear rate(g/min)	Standard deviation
With solder	8,67E-3	0,11E-3
BM	5,765E-3	0,07E-3

4. Conclusion

The FeMnCr coating did not show defects such as cracks and porosity, but it showed a lower wear resistance compared to the base metal of ASTM 128 Grade C steel.

5. References

[1] Minatto, R.M., Costa, A.F., et. al., A. *Estudo coomparativo da resistencia ao desgaste abrasivo de baixa tensão de três ligas metálicas aplicadas em revestimento duro sobre aço manganês hadfield. Braz J. Develop.*, 2020 *6*(11), p. 84267–84278.

Identification of the Wear Mechanisms in the Homogenizer Plunger in Tomato Processing Industry.

Rodrigues, T.M.P.[1)], Ferreira Filho, D.[1)] and Costa, H.L.[2)]

1) School of Electrical, Mechanical and Computer Engineering, Universidade Federal de Goiás, Goiânia-GO ,74690900, Brazil
[2)] School of Engineering, Universidade Federal do Rio Grande, Rio Grande-RS, 96203900, Brazil
*Corresponding author: thales_rodrigues@discente.ufg.br;

1. Introduction

In the case of industrial tomato processing, stops for corrective maintenance caused by wear of the homogenizer plunger used to compact tomato paste is very common. The system operates by compression, so the wear of the plunger forms a depression that makes the mechanism inefficient. This issue could be mitigated by using wear-resistant coatings. However, to evaluate alternative materials, it is first essential to identify the wear mechanisms in the field. This knowledge is fundamental to both guide the choice of possible wear-resistant coatings and to choose tribological conditions to test candidate coatings. The objective of this work is to identify the wear mechanisms that occur in a homogenizer in an industry of tomato processing.

2. Methodology

With the use of a band saw, samples were taken from the worn region of a plunger made of 316L stainless steel. The specimens were ultrasonically cleaned, first in soap water, then in isopropylic alcohol and dried. Different regions of the worn surface were analysed by optical microscopy, scanning electron microscopy (SEM), energy dispersive X-ray spectroscopy (EDS), and confocal microscopy (topographic evaluation).

3. Results

Figure 1 shows secondary electron (SE, right) and backscattered electron (BSE, left) images of three different regions of the worn plunger. In the first region (a) intense grooving abrasion was observed (blue arrows), as well as some areas with large material detachment (dotted red ellipse), probably caused by adhesion, possibly combined with chemical dissolution (tribocorrosion). The BSE image in (b) shows many small dark regions distributed over the surface, indicating that they are rich in elements with small atomic number (green arrows). In the second region (c) grooving abrasion was substantially reduced and larger areas of adhesion and/or tribocorrosion were observed, combined with surface deformation and delamination (yellow arrows). The BSE images (d) showed much less of the small dark phases. In the third region (e), mainly intense plastic deformation and delamination were observed (parallel yellow arrows). The BSE images (f) showed a distribution of larger and trapezoidal-like dark regions (purple arrows). EDS maps were taken in magnified areas of Region 1 (g) and Region 3(h). They clearly show SiO_2 particles in Region 1, probably responsible for grooving abrasion, and SiC particles in Region 3, deeply embedded in the surfaces, causing intense surface plastic deformation rather than grooving.

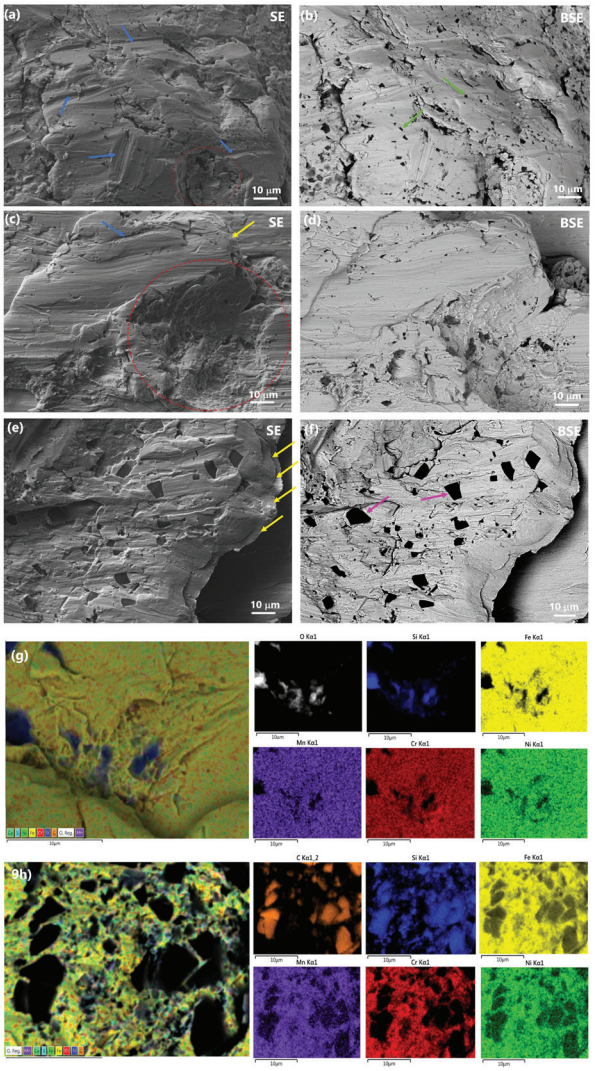

Figure 1 (a to f) SEM images of the worn plunger; (a and b): Region 1; (c and d): Region 2: (e and f) Region 3. (g-h) EDS maps of magnified areas in (g) Region 1, and (h) Region 3.

4. Conclusions

The main mechanisms found in a worn plunger used in tomato processing were abrasion, adhesion, probably tribocorrosion and delamination. Silica and SiC particles, probably coming from the tomato, play a role in this wear.

Analysis of homogeneity of the white etching layer in a deformed pearlitic steel

Pulgarin, A.*, Pereira, J. I., Souza, R.M.

Department of Mechanical Engineering, Escola Politécnica, Universidade de Sao Paulo, Av. Prof. Mello Moraes 2231, 05508-030, São Paulo, SP, Brazil
*Corresponding author: apulgarinc@usp.br

1. Introduction

Railway transportation relies on traction and braking forces between wheels and rails, which results in friction, wear, and wheel-rail contact fatigue. One common type of feature is Martensite White Etching Layers (WELs) on rail treads [1].

WELs have high hardness and wear resistance, but low ductility and deviations from matrix properties are a potential cause for cracks. These cracks may lead to spalling fatigue and potential wheel-rail failure. The formation mechanism, microstructure, and performance of WELs have been studied, but certain properties remain unclear.

This study aims to analyze the homogeneity of the WELs, based on analyses of microstructure and hardness.

2. Materials and methods

The analysis was carried out on a rail with a nominal hardness of 370HB. The rail was subjected to severe plastic deformation by heavy haul regular operation.

The samples were taken from a rail section that experienced severe deformation, resulting in a thick (> 0.5 mm) WEL and various types of defects. This condition was analyzed before [2], but the heterogeneity of the WEL was not explored. Figure 1 shows the top of rail (Region of interest), highlighting a spalling.

Figure 1 Top of rail showing a spalling.

A cross-sectional sample perpendicular to the direction of the train's motion was prepared, followed by characterization employing Scanning Electron Microscopy (SEM) and nanoindentation techniques.

3. Results and Discussions

Figure 2 presents the microstructure of the WEL at different depths from the rail surface: In Figure 2a, it is possible to observe martensite formation, while Figure 2b indicates the co-existence of martensite and divorced pearlite [3].

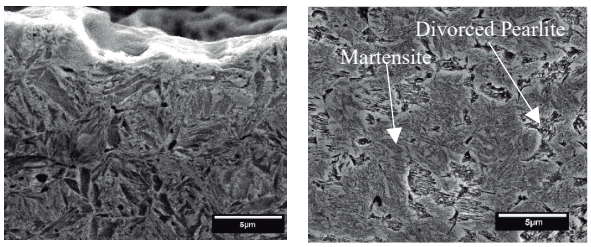

a) 0 to 15um b) 700 to 715 um

Figure 2 SEM micrograph on cross-section of the microstructure at different distances from the surface

Figure 3 illustrates the variation of nanoindentation hardness in the WEL as a function of depth from the rail surface. A decrease in hardness is evident as the depth increases, indicating a lack of homogeneity in hardness, even inside the WEL. The observed WEL in this study exhibits a notably broader thickness compared to findings from other studies, in which WEL was thinner (15-30 um) and treated as homogeneous [4].

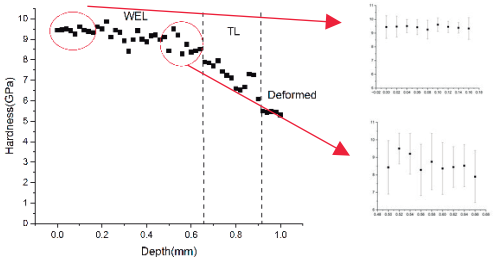

Figure 3 Hardness distribution of the WEL, TL and deformed zone

The discrepancies observed between the current research findings and the literature can be accredited to variations in the size and uncontrolled nature of the diffusion process occurring within the WEL. This study has identified similarities in hardness values between the literature and the current investigation, particularly for depths closer to the surface. However, the observed disparities in WEL size can lead to a higher occurrence of Pearlitic islands, revealing a non-homogeneous microstructure.

4. References

[1] Baumann, G., Fecht, H. J., & Liebelt, S. *Formation of white-etching layers on rail treads*. *Wear*, 1996.
[2] Pereira, J. I., Tressia, G., Kina, E. J., Sinatora, A., Souza, R. M. *Analysis of subsurface layer formation on a pearlitic rail under heavy haul conditions: Spalling characterization,* 2021.
[3] Pandit, A. S., & Bhadeshia, H. K. D. H. *Divorced pearlite in steels*, 2012.
[4] Pan, R., Ren, R., Chen, C., & Zhao, X. *The microstructure analysis of white etching layer on treads of rails*, 2017.

EFFECT OF ABRASIVE GRANULOMETRY ON THE WEAR OF ELECTRICAL SUBMERSIBLE PUMPS

Sábia, M. G.[1)], Rodrigues, F. B.[1)], da Silva, L. R. R.[1)], Ribeiro, M. P.[2)], Franco, S. D.[1)]
[1)] Department of Mechanical Engineering, Universidade Federal de Uberlandia, Uberlandia, 38400 901, Brazil
[2)] Petróleo Brasileiro S.A. (PETROBRAS), R Carlos Seidl, 188, Caju, Rio de Janeiro, RJ 20931-003, Brazil
*Corresponding author: leorrs@ufu.br

1. Introduction

Brazil is a major player in the oil industry and is researching new technologies and exploration methods [1]. Electrical submersible pumps (ESP) are commonly used when the natural flow is insufficient [2]. The impact of abrasive particle size on the wear of ESP pumps is not well-documented. A study was conducted using similar pumps and different abrasive types to investigate the relationship between abrasive particle size and pump component wear mechanisms.

2. Methodology

The study conducted by the Laboratory of Friction and Wear Technology at the Federal University of Uberlândia and compared the wear of ESP components when using fine sand (nº 100) and extra fine sand in a flow loop.

2.1. Abrasive characterization

Scanning Electron Microscopy (SEM) was used to analyze abrasive samples through particle measurements such as perimeter, aspect ratio, and circularity were made based on maximum and minimum diameters and particle area.

2.2. Pump wear measurements

The study tested the wear of ESP components with a water and sand mixture at a high concentration. The pumps were operated at 3600 rpm and 90 m³/day flow rate. Measurements of bearings' clearances and impellers and diffusers' masses were taken before and after the test to evaluate wear. Samples were taken from the diffuser, impeller, and inlet bearing sleeve for wear analysis.

3. Results

3.1. Abrasive geometry

Tests were conducted with Pump A using fine sand and Pump B using extra fine sand. 200 kg of sand was used in each test. The results are presented in Table 1.

Table 1: Particle characterization parameters for the sand.

	Parameters	New		Used	
		$\bar{x}$	σ	$\bar{x}$	σ
fine sand	Average diameter (μm)	225,27	4,62	230,39	18,04
	Aspect ratio	1,48	0,02	1,49	0,04
	Circularity	0,70	0,01	0,69	0,01
extrafine sand	Average diameter (μm)	70,31	6,70	106,96	8,76
	Aspect ratio	1,67	0,01	1,57	0,04
	Circularity	0,65	0,02	0,65	0,02

3.2. Pump wear

Figure 1 illustrates the wear surfaces of the inlet bearings of Pump A and Pump B after the wear test. The bearing of Pump A, which pumped sand with a greater granulometry, has a more irregular surface with preferential channels of greater depth formed by abrasion with bearing particles and sand grains, resulting in scratches and grooves on the surface. These preferred channels penetrate the bearing clearance and follow the abrasive wear.

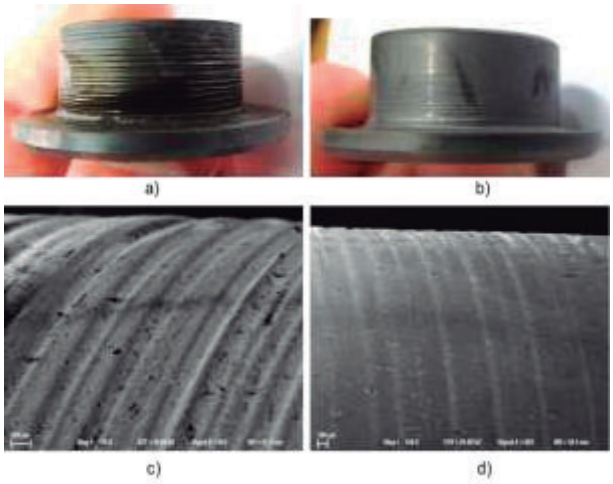

Figure 32: Inlet bearing sleeves at the end of the tests: a) Pump A bearing 1 sleeve; b) Bearing sleeve 1 of Pump B; c) Pump A sleeve surface, 100x magnification (SEM); d) Pump B sleeve surface, 100x magnification (SEM).

4. Conclusions

The study found that extra-fine sand caused more wear on bearings due to its ability to penetrate the gaps more easily. This could lead to pump failure before significant erosion occurs. Additionally, extra-fine sand resulted in smoother surfaces on bearing sleeves, while fine sand caused irregular surfaces and preferential channels for abrasive wear.

5. References

[1] Goldemberg J, Lucon O. Energy and environment in Brazil Foreword: renewable energy sources and sustainability. vol. 21. 2007.
[2] Kaplan LS. Power of submersible centrifugal pump operating on homogeneous liquid and water-petroleum mixtures. Mash Neft Oborud;(USSR) 1980;4.

Galling Resistance of a Cryogenically Treated L80 13Cr Stainless Steel for OCTG Premium Connections

Prieto, G.[1)2)*], Kafexhiu, F.[3)4)] ,Tuckart, W.R.[1)2)] and Podgornik, B.[3)]

[1)] IFISUR, CONICET-UNS, Bahía Blanca, CP8000, Argentina
[2)] Engineering Department, Universidad Nacional del Sur, Bahía Blanca, CP8000, Argentina
[3)] Institute of Metals and Technology, Ljubljana, PO1000, Slovenia
[4)] V-Research GmbH, Dornbirn, PO6850, Austria
[*]Corresponding author: german.prieto@uns.edu.ar

1. Introduction

The API L80 13Cr martensitic stainless steel is commonly utilized for premium Oil Country Tubular Goods (OCTG) connections, particularly in oil reservoirs where there are high concentrations of hydrogen sulfide and therefore there is risk of corrosion. Due to the need for tight seals, the joints require significant torque, which can result in severe adhesion and galling of the couplings.

In this study, we employed a cross-cylinder test rig to assess the resistance to adhesive wear of specimens under various heat treatments that involved cryogenic cooling of the material. Our findings indicate that the cryogenic treatments, which cause a reduction in the average size and volume fraction of carbides, had a significantly negative impact on the adhesive wear resistance of the API L80 13Cr martensitic stainless steel.

2. Materials and Methods

The chemical composition of the specimens, determined by a SPECTRO SPECTROMAXX optical emission spectrometer was (wt%): 0.17 C, 12.83 Cr, 0.76 Mn, 0.23 Ni, 0.55 Si, being in accordance with the API 5CT specification for OCTG steels [1].

The as-received material was machined to cylindrical rods of ϕ 10 mm and 100 mm in length and then heat treated, the different groups of materials are described in Table 1. The tempering stages of samples A and B followed the API 5CT specification, while those corresponding to samples C and D were selected to achieve high hardness and wear resistance [2].

Table 1 Description of the applied heat treatments

ID	Austenitizing	Cryogenic Cooling	Tempering	Hardness (HRC)
A	10 min @ 1030 °C	No	10 min @ 593 °C	33.2 ± 2.2
B	10 min @ 1030 °C	120 min @ -196 °C	10 min @ 593 °C	34.9 ± 1.6
C	10 min @ 1030 °C	No	10 min @ 410 °C	46.1 ± 0.4
D	10 min @ 1030 °C	120 min @ -196 °C	10 min @ 410 °C	45.9 ± 0.2

Galling resistance was determined using a load scanning test rig under progressive loading in dry conditions.

The test configuration involves two crossed cylinders (Ø 10 × 100 mm) which slide against each other under a constant speed of 0.01 m/s, a total distance of 85 mm. The normal force range for A and B specimens was 30 to 400 N, while for C and D specimens was 40 to 840 N. COF was continuously measured and the wear tracks were analyzed using optical and scanning electron microscopy.

3. Results and Discussion

As anticipated, specimens A and B, which were tempered at 593 °C, exhibited a greater propensity for galling due to their lower hardness when compared to specimens C and D (Fig. 1). More importantly is that cryogenic treatments had a considerably adverse effect on the tribological behavior of L80 13Cr. This phenomenon was linked to a decrease in the average size of carbides and a more refined distribution of carbides within the martensitic matrix, resulting in an increased likelihood of adhesion events between the sliding surfaces.

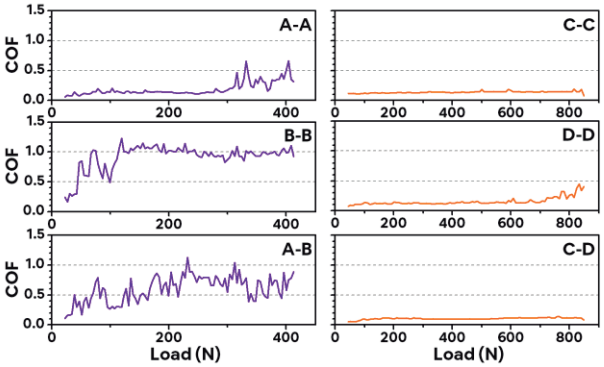

Figure 1 COF vs Normal Load for different tribopairs

4. References

[1] API 5CT Casing and Tubing Specification 10th Ed., American Petroleum Institute, 2018, Washington, USA.
[2] Prieto, G., Ipiña, J. P., & Tuckart, W. R. (2014). *Cryogenic treatments on AISI 420 stainless steel: Microstructure and mechanical properties*. Mat. Sci. Eng.: A, 605, 236-243.

The role of microstructure in the mechanical properties and wear resistance of a post-heat-treated white cast iron alloy.

Bueno, M.J.[1)*], Bortoleto, E.M[1)] and Miquelanti, E.[2)]

[1)] Vale Institute of Technology, Ouro Preto, Brazil
[2)] Vale S.A., Itabira, Brazil
[*]Corresponding author: bueno.mariojose@gmail.com

1. Introduction

The grinding media are inputs that represent a significant cost and have an impact on the entire iron ore production process. In some cases, the consumption of grinding media can account for up to 45% of the costs of comminution [1]. With that in mind, maximizing the lifespan of this material can lead to a significant reduction in the total operating cost. A difficulty in developing these materials is related to their operating conditions, as they are consumed in a mixed process that encompasses abrasive and fracturing processes [2]. Therefore, it is common to observe the simultaneous predominance of high-stress abrasion wear mechanisms, as well as the presence of impact/fracture zones resulting from the tumbling process of the load in the grinding mills. Consequently, the grinding media used in the comminution process must possess a microstructure that has high hardness but also good toughness. With that in mind, this study evaluated the wear resistance, under conditions similar to a ball mill, of a white cast iron alloy developed for use as grinding media, before and after undergoing a heat treatment (HT) process (870°C/4h). The results obtained show that the material's microstructure, before and after heat treatment, plays a crucial role in the material's performance in terms of wear resistance during the simulation of the comminution process.

2. Methods

The wear resistance of the developed white cast iron alloy (WCI-2) was compared to three commercial alloy grinding media, consisting of two steels (LAS-1 and LAS-2) and another white cast iron (WCI-1). For this purpose, a tribometer which was specifically designed to simulate the wear phenomenon that occurs inside ball mill was used. Additionally, the samples of the tested materials were also characterized using optical and scanning electron microscopy techniques. Finally, tests were conducted to evaluate the mechanical properties of the developed alloy, both before and after HT, such as hardness, Young's modulus, and fracture toughness, using the instrumented nanoindentation technique.

3. Results

In Figure 1, it is possible to observe a comparison between the microstructure of the developed alloy (WCI-2) (Figure 1a (as-cast state) and Figure 1b (HT)), with the mass loss found after testing in the tribometer for all analyzed materials (Figure 1c and Figure 1d). In the as-cast condition the microstructure is predominantly composed of a martensitic matrix (brown portion), as well as the presence of eutectic M7C3 type carbides, in white color. Additionally, the existence of pearlite (dark portion highlighted in red circles) can be observed. On the other hand, after the conducted HT, the presence of pearlite is no longer observed. It is suggested that the HT route used resulted in a more brittle alloy, as evidenced by the presence of radial cracks around the indentation after hardness testing (Figure 2), leading to a higher total mass loss after heat treatment (Figure 1d).

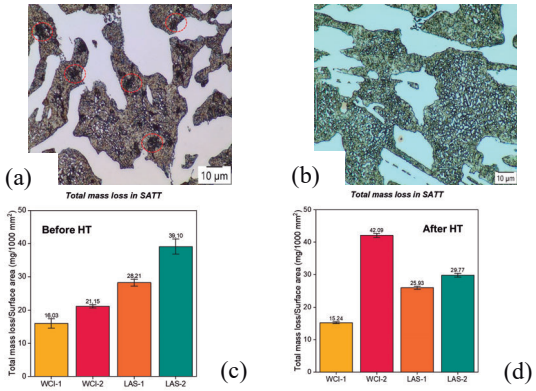

Figure 1 – Comparison of the microstructure of the WCI-2 alloy with the total mass loss after tribological test (a, c) before HT and (b, d) after HT.

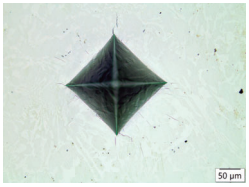

Figure 2 - Radial cracks around hardness test indentation.

4. References

[1]C. Aldrich, "Consumption of steel grinding media in mills – A review," *Miner. Eng.*, vol. 49, pp. 77–91, Aug. 2013, doi: 10.1016/J.MINENG.2013.04.023.

[2]Y. Ali, C. D. Garcia-Mendoza, and J. D. Gates, "Effects of 'impact' and abrasive particle size on the performance of white cast irons relative to low-alloy steels in laboratory ball mills," *Wear*, vol. 426–427, pp. 83–100, Apr. 2019, doi: 10.1016/J.WEAR.2019.01.048.

Thermal and Thermochemical Treatments in Co-30Cr Superalloy: Influence on Hardness and Surface Resistance

Azeredo, M.C.M. [1)*] and Franco Jr, A.R[1)]

[1)] Propemm, Instituto Federal do Espírito Santo – Campus Vitória
Vitória, 29040-780, Brazil
[*]Corresponding author: matheuscmazeredoo@hotmail.com

1. Introduction

This study aims to investigate the effects of thermal and thermochemical treatments on Co-30Cr superalloy, with the purpose of increasing the hardness and surface resistance of the material. Thermal treatments, including solubilization and recrystallization, aim to relieve stresses, improve structural homogeneity, and enhance the ductility of the alloy [1]. The thermochemical treatment of carbonitriding will be conducted to promote surface hardening, thereby increasing the hardness and abrasion resistance of the surface layer of the samples while maintaining the toughness of the core.

2. Materials and Methods

The Co-30Cr superalloy was melted in an induction furnace at 1600°C. After cooling, the obtained ingot was sectioned into discs with a thickness of 2 mm. Subsequently, a solubilization heat treatment was performed at 1200°C for 12 hours, as determined according to the CoCr binary phase diagram [2], aiming to relieve stresses and homogenize the alloy. The mechanical forming process called rolling was then applied to achieve the desired shape and reduce the thickness by 5%. The samples were subsequently recrystallized at 1200°C for 1 hour. Rapid quenching in water was carried out based on previous studies [3]. After these treatments, the superalloy underwent the thermochemical treatment of carbonitriding at different temperatures for a period of 4 hours.

The microabrasion test was performed using a stainless steel free sphere with a diameter of 25.4 mm and a hardness of 990 ± 40 HV, with a concentration of 97.6% Silicon Carbide; 0.60% SiO2; 0.80% Si; 0.20% Fe; 0.30% Al; and 0.50% C in distilled water at a concentration of 100 mg/cm³, with a dripping rate of approximately 30 drops per minute.

3. Results and Discussion

The results showed that the thermal treatments resulted in a more homogeneous microstructure and increased material ductility. The recrystallization process enabled the development of equiaxed grains, enhancing the malleability of the material. The rolling led to a slight alteration in the phase composition through mechanical shaping, at ambient temperature, of the heterogeneous structure comprising the α phases, characterized as metastable CFC, and ε with HC structure transitioning to CFC, thereby playing a role in the creation of the S layer during carbonitriding. Optical microscopy (OM) analysis revealed the presence of a modified layer on the surface of the carbonitrided samples. Scanning electron microscopy (SEM) confirmed the formation of a layer of carbonitrides, referred to as phase S, uniformly distributed and adhered to the surface, with morphology and thickness varying according to the carbonitriding temperature. According to the obtained results, an improvement in surface wear resistance was observed, as shown in the figure 1.

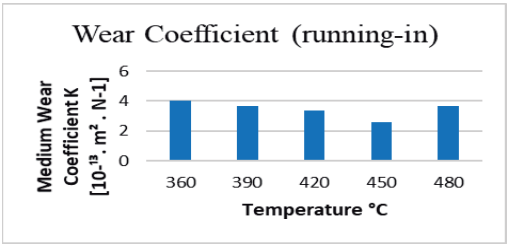

Figure 1: Abrasive wear

4. Conclusion

This study demonstrated that thermal and thermochemical treatments are effective in improving the mechanical properties of Co-30Cr superalloy. The solubilization and recrystallization heat treatment resulted in a more homogeneous microstructure and increased ductility. The thermochemical treatment of carbonitriding significantly increased the hardness and surface resistance without compromising the core toughness within the temperature range of 360 to 450ºC. However, at higher temperatures, a reduction in its resistance begins. Therefore, thermal and thermochemical treatments are ways to optimize the properties of Co-30Cr superalloy.

References

[1] Ribeiro, Kleber José Barros, *Plasma Nitriding with Cathodic Cage: Characterization and Performance Evaluation of Nitrided Layer in Cutting Knives,* 2007.

[2] Ishida, K.; Nisnizawa, T. *The Co-Cr (Cobalt-Chromium) System.* Alloy Phase Diagram, 1990.

[3] Giacchi, J. V.; Fornaro, O.; Palacio, H. *Microstructural evolution during solution treatment of Co-Cr-Mo-C biocompatible alloys*. Materials Characterization, Buenos Aires, v. 68, p. 49-57, 2012.

COMPARATIVE ANALYSIS OF THE WEAR RESISTANCE BY PURE SLIP AND ROLLING/SLIDING OF TWO SUPER PREMIUM HEAVY HAUL STEEL RAILS

Souza, S.S.[1] Pereira, H.B.[1], Tressia, G.[2], Centeno, D.M.A.[3], Alves, L.H.D.[4], e Goldenstein, H.[1]

[1] Department of Metallurgical and Materials Engineering, Universidade de São Paulo, São Paulo, 05508-030, Brazil
[2] Vale Institute of Technology, Ouro Preto, Brazil
[3] Metallurgical Processes Laboratory, Instituto de Pesquisas Tecnológicas, São Paulo, 05508-901, Brazil
[4] Federal University of Juiz de Fora, Minas Gerais, 36036-900, Brazil
*Corresponding author: hgoldens@usp.br

1. Introduction

The objective of this work was to compare in terms of pure sliding wear and rolling/sliding wear two Super Premium rails intended for heavy haul. The pure sliding mode is often found on small radius curves and external rails, whereas rolling/sliding is representative of the demand in straight paths (tangent).

Hardness is usually used as the main parameter in the tribological field and the wear rate can be frequently related to it in the form of the Archard equation [1]. However, other factors as the presence of inclusions or pro-eutectoid phases can affect the wear response as well [1].

So as to evaluate the possibility of replacing A rails for B rails, the present study was conducted. Pin-on-disc and disc/disc tribological experiments were used.

The chemical composition of the steels was analyzed by optical spectrometry and their bulk hardness was measured averaging 10 indentations, a load of 30kg and using the Vickers scale. The A rail composition is (wt%) 1.01%C, 0.52%Si, 0.70%Mn, 0.0199%P, 0.0088%S, 0.22%Cr and 0.0014%V. Its hardness is 433+-14 Hv30. The B rail composition is (wt%) 0.96%C; 0.59 %Si; 0.84 %Mn; 0.018 %P; 0,008 %S; 0.27 %Cr; 0.044 %V. Its hardness is 440+-17 Hv30.

The pin/disc tests were conducted in a PLINT TE67 machine. The parameters were: 100N of normal load, 1 hour, dry, without debris removal and 25mm of radial distance. The counter body was a AISI H-13 quenched and tempered steel (600+-10 Hv30). More details about the details of the test can be found in [2]. Nanohardness and MEV techniques were used to characterize the pins.

The disc/disc experiments parameters were: load of 160Kg, (1100MPa), 200.000 cycles, slip ratio of 1%, dry, without debris removal and at ambient temperature. More details about this test are explained in [3]. Microhardness, optical microscopy and MEV, were used to characterize the discs.

The results of the tribological experiments are presented in Figure 1. The A pins presented a slightly higher mass loss whereas their respective counter bodies presented smaller mass losses. Parameters as steel cleanness, colony size and prior austenite grain size can help to explain the differences seen in the wear rates [4]. They can affect the work hardening behavior of the steels [4]. Nanohardness measurements will be conducted to investigate this possibility.

On the other hand, the studied steels presented similar results in terms of mass loss in the disc/disc configuration. Other authors found similar results for pearlite microstructures with similar hardness values [5].

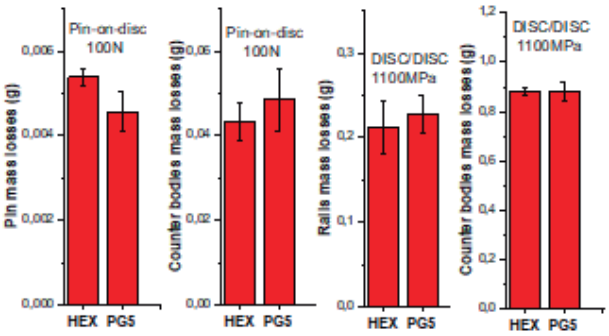

Figure 1 Tribological experiments results

2. References

[1] Lewis, R.; Olofsson, U. 2009. Wheel-rail interface handbook Edited by. Cambridge: Woodhead publishing limited, 2009.

[2] Tressia, G; Pereira, J.I; Penagos, J.J; Bortoleto, E & Sinatora, A. Effect of in-service work hardening on the sliding wear resistance of a heavy haul rail in the gauge corner. Wear. 482, 2021.

[3] Pereira, H. B; Alves, L.H.D; Rezende, A. B; Mei, P. R; Goldenstein, H. Influence of the microstructure on the rolling contact fatigue of rail steel: Spheroidized pearlite and fully pearlitic microstructure analysis. Wear. v.498-499.2022.

[4] Li, X.C; Ding, H.H; Wang, W.J; Guo, J; Liu, Q.Y & Zhou, Z.R. Investigation on the relationship between microstructure and wear characteristic of rail materials. Wear. v.163.2021.

[5] Kalousek, J; Fegredo, D.M; Laufer, E.E. 1985. The wear resistance and worn metallography of pearlite, bainite and tempered martensite rail steel microstructures of high hardness. Wear. v.105(3):199-222. 1985.

Dry Sand/Rubber Wheel tests for Abrasiveness analysis

Nins, B..D.[1),2)*], Münch, D.[2)] da Costa, A.R.[1)]

[1)] Department of Materials Engineering, Universidade Federal de Ouro preto, Ouro Preto, 35400 000, Brazil
[2)] Instituto Tecnológico Vale, Ouro Preto, MG, Brazil
[*]Corresponding author: barbaradiniznins@gmail.com

1. Introduction

The wear behavior is not intrinsic to the material but a combination of factors in the tribosystem [1]. Therefore, creating a tribosystem similar to the actual application of materials provides a reliable experimental better simulation.

The most commonly used abrasiveness measurement methods are the Miller test for slurry, the CERCHAR abrasiveness test, and the Bond test, which combines abrasion and impact conditions. However, a dry material tribosystem operating under pure abrasion is not covered by these tests.

The dry Sand/Rubber Wheel apparatus consists of a loose abrasive wear test that simulates pure abrasion [2]. In its origin [3] and in most of published studies, the test is used to study the wear of test pieces. However, it can also be applied to abrasiveness analysis [4]. This study aimed to compared the wear behavior of tested samples in laboratory conditions with the observed service-worn surfaces of a specific belt.

2. Experimental procedure

This work adapted the ASTM G65 test with rubber test pieces and iron ores as abrasive, as shown in Figure 1. The rubber test pieces were from a ST8000 commercial belt with 90 mm^3 maximum abrasion according to the ISO 4649 test. The selected iron ores are from Carajás Mineral Province, Brazil. As they are not standard abrasives, they require a series of preparation steps. They were dried, crushed, and classified into fine granulometry (between 0.15mm and 0.30mm) and coarse (between 0.30mm and 0.60mm). Procedure A of the ASTM G65 standard was selected: test time of 600s, a normal load of 130N, and wheel rotation speed of 200rpm. Finally, the surfaces worn in the Dry sand/Rubber wheel test were compared with the service-worn surfaces through SEM analysis.

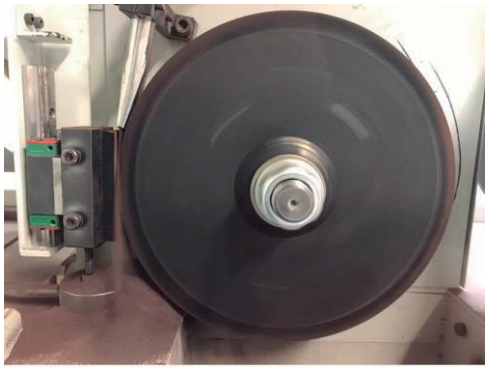

Figure 1 ASTM G65 adapted test with iron ores.

3. Results and discussion

Initial tests showed that the load of 130N was too high for that specific condition, generating macroscopic grooves in the rubber surface of the sample and the wheel. In order to minimize the formation of these grooves, procedure D of ASTM G65 proved to be more appropriate, which is a lighter load variation of procedure A using a normal load of 45N. These parameters ensured a uniform wear mark.

Figure 2 shows that the test piece worn in the laboratory presented a wear surface similar to that observed in the service-worn surface, predominantly characterized by Schallamach waves, indicating that the laboratory test promoted wear mechanisms similar to the real application of the material.

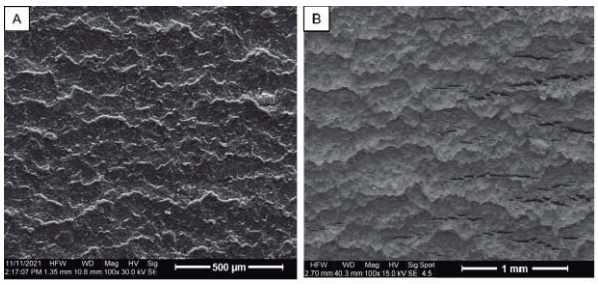

Figure 2 Rubber surface worn in A) the Dry sand/rubber wheel test and B) in service [4].

4. Conclusion

This study proved experimentally that the adapted ASTM G65 test can approach the wear mechanisms acting in tribosystems with loose abrasives and compare the response of samples tested with different abrasives (iron ores) allowing estimate their abrasiveness and compare to in service response of the belt.

5. References

[1] K. Zum Gahr, *Microstructure and wear of materials,* volume 10, Elsevier, **1987**.
[2] J. Gates, *Two-body and three-body abrasion: a critical discussion,* Wear 214 (1998) 139–146
[3] ASTM, *G65: Standard test method for measuring abrasion using the dry sand/rubber wheel apparatus,* American Society for Testing and Materials, **2010**.
[4] Nins, B., et. al. *Abrasiveness of iron ores: Analysis of service-worn conveyor belts and laboratory Dry Sand/Rubber Wheel tests. Wear*, ***2022***.

Study of the rotating arc on the tribological behavior of hardbanding for oil drilling tubes

Gramajo, J.[1)*], Gualco, A.[2)] and Svoboda, H.[3)]

[1)] Institute of Materials Science and Technology (ICyTM), Faculty of Engineering UNLZ, Buenos Aires Buenos Aires, Argentina
[2)] CONICET, Av. Godoy Cruz 2290, C.A.B.A., Argentina
[3)] GTSyCM3, INTECIN, Faculty of Engineering - UBA. Av. Las Heras 2214 (1427), CABA, Argentina
[*]Corresponding author: nahuel_jona@yahoo.com.ar

1. Introduction

Recently, alloys for weld deposits have been designed to achieve a smooth, crack-free surface with a low friction coefficient, creating a design that reaches a balance between casing-friendly performance and minimizing tool wear. This is achieved with a slag-free weld deposit in which a dispersion of niobium carbides and complex Cr-V phases precipitate finely distributed in a matrix of retained austenite and martensitic. High resistance to abrasion and erosion, even when combined with strong impact or pressure, is commonly expected in both open hole and pipe jacketing environments. The deposition using semi-automatic electric arc processes of these alloys produces a high dilution with the base metal which promotes a decrease in wear resistance. A modern and efficient method to reduce penetration is to produce the rotation of the wire, changing the dynamic forces on the drops in the metal transfer and uniformly distributing the arc [1]. These changes not only produce lower dilution, but also in the solidification and phase transformations, consequently affecting the wear resistance [2]. The aim of this work was to analyze the effect of rotating arc on microstructures and tribological properties.

2. Procedure and results

Eight coupons were welded, 4 without rotation and 4 at 500 rpm, in each case with welding speeds (WS) of 5, 9, 11 and 13 mm/s, using Metal Cored Arc Welding (MCAW) process under mixture of Ar-2%O_2 as shielding gas. The voltage was 28V and the current intensity was 250A. The microstructure was characterized on cross sections by scanning electron microscopy and Vickers microhardness profiles (HV2). Dilution percentage was measured, and the chemical composition was determined by optical emission spectrometry. Pin-on-disk wear tests were performed accordance with the ASTM G99. The reference material was tungsten carbide (disc) and the hardbanding samples were pins with a hemispherical contact surface. The rotation speed was 600 rpm and the applied load was 20 N.

The chemical composition of the dilution-free weld metal was 1.30%C, 1.06%Si, 1.18%Mn, 6.95%Cr, 4.3%Nb, 0.23%Ti and 0.68% V, Fe based. The samples welded without rotation showed a decrease in dilution with increasing WS. Regarding the samples welded with a rotating arc, the increase in WS produced an increase in dilution, as shown in figure 1a.

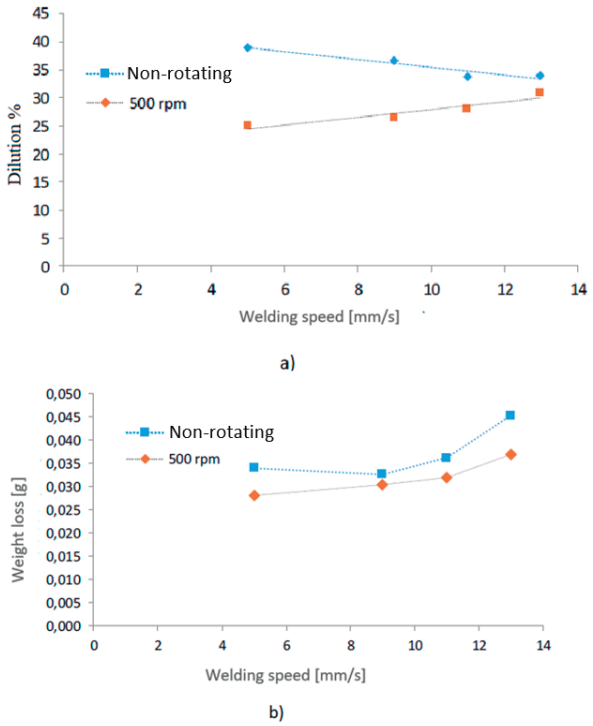

Figure 1a. Dilution. 1b. Weight loss vs welding speed

The dilution with rotating arc was lower than in non-rotating arc, for any WS.

The microstructure was formed by phases of primary polygonal Nb carbides, martensite and retained austenite, and Cr and V carbides, increasing the size and fraction of these hard phases with decreasing WS. The rotating arc (RA) produced an increase in the primary carbide precipitation. Chromium carbide solidified in segregated zones of dendritic growth. The RA produced a decrease in dilution, reaching higher hardness values and greater resistance to wear (figure 1b), with a slight increase in the friction coefficient from 0.84 to 0.9.

3. Reference

[1] FSilva RHG, Schwedersky MB, Santos AGM, Okuyama MP. Effects of the rotating arc techniqueon the GMA welding process. Soldagem & Inspeção 8259 2020.

[2] Coronado, J. J. (2011). Effect of (Fe,Cr)7C3 carbide orientation on abrasion wear resistance and fracture toughness. Wear, 270(3-4), 287–293.

The effect of test parameters on CERCHAR abrasiveness index of iron ores

Münch, D.[1)*], Bergami, L.B.[2)] and Bortoleto, E.M.[1)]

[1)] Instituto Tecnológico Vale, Ouro Preto, MG, Brazil
[2)] Department of Mechanical Engineering, University of São Paulo, SP, Brazil
[*]Corresponding author: daianemunch90@gmail.com

1. Introduction

The CERCHAR test is commonly used to assess the abrasiveness of rocks. The method consisted of a conic steel stylus, sharpened at 90°, scratching a rock surface at a distance of 10 mm under a load of 70 N [1,2]. The wear is obtained by measuring the flat diameter loss of the stylus, transformed into a CERCHAR Abrasiveness Index (CAI). This study aimed to compare two types of equipment and investigate the applied load and rock surface parameters using iron ores.

2. Materials and Methods

Samples of jaspilite, itabirite, hydrated iron ore, and compact hematite were tested using a martensitic steel stylus. The tests were performed on two equipment designs: the CERCHAR [3] and the Bruker Universal Macro-Tester (UMT-2) with DFH-10-G sensor model (without a damping system), both using a normal load of 50N and polished rock surfaces. The CERCHAR tester was also used with a normal load of 70N and a natural surface as the standards [1,2] recommended. A hypothesis testing was conducted with a significance level of 5%, and the null hypothesis stated that the abrasiveness was equal for the parameters compared.

3. Results

Figure 1(a) presents the CAI obtained from the two designs. The UMT-2 controlled the test parameters, but the applied load was unstable during the tests. For the CERCHAR tester, the applied load was ensured, but the speed was not controlled. Despite these limitations, the hypothesis tests indicated no significant difference in abrasiveness between the CAI values obtained using different types of equipment.

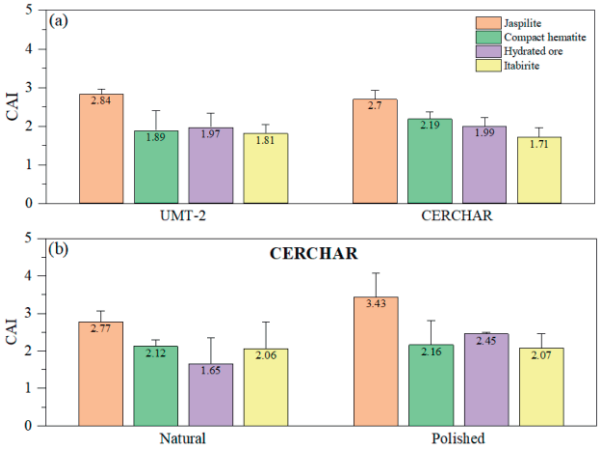

Figure 1 CAI results from (a) different equipment using 50N and (b) different rock surfaces using CERCHAR with 70N.

Increasing the applied load to 70N and specifically considering the design of CERCHAR equipment (Figure 1b), the results presented a higher average abrasiveness, except for the compact hematite sample. A natural rock surface did not increase CAI values compared to a polished surface.

4. Discussion

The lack of differentiation among the analyzed parameters was associated with the geometry loss method of quantifying abrasiveness. High standard deviations were obtained for all conditions. Surprisingly, the natural condition did not exhibit significantly higher abrasiveness. A natural surface generated wear adjacent to the stylus (Figure 2a) due to the sample's roughness and deformation of the stylus tip (Figure 2b). The loss of the stylus tip does not describe both phenomena. Although it is recommended to discard samples with burrs [3], there has been insufficient discussion about the measurement method of the worn stylus.

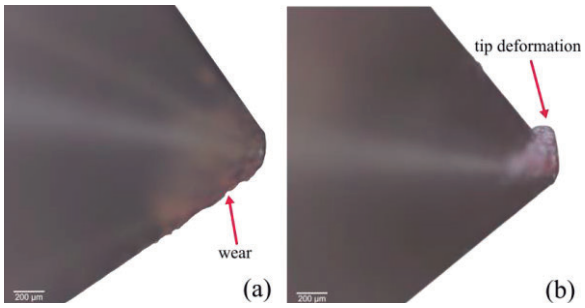

Figure 2 Steel tip wear tested with a natural surface for (a) hydrated iron-ore, and (b) itabirite.

5. Conclusions

Different CERCHAR test setups were applied with iron ores samples. Even with the equipment limitations, both provide similar values of CAI. Besides, a slight increase in abrasiveness occurred with the applied load, and the natural surface decreased the abrasiveness due to unequal wear of the stylus.

6. References

[1] ASTM D7625. *Standard Test Method for Laboratory Determination of Abrasiveness of Rock Using the CERCHAR Method.* ASTM Standards, 2010. 1–6.
[2] Alber, M.; Yarali, O.; Dahl, F.; et al. *ISRM suggested method for determining the abrasivity of rock by the cerchar abrasivity test*. Rock Mechanics & Rock Engineering, 2014. **47**:261–266.
[3] West, G. *Rock abrasiveness testing for tunnelling*. In. J. of Rock Mechanics and Mining Sciences, 1989. **26:**151–160.

The effects of heat treatment on the mechanical properties of 450 HB wear resistant steel

Murari, F.D.[1)*], Gusmão, A.M.R.[2)] and Turani, L.O.[3)]

1) *Research and Development General Management, Usiminas, Ipatinga, 35160 0900, Minas Gerais, Brazil,*
2) *Product Integrated Control Management, Usiminas, Ipatinga, Minas Gerais, Brazil*
3) *General Management of Customer Service and Quality Assurance, Usiminas, Belo Horizonte, Minas Gerais, Brazil*
*Corresponding author: fabio.murari@usiminas.com

1. Introduction

Wear resistant steel plates can be produced by means of direct quenching after hot rolling or off-line quenching process. In this case, after conventional or controlled hot rolling followed by air cooled to room temperature, the plate is reaustenitized in a heat treatment furnace and then water quenched. In both cases, the microstructure is mainly formed by martensite with some degree of tempering.

In these steels, the mechanical properties and abrasion wear resistance are strongly affected by the additional tempering of martensite, which occurs during the gas cutting and the application in some components that work at elevated temperatures in the mining and processing industries [1]. Depending on the microstructure changes that occur during the steel heating, the mechanical properties and abrasion wear resistance can be seriously compromised, reducing the length of life of a component, and increasing costs with its substitution or maintenance.

In this context, the effect of tempering temperature on the mechanical properties and three-body wear resistance of 450 HB abrasion martensitic steel produced by Usiminas steelworks (RAVUR450 steel) in the form of heavy plates via off-line quenching process was investigated.

2. Materials and Methods

The material used in this investigation was an industrial wear resistant steel heavy plate of 30 mm thickness, whose chemical composition is shown in Table 1.

Table 1. Chemical composition of the steel investigated (wt.%).

C	Si	Mn	P	S	Al	N
< 0,30	0,50 - 1,00	1,00 – 2,00	< 0,015	< 0,0012	0,01 – 0,05	< 0,0080

Samples of 300 x 300 x 25 mm were heated in a controlled atmosphere furnace to temperatures ranging from 100 to 600°C.

The wear resistance of the steel was evaluated by dry sand rubber wheel (DSRW) wear test according to ASTM G065 [2] and was correlated to the microstructure and mechanical properties.

3. Results and Discussion

The additional tempering of the as-delivered microstructure resulted in a smaller volume loss, that is, greater wear resistance, for the temperature range from 100 to 500°C, figure 1. Furthermore, the volume loss remaining practically constant in this region. As the tempering temperature increased to 600°C, the volume loss went up, approaching the as-delivered condition (DC). In addition to hardness, the ductility (TE) and toughness (E) of the material played an important role in its wear abrasive resistance by sliding contact at low stress. As shown in figure 1, the sudden drop in hardness from 400°C onwards was offset by the increase in ductility and toughness, which contributed to maintain wear resistance at a high level, comparable to the as-delivered condition.

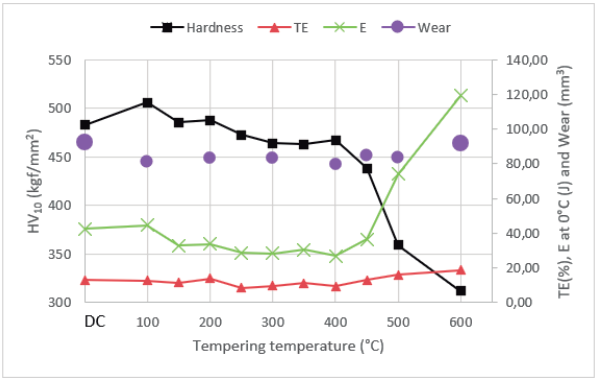

Figure 1. Influence of tempering temperature on the wear resistance and mechanical properties of the steel evaluated.

4. Conclusions

The results obtained indicate that for tempering temperatures of up to 400°C there are no remarkable changes in mechanical properties that can compromise the application of the steel evaluated. At higher temperatures, due to the microstructural changes related to tempering of martensite, there is a deterioration in mechanical strength, whereas toughness and ductility are improved. Concerning to sliding abrasive wear resistance, there is no compromise in performance for temperatures up to 600°C. The results also indicate that this property was significantly affected by absorbed energy and total elongation, in addition to hardness, as reported in literature.

5. References

[1] Gutman L. *Selection of high-temperature abrasion resistant steels for the mining and processing industry.* Materials Engineering, master's level. Lulea University of Technology. Department of Engineering Sciences and Mathematics. 2020. 39p.

[2] American Society for Testing and Materials, Philadelphia. ASTM G65-04; Standard Test Method for Measuring Abrasion Using the Dry Sand/Rubber Wheel Apparatus.

ABRASIVE WEAR RESISTANCE OF COMMERCIAL CERAMIC MATERIALS USED AS CHUTE LININGS

Mota de Souza, I.M. [1,2)*], Suarez, L.[1,2)] Chaves, R. [2)] Viáfara, C.C. [2)]. and Penagos J.J [2)].

[1)] Department of Mechanical Engineering, Universidade Federal de Ouro Preto, Ouro Preto, 35400-000, Brazil
[2)] Instituto Tecnológico Vale, Ouro Preto, MG, Brazil
[*]Corresponding author: isabella.souza@pq.itv.org

1. Introduction

Transfer chutes are of outmost importance in ensuring the continuous and efficient transfer of granulated materials from conveyor belts to different equipment within the mineral processing chain. The continuous exposure to diverse ore particles, variations in material flow, and the irregular sizes and shapes of the ore particles result in premature wear of the chute lining plates. Therefore, significant operation and maintenance costs are incurred in the mining activities [1]. On the other hand, preliminary studies and practical experience show that ceramic materials present better tribological performance than other types of metallic linings when used in abrasion conditions due to ore sliding (non-impact conditions). Therefore, different ceramic materials were carefully characterized and classified in the present work.

2. Materials and methods

The microstructures of the seven materials studied were characterized using optical microscopy (OM), as shown in Figure 1. Three samples of each material were tested with the rubber wheel abrasion test (ASTM G65 method) following the B procedure [2], which involves severe wear conditions. The quantitative wear characterization was determined by measuring the gravimetric mass loss of the test specimens after the wear test. Hardness measurements were conducted using the standard Vickers hardness technique HV30kg.

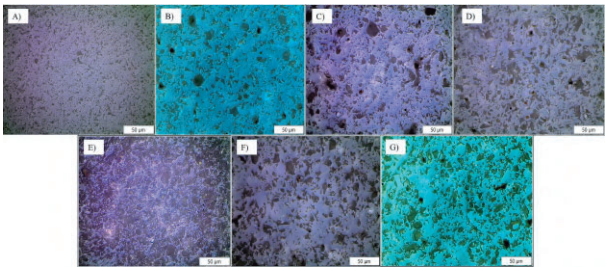

Figure 1. Optical microscopy of ceramic materials A-G.

3. Results and discussion

Typical microstructures of high-alumina materials are shown in Figure 1. The ceramic grains in each of these materials exhibit anisotropic shapes and a wide range of sizes, and a low grade of porosity visible at the grain boundaries. A material in Figure 1A shows a high refined microstructure and the lowest grade of porosity. The characterization of the phases present in each material will be studied in later stages of the project.

Figure 2 exhibits the mass losses and hardness of tested materials. A, B and C exhibited minimal wear, whereas F and G displayed poor tribological performance under severe wear conditions.

The material's response to a wear environment is influenced not only by its intrinsic properties but also by its response to a complex combination of stresses imposed by the tribosystem. In these specific conditions, there is a slight inverse proportionality between hardness and the level of abrasive wear experienced by these ceramic materials.

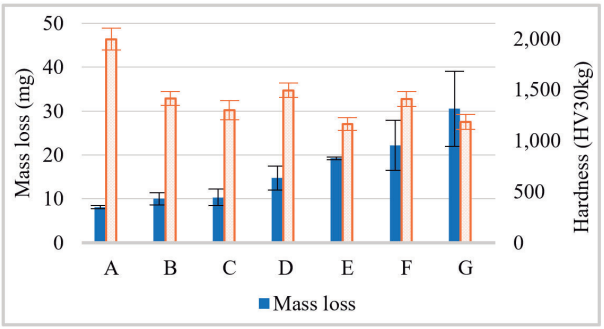

Figure 2. Mass losses after wear test and hardness values of each material.

The next stages of the project involve microstructural and mechanical characterization of the materials and, finally, comparison of the wear mechanisms observed in the laboratory and in field tests.

4. Conclusion

Under severe wear conditions, the A ceramic material (which exhibited the highest hardness and a refined microstructure), showed superior tribological performance compared to other ceramics. Therefore, it can be considered the most suitable option for field operating conditions.

5. References

[1] Penagos, J. Viáfara C. Chaves R. 2021. "Ensaio de desgaste de chapas de revestimento de chutes de transferência – Vitória. Produção técnica ITV-MI. Ouro Preto, Minas Gerais, Brasil, Fevereiro de 2021. DOI:10.29223/PROD.TEC.ITV.MI.2021.6.Penagos.

[2] ASTM G65-16, 2021. Standard test method for measuring abrasion using the dry sand/rubber wheel apparatus. DOI: 10.1520/G0065-16R21.

Influence of The Ball (Counter-Body) Material on Micro-Abrasion-Corrosion

M. A. N. Ardila[1)*], W.S. Labiapari[2)], H.L. Costa[1),3)], J.D.B. de Mello[1)]

[1)] College of Mechanical Engineering, Federal University of Uberlândia, Brazil
[2)] Aperam South America, Brazil
[3)] Federal University of Rio Grande, Brazil
[*]Corresponding author: miguelnpb@gmail.com

1. Introduction

In a previous study [1], we analyzed the influence of the ball material (polypropylene, polyacetal, polyamide, silicon nitride, and AISI 52100 steel) on pure micro-abrasion. The ball material influenced the friction coefficient and thus the ease of hard particles to enter the contact. Furthermore, the harder balls showed a few broad and deep grooves with micro-indentations between grooves, thus reducing wear when compared with the softer balls [2]. However, the effect of the ball material in micro-abrasion-corrosion tests is still unknown. Therefore, under the action of another variable (corrosion) interacting with micro-abrasion, this work aims to observe the influence of the counter-body nature on micro-abrasion-corrosion of stainless steel. The hypothesis we investigate in the present work is that passivation and removal of passivation layers are crucial in micro-abrasion -corrosion; the ball material might influence particle dynamics and thus the complex passivation/removal phenomena.

2. Methodology

For the objective of helping to understand the influence of counter-body material in the abrasion-corrosion, the tests were performed on a fixed-ball micro-abrasion-corrosion test rig described in previous work [3], as well as its optimizations and adaptations [1, 4, 5]. The test bench has a vat to create an electrochemical cell during testing. This test equipment has a BioLogic® SP150 potentiostat attached. Three different spherical counter-bodies were used (Ø25mm): one ceramic (Si_3N_4) and two thermoplastic polymers (polypropylene - PP and polyacetal – POM). AISI 304 austenitic stainless steel specimens (18Cr8Ni) were used as specimens. The average hardness of the specimens was 1.91 ± 0.05 GPa. The 2 cm^2 (0.8×2.5 cm) working area (exposed area) was delimited according to a methodology developed previously [3, 5], The micro-abrasion -corrosion tests were carried out using a slurry (SiO_2 abrasive particles (10%wt) in 1N H_2SO_4 solution in distilled water), pumped onto the austenitic stainless steel specimen at a rate of 1.7 ml min^{-1}. The specimen was partially submerged in 180 ml of 1N H_2SO_4 electrolytic solution in distilled water. The monitored normal load was between 0.85 and 1.02 N. The counter-bodies rotation speed was 150 rpm. Potentiodynamic polarization curves were made with a potential increase rate of 0.85 mV/s.

3. Results

The average values of wear coefficients (k) and friction coefficients on AISI 304 steel of five repetitions of micro -abrasion-corrosion tests, for the three different counter-bodies, were computed and are summarized in Figure 1. The results evidenced that the counter-body nature influences micro-abrasion-corrosion. This influence reflects on friction, particle dynamics, and wear rates during testing. Thus, the effects observed should be mainly related to the friction between the abrasives and the specimens and counter-bodies and the counter-body surface characteristics (hardness, topography). The results for the wear and friction coefficients showed that these were higher when using polymeric (softer) counter-bodies than when using ceramic (harder) counter-bodies. The potentiometric polarization results (Figure 2) showed that tests performed using ceramic counter-bodies resulted in lower current density and higher corrosion potentials (E_{corr}). The lower current densities show that the surface of the samples has more effective repassivation dynamics, keeping the lubricating film of F_2SO_4 more consistent and thus reducing the friction coefficient between the particles and the specimen surfaces (μ_{as}). This hypothesis can be confirmed by the appearance of the wear scars (Figure 3), which suggests a more difficult carryover of abrasive particles to the ceramic counter-bodies.

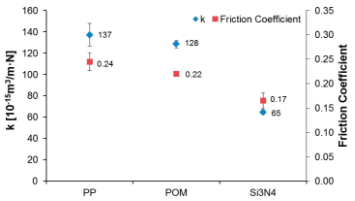

Figure 1 Friction and wear coefficients on AISI 304 specimen after micro-abrasion-corrosion tests with different counter-body types. The error bars represent the standard deviation (68,27% confidence level).

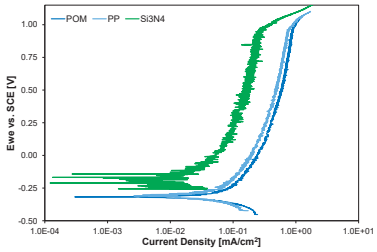

Figure 2 Characteristic polarization curves for micro-abrasion -corrosion tests on AISI 304 stainless steel with different counter-bodies.

Figure 3 SEM images in the centre of wear scar on AISI 304 samples after the micro-abrasion-corrosion tests with different counter-bodies : (a) PP; (b) POM; (c) Si3N4.

4. Conclusions

The wear coefficient, friction coefficient, and passive layer regeneration (current density) have a dependency: one is the cause of the other. The higher regeneration capacity of the passive layer leads to lower friction, which in turn leads to lower wear, leading to a greater regeneration capacity of the passive layer. The nature of the counter-body influences the dragging of abrasive particles at the interface. Polymeric counter-bodies have a greater ability to carry larger amounts of abrasive particles to the interface, promoting greater effectiveness in removing corrosion products, including the $FeSO_4$ film, when compared to ceramic counter-bodies, and thus leading to higher wear and friction coefficients.

5. References

[1] M.A.N. Ardila, H.L. Costa, J.D.B. de Mello, *Influence of the ball material on friction and wear in microabrasion tests*, Wear, 450-451 (2020).
[2] D.N. Allsopp, R.I. Trezona, I.M. Hutchings, *The effects of ball surface condition in the micro-scale abrasive wear test,* Tribology Letters, 5 (1998) 259-264.
[3] M.B. Santos, W.S. Labiapari, M.A.N. Ardila, W.M. da Silva, J.D.B. de Mello, *Abrasion–corrosion: New insights from force measurements*, Wear, 332-333 (2015).
[4] M.A.N. Ardila, H.L. Costa, J.D.B. de Mello, *Topographic evolution of balls used in microabrasion tests*, Wear, (2020).
[5] M.A.N. Ardila, W.S. Labiapari, H.L. Costa, J.D.B. de Mello, *Influence of stainless steel specimen topography on micro-abrasion and micro-abrasion-corrosion*, Wear, 426-427 (2019).

ABRASIVE WEAR RESISTANCE OF WEAR PLATE MATERIALS FOR CHUTE LININGS, WITH DIFFERENT TEST CONFIGURATIONS USING ASTM-G65 TEST TRIBOMETER

Suarez, L.[1,2)*], Mota de Souza, I.M. [1,2)] Chaves, R. [2)] Viáfara, C.C. [2)] and Penagos J.J. [2)]

[1)] Department of Mechanical Engineering, Universidade Federal de Ouro Preto, Ouro Preto, 35400-000, Brazil
[2)] Instituto Tecnológico Vale, Ouro Preto, MG, Brazil
*Corresponding author: luis.acevedo@pq.itv.org, luis.acevedosuarez7@gmail.com

1. Introduction

Transfer chutes play a crucial role in facilitating the continuous and efficient transfer of granulated materials between conveyor belts and various equipment in the mineral processing chain. However, due to the constant exposure to different types of ore particles, the flow of transported material, and the varying sizes and shapes of the ore, the chute lining plates experience premature wear, leading to substantial maintenance expenses for the industry [1]. To assess the abrasion resistance of the materials used in the field, wear tests were conducted following the ASTM-G65 standard, which simulates both mild and severe wear conditions.

2. Materials and methods

Table 1 presents the characteristics of the eight materials studied. Three samples of each material were subjected to rubber wheel abrasion test (ASTM G65 method) [2], following D (Test 1) and B (Test 2) procedures.

Table 1. Specification and hardness of studied materials.

Code	Specification	Hardness [HV30kg]
FFB1	ASTM A 532 class III A	820 ± 11
FFB2	ASTM A 532 class II D	824 ± 13
FFB-Ref	ASTM A 532 Class III A	830,7 ± 12
Rev1	Cr-based coating	913 ± 16
Rev2	Ni, V and Mo-based coating	865 ± 12
WC-Co	WC-Co in a nodular cast iron matrix (Composite)	1637,0 ±14 349 ± 23
CB92B	Ceramic (92% Alumina Al2O3)	1413.8 ± 67.8
Ref	AISI H13	478 ± 11

3. Results and discussion

The microstructures of the studied materials characterized by SEM (Scanning Electron Microscopy) are shown in Figure 1.

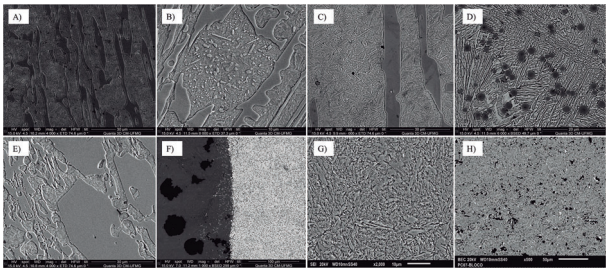

Figure 1. SEM micrographs of materials: A) FFB1, B) FFB2, C) FFB-Ref D) Rev2, E) Rev1. F) WC-Co G) Ref H). CB92B.

After tests 1 and 2, which represent mild and severe wear conditions, respectively, the WC-Co material showed the highest mass loss (between the tested materials) according to the results summarized in Figure 2. Due to the abrasive size, the WC-Co matrix (Hardness: 349 ± 23 HV nodular cast iron) exhibited greater wear compared to tungsten carbide (Hardness: 1637.0 ± 14).

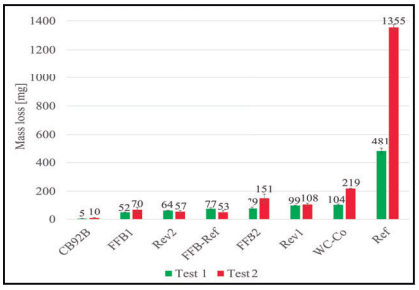

Figure 2. Mass loss of each material following Test 1 and Test 2.

The mass loss of Rev1 was higher than that of the other hard coating applied by welding (Rev2), making the latter material one of the best-performing materials in both tests, as shown in Figure 2.

The materials that exhibited minimal wear during test 1 (mild wear conditions) were CB92B, FFB2, and Rev2, as shown in Figure 2. However, the tribological performance of FFB2 decreased under more severe wear conditions during test 2, as illustrated in Figure 2.

4. Conclusion

Under mild wear conditions, the ranking of materials exhibited lower standard deviation values than the severe wear conditions. The ceramic material (CB92B) demonstrated superior performance in both abrasive wear conditions, representing the desired in-field operating behavior for chute plates.

5. References

[1] Penagos, J. Viáfara C. Chaves R. 2021. "Ensaio de desgaste de chapas de revestimento de chutes de transferência – Vitória. Produção técnica ITV-MI. Ouro Preto, Minas Gerais, Brasil, Fevereiro de 2021.

[2] ASTM G65-16, 2021. Standard test method for measuring abrasion using the dry sand/rubber wheel apparatus.

The removal coefficient (f_{ab})of high chromium white cast irons and tool steels.

Mello, V,S,[1)*], Strey, N.F [1)], Vieira, S.L, K [1)], Scandian, C[1)] and Alves, S, M.[2)]

[1)] Tribology, Corrosion and Materials Laboratory - TRICORRMAT, Department of Mechanical Engineering, Federal University of Espírito Santo - UFES, Vitória, 29075-910, Brazil
[2)] Science and Technology School, Universidade Federal do Rio Grande do Norte, Natal, 59075-000, Brazil
*Corresponding author: valdicleide.mello@ufes.br

1. Introduction

The manufacturing industry of injection-molded parts for automotive applications needs molds made of materials with high mechanical strength, resistance and they need to ensure high machinability and surface finishing capability.

The resistance that materials exhibit to processes involving material removal can provide insights for selecting tools and processes for manufacturing operations [1].

This work aims to provide insights into evaluating the removal coefficient (f_{ab}) through scratch tests in high chromium white cast irons and tool steels used for the manufacturing of injection molds.

2. Materials

Four high white chromium cast irons were studied, coded according to the chromium percentage and arrangement of carbides in the matrix. These alloys are 19E - 19 %wt Cr, eutectic, (56 ± 1,0) HRC, 19H - 19 % wt Cr, hypoeutectic, (60 ±0,9) HRC, 26E - 26 %wt Cr, eutectic, (55 ± 0,7) HRC and 26H - 26 % wt hypoeutectic,(55 ± 0,5) HRC, using the P20 steel as reference.

Scratch tests were conducted using a Universal Macro-Tribometer (Apex CETR-Bruker). The test was performed in the linear scratch configuration transversally to the chromiun carbide orientation, with a Rockwell-C diamond indenter with a 200 µm tip radius sliding against the surface under a constant loads of 40 N and 102 N and progressive applied normal load (from 2 N to 102 N) at a rate of 10 N/mm and a constant speed of 2 mm/min. The length of the scratches was 10 mm. To support the analysis and calculate the f_{ab}, a confocal profilometer (S neox- Sensofar) was used. The metalographic analysis of samples was performed by the Murakami etchant.

The f_{ab} was calculated by the L.A. Franco and A. Sinatora [2] method using the equation 1 outlined in figure 1.

$$f_{ab} = 1 - (A_p / A_v) \quad (1)$$

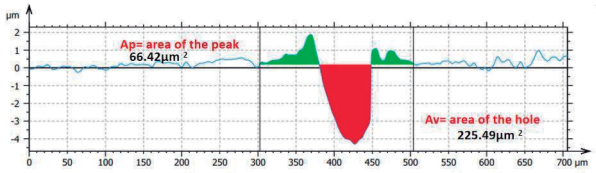

Figure 1: Schematic diagram of the area used for the calculation of f_{ab}.

The statistical analysis (ANOVA) was performed to assess the effect of the load and material on the f_{ab} value.

3. Results and discussions

The results indicated that the load did not have a significant influence on the fab values (at a 95% confidence interval). However, the material had a significant influence on the fab value. A linear relationship was found for sample 26E, where fab increases with increasing load, resulting in f_{ab} values that suggest an efficiency in the material removal process.

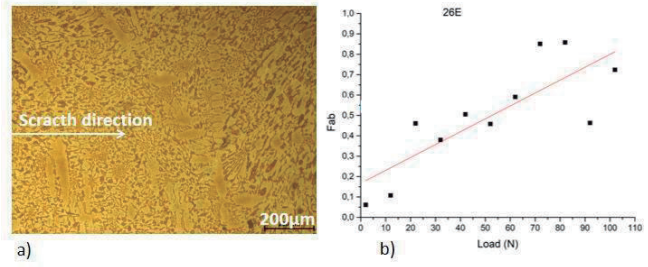

Figure 2: Data to sample 26E: a) surface topography and b)behavior of the f_{ab} for sample 26E during increasing load.

4. References

[1] K.H. Zum Gahr, D. Mewes. *Severity of material removal in abrasive wear of ductile metals*, in: K.C. Ludema (Ed.), Wear of Materials, ASME, N. York, 1983.

[2] L.A. Franco, A. Sinatora. *Material removal factor (f ab): A critical assessment of its role in theoretical and practical approaches to abrasive wear of ductile materials.* Wear, 2021, **382–383,** p. 51–61.

Microstructural and Wear Resistance Analysis of CoCr Alloy after Plasma Carbonitriding Using Cathodic Cage

Binda, R.M. [1)*] and Franco Jr, A.R[1)]

[1)] Propemm, Instituto Federal do Espírito Santo – Campus Vitória
Vitória, 29040-780, Brazil
[*]Corresponding author: rodolfombinda@gmail.com

1. Introduction

In conditions involving extreme temperatures and mechanical requirements, cobalt-chromium (Co-Cr) alloys are widely applied, mainly because they combine high corrosion resistance and good mechanical properties. Additionally, such alloys exhibit an easy weldability, formability, and manufacturing, as well as biocompatibility with the human body [1].

Studies have reported that carbonitriding conducted at low temperatures can improve the surface hardness and consequently the tribological performance of Fe-Cr-Ni alloys (austenitic stainless steels) without impairing corrosion resistance when the S phase is formed [2], [3].

2. Material and Procedures

Samples 3 cm long, 2 cm wide and 4 mm thick were cut from Co-30Cr ingot casted at 1600 °C, and subsequentially subjected to solubilization during 12 h at 1200 °C, defined from the CoCr binary diagram [4].

Subsequently, the samples were rolled imposing reduction degrees of 5%, as above it they present many cracks, recrystallized at 1200 °C and 1 h, and quenched in water considering previous studies [5]. Carbonitriding was performed using fixed parameters of 420 ^{0}C at 4.5 mbar and varying the treatment time by 1.5; 5; 8 and 11 hours.

Wear tests were performed using a CSM CALOWEAR "free ball" micro-abrasion apparatus with a 25.4 mm diameter AISI 52100 martensitic steel ball., with a hardness of 990 ± 40 HV. The rotation of the drive shaft, which causes the sphere to move, was set at 60 rpm, the applied load was 0.27 N. As abrasive, an slurry consisting of silicon carbide (SiC), with particles of size of about 5 µm at a concentration of 100 mg/ cm³ and with approximately 30 drops per minute.

Carbonitrided layers were observed using both light microscopy and scanning electron microscope (SEM/MEV).

3. Results and Discussion

Solubilization heat treatment was effective in reducing residual stresses and obtaining a more homogeneous microstructure. The recrystallization treatment carried out after rolling allowed the formation of equiaxed grains, improving the ductility of the material. However, the gain offered by lamination was low, as the microstructure of the material continued to show the same proportion of both phases, metastable CFC α phase and ε HC phase, which is responsible for the formation of the S layer during carbonitriding. Figure 1 shows that the presence of S layer improves the wear resistance of the material.

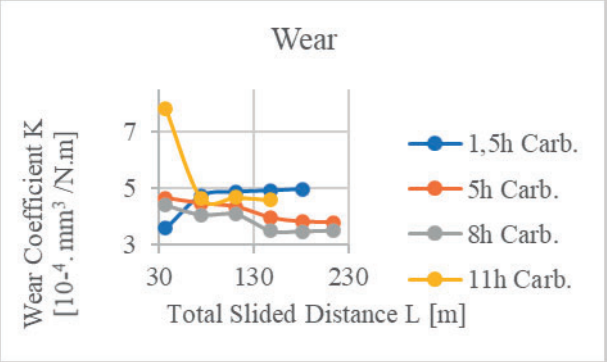

Figure 1: Abrasive wear of Co30Cr as a function of carbonitriding times.

4. Conclusion

Carbonitriding of Co30Cr alloys resulted in improvements in the wear resistance. Recrystallization conducted after solubilization and rolling provided microstructural homogeneity. However, rolling resulted in a small increase in the S layer thickness, after carbonitriding. Increasing the carbonitriding times until 9 h allows improvements in the wear resistance; however, the use of long treatments, as 11 h, promoted a lost in wear resistance. All treatments carried out were effective, however, carbonitring at 8 h offered the best wear resistance.

5. References

[1] Kilner, T.; Dempsey, A.J.; Pilliar, R.M. ET AL. *The effects of nitrogen additions to a cobalt-chromium surgical implant alloy.* J Mater Sci no. 22, 1987.

[2] Kane L.M; Chronaios D; Sierraalta M.; George F.M. *Marginal and internal adaptation of milled cobalt-chromium copings.* J Prosthet Dent, 2015.

[3] Li C.X.; Bell T. *Principles, mechanisms and aplications of active screen plasma nitriding, Heat Treatments of Metals*, (2003).

[4] Ishida, K.; Nisnizawa, T. *The Co-Cr (Cobalt-Chromium) System.* Alloy Phase Diagram, 1990.

[5] Giacchi, J. V.; Fornaro, O.; Palacio, H. *Microstructural evolution during solution treatment of Co-Cr-Mo-C biocompatible alloys*. Materials Characterization, Buenos Aires, v. 68, p. 49-57, 2012.

Correlation of field and laboratory wear results of commercial materials for transfer chute linings.

Penagos, J.J.[1)*], Viáfara, C.C.[1)], Silva, R.C.P.[1)], Suárez, L.A.[1)], Castanheira, M.[2)] and Machado, W.[2)]

[1)] Tribology Group, Vale Institute of Technology - Mining, Ouro Preto, 35400 000, Brazil.
[2)] Vale S.A.
[*]Corresponding author: jimmy.penagos@itv.org

1. Introduction

The wear of chute linings is a challenge in the mining industry due to the high costs associated with replacement materials, maintenance activities, and high safety risks.

Field wear tests offer a practical opportunity to assess various lining materials and measure their potential service lifespans. However, field tests are expensive, time-consuming, and have high results dispersion, among other difficulties. In this way, it is necessary to develop a laboratory test methodology that represents wear conditions in the field and thus be able to evaluate candidate materials to be used in chute linings. Such laboratory tests are quick and inexpensive to select the best chute lining materials.

In this work, the results of field and laboratory wear tests of commercial materials for chute linings are presented in order to establish a correlation between the field and laboratory tests.

2. Methodology

Field and laboratory wear tests were executed to evaluate the tribological behavior of commercial materials for transfer chute linings. Sample materials are listed in Table 1.

Table 1 Description and hardness of materials.

Sample name	Material description	Hardness [HV 30]
Reference	ASTM A 532 III A class	831 ± 12
WCI-1	ASTM A 532 III A class	820 ±11
WCI-2	ASTM A 532 II D class	824 ± 14
Weld-1	Weld Overlay	914 ± 17
Weld-2		866 ± 19
WC-Co	WC-Co dispersed in a ductile iron matrix	1637± 14
Cer. 1	Ceramic (Al_2O_3 and SiO_2)+ Rubber	1104 ± 41
Cer. 2		1166 ± 36
Cer. 3		1179 ± 14
Cer. 4	Ceramic (Al_2O_3 and SiO_2)	1188 ± 32

Field wear tests were executed at a transfer chute of an industrial plant of Vale S.A Company. Laboratory sliding abrasion tumbler and impeller-tumbler [1, 2] tests were also performed.

3. Results

The results of field and laboratory wear tests are shown in Figure 1. WC-Co and ceramic materials were the most wear-resistant materials in field wear tests.

As can be observed in Figure 1(c), samples of ceramics material were not tested in impeller-tumbler equipment, considering that impact contact is involved and ceramic samples fractured in preliminary tests. In this laboratory test, the WC-Co and white cast iron samples achieved the lowest volumetric losses. Then, in this case, the results did not correlate well with the field wear results. It could be explained by the impact contact condition characterizing this test configuration.

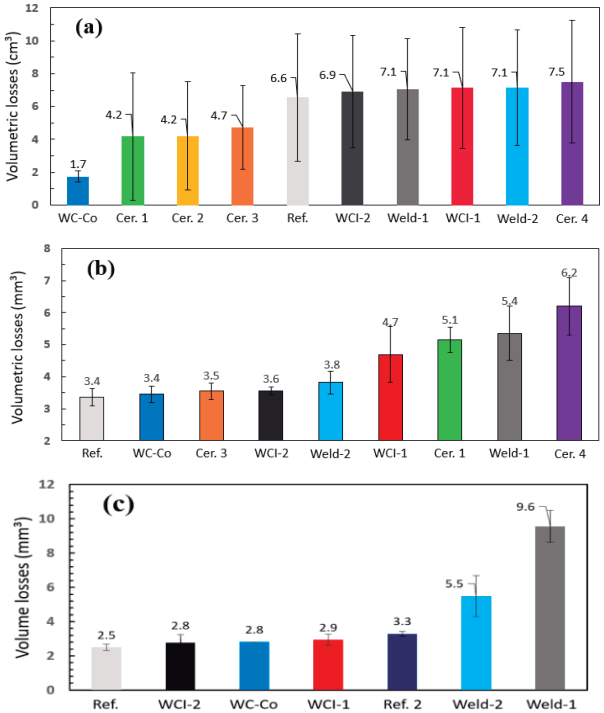

Figure 1 Field (a), sliding abrasion tumbler (b) and impeller-tumbler (c) tests results.

4. Conclusion

The field test shows high dispersion of the wear results due to the multiple variables. When comparing the types of materials (WCI, Weld, WC-Co and Cer), laboratory wear tests showed a good correlation with the field.

5. References

[1] Ratia, V., Valtonen, K., Kemppainen, A., and Kuokkala, V. T. *The role of edge-concentrated wear in impact-abrasion testing*. Tribology Online, v. **11**, n. 2, p. 410-416, 2016.

[2] Wilson, R. D., and Hawk, J. A. *Impeller wear impact-abrasive wear test*. Wear, 225, 1248-1257, 1999.

Abrasion Resistance of Work Hardening Layer of Hadfield Steel

Machado, P.C.[1]* and Sinatora, A.[2]

[1)] Institute of Technology, Federal University of Pará, Belém-PA, Brazil
[2)] Instituto Tecnologia Vale, Ouro Preto-MG, Brazil
*Corresponding author: paulomachado@ufpa.br

1. Introduction

The abrasive wear resistance of the Hadfield steel (austenitic manganese steel - 1.2 %C and 12 %Mn) is related to its metallurgical features, such as work hardening capability, crystallographic orientation, and depending on manganese concentration and stacking fault energy, phase transformation [1-4]. The work hardening layer reach 700 HV with work hardening [2-5] and it is related to nanocrystalline layer formation, twinning [4] and martensitic transformation [5]. Its main applications are coatings for ore crushers and railways frogs, in which have impact and abrasion conditions. The objective of this work is to evaluate the effects of Hadfield steel work hardening via linear scratch test.

2. Methodology

An ASTM A128 grade C Hadfield steel (12.4Mn–1.2C–1.5Cr (% wt), [6]) was used in the undeformed and deformed condition (field-deformed in jaw crusher). The scratches were carried out with the UMT-2 Bruker Tribometer with scratching in the direction of the edge of the Vickers indenter. The tests in the deformed material were performed along the cross-section surface in the direction from the core to the worn surface, one pass with length of 7 mm, constant load of 8 N and speed of 1 mm/s. The scanning electron microscope JEOL JSM-6010LA and the 3D optical interferometer Taylor-Hobson CCI MP were used to evaluate, respectively, the micrography and the scratches geometries to obtain the f_{ab}, from that the wear coefficient (k_{ab}) was calculated [7].

3. Results

The Figure 1 shows the scratch micrography highlighting a grain boundary transition, that reveals the effect of each grain on the wear (different pile-up configurations), and the scratch end (highest hardness). The highest f_{ab} values show in the Figure 2 are not in the most deformed region of the material. The highest f_{ab} value obtained was 0.19 at 4.5 mm from the start of scratch, that is, ~1.5 mm from the deformed surface in the field. Although the 6.5 mm position (~700 HV) has the lowest coefficient of wear resistance, the 2.5 mm (300 HV) position has the second lowest value, as indicated in the Figure 2. It is also noted that the data obtained for the non-deformed material has a significant f_{ab} variation. Machado et al. 2017 [4] evaluated the strain hardening layer of the Hadfield steel via microscratch test (i.e. nanoindenter equipment) and found that the hardness profile did not present significant effect on the abrasion resistance.

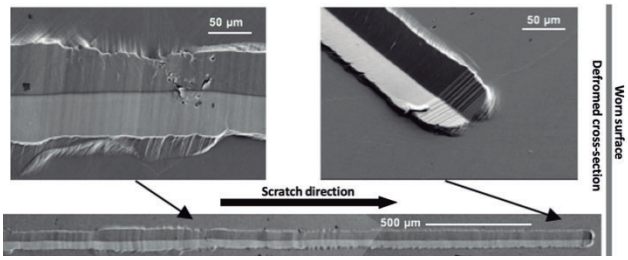

Figure 1. Micrographs (SEV-SE) of the scratch.

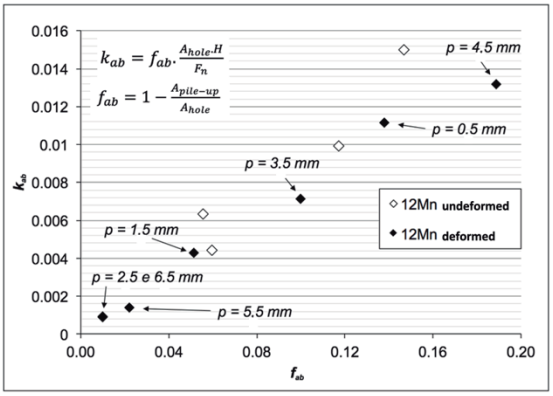

Figure 2. Coefficient of wear (k_{ab}) as a function of fab for field-deformed and undeformed Hadfield steel

4. Conclusions

The abrasion wear resistance of field-deformed Hadfield steel evaluated via scratch test shows no dependence of the work hardening layer. On the other hand, the results present the effect of the grain orientation on the wear.

5. References

[1] ADLER, P. H.; OLSON, G. B.; OWEN, W. S. Strain hardening of hadfield manganese steel. Metallurgical and Materials Transactions A, v. 17, n. 10, p. 1725–1737, 1986.
[2] LINDROOS, M.; et al. The deformation, strain hardening, and wear behavior of chromium-alloyed Hadfield steel in abrasive and impact conditions. Tribology Letters, v. 57, n. 3, p. 1–11, 2015.
[3] TRESSIA, GUSTAVO; SINATORA, AMILTON. Effect of the normal load on the sliding wear behavior of Hadfield steels. Wear, v. 520-521, p. 204657, 2023.
[4] MACHADO, P. C.; PEREIRA, J. I.; PENAGOS, J. J.; YONAMINE, T.; SINATORA, A. The effect of in-service work hardening and crystallographic orientation on the micro-scratch wear of Hadfield steel. Wear., v. 376-377, p. 1064-1073, 2017.
[5] AVERY, H. S. Austenitic Manganese Steel. American Brake Shoe, p. 834–842, 1949.
[6] ASTM G128, A128: standard Specification for Steel Castings, Austenitic Manganese, ASTM Int. 93, 2012.
[7] ZUM GAHR, K. Microstructure and wear of materials. Elsevier, 1st edition, p. 560, 1987.

Influence of austenitising temperature on micro-scale abrasive wear of Ni-modified ferritic stainless steel

Labiapari, W.S.[1)*], Teles, V.C.[2)], Pagani, V.[1)], de Alcântara, C.M.[1)], Ishizaki Neto, I.[1)], Fialho, R.L.[1)], da Silva Jr, W.M.[3)], de Mello, J.D.B.[3)]

[1)] Aperam South America, Timóteo, 35180-018, Brazil,
[2)] Department of Mechanical Engineering, Federal University of Ouro Preto, Ouro Preto, 35400-000, Brazil
[3)] College of Mechanical Engineering, Federal University of Uberlândia Uberlândia, 38400-902, Brazil
[*]Corresponding author: vinicius.teles@ufop.edu.br

1. Introduction

Applications of low alloy ferritic stainless steel in the biofuel industry reduced maintenance costs and improved final product quality due to its higher wear-corrosion resistance than structural carbon steel [1]. In this sense, having a higher mechanical resistance material while maintaining its corrosion resistance would be a crucial differential for this sector. This work aims to verify the effect of the austenitising temperature on the abrasive wear resistance of Ni-modified P410D ferritic stainless steel.

2. Experimental methods and materials

A UNS S41003 stainless steel with the addition of Ni was used in this work. The evaluated 'material's chemical composition was 11%wt Cr, 0.01%wt C and 0.3%wt Ni. They were initially subjected to annealing for 10 minutes at 800 ºC to homogenise the samples. Then, five different temperatures (850 ºC, 900 ºC, 950 ºC, 1000 ºC and 1050 ºC) were used to evaluate the effect of the austenitising temperature on quenching and wear resistance. The samples were named T0 to T5, respecting the austenitising temperature. The first two temperatures were inside the inter-critical area, between A_{c1} and A_{c3}, and the other three were within the gamma loop.

The micro-scale abrasion tests were conducted in a Plint TE66 device, consisting of a fixed ball rotating against the sample in an abrasive slurry. The normal load used was 2.0 N applied by dead weight. The abrasive slurry was composed of 5 µm silica particles suspended in distilled water, and the abrasive concentration used was 0.5 g/cm^3. The counter body was a 25.4 mm diameter zirconia ball.

A tensile test was carried out to evaluate the sample's mechanical properties.

3. Results and Discussion

The stress vs strain plots are shown in Fig. 1(a). Young's modulus remains unchanged by the quenching. However, the yield strength varies significantly with austenitising temperature; it increased to 950 ºC and remained almost the same for higher temperatures.

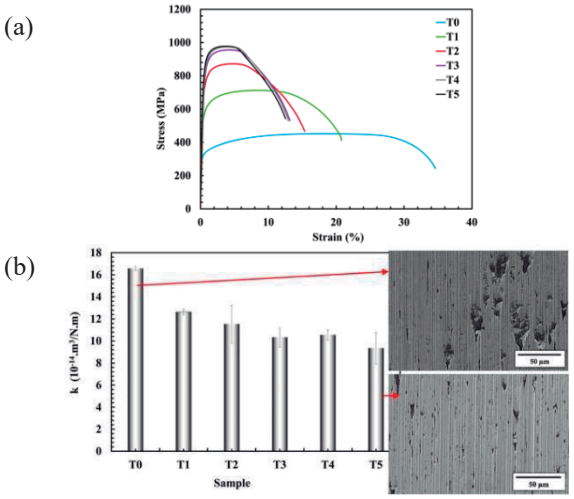

Figure 1 (a) Stress vs Strain curves and (b) Wear coefficient as a function of heat treatment.

The increase in abrasive wear resistance was 77% comparing the T0 the T5 samples, Fig.1(b). Higher tensile strength of steels can lead to higher abrasive resistance. However, due to ductility losses, evidenced using micro-scratch tests, the gain in abrasion resistance was not proportional to the increase in tensile strength, as it usually occurs with annealed materials. The wear mechanism was microploughing with craters between the scratches. The T5 sample presented smaller craters than T0.

4. Conclusions

The tests showed that increasing the tensile strength of Ni-modified ferritic stainless steel by austenitising followed by quenching is an efficient approach to increasing abrasion resistance. The austenitised at 1050 ºC sample presented a micro-abrasive wear rate 77% lower than the annealed material. The wear mechanism was predominantly micro-ploughing with craters between the scratches.

5. References

[1] Labiapari, W.S., Alcântara, C.M., Costa, H.L., de Mello, J.D.B.: *Stainless steel as an antiwear material for the bio-fuel industry*. Wear, 2013. **302**, 1536–1545.

Tribological Behavior of Composite Epoxy Coatings for Premium OCTG Threaded Connections

Prieto, G.[1)2)], Marini, C.B.[2)], Iriarte, M.V.[2)], Abdelnabe, J.P.[1)2)*], Tuckart, W.R.[1)2)]
[1)] IFISUR, CONICET-UNS, Bahía Blanca, CP8000, Argentina
[2)] Engineering Department, Universidad Nacional del Sur, Bahía Blanca, CP8000, Argentina
[*]Corresponding author: juan.abdelnabe@uns.edu.ar

1. Introduction

Premium Oil Country Tubular Goods (OCTG) connections are used in the exploration and production of oil and gas, particularly in applications where high-performance pipes are required to withstand the harsh environments and extreme pressures encountered during drilling and completion operations.

OCTG threaded connections are prone to suffering galling and seizure, often due to poor lubrication. This can lead to severe delays during production and large loss-profits.

In this work, novel formulations for composite epoxy coatings using MoS_2, Bi_2S_3, graphite and carbon nanotubes (CNTs) were tested on a ring-on-disc apparatus, using a standard testing protocol for OCTG connections.

It was found that the combination of these compounds presented up to 80% more wear resistance than the traditional ones, while maintaining a low and stable COF.

2. Materials and Methods

The composite epoxy coatings were produced using a high-performance epoxy resin (GekkoTool 4005) with the addition of MoS_2 (Climax Molybdenum Inc.), Bi_2S_3 (Tribotecc GmbH) and CNTs (Cheap Tubes Inc.). The resulting formulations were identified as follows:

Table 1 Composite Epoxy Formulations

ID	Solid Lubricants
A	5 wt% MoS_2 + 5wt% Graphite
B	5 wt% MoS_2 + 5wt% Bi_2S_3
C	5 wt% MoS_2 + 5wt% Bi_2S_3 + 0.1wt% CNT

The solid lubricants were added to the epoxy resin and stirred in a magnetic agitator for 1 h. Then, the hardener agent was added and the stirring continued for 10 min before applying the resin on top of the disc specimens. Thickness and hardness were measured in each coated specimen.

Both the disc and the ring specimens were machined using SAE 4140 steel. The discs have a diameter of 40 mm, while the rings have an outer diameter of 22 mm and an inner of 18 mm. The discs were polished using abrasive paper up to grit 400 and then sand-blasted using alumina.

Tests were performed in a pin-on-box tribometer, in which the coated disc specimen rotates at 10 RPM, while the ring specimen is pressed against it at a constant loading rate until reaching 37,700 N in 120 s (Fig. 1a), generating a contact pressure of 300 MPa. This load level is maintained until failure of the coating (Fig. 2), which occurs when the COF reaches 200% of its initial stable value.

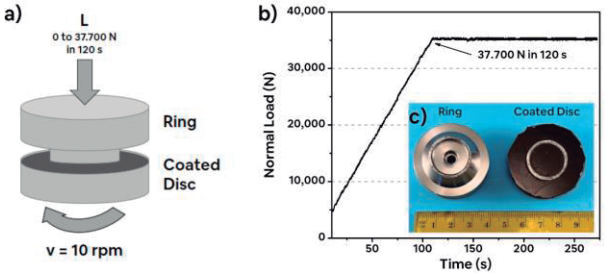

Figure 1 a) Ring-on-Disc setup, b) Load vs Time registry, c) Specimens after testing.

3. Results

All the tested compositions showed an initial running-in period, before achieving a stable region with COF values of 0.2-0.25. It was found that the formulations containing Bi_2S_3 and CNTs provided better surface protection, showing times-to-failure up to 80% higher than the A coating. This behavior was expected, as composite MoS_2/Bi_2S_3 tribolayers have increased durability [1, 2]. Also, it is known that the addition of CNTs increases the mechanical strength of epoxy resins, which contributes to the enhancement of the coating durability.

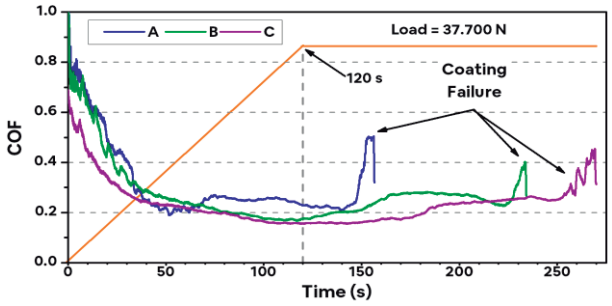

Figure 2 COF vs Time (s)

4. References

[1] Pilotti, B., Prieto, G., Juan, A., et al. (2021). *Bi_2S_3 and MoS_2 Soft Coatings: A Comparative Study of Their Frictional Behavior Under Different Humidity Levels, Normal Loads, and Sliding Speeds*. Trib. Lett. 69(3), 1–24.

[2] Prieto, G., Pilotti, B., Sobanski, G. et al. (2023). *Enhancing the Tribological Performance of MoS_2 Coatings in Humid Environments with the Addition of Bi_2S_3*. Trib. Lett. 71(1), 18.

PRODUCTION AND TRIBOLOGICAL CHARACTERIZATION OF BRONZE COMPOSITES REINFORCED WITH SILICA FROM RICE HUSK DEPOSITED BY THERMAL PLASMA SPRAY

Fonseca, M.G.[1)*], HL, Costa[1,2)].

[1)] Universidade Federal de Pelotas, Brazil
[2)] Graduate Program in Materials Science and Engineering
[*]Corresponding author: marcelofonseca@furg.br

1. Introduction

Thermal plasma spray has undergone great evolution, having wide applicability, It allows combining powders in order to produce versatile composite coatings. The use of sustainable resources such as silica, from the process of burning rice husks as agro-industrial waste has been a trend within science and research, with a focus on sustainability in the production of coatings (MOJTABA KHORRAM NIAKI, 2017). The use of silica nanoparticles could be an interesting alternative to reduce wear of parts and components, since materials containing Si seem to have very interesting tribological properties. (LI et al., 2021) used different types of tribological tests for Si_3N_4 ceramics with aqueous lubricant with silicon nanoparticles. The results showed the formation of a homogeneous surface film reducing wear and reaching dynamic balance. (STREY; RAMOS; SCANDIAN, 2022) also achieved superlubricity for certain combinations of load and sliding speed after a running-in period when testing 5 different tribopairs (Si_3N_4–Al_2O_3, Si_3N_4-ZTA, Si_3N_4–SiC, Al_2O_3–SiC, ZrO_2–SiC).

This work verifies the hypothesis of reinforcing bronze coatings with silica nanoparticles from rice husk burning and its effect on the dry and water-lubricated tribological properties of the coatings.

2. Methodology

In order to carry out this work, the infrastructure and manufacture of the components of a plasma thermal spray system were developed. The material used in the coatings was bronze (90% Cur, 10% Sn), bronze + 5%wt. rice husk ash and bronze + 20%wt. rice husk ash. The materials and coatings were characterized by SEM (EDS) and XRD. Reciprocating wear tests (dry and lubricated with water) were carried out, using a Tribometer model RTEC MFT -5000, under a normal load of 45 N, speed of 3,5 mm/s and acceleration of 1,53 mm/s.

3. Results and discussion

Figure 1 shows cross-sections of coatings with different silica contents, where it is seen that increasing the amount of silica reduces the deposition rate and therefore the thickness of the coating.

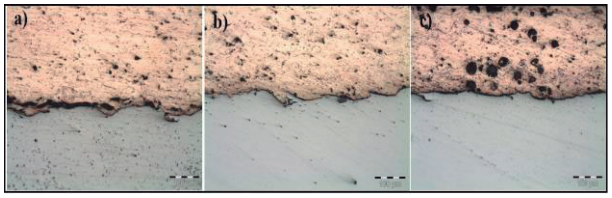

Figure 1 a) pure bronze coating b) bronze +5% rice husk ash and c) bronze with 20% rice husk ash.

Figure 2 shows the COF graph with trend lines for the six tests performed. In the black lines, the moving average and the trend line can be seen, showing a significant reduction in the coefficient over time. It is observed that what showed the best performance was the bronze +5% dry rice husk ash.

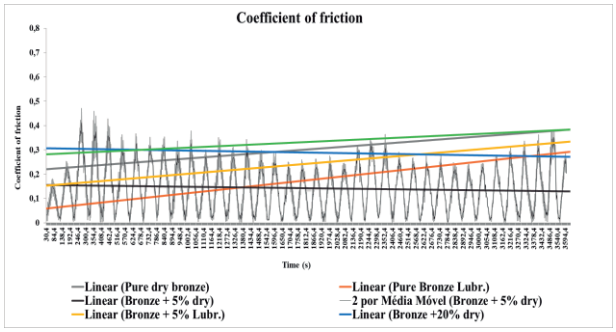

Figure 2 Results of wear tests

3. References

[1] LI, L. et al. Influence of silica nanoparticles on running-in performance of aqueous lubricated Si3N4 ceramics. **Tribology International**, v. 159, n. February, p. 106968, 2021.

[2] MOJTABA KHORRAM NIAKI, F. N. Impact of additive manufacturing on business competitiveness: a multiple case study. **Journal of Manufacturing Technology Management**, 2017.

[3] STREY, N. F.; RAMOS, R.; SCANDIAN, C. Superlubricity and running-in wear maps of water-lubricated dissimilar ceramics. **Wear**, v. 498–499, n. March, 2022.

Chromium- and cobalt-based oxide materials for elevated temperature applications

Castilho, B. C. N. M. de [1)*], Mayer, A. [2)], Madrigal, C.P. [1)], Nguyen N.T.[1)], C Moreau, C. [2)],Stoyanov, P. [1)]

[1)] Department of Chemical and Materials Engineering, Concordia University, Canada,
[2)] Department of Mechanical, Industrial and Aerospace Engineering, Concordia University, Canada;
[*]Corresponding author: bruno.noronhacastilho@concordia.ca

1. Introduction

The continuous development of gas turbine engine components relies on the discovery and improvement of high-performance materials that can endure harsh conditions throughout the flight, such as the high pressures and temperatures during its operation and its lifetime [1]. A significant number of parts inside the engine are exposed to severe tribological contacts, such as shown in Figure 1, to which the development of novel advanced materials is key to improve performance.

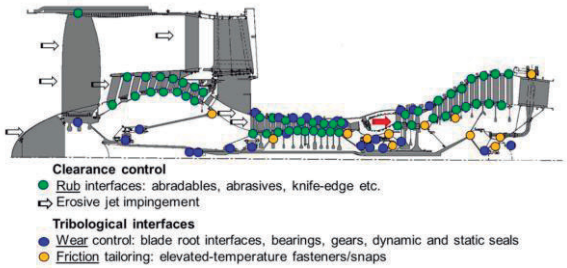

Figure 1 Cross-section of a gas turbine engine with key tribological contacts [1]

These materials should perform in demanding environments, thus holding the potential to address a wide spectrum of issues, such the enhancement of aircraft durability, prevention of premature component failures, and the advancement of innovative gas turbine engines. Current engines use different metals (mainly Ni-based and Co-based superalloys) which, when exposed to high temperature conditions, form glaze layers (lubricious oxide layers capable of reducing wear and friction) [2,3].

However, these layers are not instantly formed, and the surfaces of the metallic materials must go through significant wear before developing protective layers. One of the main challenges of tribology is finding ways of producing such layers or how to reduce the time for their formation. In this study, three different approaches for lubricating a surface with oxides and anticipating the formation of glaze layers are explored: applying loose submicron particles at the surface, dispersing the particles by spin coating and thermally spraying these particles by suspension plasma spray.

2. Materials and methods

The friction and wear behavior of Co-based and Cr-based oxide coatings was assessed using different means of adding oxides at the surface: In a first approach, sub-micron sized powder was applied on the surface of the pin of Inconel 718 and tested at elevated temperature. A second approach consisted of using a suspension containing the oxide powders and applying the powder at the surface of the same substrate with a spin coater. Lastly, suspension plasma spray (SPS) was used to produce a coating from the same powder feedstock. All samples were tested at 800°C with a POD 4.0 (Ducom, India) in reciprocating pin-on-disk conditions against a pin of Inconel 718 to determine the friction and wear behavior of the materials. The worn samples were analyzed by Raman and Scanning Electron Microscopy (SEM), and the wear rates were calculated by using a confocal microscope to determine the cross-sectional profiles of the wear tracks.

3. Preliminary results

Figure 2 shows the SEM images (left – Cr_2O_3, right – CoO) of the powder feedstock used for this study. The same feedstock was used to produce the suspension for the spin coater and for thermal spraying. Both powders show similar particle size distribution (D50~500nm), which removes any possible influence of the size of the particle in the comparison between both materials.

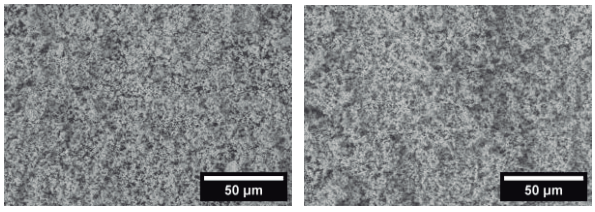

Figure 2 Backscattered electron microscopy of Cr_2O_3 (left) and CoO (right) powder feedstock

Preliminary results showed better friction and wear behavior for the CoO thermally sprayed coating when compared to the Cr_2O_3 coating.

4. References

[1] Stoyanov P., Harrington, K.M, Frye, A., *Insights into the Tribological Characteristic of Cu-Based Coatings Under Extreme Contact Conditions*, JOM, 2020. **72**: 2191–2197.
[2] Stott, F.H, Lin D.S., Wood G.C., *The structure and mechanism of formation of the 'glaze' oxide layers produced on nickel-based alloys during wear at high temperatures.* Corros. Sci., 1973. **13**: p. 449-454.
[3] Viat, A. et al., *Brittle to ductile transition of tribomaterial in relation to wear response at high temperatures.* Wear, 2017. **392-393**: p. 60-68.

Effect of the shielding gas and heat treatment on microstructure and sliding wear behavior of Inconel 625 coatings onto carbon steel

Kihara, E.A.[1)*], Costa, H.L.[2)], and Filho, D.F[1)]

[1)] Department of Mechanical Engineering, Universidade Federal de Goiás, Goiânia, 74045 155, Brazil
[2)] School of Engineering, Universidade Federal do Rio Grande, Rio Grande, Brazil
[*]Corresponding author: eliane_kihara@discente.ufg.br

1. Introduction

In coastal and offshore installations, deterioration of materials due to corrosion can reduce reliability. The surface properties of materials can be improved by applying protective coatings to prolong life in severe environments [1]. Among many possible coating methods, welding techniques are very versatile and produce metallic coatings with very high adhesion, but lead to dilution of the substrate into the coating. On one hand, gas metal arc welding (GMAW) is known for producing coatings with particularly high dilution and thus are less used to produce corrosion-resistant coatings, but on the other hand have high deposition rates, increasing productivity. The shielding gas in GMAW can affect dilution and microstructure. Post-deposition heat treatment can also tailor the microstructure of coatings. This work aims to evaluate the microstructure and wear behavior of Inconel 625 deposited by GMAW process onto carbon steel surface using different shielding atmospheres and post-deposition heat treatment.

2. Experimental Procedures

Coatings were deposited onto A36 carbon steel plate with two mixtures of shielding gases (Ar + 25%CO_2 and Ar +25%He). Samples were tested both as welded and after heat treatment (heating for 1 h at 1000 °C and air cooling). To evaluate the microstructure of the coatings, Vickers hardness tests (HV), scanning electron microscopy (SEM), energy dispersion spectrometer (EDS), and wavelength dispersion spectrometry (WDS) were employed. The tribological behaviour of the coatings was evaluated via reciprocating wear tests between a flat surface and a spherical counter in saline solution (10%wt. iodized NaCl). After the tests, the wear mechanisms were assessed via SEM and topographic analysis by confocal microscopy.

3. Results and discussion

The shielding gas had a strong effect on the microstructure of the coatings (Figure 1). When He was used in the mixture (c,d), intense cracking was observed in the interdendritic region. The coatings that used CO_2 showed better wear behavior, Figure 2. The microstructural examination, figure 1, revealed that Inconel 625 undergoes distinct microstructural changes according to the welding process. The higher sliding wear resistance of the samples using CO_2 was attributed to the high content of precipitates in its coating, while the lower resistance of the samples that used He was attributed to the microstructure formed by the coating process. The microstructure formed showed hot cracking in the dendritic and interdendritic regions that caused the weakening of the coated surface. The use of post-welding heat treatment did not affect the wear resistance of the coatings.

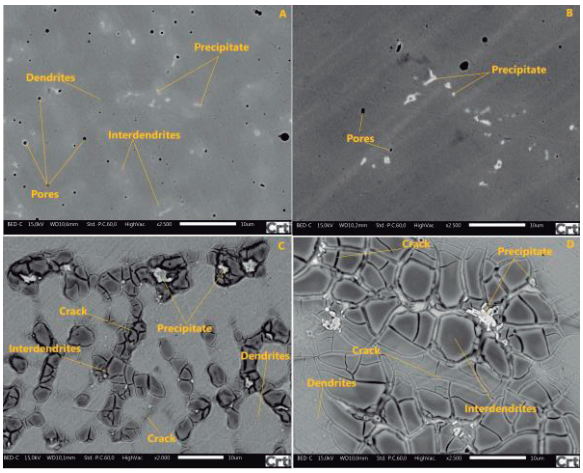

Figure 1 SEM (BSE) micrographs of the Inconel 625 coating deposited by GMAW on carbon steel under the conditions: (a) CO_2, (b) CO_2 after heat treatment, (c) He (d) He after heat treatment.

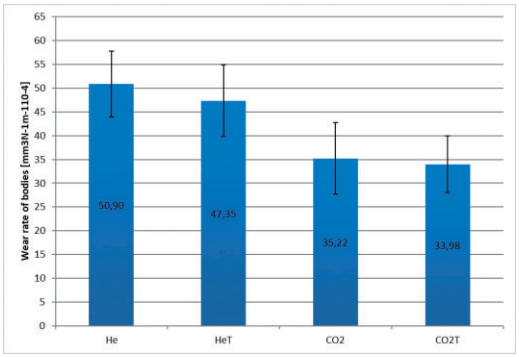

Figure 2 Wear rate of the specimens.

4. References

[1] Mohammadi Zahrani, E., Alfantazi, A.M., 2014. *High temperature corrosion ande-lectrochemical behavior of INCONEL 625 weld overlay* in $PbSO_4$–Pb_3O_4–$PbCl_2$–CdO– ZnO molten salt medium. Corros Sci. 85, 60– 76.

Microabrasion Resistance of Laser-cladded 316L/NbC Composite Coating

Duarte, G.D.M.[1)], de Carvalho, S.M.[2)], Scandian, C. [1)] and Strey, N.F.[1)*]

1) Tribology, Corrosion and Materials Laboratory – TRICORRMAT, Department of Mechanical Engineering, Federal University of Espírito Santo, Vitória, 29075-910, Brazil
2) Welding Laboratory, Department of Mechanical Engineering, Federal University of Espírito Santo, Vitória, 29075-910, Brazil
*Corresponding author: nathan.strey@ufes.br

1. Introduction

Among the coating processes, laser cladding stands out for its excellent process control, in addition to high precision and low heat input, consequence of the concentrated beam [1]. From the materials selection perspective, NbC particle reinforcements to metal-matrix composites show high potential for wear protection [2]. This study investigated the influence of laser power on the microabrasive wear resistance of laser-cladded 316L/NbC composite coating.

2. Materials and Methods

AISI 1020 was the substrate, while the coating was composed of NbC particles (50 %wt) in an AISI 316L matrix (50 %wt). Coatings were deposited as powders using a disk solid-state laser (TruDisk 6002, Thumpf inc.), coupled with a KUKA robotic arm (model KR 60HA). Parameters were: powder flow rate = 19.6 g/min; feeder disk rotation = 10 rad/s; focal distance = + 25 mm; beam diameter = 3.2 mm; scanning speed = 25 mm/s. Laser powers of 2400 W, 2600 W and 2800 W resulted in three different coating conditions, which were characterized by microhardness and metallography.

Wear tests were performed on coatings and bulk 316L in a PLINT TE66 micro-scale abrasion tester. Ball's rotation speed was 40 rpm, applied load was 0.3 N, under a Fe_2O_3 abrasive slurry (0.2 g/cm³, 90 % between 1-5 µm diameter particles). Three experiments were run for each material, in a random order. Wear craters were analyzed by confocal profilometry (Sensofar S neox).

3. Results and Discussions

Figures 1 to 4 show the microstructures, microhardness, wear and profilometry results, respectively. Microhardness of coatings are higher than the substrate, due to the second phase strengthening of the NbC. Wear rates of 316L/NbC coatings were 1.8-2.5 times lower than 316L, what shows the wear resistance potential of the first. Laser power, despite being the most influential parameter on the weld bead shape [1], has little effect on wear resistance of the coatings in the 2400 W to 2800 W range. Finally, confocal profilometry revealed the wear dominates in the 316L matrix, by a grooving mechanism.

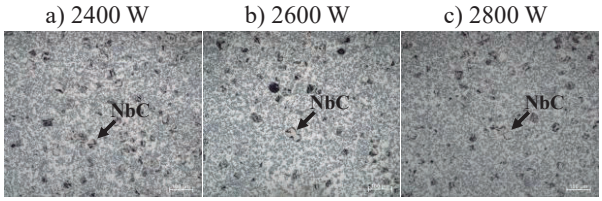

Figure 1 Microstructures of coatings: a) 2400W; b)2600W; c)2800W.

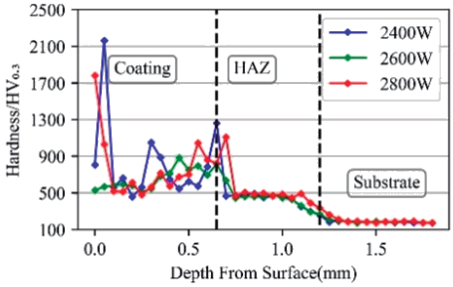

Figure 2 Microhardness profiles of coatings.

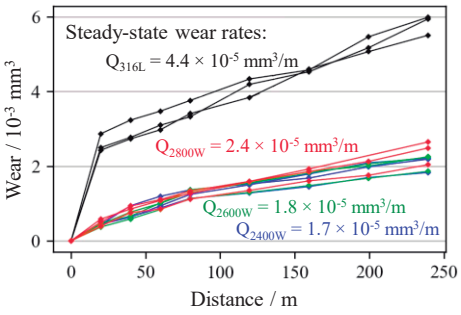

Figure 3 Wear evolution and wear rates during microabrasion tests.

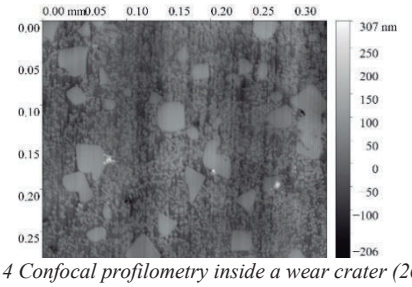

Figure 4 Confocal profilometry inside a wear crater (2600 W).

4. References

[1] GOODARZI, D. M.; PEKKARINEN, J.; SALMINEN, A. *Effect of process parameters in laser cladding on substrate melted areas and the substrate melted shape*. **Journal of Laser Applications**, v. 27, n. S2, p. S29201, 2015.

[2] WOYDT, M. et al. *Niobium carbide for wear protection–tailoring its properties by processing and stoichiometry*. **Metal Powder Report**, v. 71, n. 4, p. 265-272, 2016.

On the relationship between contact temperature and tribological behavior of wagon brake shoes

Camporez, R.M.[1)*], Furlan, A. A.[1)], Romero, M. C.[1)], De Souza, R. M.[2)], Strey, N.F. and Scandian, C.[1)]

[1)] Tribology, Corrosion and Materials Laboratory - TRICORRMAT, Department of Mechanical Engineering, Federal University of Espírito Santo, Vitória, 29075-910, Brazil
[2)] Surface Phenomena Laboratory - LFS, Department of Mechanical Engineering, Polytechnic School of the University of Sao Paulo, São Paulo, 05508-900, Brazil
[*]Corresponding author: rubsonmc@gmail.com

1. Introduction

Brake shoe is one of the most important components of railway vehicles braking systems. These components get in direct contact with the wheel to reduce the speed of the vehicle. During brake, friction heat is dissipated leading to materials thermal degradation and metallic film transfer, which results in performance loss and in potential risk of accidents. Organic composite brake shoes have been widely used in recent years due to its friction stability and low noise. However, they are a complex mixture, containing the resin matrix, fillers, mineral fibers, abrasives, and metallic particles [1]. Wear of brake shoes also have an important thermal contribution, which involves chemical reactions and friction on the surface. During braking, the kinetic energy is transformed into heat, which is portioned between the brake and the wheel, according to the heat partition factor. The heat is then transferred through conduction to the contact area or is dissipated through convection of the wheel. This work aims to calculate the brake shoe contact temperature and its tribological behavior [2].

2. Methods

2.1. Materials

Commercially available wagon brake shoes were used to manufacture the pins. Two different conditions were studied: end-of-life brake shoes with adhered metal film (BSM) and new brake shoes (BS). Discs were machined from Class D (AAR Standard - Association of American Railroads) railway wheels.

2.2. Tribological test

Dry sliding wear tests were carried out using a pin-on-disc configuration, Fig. 1a, in a PLINT TE67 tribometer. Sliding speed was 0.9 m/s and contact pressure of 0.8 MPa in order to reproduce service condition. Tests were done in two different conditions: continuous and intermittent. Duration of continuous tests was 30 min. Intermittent tests consisted of cycles of 3 min of slide and 3 min of stop (no pin-disc contact), representing 10 braking cycles. The BS temperature was monitored during the test using an infrared (IR) thermographic camera (OPTRIS PI – 450i).

2.3. Contact temperature

Based on Kennedy, Lu and Baker [2] work, $T_c = T_{amb} + \Delta T_{ss} + \Delta T_f$, where T_{amb} is the ambient temperature, ΔT_{ss} is the nominal temperature rise in steady state and ΔT_f is the flash temperature rise. T_c depends on friction, contact pressure, sliding speed, material properties and environment.

3. Results and discussion

BS and BSM continuous tests showed a mean steady-state friction coefficient of 0.63 ± 0.06 and 0.66 ± 0.10, respectively. The evolution of friction (Fig. 1b) can be attributed to the dependence of the organic phenolic resin matrix and rubber properties on temperature. This causes mobility of the polymeric chains, facilitating the removal of the fillers from the matrix and increasing the elastic deformation of the rubber and, consequently, increasing friction. However, if the temperature continues to increase, the rubber begins to thermally degrade and the phenolic resin matrix becomes inorganic and less sensitive to temperature, thus reducing the friction coefficient [3]. The specific wear rate (mm³/N·m) for the continuous and intermittent test of the BS was (19.0 ± 1.6) × 10^{-6} and (6.6 ± 2.3) × 10^{-6}, respectively, while for the BSM it was (26.7 ± 5.5) × 10^{-6} and (31.6 ± 6.6)×10^{-6}, respectively.

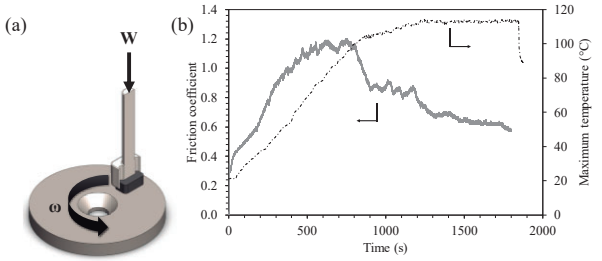

Figure 1 (a) Test configuration. (b) Friction and Temperature IR camera of BS test.

4. References

[1] Y. Lyu, E. Bergseth, M. Tu, U. Olofsson, *Effect of humidity on the tribological behaviour and airborne particle emissions of railway brake block materials.* Tribol Int. **118** (2018) 360–367.
[2] F.E. Kennedy, Y. Lu, I. Baker, *Contact temperatures and their influence on wear during pin-on-disk tribotesting*, Tribol Int. **82** (2015) 534–542.
[3] K.H. Cho, M.H. Cho, S.J. Kim, H. Jang, Tribological properties of potassium titanate in the brake friction material; morphological effects, Tribol Lett. 32 (2008) 59–66.

Characterization of tribolayers formed during sliding wear of railway wheels

Oliveira, D.N.[1)], Nogueira, J.B.[1)], Rosa Neto, C.A.[1)], Scandian, C.[1)] and Strey, N.F.[1)*]

[1)] Tribology, Corrosion and Materials Laboratory - TRICORRMAT, Department of Mechanical Engineering, Federal University of Espírito Santo - UFES, Vitória, 29075-910, Brazil
[*]Corresponding author: nathan.strey@ufes.br

1. Introduction

The contact between wheels and railway tracks is subjected to high levels of mechanical stress, which results in the degradation of these components during service, leading to a range of surface defects. In this context, it is important to understand and simulate these defects in laboratory tests [1].

Thus, the objective of this work is to compare the microstructure, microhardness and topography of the tribolayers present in railway wheel flange with those of laboratory samples worn in the pin-on-disk test.

2. Materials and Methods

Pins made from a high-strength AREMA TR68 rail, disks made from AAR Class C and AAR Class D wheels and an AAR Class D wheel with a worn flange were studied. The wheels were made of ferritic-pearlitic steel with 2 % pro-eutectoid ferrite. Sliding wear tests were carried out in a PLINT TE67 tribometer (Phoenix Tribology Ltd.), in a pin-on-disk configuration, without lubrication, at two temperatures (25 °C and 300 °C) and two different loads (300 N and 600 N).

The surface characterization of the tribolayers consisted of macrography, stereomicroscopy, qualitative and quantitative metallography, Vickers microhardness and confocal profilometry (Sensofar S neox).

3. Results and Discussion

The thickness of the tribolayer in the wheel is about 5 times greater that of the disks, but the roughness is smaller, as shown in Figures 1 and 2, respectively.

Figures 3 ratifies that the hardened thickness of the wheel's tribolayer is greater than that of the disks. This is due to the greater contact area of the wheels with the rails, resulting in greater depth of the contact stress field. Although the microhardness in the wheel presents magnitudes higher compared to the disks, the ratio between the maximum surface microhardness and the bulk hardness is similar, 1.2 for both cases, suggesting that there is similitude in the evolution of microstructure and strain hardening phenomena in both cases [2].

The results point that normal load and temperature in the pin-on-disk test did not affect the microhardness and thickness of the tribolayers, for the tested conditions.

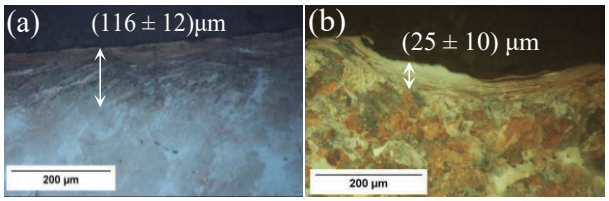

Figure 1 Micrographs of the tribolayers: (a) Wheel; (b) Disk (600 N / 300 °C).

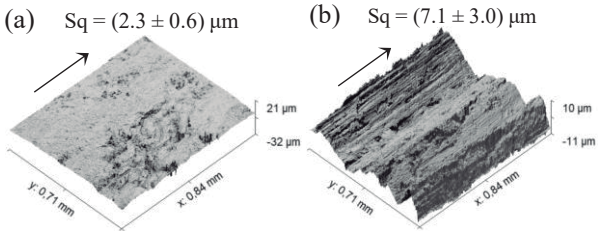

Figure 2 Confocal profilometry of worn surfaces: (a) Wheel; (b) Disk (600 N / 300 °C).

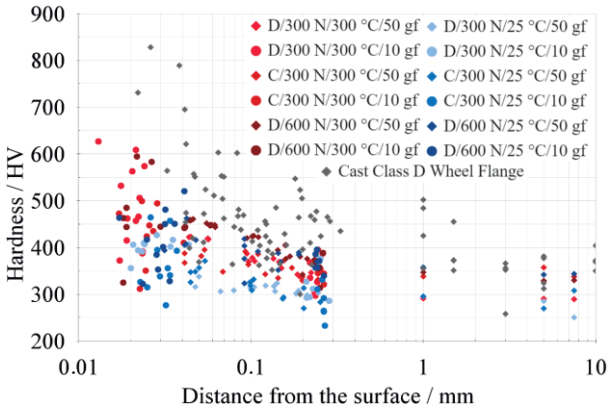

Figure 3 Microhardness profiles for each tested condition and for wheel flange.

4. Conclusion

The pin-on-disk test has limitations to reproduce the thickness and roughness of the tribolayers of railway wheels, under the tested conditions, but reproduces the microstructure evolution and strain-hardening process.

5. References

[1] LEWIS, Roger; OLOFSSON, U. Wheel-rail interface handbook. 1st Edition. Elsevier, 2009.

[2] WOLFF, Karsten, et al. Chronology of the microstructure evolution for pearlitic steel under unidirectional tribological loading. Tribology International 102 (2016): 540-545.

Design, manufacturing, assembly and operation of high-stress abrasion tester according to ASTM B611-21

Sousa, N.O.[1)*], Souza, L.L.[1)], Sousa, A.C.D.[1)], Magnol, R.V. [1)], Scandian, C. [1)] and Strey, N.F.[1)]

[1)] Tribology, Corrosion and Materials Laboratory - TRICORRMAT, Department of Mechanical Engineering, Federal University of Espírito Santo - UFES, Vitória, 29075-910, Brazil
[*]Corresponding author: natalia.sousa@edu.ufes.br

1. Introduction

To understand wear and its mechanisms, it is essential to simulate tribological systems [1]. A high-stress abrasion tester is suggested in ASTM B611-21 standard test for hard materials, as cermets and ceramics, using a water slurry and a rotating steel wheel, to force the abrasive against the test specimen, all immersed in the slurry [2]. Therefore, the objective of this work is to design, manufacture, assemble and operate an abrasion tester, according to ASBM B611-21.

2. Project Design

Design conception was done on Solid Works®, as shown in Figure 1, and critical parts, as cantilevers and axis, were submitted to analytic structural calculus conforming to solid mechanics. The lowest security coefficient obtained was 1.67 in the wheel axis. The equipment was mainly built out of galvanized structural steel ASTM A36, whose yield strength is 250 MPa.

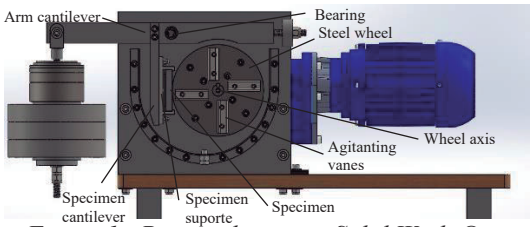

Figure 1 Project design on Solid Works®.

3. Materials and Methods

Prismatic ferritic-pearlitic low carbon steel samples were prepared, with hardness of 67±2 HRB, roughness average of 0,15±0,03 µm, and 76,5x25x9 mm dimension. Metallic samples were used for operational concept proof.

Operational parameters are displayed in Table 1. In each test, a load of 220 N was applied on wheel-specimen contact, and the rotational speed was 50 rpm.

Table 1 Operation parameters

Test	Abrasive type	Time
1	Fused Alumina, 60 µm	20 min
2	Standard Brazilian Sand – IPT, 600 µm	20 min
3	Standard Brazilian Sand – IPT, 600 µm	10 min
4	Standard Brazilian Sand – IPT, 600 µm	15 min
5	Standard Brazilian Sand – IPT, 600 µm	15 min

4. Results and Discussion

Figure 1a shows final equipment assembly. The sample and its support, in contact with the steel wheel, are shown in grater details on Figure 1b.

Wear rate was increased after changing the abrasive particle from alumina to sand, as shown in Figure 2. This is due to the latter's larger particle size, even though alumina presents higher hardness the silica. Detection of a slurry make-up depends on the visualization of the grit being carried up by the wheel and on hearing a crushing sound, due to wheel-specimen contact, indicating grit comminution. Not all tests presented this phenomenon, as Test 3, due to its duration time, and as Test 4, due to a water loss in the slurry, provoking metallic contact between the sample and wheel.

Considering just sand grit tests, there was an increase on the wear rate with time. A hypothesis for this is morphologic changes in the grit during the comminution, on test, becoming more sharp than spherical.

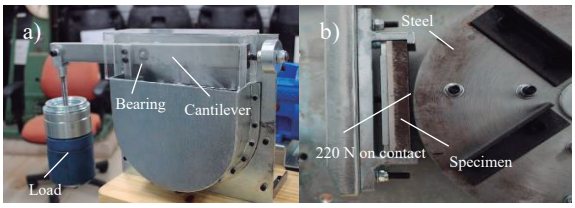

Figure 2 ASTM B611-21 abrasion tester.

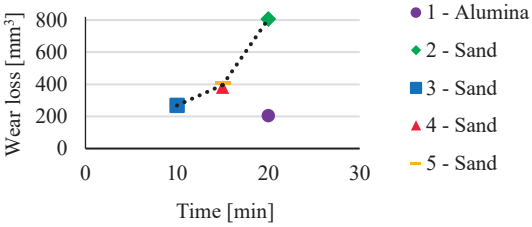

Figure 3 Wear rate per time.

5. Conclusion

The project design was proven to fit the requirements, after the operation of the equipment. It was established that the test occurred under high stress, due to the slurry make-up from particle comminution. It is intended, in following studies, to utilize ceramic samples in accordance with ASTM B611-21.

6. References

[1] Stachowiak, Gwidon; Batchelor, Andrew W. *Experimental methods in tribology*. Elsevier, 2004.
[2] ASTM Standard B611-21, *"Standard Test Method for Determining the High Stress Abrasion resistance of Hard Materials"* ASTM International, West Conshohocken, PA, 2021, DOI: 10.1520/B0611-21, www.astm.org

Computational method for evaluating the sliding wear rate in a pin-on-disc tribometer

Silva e Silva, J.V. R [1)*], Corrêa, L. F. V [1)], Neves, D. R [1),] Scandian, C [2)] and Santos, G. F. M [1)]

[1)] Tribology and Railway Dynamics Laboratory (Lab TDF), Federal University of Espírito Santo, Brazil
[2)] Tribology, Corrosion and Materials Laboratory (TRICORRMAT), Federal University of Espírito Santo, Brazil
*Corresponding author: eng.jvrss@outlook.com

1. Introduction

The wheel-rail system in railways is prone to sliding wear during curves, which can lead to detrimental effects such as reduced wheel lifespan. Laboratory pin-on-disc tests aim to replicate the operational conditions found in the field, helping to understand and predict wear phenomena. However, due to cost and time constraints, computational approaches are being explored as an alternative in this domain [1].

Semi-analytical simulations offer an efficient means to predict wear rates resulting from the sliding between train wheels and rails [1]. Therefore, the objective of this study is to evaluate the accuracy of a semi-analytical computational method in predicting wear rates in rails through the simulation of pin-on-disc tests.

2. Materials and Methods

Samples of predominantly pearlitic rail and cast microalloyed steel wheels were used to create pins and discs, respectively. The elastic modulus of the materials was assumed to be 200 GPa, with a Poisson's coefficient of 0.3.

The GIWM method [2] was adapted to estimate wear rate (m³/m) from pin-on-disc tests. The initial fitting involved using experimental data from the test conducted at 300 N normal load and 0.1 m/s tangential velocity as inputs for the Python-based algorithm. The adjusted algorithm was then used to determine the wear coefficient (k), which was subsequently utilized to predict the wear rate in rail samples from tests conducted at 600 N normal load.

3. Results and Discussions

Figure 1(b) demonstrates that the wear rates predicted by the algorithm for railway rail samples (pin) are in accordance with the experimental results. The simulated wear rate underestimated the experimental value by approximately 12.8%. The algorithm identified the wear coefficient (k) as 2.48 ± 0.33E-13 m³/N.m. The simple geometry and wear profile of the pin may have positively influenced the algorithm's fitting (Fig. 1a) and, consequently, its prediction capability for other simulated loads.

However, despite the acceptable percentage discrepancy between experiments and simulation, the fact that the algorithm is based on elastic mechanics may have negatively influenced its accuracy, as it does not consider the plasticity involved in wear.

Another factor contributing to the method's imprecision is the alteration of wear mechanisms in the experiment. Doubling the applied normal load likely changed the wear regime, making it more aggressive. Consequently, a shift in the dominant wear mechanism may have occurred, leading to imprecise wear rate predictions by the GIWM. This imprecision aligns with [2], but it remains unclear why the algorithm underestimated the wear rate in the current study while overestimating it in the original study.

Finally, the method proved to be computationally efficient, delivering results in approximately 60 seconds.

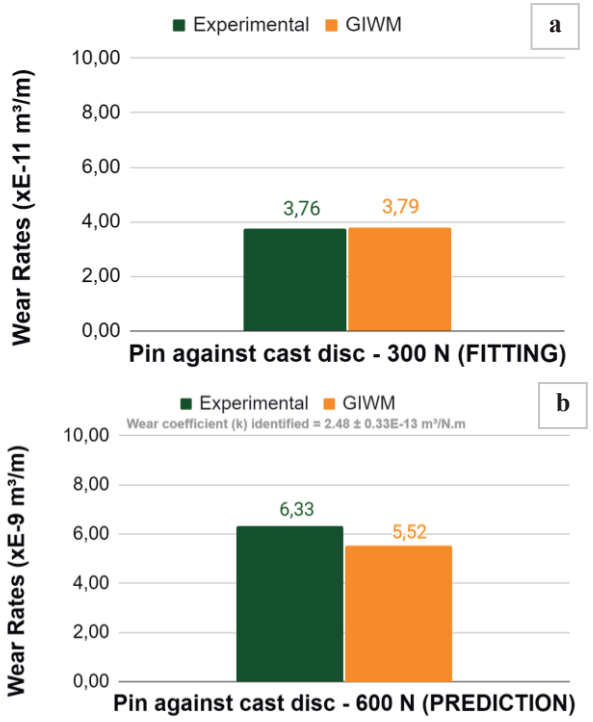

Figure 1: (a) Algorithm calibration with experiments; (b) Comparison between experimental and computational wear rate results

Based on the presented results, the evaluation of the semi-analytical GIWM method has proven to be a fast and cost-effective tool for guidance regarding rail wear resulting from contact with railway vehicles during curves.

4. References

[1] Silva e Silva, J. V. R, Corrêa, L. F, Camporez, R. M, Scandian, C, & Santos, G. F. M. *Computer simulation to predict the sliding wear of pearlitic rails in contact between cast and forged railway wheels*. WIT Transactions on The Built Environment, 89-98, 2022;

[2] Hegadekatte, V, Huber, N. & Kraft, O. *Modeling and simulation of wear in a pin on disc tribometer*. Tribology Letters, 51–60, 2006.

Adhesion of protective patinas formed in high-performance weathering steels

Costa, H.L[1)], Alano, J.H. [1)], Bianchi, K.E. [1)], Souza, D[1)]., Passos, T. A. [1)], Leivas, M.M. [1)], Cortopassi, C.E.G. [1)], Celente, C. [1)], Laner, B.S. [1)], Oliveira, J. A. B. [1)], Colares, H.X. [1)], Mendes, H.E.G. [1)], Cunha, M.L.A..[2)]

[1)] Surface Engineering Group, Universidade Federal do Rio Grande, Rio Grande, 96203-900, Brazil
2) ArcelorMittal Brasil, R&D Department, Distrito Carapina, Serra, 29163-970, Brazil
*Corresponding author: henaracosta@furg.br

1. Introduction

Weathering steels exhibit enhanced corrosion resistance when exposed to harsh environments due to the development of a protective layer of rust on its surface, called patina, which slows down further corrosion and eliminates the need for painting or protective coatings. Unlike ordinary steel, which corrodes uniformly, weathering steel undergoes an initial period of accelerated corrosion, followed by a stabilization phase where the corrosion rate decreases significantly. Weathering steel is primarily composed of iron, along with small amounts of copper, chromium, and nickel. In addition to its corrosion resistance, weathering steels generally possess high strength and durability [1].

When used in applications that require welding, the microstructure can be affected the heat input and thermal cycles imposed, which in turn can affect the formation of patinas and their adhesion to the substrate. This work compares the adhesion of patinas formed on different weathering steels. It also investigates the effects of arc energy on the microstructure and adhesion of the patinas.

2. Methods

The two steels investigated in this work were a commercial weathering steel (A242) and a high-strength weathering steel with a nominal tensile strength of 750 MPa (steel B). The chemical composition of steel B is proprietary. The multi-pass welding experiments were carried out with a constant voltage inverter type power supply, model Lincoln Electric Flextec 450, an air-cooled MIG/MAG torch and a tractor-type linear robot model BUG-O. Welding current and voltage were acquired at a frequency of 5 kHz. The electrode wires were 1.2 mm ER70S-6 for ASMT A242 steel and ER110S-1 for steel B. The shielding gas was 100% CO_2 with a flow rate of 17 L/min.

For producing the patinas, accelerated corrosion tests followed the ASTM G1 standard. Before being subjected to weathering cycles, the specimens were carefully cleaned in acetone and alcohol by ultrasound, dried, weighed and measured. Wet and dry cycles were performed, totaling 24 hours per cycle, as follows: *i.* 3 h in salt mist; *ii.* 2 h of drying; *iii.* 17 h in saline mist, followed by cleaning in running water; *iv.* 2 h of drying. These steps are fundamental, as they simulate the action of weathering on steel, including environmental deterioration, reducing the concentration of chlorides and allowing the formation of a protective patina. At pre-established intervals, mass loss measurements were performed on two specimens of each steel. The specimens were immersed in HCl (50% v/v) containing a corrosion inhibitor [$(CH_2)6N_4$] until the complete elimination of corrosion products. Afterwards, they were rinsed with distilled water, dried and weighed. The thickness loss as a function of the number of cycles was obtained from the mass loss data according to the ASTM B117 standard.

The adhesion of the patinas was assessed via room temperature linear unidirectional tests with linearly increasing loads in a universal tribometer model Rtec Mft 5000 in order to obtain the critical loads for initial delamination (Lc1) and total delamination (Lc2). The counterbody was a 6 mm 52100 steel ball. After the tests, the worn tracks were observed by scanning electron microscopy (SEM) and Energy dispersive X-ray spectroscopy (EDS) to identify the delamination of the patinas and the removal mechanisms.

3. Results and discussion

Due to the large thickness of the plates, the macrostructure (Figure 1) and microstructure of the weld beads was very complex. The differences in microstructure between the different macro regions can influence the patinas formed. Therefore, the adhesion of the patinas was measured when formed in each of the regions individually (base metal, heat affected zone and weld region).

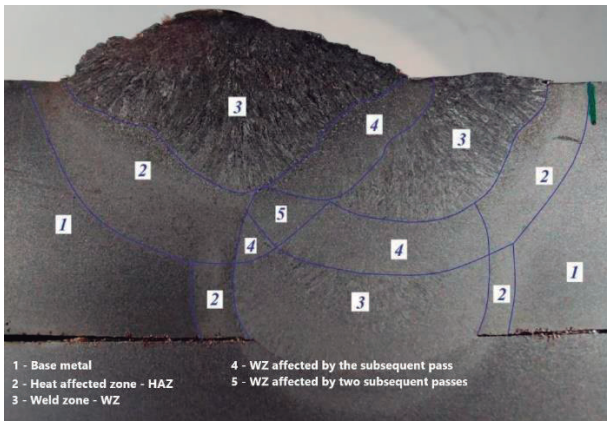

Figure 1 Macrostrucure of the welded joint for A242 steel

4. References

1. Artigas, A., et al., *Development of accelerated wet–dry cycle corrosion test in marine environment for weathering steels.* Corrosion Engineering, Science and Technology, 2015. **50**(8): p. 628-632.

The impact of high chromium cast iron modified with niobium and boron on abrasive wear assessed by industrial tests under different severity conditions

Godoy, C.[1)*], Scal, M.W.[2)], Oliveira, C. [3)] and Bueno, M. [4)]

[1, 3,4)] Department of Metallurgical and Materials Engineering, Federal University of Minas Gerais - UFMG, Brazil
[2)] MScal Steelmaking Consulting Co., Brazil
*Corresponding author: cristinagodoyufmg@gmail.com

1. Introduction

The austenite (γ) destabilization heat treatment aims to get the highest hardness through a martensite (α')-based microstructure with low retained austenite in white cast iron (WCI). Computational Thermodynamic (CT) is a good tool to define the austenitization temperature and equilibrium phases. With enough time, at high temperature, the equilibrium chemical composition is reached, the solid solution elements get the minimum value, increasing Ms temperature (thermodynamic factor for γ-α' transformation). Depends on the cooling rate a low γ content can be obtained in a martensitic matrix with secondary carbides (M_7C_3 and $M_{23}C_7$) – kinetic factor [1]. This study aims to clarify that not only alloy microstructure and hardness influence the wear resistance, but also that the same alloy may have different responses to wear when subjected to varying severity conditions.

2. Methods

The abrasion resistance was obtained through industrial tests in an iron ore transfer chute and a belt feeder conveyor. X-ray diffraction (XRD), OM, and SEM analyses were used to detect phases and microstructure. A destabilization treatment at 1020ºC for 2 h was carried out followed by air quenching and tempering at 250ºC for 2h. A high severity occurred in the transfer chute: transport rate of 1180 ton/h, speed of 3.0 m/s and a drop height of 12 m after 75 operating days. A low severity took place in belt feeder: transport rate of 2834 ton/h, speed of 0.5 m/s and with no drop height after 57 operating days. Based on the eutectic composition of 25%Cr and 2.8%C, four different WCI were designed: WCI, Nb-WCI, B-WCI, and NbB-WCI.

3. Results and Discussion

The WCI showed a eutectic microstructure with carbides surrounded by martensite and with austenite occupying the available space between these phases. The Nb addition leads to NbC precipitates at a temperature higher than eutectic promoting a hypoeutectic microstructure. According to CT the addition of B causes M_2B (M=Cr,Fe) formation at the eutectic temperature leading to a hypereutectic microstructure. These structural aspects are fundamental in abrasive wear resistance [2]. All Nb-B modified alloys have just martensite and no remaining austenite. Eutectic alloys showed greater wear resistance at high severity and hypereutectic alloys showed better performance at low severity tests, faced with different severities in industrial tests.
The distinct chemical compositions explain the microstructure variation in the materials (Fig.1a-d). B-WCI contain large primary carbides, B nitrides, and Fe-B carbides, whereas WCI retains austenite that contributes to the lowest wear rate under greater severity conditions (Fig.2a,b). On the other hand, NbB-WCI with a hypereutectic microstructure exibits the same effect but under less severe conditions in the Belt Feeder (Fig.2c,d). It is worth noting that even though the hardness of different alloys varies in a narrow range, these microstructural differences play a crucial role in their performance.

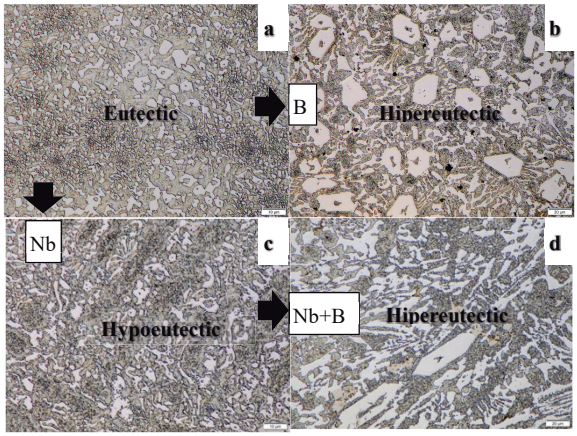

Fig.1: Microstructure: (a)WCI, (b)B-WCI, (c) Nb-WCI, and (d) NbB-WCI.

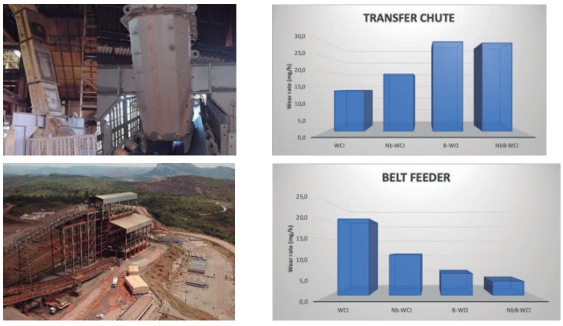

Fig 2: Wear Rate of alloys in industrial equipment.

4. Conclusions

An alloy responds differently to wear when subjected to different severities of industrial applications on mining process. Equal microstructures subjected to different severities lead to different responses in wear rate.

5.References

[1] Albertin E., Beneduce F., Matsumoto M. and Teixeira, I., *Optimizing heat treatment and wear resistance of high chromium cast irons using computational thermodynamics*. Wear, 2011. **271**: p.1813–1818.
[2] Pintaude G., Bernardes, F.G., Santos, M.M., *Sinatora A., Albertin E., Mild and severe wear of steels and cast irons in sliding abrasion.*Wear, 2009. **267:** p. 19–25.

Improving the tribotechnical properties of friction surfaces by using mineral coatings

Kislov, S.[1)], Savin, L.[2)] and Polyakov, R.[2)*]

[1)] LLC MicoTech, Kaluga, 248010, Russian Federation
[2)] Department of Mechatronics, Mechanics and Robotics, Orel State University named after I.S. Turgenev, Orel, 302026, Russian Federation
*Corresponding author: romanpolak@mail.ru

1. Introduction

The irreversibility of the wear process requires the search for more and more new approaches of increasing the wear resistance of friction pairs of machines and mechanisms: sliding bearings, rods, seals, gear and worm gears, threaded connections, sliding guides, rollers of rolling equipment and many others. In the most critical mechanisms, the assumption of extreme wear of parts leads to damage of the associated parts and a significant increase in repair costs, not to mention losses in accidents and sudden failures.

The scientific and production association Mineral Coating Technologies [1] has developed a unique technology for obtaining friction surfaces with improved qualities by penetrating mineral particles through the surface layer of the material.

2. Description of Technology

Mineral coating technology is set of techniques for forming friction pair surfaces by combining mechanical, electrical and sound effects of the object of application and mineral particles with a size of less than 100 nm. The raw materials are natural minerals, for example serpentines and the like, consisting mainly of structures of the type Mg_3 $[Si_2O_5]$ $(OH)_4$, and also sometimes including impurities Fe^{2+}, Fe^{3+}, Al, Ni, sometimes Ti, Mn, Ca.

As a result, mineral particles are introduced into the crystal lattice of the treated metal and, thereby, modify the surface and border layers with a depth of up to 50 microns in the following directions: increase in microhardness, decrease in friction coefficient, decrease in grain size, decrease in roughness of the original surface.

The versatility of the technology allows mineral coating to be applied to virtually any surface used for the production of friction pairs: bronze, brass, copper, aluminum, babbits, low-alloy and high-alloy steels, stainless and non-magnetic steels, cast iron, titanium, plastics (fluoroplastic, caprolone) and hard rubber.

3. Results of Experimental Research

The picture 1 shows an enlarged image of a cut of a treated metal sample made of 20Cr613 steel with applied mineral coatings.

The results of the experiments performed at the BAM Institute [2] proved an improving in the tribotechnical qualities of friction surfaces with mineral coatings in terms of increasing the microhardness of the surface compared to the base material (up to 40%), a decrease in wear intensity (from 25% or more), a decrease in the coefficient of friction (up to 40%).

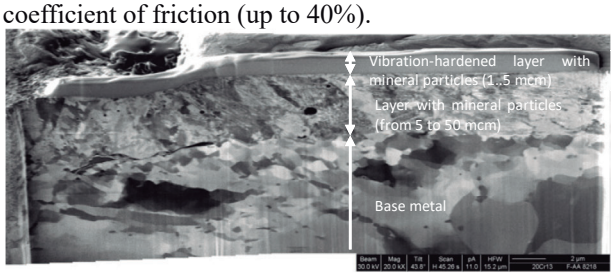

Figure 1 Structure of metal layer with mineral coating

The results of studies of the friction pair «steel-steel», the contact «plane-cylinder» are partially presented in Table 1.

Table 1 Results of experiments

Material 102Cr6	Hardness, MPa	Wear rate, mm^3/Nm	Coef. of friction
Untreated	2139	$1{,}97 \cdot 10^{-9}$	0,09
Treated	3585	$0{,}884 \cdot 10^{-9}$	0,07

4. Conclusion

Summarizing the experience gained over 15 years in introducing the technology at power plants, sea and river transport,

The following key aspects can be identified that may be the interests of potential partners to decide on the implementation of the technology:

-increase of friction pair service life up to 3-10 times;
-preservation of geometric dimensions of machined parts;
-the temperature of the technological process does not exceed 50-70°C;
-possibility of coating only on the working area;
-there is no restriction of the size and shape of the machined elements.

Abroad, the technology is implemented or is under implementation at the following enterprises: SMS GROUP (Germany), KSB AG (Germany), WILO (Germany), Termomeccanica Pompe (Italy), Zhejiang SF Oilless Bearing (China).

5. References

[1] Mico-Tech, LLC: http://mico-tech.com.
[2] Federal Institute for Material Research and Testing: https://www.bam.de.

AUTHOR INDEX

Bruno Soares Laner	4DTC

C

Caio Augusto Garcia Sampaio Valente	4DQ2
Camila Belén Marini	4DPM
Camilo Andrés García	4DSB
Camilo Perdomo Madrigal	4DTQ
Carlos Alberto Achete	4DNN, 4DNP
Carlos Alberto Fonzar Pintão	4DQZ, 4DR2
Carlos Alberto Rosa Neto	4DS6, 4DSP
Carlos Alejandro Figueroa	4DN6
Carlos Eduardo Grisolia Cortopassi	4DTC
Carlos Enrique Niño	4DNM
Carlos Henrique Da Silva	4DQ2
Carlos Roberto Grandini	4DR2
Carlos Rodrigo Melo Roesler	4DR6
Caroline Francisco Dorneles	4DQB
Celso Ricardo Adami	4DRT
César Perez	4DNQ
Cherlio Scandian	4DP6, 4DS6, 4DSA, 4DSC, 4DSD, 4DSE, 4DSP, 4DSQ, 4DSV, 4DSZ, 4DTB, 4DTD, 4DTR
Chinwuba Victor Ossia	4DRY
Christian Moreau	4DMX, 4DTP, 4DTQ
Christine Boher	4DSP
Clara Muniz Almeida	4DR6
Cláudio Gonçalves de Oliveira	4DQE
Claudio Gonçalves Oliveira	4DQG
Cláudio Moreira Alcântara	4DN4
Clidio Hort Filho	4DPS
Cosimi Corleto	4DTS
Cristian Camilo Viáfara Arango	4DRA, 4DRF
CRISTIANE ARPINO SILVA	4DPG
Cristiano Azevedo Celente	4DTC
Cristiano Binder	4DMJ, 4DNE, 4DNF, 4DP4, 4DPW, 4DPY, 4DQB, 4DTB
Cristiano José Scheuer	4DNH
Cristiano Simões Abreu	4DMH
Cristian Viafara Arango	4DQD

D

Daiane Münch	4DMS, 4DNA, 4DQM
Daniela Nunes Oliveira	4DS6
Daniele Rodrigues das Neves	4DP6
Daniel Souza	4DTC
Danilo Assad Ludewigs	4DPH
Danilo Mota Campos	4DNV
Dany Michell Andrade Centeno	4DSX, 4DTA
Daria Kolbas	4DMQ
David Cano	4DSB
Davi Franzosi	4DQQ
Delfim Fernandes Soares	4DMV
Demostenes Ferreira	4DSR
Diego Berti Salvaro	4DMJ, 4DP4, 4DPW, 4DPY, 4DR4

Diego Piazza	4DRT
Diego Rafael Nespeque Correa	4DR2
Diego Tolotti de Almeida	4DNH, 4DQ6
Dirk Drees	4DTV
D Kesavan	4DME

E

Edja Iandeyara Freitas Moura	4DNJ
Edson Pinheiro Lima	4DSY
Eduardo Albertin	4DQF
Eduardo Alberto Fancello	4DR6
Eduardo Tomanik	4DRB, 4DSN
Eleir Mundim Bortoleto	4DNA, 4DPD, 4DQM, 4DRP, 4DRS, 4DRV
Eliane Alves Kihara	4DSR
Elismar Miquelanti	4DRV
Elton Yvens Godoy de Oliveira	4DPF
Emilio Carlos Nelli Silva	4DPV
Emmanuel Georgiou	4DTV
Enrique Giménez	4DMR
Enzo Ovando	4DNW
Erick Cardoso Costa	4DPS, 4DPT, 4DPZ
Erika Lira Buthers	4DNN
Erivaldo Santos Jales	4DPD
Esteban Rave	4DSB
Eurico Felix Pieretti	4DRK, 4DRX
Eziwhuo Second Justice	4DRY

F

Fabio Antonio Xavier	4DPS, 4DPT, 4DPZ
Fábio Dian Murari	4DNR
Fabio Tatzgern	4DSM
Fadhel Ben Ettouil	4DMX
Felipe Gustavo Ebersbach	4DQB
Felipe Kessler	4DTT
Felipe Kevin Correia Luz	4DQ6, 4DQX
Felipe Santos de Almeida	4DQV
Fernanda Correa	4DNM
Fernanda de Melo Fernandes	4DP2
Fernando Alvarez	4DN6
Fernando Buiatti Rodrigues	4DNK
Fernando Galembeck	4DRB
Fernando H. Gruber Colaco	4DTK
Fernando Moreira Bordin	4DPS, 4DPT, 4DPZ
Fevzi Kafexhiu	4DNX
Filomena Viana	4DT4
Franciele Dias de Castro	4DSJ
Francisco das Chagas Marques	4DQV
Francisco José Profito	4DMM, 4DPE, 4DPF, 4DPR, 4DQN, 4DQQ, 4DQX, 4DRN, 4DSN
Funsho Olaitan Kolawole	4DPH

G

Gabriela Papoulias França	4DSN
Gabriel Borges Ferreira	4DSA
Gabriel Del Maestro Duarte	4DSC
Gabriel Macêdo	4DMW
Geralda Cristina Duraes de Godoy	4DQE, 4DQG
Germán Prieto	4DNW, 4DNX, 4DPM, 4DPQ

Giuseppe Pintaude	4DPB, 4DRJ, 4DTB, 4DTK
Gnanamoorthy R	4DMB
Guilherme Fabiano Mendonça dos Santos	4DP6
Guilherme Oliveira Neves	4DNE, 4DNF, 4DPW
Guilherme Ribeiro Capelin	4DQZ
Guilherme Santos Vacchi	4DPN
Guilherme Yuuki Koga	4DRH, 4DRM
Gustavo Tressia	4DQJ, 4DRP, 4DRS, 4DSX, 4DTA
G V Balakrishna	4DMB

H

Hadille Emanuele Gonçalves Mendes	4DTC
Hélio Goldenstein	4DSX, 4DTA
Henara Lillian Costa	4DMM, 4DNH, 4DPB, 4DPF, 4DPG, 4DPX, 4DQ6, 4DQR, 4DQX, 4DSJ, 4DSM, 4DSR, 4DTB, 4DTC, 4DTT
Henrique Boschetti Pereira	4DPN, 4DSX, 4DTA
Hermes Xavier Colares	4DTC

I

Ignacio Hernán Silva Cardenas	4DNW
Isaac dos Santos Nunes	4DTT
Isaac Vinícius do Nascimento	4DPE
Isabela Alves dos Santos	4DNG
Isabella Maria Mota de Souza	4DQD, 4DRA
Istiak Mahmud Saikat	4DTP
Iwao Ishizaki Neto	4DN4
Izabel Fernanda Machado	4DPK, 4DPV, 4DQF, 4DQH, 4DQP, 4DRN, 4DSH

J

Jacobo Porteiro	4DPR
Jaime Alberto Sanchez Caceres	4DSY
Javier Blanco Rodríguez	4DPR
Jean Valdir Uchôa Teixeira	4DQZ, 4DR2
Jeferson Trevisan Pacheco	4DNM
Jens Hardell	4DMQ, 4DMW
Jhonattan Gutjahr	4DMJ
Joana Silva Gomes	4DMH
João Carlos Fernandes de Queiróz	4DQN
João Eduardo Ribeiro	4DMV
João Henrique Corrêa de Souza	4DQ6
João Vinícius da Silva	4DNT
João Vitor Raimundo Silva e Silva	4DP6
Joice Miagava	4DSN
Jonathan Gramajo	4DMZ, 4DN2
Jorge Airton Badin de Oliveira	4DTC
Jorge Miguel Vieira	4DMH
José Daniel Biasoli de Mello	4DMT, 4DN4, 4DNE, 4DNF, 4DP4, 4DPW, 4DQR, 4DR4, 4DTB
Josefina Andrea Dib	4DT2
Jose Guilherme Andrade Carvalho	4DP2
José Henrique Alano	4DTC
Joseir Gandra Percy	4DNJ

Jose Jimmy Penagos	4DQD, 4DQM, 4DRA, 4DRF, 4DRS
José Ramos Gomes	4DMH
Juan Felipe Santa Marín	4DSS
Juan Ignacio Pereira	4DSK
Juan Manuel González Carmona	4DSF
Juan Pablo Abdelnabe	4DNW, 4DPM, 4DPQ
Júlia Afonso Pires	4DR4
Julia Bernardes Nogueira	4DS6
Juliane Ribeiro da Cruz Alves	4DMJ
Jurandir Marcos Sá de Sousa	4DMJ

K

Kaio Lucas Sousa Vieira	4DSV, 4DTD
Kezia Calmon	4DNQ
Kleber Eduardo Bianchi	4DTC

L

Lais M. Lopes	4DTV
Lanna Cristina Costa	4DNQ
Larissa Driemeier	4DRN
Larissa Solano de Almeida	4DNT, 4DPP
Laura Vanessa Giraldo	4DSB
Leandro Bastos Bergami	4DNA, 4DQF
Leandro Luiz de Oliveira e Silva	4DPT, 4DPZ
Leandro Moreira	4DQM
Lenine Marques de Castro Silva	4DQK
Leonardo de Oliveira Turani	4DNR
Leonardo Mathias Leidens	4DN6
Leonardo Medeiros Xavier	4DSP
Leonardo Pelcastre	4DMQ, 4DMW
Leonardo Rosa Ribeiro da Silva	4DNJ, 4DNK
Leonid Savin	4DMP
Lígia Raquel Rodrigues	4DMH
Lilian Vanessa Rossa Beltrami	4DRT
Lucas A. Manfroi	4DQV
LUCAS BIAZON	4DRR
Lucas Gimenis de Moura	4DR6
LUCAS KALEBE ARAUJO DE ALMEIDA	4DRH
Lucas Luiz de Souza	4DTR
Luciana Sgarbi Rossino	4DNS, 4DNT, 4DPN, 4DPP
Lucia Vieira	4DQV, 4DT4
Luis Alfredo Acevedo Suarez	4DQD, 4DRA, 4DRF
Luis Felipe Jiménez	4DSB
Luis Miguel Ballesteros	4DSB
Luis Vilhena	4DRC
Luiz Fernando Vieira Corrêa	4DP6
Luiz Henrique Dias Alves	4DSX, 4DTA

M

Maicon Machado Leivas	4DTC
Maicon Roberto Teodoro	4DPN
Manuelle Corbani Romero	4DSD, 4DSQ
Mara Cristina Lopes Oliveira	4DRK, 4DRX
Marcel Bartz	4DRZ
Marcelo Braga dos Santos	4DQX

Marcelo Gautério Fonseca	4DPX, 4DSJ
Marcelo Gouveia Sábia	4DNK
Marcel Roberto Castanheira	4DRF
Marcia Marie Maru de Moraes	4DNN, 4DNP, 4DNQ, 4DR6
Márcio L. A. Cunha	4DTC
Marcos Dantas dos Santos	4DT4
Marcos Dorigão Manfrinato	4DNS, 4DNT, 4DPN, 4DPP
Marcos Pellegrini Ribeiro	4DNK
Margarete Regina Freitas Gonçalves	4DPG
María Cristina Moré Farias	4DRT
María Margarita Echeverri Rodríguez	4DSS
María Mercedes Antonelli	4DNW
María Victoria Iriarte	4DPM
Marília Mendonça Lima	4DQE
Marina Cardozo Vasco	4DRJ
Marina Fuser Pillis	4DRK
Mário Antônio Caixeiro Castro Pereira	4DMV
Mário José Bueno de Souza Freitas	4DQE, 4DQG, 4DRV
Marjorie Benegra	4DSG
Marta-Lena Antti	4DMQ
Martha Simões Ribeiro	4DRX
Martín Iván Crespo	4DPQ
Mateus da Silva Cardoso	4DPY
Mateus Lube Uliana	4DSA
Matheus da Costa Mattos Azeredo	4DST
Mauricio Martins das Neves	4DRK, 4DRX
Maurício Waineraich Scal	4DQE, 4DQG
Max Marian	4DRZ, 4DS2
Mehmet Baykara	4DM6
Melanie Jane Hazlett	4DTP
Metallurgy and Materials Engineering	4DPN
Miguel Angel Narvaez Ardila	4DQR
Miguel Carvalho Silva Barcelos	4DPT, 4DPZ
Miguel Rubira Danelon	4DNS, 4DNT
Milton Pereira	4DMJ
Modesto Valci Moreira Lopes	4DRN
Mohamed El Mansori	4DSH, 4DTS
Muthuswamy Kamaraj	4DME

N

Nan Kang	4DSH
Natália de Oliveira Sousa	4DTR
Natália Dreveck	4DNM
Nathan Fantecelle Strey	4DS6, 4DSA, 4DSC, 4DSD, 4DSE, 4DSP, 4DSV, 4DSZ, 4DTD, 4DTR
Newton Kiyoshi Fukumasu	4DPH, 4DPK, 4DRB, 4DRN
Nhat Truong Nguyen	4DTQ
Nicola Getschko	4DSN
Nicolás Ignacio Araya Rivera	4DNE, 4DNF, 4DPW

O

Odila Florencio	4DPP
Olandir Vercino Correa	4DRK
Oliver Koch	4DQC, 4DQK
Osmar Custódio de Moura Filho	4DNM

Otávio José Costa de Oliveira	4DRB

P

Pantcho Stoyanov	4DMX, 4DTP, 4DTQ
Patrick Wingertszahn	4DQC
Paulo Cordeiro Machado	4DRQ
Paulo Marengo Trindade Júnior	4DTT
Paulo Noronha Lisboa-Filho	4DQZ, 4DR2
Paulo Roberto Mei	4DP2
Paulo Vanconvsky	4DPH
PEDRO TAYER	4DRR
Polyana Alves Radi	4DT4

R

Rafael Arenhart	4DNE
Rafael Lopes Fialho Penedo	4DN4
Raimundo Nonato Alves da Silva	4DT4
Rayan Paulo Santiago Santos	4DNG
Renan Oss Giacomelli	4DNM, 4DPW
Renan Santos da Silva	4DQ6
Renan Valter Magnol	4DSZ, 4DTR
Renata Antoun Simão	4DNN
Renata Strubbia	4DT2
Renato Altobelli Antunes	4DRK, 4DRX
Renato Chaves Pereira da Silva	4DMG, 4DQD, 4DRA, 4DRF
Ricardo Knoblauch	4DTS
Rinara Gregório Silva	4DRM
Roberto Carlos Vega Móron	4DPP
Roberto Fernández-Lafuente	4DNG
Roberto Martins de Souza	4DPH, 4DPK, 4DQF, 4DQJ, 4DQP, 4DQQ, 4DRB, 4DRN, 4DSD, 4DSH, 4DSK, 4DTB
Rodolfo Miranda Binda	4DRE
Rodolpho Ramilton de Castro Monteiro	4DNG
Rodrigo da Silva Miranda	4DP2
Rodrigo Silveira Vieira	4DNG
Rolf Bertrand Schroeter	4DQB
Roman Polyakov	4DMP
Ronnie Rodrigo Rego	4DPK
Ronny Peterson da Nóbrega Gonçalves	4DRB
Rubson Mação Camporez	4DSA, 4DSD, 4DSE
Rui Neto	4DT4
Rui Rodrigues	4DMH
Rui Soares	4DT4

S

Salete Martins Alves	4DSV, 4DTB, 4DTD
Samira Tahanzadeh	4DQH
Samuel Anisio Nunes Silva	4DMM
Samuel da Silva de Souza	4DSX, 4DTA
Sandro Wartzack	4DRZ
Sangharatna Ramteke	4DS2
Santiago Maya Johnson	4DNH
Santiago Moreno Sánchez	4DQJ
Sara Diaz Builes	4DPS, 4DQB
Sara Silvério	4DMH
Sebastian Gomez Durango	4DSS
Sebastían Rudas	4DSB
Sergio da Silva Cava	4DTB

SPONSORS AND EXIBITHORS

Gold sponsors

CAPES

FAPES

GOVERNO DO ESTADO DO ESPÍRITO SANTO
Secretaria da Ciência, Tecnologia, Inovação e Educação Profissional

VALE

Sponsors

CT-TRIB
Green Tribology for the Energetic Transition

FALEX TRIBOLOGY

Anton Paar

analítica

Rtec instruments

Essencis

PHOENIX TRIBOLOGY

CREA-ES
Conselho Regional de Engenharia e Agronomia do Espírito Santo

SEE

ENDORSEMENT

IFToMM Technical Committee for Tribology

PETRO Industry News